Studies on the Extraction/Complexation of Actinide and Fission Product Elements using Selective Ligands in Room Temperature Ionic Liquids

By

ARIJIT SENGUPTA
CHEM 012 011 04011
Bhabha Atomic Research Centre, Mumbai

A thesis submitted to the
Board of Studies in Chemical Sciences
In partial fulfillment of requirements
For the Degree of

DOCTOR OF PHILOSOPHY

of

HOMI BHABHA NATIONAL INSTITUTE

November 2014

HOMI BHABHA NATIONAL INSTITUTE

Recommendations of the Viva Voce Board

As members of the Viva Voce Board, we certify that we have read the dissertation prepared by **Arijit Sengupta** entitled **"Studies on the extraction/ complexation of actinide and fission product elements using selective ligands in room temperature ionic liquids "** and recommend that it may be accepted as fulfilling the dissertation requirement for the Degree of Doctor of Philosophy.

Date: 20.11.2014

Chairman: Prof. K. L. Ramakumar

Date: 20.11.2014

Guide: Dr. P. K. Mohapatra

Date: 20/11/2014

Member 1: Dr. P. N. Pathak

Date:

Member 2: Dr. P. S. Dhami

Date: 20/11/2014

External Examiner: Prof. A. K. Singh AK Singh

Final approval and acceptance of this thesis is contingent upon the candidate's submission of the final copies of the thesis to HBNI. I/We hereby certify that I/we have read this thesis prepared under my/our direction and recommend that it may be accepted as fulfilling the thesis requirement.

Date: 20.11.2014

Place: BARC, Mumbai

<Signature>

Guide

STATEMENT BY AUTHOR

This dissertation has been submitted in partial fulfillment of requirements for an advanced degree at Homi Bhabha National Institute (HBNI) and is deposited in the Library to be made available to borrowers under rules of the HBNI.

Brief quotations from this dissertation are allowable without special permission, provided that accurate acknowledgement of source is made. Requests for permission for extended quotation from or reproduction of this manuscript in whole or in part may be granted by the Competent Authority of HBNI when in his or her judgment the proposed use of the material is in the interests of scholarship. In all other instances, however, permission must be obtained from the author.

Arijit Sengupta.

ARIJIT SENGUPTA

DECLARATION

I, hereby declare that the investigation presented in the thesis has been carried out by me. The work is original and has not been submitted earlier as a whole or in part for a degree / diploma at this or any other Institution / University.

Arijit Sengupta

Arijit Sengupta

Dedicated to …..

My Family

List of Publications

Journals

1. Extraction of Am(III) using novel solvent systems containing a tripodal diglycolamide ligand in room temperature ionic liquids: a ‘green’ approach for radioactive waste processing.

   A. Sengupta, P. K. Mohapatra, M. Iqbal, W. Verboom, J. Huskens and S. V. Godbole, *The Royal Society Advances*, 2 **(2012)** 7492-7500

2. Extraction of radiostrontium from nuclear waste solution using crown ethers in room temperature ionic liquids.

   Arijit Sengupta and Prasanta Kumar Mohapatra, *Supramolecular Chemistry*, 24(11) (**2012**) 771-778.

3. A highly efficient solvent system containing functionalized diglycolamides and an ionic liquid for americium recovery from radioactive wastes.

   Arijit Sengupta, Prasanta K. Mohapatra, Mudassir Iqbal, Jurriaan Huskensb, Willem Verboom, *Dalton Trans*. 41(23) (**2012**) 6970-6979.

4. Remarkable acidity independent actinide extraction with a both-side diglycolamide-functionalized calix[4]arene.

   Prasanta K. Mohapatra, **Arijit Sengupta**, Mudassir Iqbal, Jurriaan Huskens, Shrikant V. Godbole and Willem Verboom, *Dalton Trans.*, 42 (**2013**) 8558–8562,

5. Highly Efficient Diglycolamide-Based Task Specific Ionic Liquids: Synthesis, Unusual Extraction Behaviour, Irradiation, and Fluorescence Studies.

   Prasant K. Mohapatra, **Arijit Sengupta**, Mussadir Iqbal, Jurriaan Huskens, Willem Verboom, *Chemistry A European Journal*, 19(9) (**2013**) 3230–3238.

6. A diglycolamide-functionalized task specific ionic liquid (TSIL) for actinide extraction: Solvent extraction, thermodynamics and radiolytic stability studies**.**

   Arijit Sengupta, Prasanta Kumar Mohapatra, Mudassir Iqbal, Jurrian Huskens, Willem Verboom, *Separation and Purification Technology* 118 (**2013**) 264–270

7. Diglycolamide-functionalized calix[4]arenes showing unusual complexation of actinide ions in room temperature ionic liquids: Role of ligand structure, radiolytic stability, emission spectroscopy, and thermodynamic studies.

   Prasanta K. Mohapatra, **Arijit Sengupta**, Mudassir Iqbal, Jurriaan Huskens, Willem Verboom, *Inorg. Chem.*, 52 (5) (**2013**) 2533–2541.

8. Role of alkyl substituent in room temperature ionic liquid on the electrochemical behavior of uranium ion and its local environment.

   Arijit Sengupta, M. S. Murali, P. K. Mohapatra, *J Radioanal. Nucl. Chem.*, 298 (**2013**) 209-217.

9. A comparative study on the complexation of Am and Eu with TODGA in room temperature ionic liquid.

   Arijit Sengupta, M.S.Murali, P.K.Mohapatra, *J Radioanal. Nucl. Chem.*, 298 (**2013**) 405-412.

10. Role of organic diluent on actinide ion extraction using a both-side diglycolamide-functionalized calix[4]arene.

    Arijit Sengupta, Prasanta K.Mohapatra, Mudassir Iqbal, Jurriaan Huskens, Willem Verboom, *Supramolecular Chemistry*, 25 (9-11) (**2013**) 688-695.

11. Judd-Ofelt parameters of diglycolamide-functionalized calix[4]arene Eu^{3+} complexes in room temperature ionic liquid for structural analysis: Effects of solvents and ligand stereochemistry.

Arijit Sengupta, Shrikant V. Godbole, Prasanta K. Mohapatra, Mudassir Iqbal, Jurriaan Huskens and Willem Verboom, , *J of luminescence*, 148(**2014**)174-180.

12. Solvent systems containing diglycolamide-functionalized calix[4]arenes in room temperature ionic liquids for metal ion extraction: Studies with simulated high level wastes

    Arijit Sengupta, Prasanta K.Mohapatra, Mudassir Iqbal, Jurriaan Huskens, Willem Verboom, *Supramolecular Chemistry*, 26(7-8), (**2014**) 612-619

13. Spectroscopic investigation of Eu^{3+} - complexes with ligands containing multiple diglycolamide pendant arms in a room temperature ionic liquid

    Arijit Sengupta, Prasanta K. Mohapatra, Mudassir Iqbal, Jurriaan Huskens, Willem Verboom, *J of Luminescence*, 154 (**2014**)392 - 401.

14. Diglycolamide-Functionalized Task Specific Ionic Liquids for Nuclear Waste Remediation: Extraction, Luminescence, Theoretical and EPR Investigations.

    Arijit Sengupta, Prasanta K. Mohapatra, Ramakant M. Kadam, Debashree Manna, Tapan K. Ghanty, Mudassir Iqbal, Jurriaan Huskens and Willem Verboom, RSC Adv., 4 (2014) 46613–46623

Symposium

1. Selective extraction of Strontium (II) from SHLW using room temperature ionic liquid. **Arijit Sengupta** and P.K. Mohapatra, *SESTEC* (**2012**).
2. Extraction and radiolytic degradation studies using a novel actinide selective solvent system containing a tripodal diglycolamide in room temperature ionic liquids.

   A. Sengupta, M. Iqbal, W. Verboom, and P.K. Mohapatra, *SESTEC* (**2012**).
3. Actinide extraction using two novel task specific ionic liquid.

   A.Sengupta, M.Iqbal, W. Verboom, P.K.Mohapatra, *NUCAR* (**2013**) 283-284.
4. Structurally modified diglycolamide functionalized calixarenes in room temperature ionic liquid for actinide extraction.

   A.Sengupta, M.Iqbal, W. Verboom, P.K.Mohapatra, *NUCAR* (**2013**) 285-286.
5. Complexation of TODGA in room temperature ionic liquid, electrochemical study.

   A. Sengupta, M.S.Murali, P.K.Mohapatra, *NUCAR* (**2013**) 307-308.
6. Effect of structure of room temperature ionic liquid on the electrochemical behavior of uranium.

   A. Sengupta, M.S.Murali, P.K.Mohapatra, *NUCAR* (**2013**) 309-310.
7. Studies on diglycolamide functionalized calix[4]arenes in room temperature ionic liquid for actinide partitioning

   A.Sengupta, P.K.Mohapatra, *25th Research scholar meet* (**2013**), 48.
8. Use of a digycolamide functionalized Task Specific Ionic liquid for actinide separation from Simulated High Level Waste.

Arijit Sengupta, Prasanta K. Mohapatra, M. Iqbal, J. Huskens, W. Verboom, *1st European congress on green and sustainable chemistry* (**2013**).

9. A comparative study on radiolytic degradation of diglycolamide functionalized ligands in ionic liquids and molecular diluents.

   Arijit Sengupta, P.K.Mohapatra, Mudassir Iqbal, Jurrian Huskens, Willem Verboom, *SESTEC* (**2014**).
10. Spectroscopic investigation of Eu^{3+} - complexes with ligands containing multiple diglycolamide pendent arms in room temperature ionic liquid.

    Arijit Sengupta, P.K.Mohapatra, Mudassir Iqbal, Jurrian Huskens, Willem Verboom, SESTEC (**2014**).
11. Studies on the complexation of UO_2^{2+} with DGA-TSIL.

    Arijit Sengupta, M.S.Murali, P.K.Mohapatra, Mudassir Iqbal, Jurrian Huskens, Willem Verboom, *SESTEC* (**2014**).
12. Study the complexation of Np(IV) with task specific ionic liquids by cyclic voltammetry. **Arijit Sengupta**, M.S.Murali, P.K.Mohapatra, Mudassir Iqbal, Jurrian Huskens, Willem Verboom, *SESTEC* (**2014**).
13. Study on Eu^{3+}-Calix-DGA complex in room temperature ionic liquid, effects of media and structural modification of CDGA by fluorescence spectroscopy.

    Arijit Sengupta, P.K.Mohapatra, Mudassir Iqbal, Jurrian Huskens, Willem Verboom, *TSRP* (**2014**).
14. Study on radiolytic degradation of Diglycolamide functionalized room temperature ionic liquid by EPR spectroscopy.

    Arijit Sengupta, P.K.Mohapatra, R.M.Kadam, Mudassir Iqbal, Jurrian Huskens, Willem Verboom, TSRP (**2014**).

15. Separation of Lanthanides and actinides from Simulated High Level Waste using diglycolamide-functionalized calix[4]arene.

    Arijit Sengupta, P.K.Mohapatra, Mudassir Iqbal, Jurrian Huskens, Willem Verboom, *NAC -5* (**2014**).

Arijit Sengupta.

Arijit Sengupta

ACKNOWLEDGEMENTS

This thesis would not have been possible without the support and encouragement of many people who contributed and extended their valuable assistance in the completion of the research work. I feel short of words in expressing my appreciation for their help at various stages of this work.

First and foremost, I would like to express my sincere gratitude to my research guide Dr. P.K. Mohapatra for his continuous support to my work, his patience, encouragement, enthusiasm and immense knowledge. His intellectual ideas and guidance helped me in my research work and writing this thesis. He has always been a source of motivation for me in difficult times in research or otherwise. I express my deep sense of appreciation for his support and for energizing me to overcome all the hurdles.

Besides my advisor, I would like to thank members of my doctoral committee; Prof. K. L. Ramakumar, Director, RC & I Group, Dr. P.N.Pathak, Dr. P.S. Dhami, for their encouragement, insightful comments and fruitful ideas during the course of the thesis work which have been useful for the progress of the work.

I also wish to express my sincere gratitude to Dr. A. Goswami, Head, Radiochemistry Division and Dr. V. Natarajan, Head, Actinide Spectroscopy Section, Radiochemistry Division, for allowing me to presue my PhD work programme and their keen interest in my work.

I am greatly thankful to Dr. M. S. Murali, Dr. R.M.Kadam, Dr. A. Bhattacharya, Dr. S.A. Ansari, Dr. D.R. Raut, Dr. R.B.Gujar, Mr. D.R.Prabhu, Mr. A.S.Kanekar, Mr. P.K.Verma for their help and encouraging discussions during the course of my doctoral research. I would like to acknowledge my sincere gratitude to all my lab mates, friends and well wishers.

Last but not the least, my deepest gratitude is to my family for their warm support which brings belief and hope into my life; to my beloved parents, my wife and son, who have been so caring and supportive to me all the time, who have always been a source of inspiration towards achieving the goals in life.

Apart from all the people mentioned in this acknowledgment, there are many others who have helped me in various ways during the course of this thesis work. My sincere thanks and apologies to all those I may have forgotten to mention.

Arijit Sengupta.

November, 2014

Arijit Sengupta

CONTENTS

CHAPTER - 1

CHAPTER - 2

CHAPTER - 3

CHAPTER-4

CHAPTER-5

CHAPTER-6

CHAPTER-7

SYNOPSIS

Homi Bhabha National Institute

SYNOPSIS OF Ph. D. THESIS

1. Name of the Student: ARIJIT SENGUPTA

2. Name of the Constituent Institution: Bhabha Atomic Research Centre, Mumbai, India

3. Enrolment No. : CHEM 012 011 04011

4. Title of the Thesis: Studies on the Extraction/ Complexation of Actinide and Fission Product Elements using Selective Ligands in Room Temperature Ionic Liquids

5. Board of Studies: Chemical Sciences

Studies on the extraction/ complexation of actinide and fission product elements using selective ligands in room temperature ionic liquids

With the ever increasing demands for energy, nuclear power is slowly becoming one of the most viable sources along with the renewables. However, due to limited natural resources of the fissile material (^{235}U), the future nuclear energy program largely depends on the availability of man made fissile materials such as ^{239}Pu and ^{233}U. To sustain nuclear power program beyond the availability of naturally occurring ^{235}U, it is imperative to follow the closed fuel cycle option. During the reprocessing of the ^{235}U based spent fuel, the fissile elements such as plutonium and uranium are recovered leaving behind a highly radioactive liquid waste solution referred to as High Level Waste (HLW). This HLW solution comprises long-lived alpha emitting actinides such as ^{241}Am, ^{243}Am, ^{245}Cm and ^{237}Np (referred as minor actinides) apart from the small amounts of un-recovered plutonium and uranium as well as beta / gamma emitting fission products (^{137}Cs, ^{90}Sr etc.) and significant concentrations of structural materials along with several process chemicals. Since the half lives of minor actinides and some of the fission products range from few hundreds to millions of years, HLW poses long term radiological risk to the Environment [1]. Apart from the high radiological risk, some of the minor actinides and fission products, if recovered, may find various applications. The sustainability of the future nuclear energy program, therefore, depends on an efficient and effective radioactive waste management strategy which must be aimed at mitigating the long term hazards of the radioactive wastes.

One of the major challenges in radioactive waste remediation is the selective separation of the long-lived minor actinides (Am, Cm) which have been proposed to be achieved by a strategy known as ‘actinide partitioning’ [2]. Extractants such as CMPO (carbamoyl methyl phosphine oxide), malonamide, TRPO (trialkyl phosphine oxide), DIDPA (diisodecyl phosphoric acid) and DGA (diglycolamide) are well known for the extraction of trivalent actinides from a moderately acidic medium [3-4]. The favourable extraction of these trivalent actinides by TODGA (*N,N,N′,N′*-tetraoctyl diglycolamide) have been attributed to a reverse micellar mechanism where four extractant molecules are believed to be involved in the formation of an aggregate with a hydrophilic interior [5]. The aggregate formation is, however, dependent on the nature of the diluents [6]. In order to effect a diluent independent cooperative complexation, equivalent to that displayed by four TODGA molecules in non polar diluents, four TODGA moieties were appended onto a calixarene scaffold resulting in spectacular extraction / separation properties [7]. Heat emitting fission products such as ^{90}Sr are reported to be extracted by size selective extractants such as crown ethers. Literature reports show that ditertiary butyl dicyclohexano 18-crown-6 (DTBCH18C6) and dicyclohexano 18-crown-6 (DCH18C6) have been extensively used for the extraction of radiostrontium from acidic feed solutions.

Due to the growing awareness of the environmental impact associated with the use of volatile organic compounds (VOC), room temperature ionic liquids (RTIL) have been proposed as alternatives to the molecular diluents due to favourable properties like negligible vapour pressure, wide liquid range, good thermal stability, non flammability, good thermal conductivity, large potential window, good solvents for broad spectrum of inorganic, organic and polymeric compounds etc. Though there are numerous reports on the use of ionic liquids as diluents for the extraction of actinides and fission products [8-9], there is no report on the extraction behavior of these ions using DGA functionalized calixarene (C4DGA) ligands in RTIL. Furthermore, DGA functionalized task specific ionic liquids (TSIL) synthesized for the first time and hence are required to be tested for the actinide ion extraction. It is therefore, thought of interest to carry out a systematic study on the extraction of actinides and fission products such as ^{90}Sr using C4DGA and TSIL (for actinides) and crown ethers (for ^{90}Sr) in room temperature ionic liquids.

Objectives:

The main objectives of the present study are:

I. Conventional extractants in RTILs were reported to show very high extraction efficiency towards metal ions compared to that in molecular diluents. Therefore, it was thought to be interesting to study the extraction / separation behavior of actinides by using several multiple – DGA-functionalized ligands such as T-DGA (tripodal diglycolamide) and C4DGA in RTILs. It was also thought of interest to study the extraction efficiency of different oxidation states of actinides and their separation behavior with respect to themselves and long lived fission products in terms of separation factors. Changes in diluents from molecular solvents like n-dodecane to RTILs can lead to change in extraction mechanism of metal ion suggesting the need for such investigation. Finally, the stripping of the metal ions from RTILs is one of the major challenges and studies will be undertaken to back extract the actinides from the loaded RTIL phase. It is also of interest to evaluate the DGA functionalized TSILs and two substituted 18 crown 6 ethers in RTIL for extraction of actinides and Sr^{2+} ion, respectively.

II. Apart from separation aspects, it is essential to understand the complexation, kinetics and thermodynamics behavior associated with the extraction procedure. In this context, it is of interest to study the metal – ligand stoichiometry, nature of bonding, amount of covalence between metal – ligand bond, symmetry of the complex, perturbation of actinide – oxygen bond on complexation of actinyl ion etc. Nature of complex (inner sphere / outer sphere); conformational changes of the ligands due to complexation (which is of significance when large size ligands are used), spontaneity of complexation process etc. are also required to be investigated through thermodynamic study.

III. The central idea of developing a solvent system for 'actinide partitioning' is its successful application in the preferential extraction of the target metal ions from the HLW. It is also required to know the extraction behavior of the concomitant metal ions present in the HLW solution. For the long term application of the solvent system for actinide extraction, one needs to understand the radiolytic degradation behaviour which can address issues related to the sustainability and recycling possibilities. It is also of interest to identify the radicals and the products generated during the irradiation of the solvent systems and responsible for deterioration of the performance of the solvent systems.

Chapter 1: Introduction

This introductory Chapter gives an overview of the nuclear fuel cycle. Various types of nuclear wastes generated during the spent fuel reprocessing and their impact on the Environment have been elaborated. Knowledge of the chemistry of actinides is important for their separation and, therefore, is briefly mentioned including topics such as electronic configuration, ionic species, variable valency, disproportionation etc. which includes basis of luminescence spectroscopy relevant for studies involving lanthanides such as Eu^{3+} used as a surrogate for trivalent minor actinides. The solution chemistry of actinide ions including their spectral properties has also been discussed. The Chapter also describes the various separation methods for the partitioning of actinides from different waste solutions. Solvent extraction based separation methods are particularly elaborated and factors influencing the selection of a solvent system are also discussed. A brief introduction of RTILs and its application in nuclear fuel cycle are discussed. This Chapter also lists the motivations for the present study.

Chapter 2: Experimental

This Chapter deals mainly with instrumentation, materials and methods. The brief description of the instruments, optimization of instrumental and experimental parameters, working principles of different techniques viz. solvent extraction, inductively coupled plasma optical emission spectroscopy (ICP-OES), luminescence spectroscopy, electron paramagnetic resonance (EPR) spectroscopy etc are given in this Chapter. Synthesis / source of different ligands such as TODGA, T-DGA, C4DGA, TSILs etc. and RTILs are discussed in a brief manner along with their purity and characterization methods. The sources of different radiotracers used in the present work along with their purification and assaying methods have also been discussed. The estimation of gamma ray emitting radiotracers was carried out by employing NaI(Tl) and HPGe detectors. The assay of beta-emitting isotopes was performed by liquid scintillation counter. The basic principles and working of these detectors have been elaborated in this Chapter. The experimental procedures adopted to achieve meaningful conclusions are also discussed.

Chapter 3: Evaluations of DGA based systems in RTILs for the extraction of actinides

In this Chapter, extraction of actinides by solvents containing multiple-DGA-functionalized ligands in different RTILs ([$C_n$mim] [PF_6], where, n = 4, 6, 8)) was studied from acidic feed solution. The multiple-DGA-functionalized ligands used as T-DGA (**L-I**) and C4DGA (**L-II**) and the results obtained with these ligands are compared with TODGA (**L-III**) with a single DGA functionality. The use of RTILs gives rise to significantly improved extraction properties than the commonly used n-dodecane. The unusually high extraction of Am^{3+} can be attributed to the unique ion-exchange extraction mechanism in the RTIL medium, while the high viscosity of the RTILs is responsible for the slower extraction kinetics. The stoichiometry of metal ligand extracted complexes was ascertained by the conventional slope analysis method. The extracted species were 1 : 1 complexes formed between Am^{3+} and T-DGA and C4DGA with no inner sphere water molecules, which was confirmed by TRLFS studies using the analogous Eu(III) complexes. Solutions of EDTA or DTPA in guanidine carbonate were successfully used for quantitative stripping of Am^{3+} from the RTIL phase. The thermodynamic parameters of the extraction process and the radiolytic stability of the solvent systems were studied.

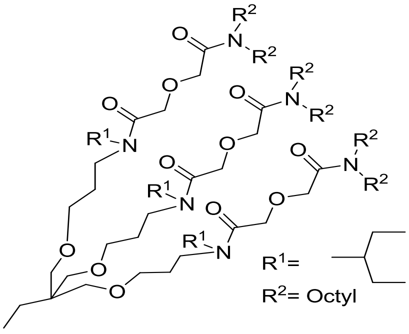

L-I
T-DGA

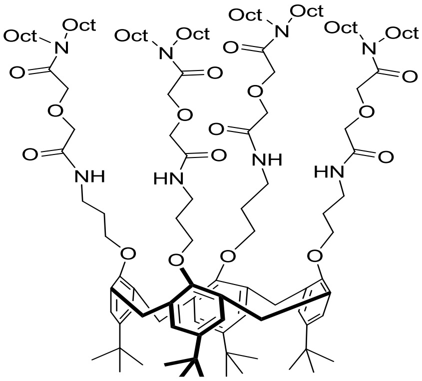

L-II
C4DGA

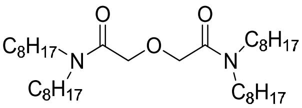

L-III
TODGA

Chapter 4: Studies on the effect of ligand structure of C4DGA on actinide ion extraction into RTIL

Ligand structure has a major role on not only the complexation of the metal ion, but also the overall extraction and separation efficiencies. Factors such as the nature of the alkyl substituents, spacer lengths and types of functionalization appended onto the calix[4]arene scaffold are deciding the overall separation efficiency of the metal ions. Role of ligand structure of the C4DGAs (**L-IV** to **L-X**) in RTIL was investigated to understand their extraction properties, separation and complexation behavior of actinides in different oxidation states. The thermodynamics of metal ion extraction was also investigated. Although the alkyl substituents on the amidic nitrogen increase the extraction efficiency of americium at lower acidity because of the inductive effect of the alkyl groups, at higher acidities the steric crowding around the ligating sites determines the extraction efficiency. All C4DGAs formed 1:1 complexes with no inner sphere water molecules resulting in complexes of C_{4v} symmetry. Judd and Ofelt (J. O.) parameters [10] (Ω_2, Ω_4) and other photo physical constants including asymmetry factors, transition probabilities of each transition, branching ratio, quantum efficiency, radiative and no radiative lifetime etc. were calculated for all Eu^{3+} C4DGA complexes. The solvent systems show promise to be employed for nuclear waste remediation, and sustainability options were evaluated from radiolytic stability as well as stripping studies.

In view of the important role of the diluents in the extraction of metal ions [11], the distribution ratio values of Am^{3+} were obtained by a both side functionalized C4DGA (**L - X**) in various diluents and the results were correlated with Schmidt's diluent parameter and the dielectric constant. The nature of the extracted species was ascertained in various diluents by the slope analysis method, while temperature variation studies were carried out to determine the thermodynamic parameters, which in turn explained the extraction mechanism. On application point of view, the solvent systems were applied for actinide partitioning from simulated HLW which revealed that Y, La, Sm, Y, Pr, Nd, Zr and Mo were found to be extracted into the organic phase along with actinide ions while Na, K, Pd, Fe, Sr, Mn, Pd, Ce, Ru and Ba remain un-extracted.

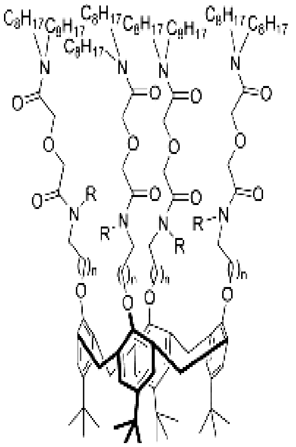

Lower rim C4DGA
L-IV: R = n-Propyl
L-V: R = n-Octyl
L-VI: R = 3-Pentyl
L-VII: R = H (n = 1)
L-VIII: R = H (n = 2)

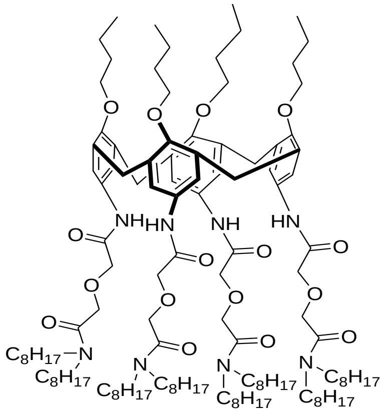

Upper rim C4DGA
L-IX

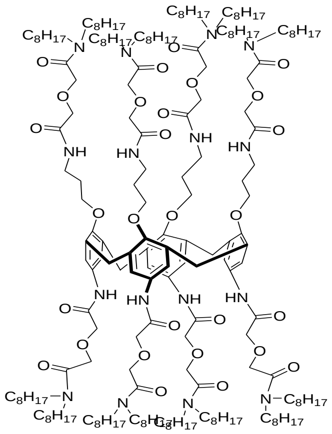

Both rim C4DGA
L-X

Chapter 5: Studies involving task specific ionic liquids (TSIL) for the separation of actinides

Two DGA-TSILs (**LXI** cation associated with PF_6^- and NTf_2^- anion) were synthesized for the first time and evaluated for the extraction of actinides and lanthanides from acidic feed solutions. The mechanism of extraction was studied by carrying out a series of studies to find out the nature of the extracted species. Other studies included luminescence studies which could throw light on the structure of the extracted species and the associated kinetics and thermodynamics. The DGA-TSILs showed an exceptionally high extraction of trivalent actinide as well as lanthanide ions. As mentioned in Chapter 3, solutions of EDTA and DTPA in guanidine carbonate, Na_2CO_3 and oxalic acid were used for the quantitative stripping of An^{3+}, AnO_2^{2+} and An^{4+}, respectively.

Radiolytic stability of the TSILs was evaluated and EPR spectroscopic measurements were performed to understand the nature of free radical species generated on gamma irradiation of TSIL.

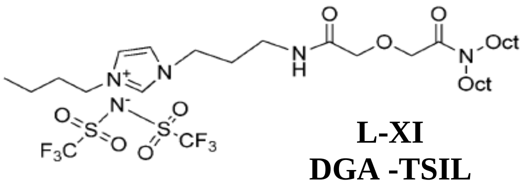

L-XI
DGA -TSIL

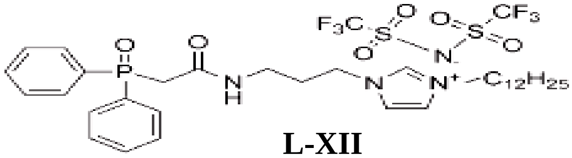

L-XII
CMPO -TSIL

Due to long half life of ^{237}Np, it was of interest to separate Np from radioactive waste solution to avoid long term surveillance. As Np usually exists in the inextractable +5 oxidation state, it is required to adjust the oxidation state of Np to the more extractable forms. A comparative study was carried out to understand the extraction behavior, extraction mechanism, stiochiometry, nature of bonding etc. of Np(IV) and Np(VI) using CMPO – TSIL (**L-XII)** and DGA – TSIL (**L-XI**) in [$C_n$mim][NTf_2] (where, n = 4,6,8). Cyclic voltammetric and UV – Vis spectroscopic studies were also carried out to understand the complexation behavior.

Chapter 6: Extraction of radio strontium from nuclear waste solution using crown ethers in RTILs

In this Chapter, the extraction of Sr^{2+} from dilute nitric acid solutions was studied using two Sr^{2+} selective crown ethers, viz. DCH18C6 (**L-XIII**), DTBCH18C6 (**L-XIV**) in several RTILs, viz. [$C_n$mim][PF_6] (where, n = 4,6,8) and [$C_n$mim][NTf_2] (where, n = 4, 6, 8). The roles of time of equilibration, feed acidity and extractant concentration were also investigated. The extracted species were found to have the metal - ligand stoichiometry of 1:1 with 'ion exchange mechanism'. Radiolytic degradation studies were also carried out which indicated decrease in

Sr^{2+} extraction with increase in the absorbed dose and it was found to be comparable with those reported in the literature [12]. Furthermore, though DTBCH18C6 is considered as an extractant superior to DCH18C6, the radiolytic stability of the former is relatively poor as compared to the latter extractant.

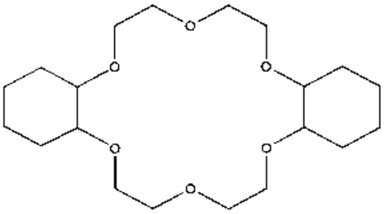

L-XIII
DCH18C6

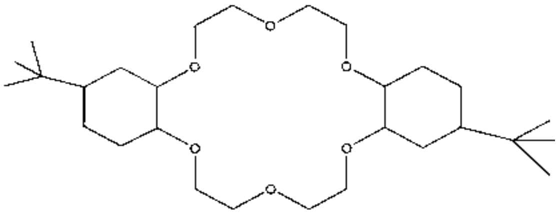

L-XIV
DTBCH18C6

Chapter 7: Summary and Conclusions

Multiple-diglycolamide-functionalized ligands in room temperature ionic liquid were studied for extraction of actinides and lanthanides from aqueous acidic solutions. The extraction kinetics, separation behavior, associated thermodynamics of extraction, nature of the extracted species formed were studied. Luminescence spectroscopy was used to understand the nature of bonding between metal and ligands, formation of inner sphere/ outer sphere complex etc. The radiolytic stability of solvent systems was studied and attempt was used to understand the degradation products. Finally, all the systems were evaluated for 'actinide partitioning' from synthetic high level waste solution. The major findings of the work included in this Thesis are summarized in this Chapter along with the future perspectives.

References

1. Status and Trends of Spent Fuel reprocessing, **1999,** IAEA TECDOC-1103.
2. J. N. Mathur, M. S. Murali, K. L. Nash, *Solv. Extr. Ion Exch.*, 19 **(2008)** 357.
3. Y. Morita, J. P. Glatz, M. Kubota, L. Koch, G. Pagliosa, K. Roemer and A. Nicholl, *Solv. Extr. Ion Exch.*, 14 (**1996)** 385.
4. Y. Sasaki, Z. X. Zhu, Y. Sugo and T. Kimura, *J. Nucl. Sci. Technol.*, 44 (**2007)** 405.
5. M. P. Jensen, T. Yaita, R. Chiarizia, *Langmuir*, 23 (**2007)** 4765.
6. S. Panja, P. K. Mohapatra, S. C. Tripathi, P. M.Gandhi, P. J. Janardan, *J. Membr. Sci*., 403 (**2012)** 71.
7. M. Iqbal, P. K. Mohapatra, S. A. Ansari, J. Huskens, W. Verboom, *Tetrahedron*, 68 (**2012**) 7840.
8. K. Binnemans, *Chem. Rev*., 107 (**2007)** 2592.
9. X. Sun, H. Luo, S. Dai, *Chem. Rev*. 112 (**2012**) 2100.
10. B.R. Judd, *Phys. Rev.*, 127 (**1962)** 750.
11. Y. Sasaki, Y. Sugo, S. Suzuki, S. Tachimori, *Solv. Extr. Ion Exch.*, 19 (**2001)** 91.
12. I.A. Shkrob, T.W. Marin, M.L. Dietz, *J. Phys. Chem. B*, 115 (**2011)** 3903.

LIST OF FIGURES

Page No.

CHAPTER - 1

CHAPTER - 2

CHAPTER - 3

CHAPTER - 4

CHAPTER - 5

CHAPTER - 6

LIST OF TABLES

Page No.

CHAPTER - 1

CHAPTER - 2

CHAPTER - 3

CHAPTER - 4

CHAPTER - 5

CHAPTER - 6

CHAPTER - 1

Introduction

In view of the fast depleting fossil fuel resources, nuclear power is emerging as one of the more viable options to meet the increasing demands for power in the twenty first century. Currently, nuclear power plants produce slightly less than 14% of the world's electricity and 5.7% of the total primary power used worldwide (**Fig. 1.1**). Nuclear power is a relatively clean source, since it contributes very little to the green house gas burden. Nuclear power is the fourth-largest source of electricity in India after thermal, hydro and renewable sources of electricity. A total number of 441 nuclear reactors are operational world-wide with a nuclear power capacity of 375 GW (e). In addition, 67 reactors are under construction [1].

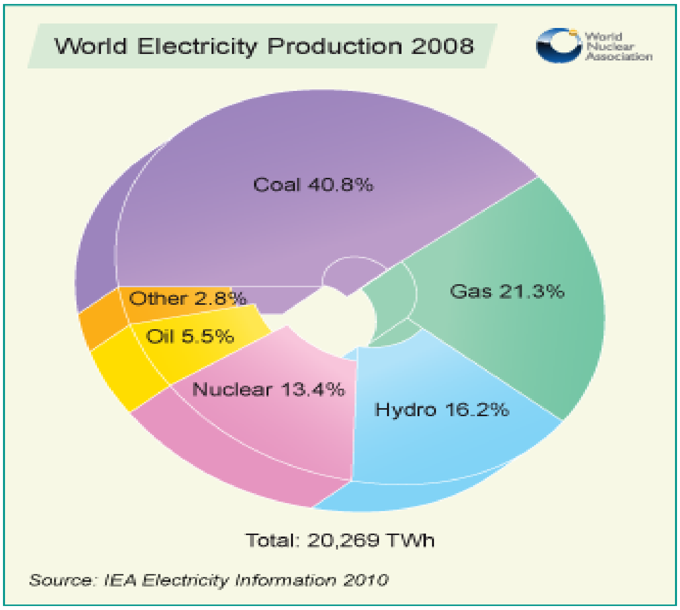

Source: IEA Electricity Information 2010

Fig. 1.1: Production of electricity from different sources, a world – wide scenario [2]

Amongst these 67, the construction of 16 new power reactors started in 2010.As of 2013, India has 20 nuclear power plants in operation generating 4,560 MW while 4 others are under construction and are expected to generate an additional 2,720 MW. India's nuclear power program is undergoing rapid expansion with plans to increase the power output to 64,000 MW by 2032 and 25 % nuclear contribution is foreseen by 2050 [3,4]. Thus, nuclear energy is going to play a crucial role for satisfying India's future energy demands. The current scenario in worldwide nuclear energy production is presented in **Fig.1. 2**.

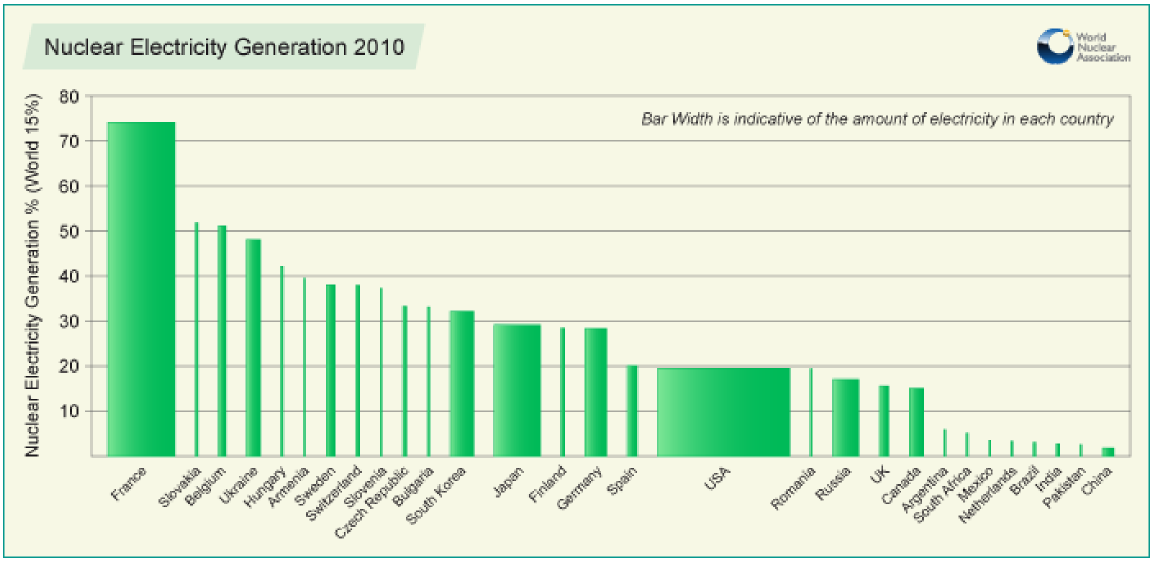

Fig. 1.2: Contribution of different countries in worldwide nuclear energy production [2]

1.1 NUCLEAR FUEL CYCLE

1.1.1 Nuclear fission

The discovery of nuclear fission is an important landmark in the history of nuclear science. ^{235}U when bombarded by thermal neutrons ($E_n < 0.025$ eV), produces enormous amount of energy (~200 MeV per fissioning atom) along with a number of fission fragments. The mass loss in this process appears as the huge energy according to the Einstein's mass-energy relation and the fission process can be expressed as

$$^{235}U + {}^{0}n_{1} = X + Y + 3{}^{0}n_{1} + E \qquad (1.1)$$

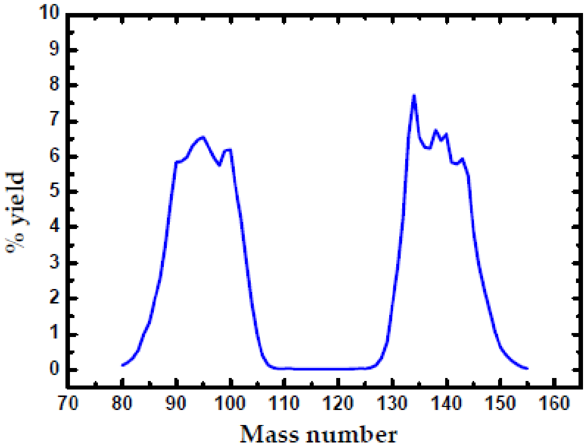

Fig. 1.3: Thermal neutron fission yield curve for ^{235}U [5]

where *X, Y* represents fission products and *E* denotes the amount of energy released per fission per atom of ^{235}U. Mass-yield curve of thermal neutron induced fission of ^{235}U is shown in **Fig. 1.3** with two maxima around mass number of 95 and 140. Production of 2-3 neutrons indicates the self sustainability of nuclear fission and also indicating the possibility of explosion due to uncontrolled chain reaction. The fundamental concept to exploit fission reaction in a controlled manner was used in designing the nuclear reactor for subsequent used for electricity production.

1.1.2 Various stages in nuclear fuel cycle

Nuclear fuel cycle comprises of various stages like mineral exploration, mineral processing, purification of uranium / thorium, fuel fabrication, reactor operation, spent fuel reprocessing, radioactive waste management etc. (**Fig. 1.4**) which can be broadly classified as the front end and back end processes of the fuel cycle.

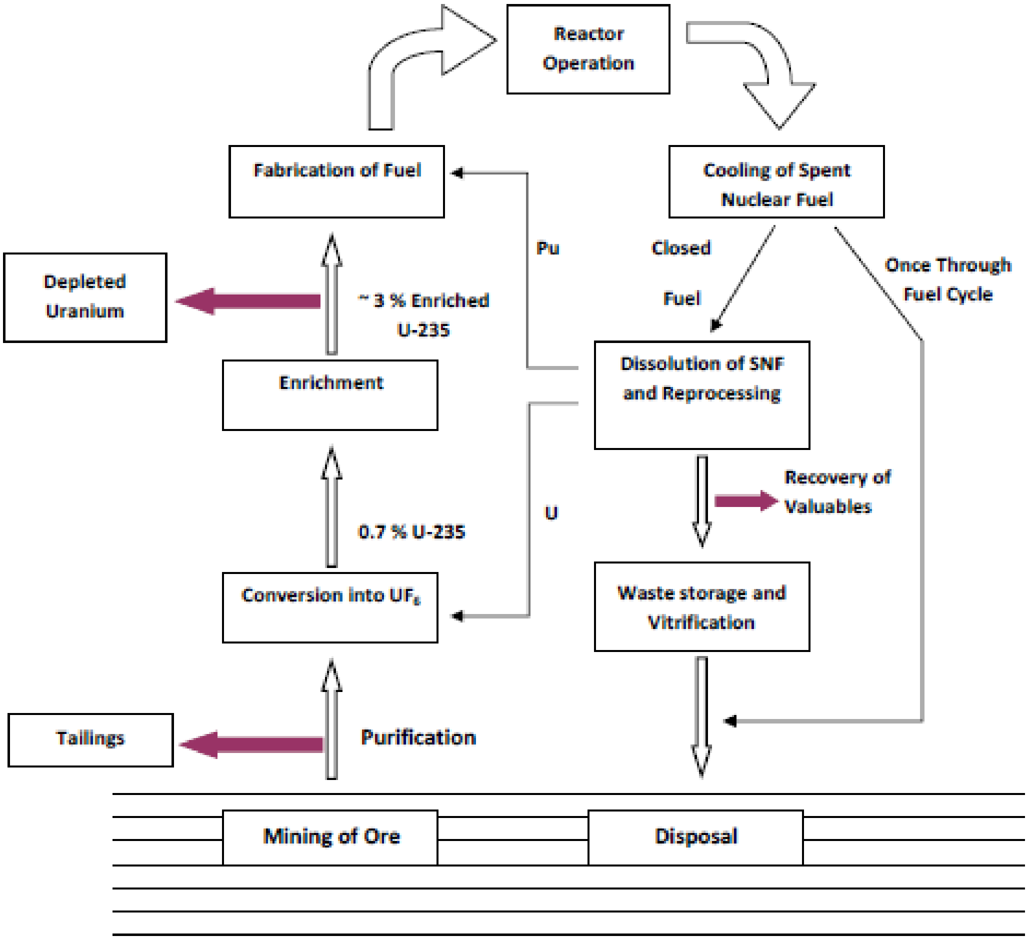

Fig. 1.4: Schematic of nuclear fuel cycle

1.1.2.1 Wastes from the "Front End" of the nuclear fuel cycle

The wastes generated at the uranium mine site comprise of the decay products of ^{238}U /^{235}U and exists in the form of radioactive dust. The wastes from the milling operation include the radioactive radium which is reverted back to the mine. When uranium is burnt in the reactor, significant quantities of highly radioactive fission / activation products are produced (**Table 1.1**). More than 99.9% of the radioactivity produced in the reactor is retained in the fuel rods, while less than 0.1% is distributed in other systems of the reactor.

1.1.2.2 Wastes from the "Back End" of the Nuclear Fuel Cycle

In the nuclear fuel cycle, most of the radioactive wastes are generated during the reprocessing of the spent fuel, i.e. at the back end of the fuel cycle. This irradiated spent fuel contains long-lived alpha emitting transuranic elements (principally Np, Pu, Am and Cm), which are formed in uranium fuelled reactors by neutron capture of ^{238}U followed by a sequence of beta emission and neutron capture reaction of the daughter products alongwith large amounts of beta/gamma emitting fission products [6].

Table 1.1: Major contributors to the radioactivity in spent fuel after a cooling period of 50 days

Nuclides	Half life	Nuclides	Half life
^{3}H	12.3 y	^{131}I	8.05 d
^{85}Kr	10.8 y	^{137}Cs	30.0 y
^{89}Sr	50.6 d	^{140}Ba	12.8 d
^{90}Sr	28.8 y	^{140}La	40.2 y
^{90}Y	68.4 h	^{141}Ce	32.4 d
^{91}Y	58.8 d	^{143}Pr	13.6 d
^{95}Zr	65 d	^{144}Ce	285.0 d
^{95}Nb	35 d	^{144}Pr	17.3 m
^{103}Ru	39.6 d	^{147}Nb	11.1 d
^{106}Ru	367 d	^{147}Pm	2.62 y
^{129m}Te	34 d		

Although nearly 200 radionuclides are produced during irradiation of the fuel, a great majority of those are relatively short lived and decay to low radioactivity level within a few decades and the long lived isotopes are of major concern. Short cooled spent fuel contains significantly large numbers of radionuclide. The major contributors to the fission product activity after a cooling period of 50 days are listed in **Table 1.1.** After cooling the spent fuel for about one year, only ^{106}Ru, ^{106}Rh, ^{90}Sr, ^{90}Y, ^{144}Ce, ^{144}Pr, ^{134}Cs, ^{137}Cs and ^{147}Pm contribute significantly to the radioactivity [6]. One of the challenges at the back end of the nuclear fuel cycle lies in the safe management of the radioactive wastes.

1.2 CLASSIFICATION OF THE RADIOACTIVE WASTE

The radioactive wastes from the back-end of the nuclear fuel cycle can be classified based on their physical state, as well as the type of radiation field (alpha, beta or gamma radiation) being produced or the radioactivity present in the waste stream. Worldwide, the nuclear waste is categorized depending on the radioactivity level of the wastes.

1.2.1 Low level waste

When the total radioactivity of the waste is less than millicurie / litre, it is referred to as low level waste (LLW). It is generated as liquid from the decontamination of equipments, radioactive laboratories, and hospitals using radiopharmaceuticals as well as from the nuclear fuel cycle. The LLW comprises of about 90% of the total volume of the radioactive wastes generated, but only < 1% radioactivity of all the wastes. To reduce the volume of solid LLW, it is often incinerated and compressed before disposal. Usually it is buried in shallow landfill sites.

1.2.2 Intermediate level waste

When the radioactivity of the waste ranges from millicurie to curie / litre, the waste is referred to as intermediate level waste (ILW). It typically comprises of resins, chemical sludges, reactor components as well as reprocessing equipments. The ILW comprises of about 7% of the total volume of the radioactive wastes, while it contains < 4% radioactivity of all the radioactive wastes.

1.2.3 High level waste

When the radioactivity of the waste is greater than curie / liter, the radioactive waste is referred to as high level waste (HLW). The HLW is the waste emanating from the reprocessing of spent fuel. While HLW comprises of only about 3% of the total volume of all the radioactive wastes, it contains more than 95% of the total radioactivity generated in the nuclear fuel cycle. This waste includes uranium, plutonium and other highly radioactive elements made up of fission products and alpha emitting minor actinides. Composition of Pressurized Heavy Water Reactor Simulated High Level Waste is summarized in **Table 1.2**.

Table 1.2: Composition of Pressurized Heavy Water Reactor Simulated High Level Waste, HNO_3 concentration: 3–4 M.

Metal ions	Concentration (g/L)	Metal ions	Concentration (g/L)
Na	5.5	Mo	0.137
K	0.224	Y	0.06
Sr	0.03	La	0.18
Ba	0.064	Cs	0.32
Fe	0.72	U	0.64
Cr	0.119	Ce	0.06
Ni	0.107	Pr	0.09
Mn*	0.426	Nd	0.12
Zr	0.004	Sm	0.085

Note: * taken as surrogate of Tc

The challenge for the final disposal of HLW is largely due to the radiotoxicity associated with the minor actinides which have half lives ranging from a few hundred to millions of years [7]. Efforts are being made by researchers to meet the challenges of radioactive waste management by developing efficient and environmentally benign processes for the separation of various radionuclides from HLW solution. This would minimize the volumes of radioactive wastes and costs of their final disposal. At present, the typical contents of spent fuel being stored along with the suggested approaches for disposals around the world are presented in **Table 1.3**.

Table 1.3: Typical percentages of components making up spent nuclear fuel along with suggested approaches for disposal [8]

Percentage	Component	Disposition
85.6	Uranium	Recycled and disposed of as low level waste
3	Stable or short - lived fission products	Decays in a short time resulting in no significant disposal problem
0.3	Major fission products	Cesium and Strontium are the primary heat sources in HLW: decays in a few centuries
0.1	Long - lived fission products	Primarily iodine and technitium can be stored or removed and transmuted
0.9	Plutonium	Can be recovered and recycled as fuel
0.1	Long - lived minor actinides	Primarily Np, Am and Cm: can be searated and fissoned using fast reactors

1.3 IMPACT OF RADIOACTIVE WATE ON THE ENVIRONMENT

The annual accumulation of high level waste (HLW) with an average accumulation rate worldwide is approximately 850 cubic meters per year [3]. This HLW, generated during spent nuclear fuel reprocessing, contains un-extracted U, Pu, minor actinides (such as Am, Np, Cm), lanthanides, fission product elements (such as Tc, Pd, Zr, I, Cs, and Sr), transition elements including Fe, Ni, Co, Zr, and some salts of Al, and Na. At present, the most accepted approach for the management of HLW is to vitrify the waste in a glass matrix followed by interim storage for ~200 years to allow the decay of heat-dissipating nuclides such as ^{137}Cs and ^{90}Sr and its subsequent disposal in deep geological repositories [9]. The half-lives of a few minor actinides and some fission product elements range between a few hundreds to millions of years. Therefore, storing vitrified blocks for such a long period is not favorable from an economic, as well as an environmental safety point of view. There is also the possible risk of the migration of long-lived α-emitting minor actinides from the repository to the aquatic environment, as in the past, more than three million liters of highly radioactive waste leaked into the surrounding soil of the Columbia Basin [10]. As shown in **Fig. 1.5**, if the actinides are not removed from the spent fuel, it will require millions of years to reduce its radiotoxicity to the level of natural uranium ore.

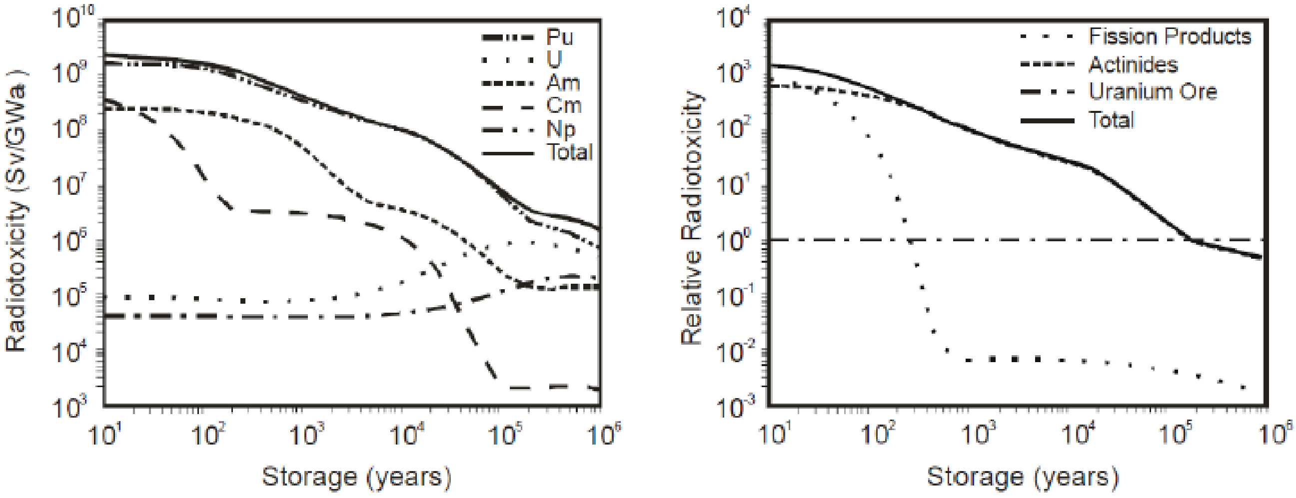

(a) **(b)**

Fig. 1.5: (**a**) The radiotoxicity per element of the actinides in spent UO_2 fuel. (GWae is a measure of electricity produced and 1 GWae equals about two times the annual production of the Borssele nuclear power plant); (**b**) the radiotoxicity of the actinides and fission products in spent fuel relative to the uranium ore needed to manufacture the fuel. The storage time needed to reach a radiotoxicity level of uranium ore is about 200,000 years [11].

1.4 CHEMISTRY OF ACTINIDES

A brief survey of the chemistry of actinide elements is considered relevant to understand its extraction and complexation behavior. The fourteen *5f* electrons enter the actinide elements beginning formally with Th (Z=90) and ending with Lr (Z=103). These fourteen elements following Ac are placed in the 7th row of the periodic table separately analogous to the lanthanides. Intensive chemical studies have revealed many similarities between the lanthanides and actinides. The ground state electronic configuration of lanthanides and actinides is shown in **Table 1.4**. Though there is over all similarity between the two groups of elements, some important differences also exist mainly because the *5f* and *6d* shells are of similar energy in actinides and *5f* electrons are not so well shielded as the *4f* electrons in lanthanides [12]. The lighter actinides (Ac to Np) show greater tendency to retain the *6d* electrons due to smaller energy differences between the *6d* and the *5f* orbitals relative to that between the *5d* and the *4f* orbitals of the lanthanides. In case of the transition series, the relative energy of the orbitals undergoing the filling process becomes lower as the successive electrons are added. In case of the actinides, the *5f* orbitals of plutonium and subsequent elements are of lower energy than the *6d* orbitals and, therefore, the subsequent electrons are filled in the *5f* orbitals with no electrons in the *6d* orbital.

Table 1.4: Ground state electronic configuration of lanthanides and actinides

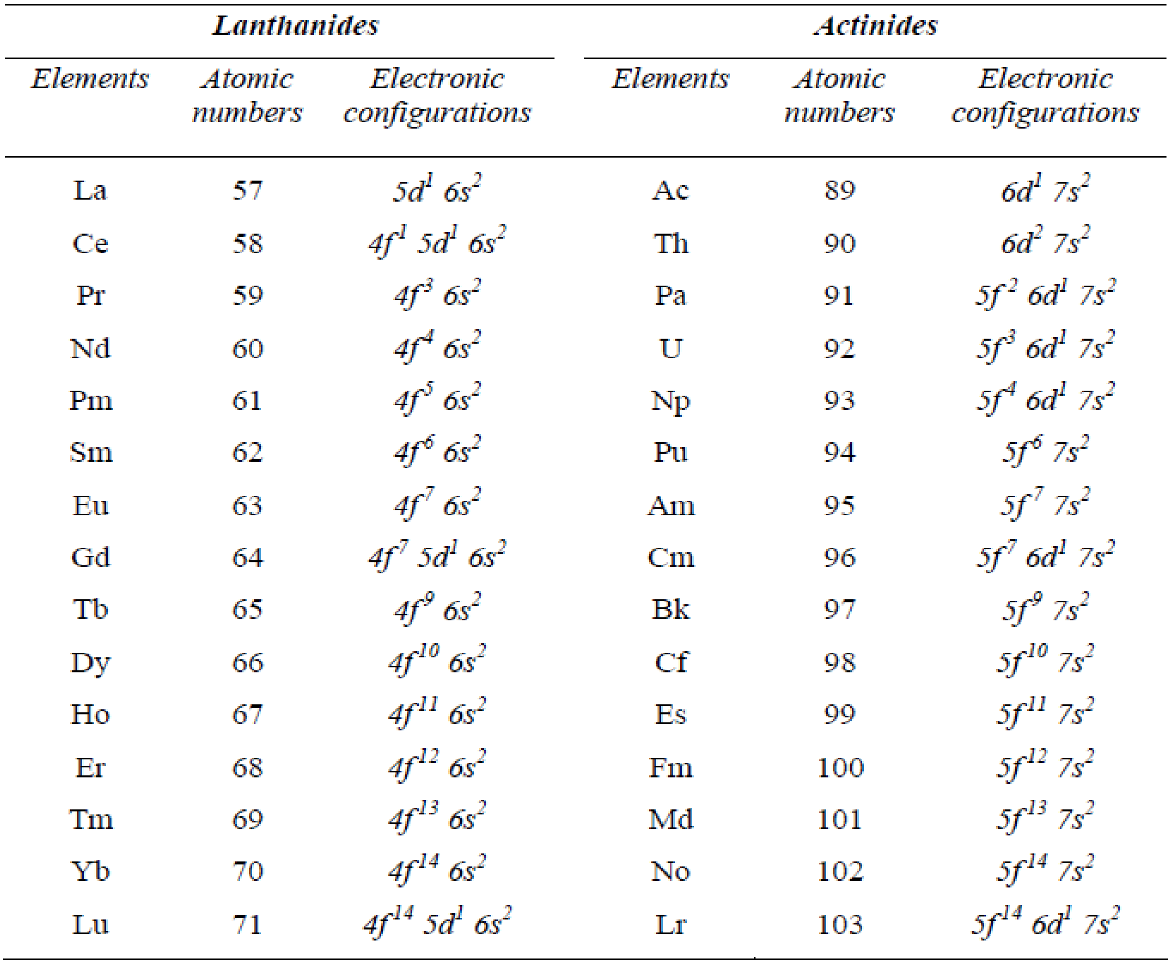

Lanthanides			*Actinides*		
Elements	*Atomic numbers*	*Electronic configurations*	*Elements*	*Atomic numbers*	*Electronic configurations*
La	57	$5d^1\ 6s^2$	Ac	89	$6d^1\ 7s^2$
Ce	58	$4f^1\ 5d^1\ 6s^2$	Th	90	$6d^2\ 7s^2$
Pr	59	$4f^3\ 6s^2$	Pa	91	$5f^2\ 6d^1\ 7s^2$
Nd	60	$4f^4\ 6s^2$	U	92	$5f^3\ 6d^1\ 7s^2$
Pm	61	$4f^5\ 6s^2$	Np	93	$5f^4\ 6d^1\ 7s^2$
Sm	62	$4f^6\ 6s^2$	Pu	94	$5f^6\ 7s^2$
Eu	63	$4f^7\ 6s^2$	Am	95	$5f^7\ 7s^2$
Gd	64	$4f^7\ 5d^1\ 6s^2$	Cm	96	$5f^7\ 6d^1\ 7s^2$
Tb	65	$4f^9\ 6s^2$	Bk	97	$5f^9\ 7s^2$
Dy	66	$4f^{10}\ 6s^2$	Cf	98	$5f^{10}\ 7s^2$
Ho	67	$4f^{11}\ 6s^2$	Es	99	$5f^{11}\ 7s^2$
Er	68	$4f^{12}\ 6s^2$	Fm	100	$5f^{12}\ 7s^2$
Tm	69	$4f^{13}\ 6s^2$	Md	101	$5f^{13}\ 7s^2$
Yb	70	$4f^{14}\ 6s^2$	No	102	$5f^{14}\ 7s^2$
Lu	71	$4f^{14}\ 5d^1\ 6s^2$	Lr	103	$5f^{14}\ 6d^1\ 7s^2$

1.4.1 Solution chemistry of actinides

As the processes of separation and purification of actinides on a large scale are essentially based on hydrometallurgical techniques, the study of solution chemistry of actinides has received considerable attention. The actinide elements exist in multiple oxidation states and most of their separation processes are based on the effective exploitation of these properties. It is, therefore, desirable to understand the various oxidation states of actinide ions in solution.

1.4.1.1 Oxidation states

The trivalent state is the most stable oxidation state for all lanthanides. However, this is not so at least in the case of earlier members of the actinide series. The *5f* electrons of actinides are subjected to a lesser attraction from the nuclear charge than the corresponding *4f* electrons of the lanthanides. The greater stability of the tetra positive ions of the early actinides is attributed to the smaller values of the fourth ionization potential for the *5f* electrons compared to the *4f* electrons of lanthanides, an effect which has been observed experimentally in the case of Th and Ce [13]. Thus, thorium exists in aqueous phase only as Th(IV) while the oxidation state of 3+ becomes dominant only for transplutonium elements. The different oxidation states of the actinide ions are listed in **Table 1.5**, where the most stable oxidation states are under lined [12]. All the oxidation states are well known except for the 7+ states for Np and Pu which exist only in alkaline solution [14]. Penta and hexavalent actinide ions exist in acid solution as oxygenated cations, viz. MO_2^+ and MO_2^{2+}.

Table 1.5: Oxidation states of different actinides

89	90	91	92	93	94	95	96	97	98	99	100	101	102	103
Ac	**Th**	**Pa**	**U**	**Np**	**Pu**	**Am**	**Cm**	**Bk**	**Cf**	**Es**	**Fm**	**Md**	**No**	**Lr**
						(2)		(2)				2	$\underline{2}$	
$\underline{3}$	(3)	(3)	3	3	3	$\underline{3}$	$\underline{3}$	$\underline{3}$	$\underline{3}$	$\underline{3}$	$\underline{3}$	$\underline{3}$	3	$\underline{3}$
	$\underline{4}$	4	4	4	$\underline{4}$	4	4	4						
		$\underline{5}$	5	$\underline{5}$	5	5								
			$\underline{6}$	6	6	6								
				7	7									

** Those underlined are the most stable oxidation states in aqueous solution; those in parentheses refer to oxidation states which are not known in solutions.*

1.4.1.2 Disproportionation reactions

"Disproportionation" is referred to as simultaneous self oxidation and reduction reactions. For disproportionation reaction to occur an element must have at least three oxidation states and these ions must be able to co-exist in solutions, which depend on the closeness of the electrode potentials of redox couples involved. In case of Pu, these values are so close that the four oxidation states, viz. III, IV, V and VI are in equilibrium with each other. The disproportionation reactions of U, Pu, Np and Am have been well studied [12]. In general, disproportionation reactions of MO_2^+ (M = U, Pu or Np) ions can be represented as follows,

$$2MO_2^+ + 4H^+ \leftrightarrow M^{4+} + MO_2^{2+} + H_2O \qquad (1.2)$$

It is clearly demonstrated from the equilibrium reaction that the presence of hydrogen ion and complexing ions like F^- and SO_4^{2-}, which complex strongly with M^{4+} and MO_2^{2+} ions, have pronounced effect on the disproportionation reactions **(Table 1.6**).

Table 1.6: Disproportionation reactions in actinides

Element	*Oxidation Numbers*	*Reaction*	*logK (25°C)*
U	V = IV + VI	$2UO_2^+ + 4H^+ \Leftrightarrow U^{4+} + UO_2^{2+} + 2H_2O$	9.30
Np	V = IV + VI	$2NpO_2^+ + 4H^+ \Leftrightarrow Np^{4+} + NpO_2^{2+} + 2H_2O$	-6.72
Pu	V = IV + VI	$2PuO_2^+ + 4H^+ \Leftrightarrow Pu^{4+} + PuO_2^{2+} + 2H_2O$	4.29
	V = III + VI	$3PuO_2^+ + 4H^+ \Leftrightarrow Pu^{3+} + 2PuO_2^{2+} + 2H_2O$	5.40
	IV + V = III + VI	$Pu^{4+} + PuO_2^+ \Leftrightarrow Pu^{3+} + PuO_2^{2+}$	1.11
	IV = III + VI	$3Pu^{4+} + 2H_2O \Leftrightarrow 2Pu^{3+} + PuO_2^{2+} + 4H^+$	-2.08
Am	IV + V = III + VI	$Am^{4+} + AmO_2^+ \Leftrightarrow Am^{3+} + AmO_2^{2+}$	12.5
	IV = III + VI	$3Am^{4+} + 2H_2O \Leftrightarrow 2Am^{3+} + AmO_2^{2+} + 4H^+$	32.5
	IV = III + V	$2Am^{4+} + 2H_2O \Leftrightarrow Am^{3+} + AmO_2^+ + 4H^+$	19.5

1.4.1.3 Hydrolysis and polymerization

The penta and hexavalent states are prone to very significant hydrolysis as compared to the lower oxidation states. The metal ions in these oxidation states exist as partially hydrolyzed actinyl ions, viz.MO_2^+ and MO_2^{2+} and can get further hydrolyzed under high pH conditions. The degree of hydrolysis for actinide ions decreases in the order: $An^{4+} > AnO_2^{2+} > An^{3+} > AnO_2^+$ which is similar to their complex formation abilities. In general, the hydrolysis of the actinide ion (M^{n+}) can be represented as follows,

$$M(H_2O)_x^{n+} \leftrightarrow M(OH)_x^{(n-x)+} + xH^+ \quad (1.3)$$

For U^{4+} and Pu^{4+}, the metal ion hydrolyzes first in a simple monomeric reaction followed by a slow irreversible polymerization of the hydrolyzed products. For Th^{4+}, however, various polymeric species exist even in very dilute solutions. Whereas the polymer formation of Pu^{4+} is irreversible, that of Th^{4+} is reversible. The hydrolysis of some of the trivalent actinides such as Am^{3+}, Cm^{3+} and Cf^{3+} is well studied which revealed the higher hydrolysis constant values for trivalent actinides as compared to their lanthanides homologs [12].

Though the polynuclear species of all actinide ions are of great interest, the polymers of Pu^{4+} have attracted particular attention because of practical considerations. Pu^{4+} polymers with varying molecular weights ranging from a few thousands to as high as 10^{10} have been observed [15]. In dilute HNO_3 or HCl solutions, Pu^{4+} polymer exists as a bright green colour with a characteristic spectrum different from that of monomeric Pu(IV) in these solutions. The rate of polymerization depends on acidity, temperature, Pu(IV) concentration as well as the nature of ions present in the solution [16, 17]. Polymerization rate for Pu(IV) is higher when the ratio of acid to Pu(IV) concentration is low. Thus, the polymerization can occur even at higher acidities if Pu(IV) concentration is raised. Depolymerization of Pu(IV) is best accomplished by heating the Pu solution in 6–10 M HNO_3. Strong complexing agents such as fluoride and sulphate ions as well as oxidizing agents such as permanganate and dichromate promote depolymerization of plutonium.

1.4.1.4 Complexation of actinides

The property of actinides to exhibit strong tendency to form complexes is widely exploited in devising methods for their separation and purification. The complexing strength of actinide ions in different oxidation states follows the order: $M^{4+} > MO_2^{2+} > M^{3+} > MO_2^{+}$ which can be explained on the basis of their decreasing trend in the ionic potential values. For a given oxidation state, the complexing ability increases with the atomic number due to increase in the ionic potential as a result of the 'actinide contraction' [12]. However, there are large number of instances where, hybridization involving *5f* orbitals, steric effects and hydration of metal ions affect the tendency of complexation. For anions the tendency to form complex with the given actinide ion generally vary in the same manner as their abilities to bind with hydrogen ion [18]. For monovalent ligands the complexing tendency decreases in the order: $F^- > CH_3COO^- > SCN^- > NO_3^- > Cl^- > Br^- > I^- > ClO_4^-$. The divalent anions usually from stronger complexes than the monovalent anions and their complexing ability decrease in the order: $CO_3^{2-} > SO_3^{2-} > C_2O_4^{2-} > SO_4^{2-}$. The complexing ability of some of the organic ligands with Th(IV) varies as: ethelene diamine tetra acetic acid (EDTA) > citrate > oxalate > HIBA > lactate > acetate. On the basis of Pearson's [19] hard – soft acid base principle, actinide ions being "hard acids" are expected to interact strongly with hard bases such as 'O' or 'F' rather than soft donor atoms like 'N', 'S' or 'P'. However, as compared to lanthanides they show marked preference for the soft donors. When the primary hydration shell is broken during complex formation, the resultant complex is referred to as 'inner sphere complex'. In contrast, 'outer sphere complexes' do not require breaking of the primary hydration shell. The actinide ions interact with soft bases in organic solvents of low solvating power, but not in aqueous solutions where the soft bases would have to replace the inner sphere water molecules which are a hard base. Thus, depending on the nature of ligand and medium actinide cations form inner or outer sphere complexes.

1.4.1.5 Spectroscopy of actinides

The absorption/ emission spectra of actinides arise due to the electronic transitions and absorption bands appear mainly from three types of transitions, viz. i) *f-f* transition, ii) *f-d* transition, and iii) charge transfer bands [12]. In *f-f* transitions, the electronic transition occurs between the two *5f-5f* orbitals of different angular momentum which is generally Laporate forbidden. The bands are sharp because the transitions take place in the inner shell and are, therefore, not affected much by the surrounding environment. The energy differences between the various energy levels are of such an order of magnitude that the bands due to *5f-5f* transitions appear in UV, visible and near IR regions. On the other hand, in case of *f-d* transitions the absorption bands are broad as these transitions are influenced by the surrounding environment. As transitions take place between the orbitals of different azimuthal quantum number they are Laporate allowed and, therefore, these bands are relatively more intense. In case of charge transfer transitions, the bands occur due to the transition between the *5f* orbitals of actinide ions and the ligand orbitals. Therefore, the nature of ligand plays an important role. These transitions are significantly affected by the surrounding environment. As a consequence, the charge transfer bands are broad.

1.5 SEPARATION OF METAL IONS

Several methods are adopted for the separation of the metal ions of interest from the associated impurities. Solvent extraction, solid phase extraction, liquid membrane, precipitation are some of the commonly used techniques for metal ion separation. Out of these, solvent extraction technique is simple and efficient.

1.5.1 Solvent extraction

Solvent extraction or liquid-liquid extraction is based on the principle that a solute can distribute itself in a certain ratio between the two immiscible solvents, one of which is usually water and the other an organic solvent. The liquid–liquid extraction systems can be thermodynamically explained with the help of phase rule [20], which is usually expressed as,

$$P + V = C + 2 \qquad (1.4)$$

where, P, V and C denote the number of phases, variances and components, respectively. In general, a binary liquid-liquid distribution system has two phases (P =2) and contains three or more components (two solvents and one or more solutes). when molecular species of the solute is same in the two phases, its concentration in one phase is related to that in the other phase (the Nernst's distribution law). Consider following equilibrium reaction,

$$M_{aq} \leftrightarrow M_{org} \qquad (1.5)$$

Where, the species with the subscripts 'aq' and 'org' represent those in the aqueous and the organic phases, respectively. According to the distribution law, the distribution coefficient (K_d), also referred to as partition coefficient, is represented as,

$$K_d = [M]_{org} / [M]_{aq} \qquad (1.6)$$

and refers to a particular chemical species. However, it has been observed that, in most cases, the molecular species of metal ions are not the same in both the phases. Therefore, the term "distribution ratio (D)" is used in the solvent extraction which is defined as the ratio of total metal ion concentration in the organic phase ($[M]_{total,org}$) to that in the aqueous phase ($[M]_{total,aq}$) and can be expressed as

$$D = [M]_{total,org} / [M]_{total,aq} \tag{1.7}$$

Another relevant term is the % extraction (% E), which is given by the following equation

$$\% E = 100D / (D + V_{aq}/V_{org}) \tag{1.8}$$

If ratio of the organic phase volume (V_{org}) to the aqueous phase volume (V_{aq}) is kept as 1, then Eq (1.8) simplifies to

$$\% E = 100D / (D + 1) \tag{1.9}$$

The solubility of the charge bearing metal ions in the organic solvents are very less as they tend to remain in the aqueous phase due to ion-dipole interaction. For the extraction of metal ions in the organic phase, the charge on the metal ions must be neutralized so as to enhance the solubility in non-polar organic solvents. Therefore, a suitable extractant (ligand) molecule is generally added in the organic solvent which upon complexation with metal ions forms neutral hydrophobic species which are then extracted into the organic phase. In such cases, the extraction of metal ions may follow one of the following extraction mechanisms.

1.5.1.1 Solvation mechanism

The extraction of metal ions by neutral ligands usually follows the solvation mechanism, where, the water molecules from the inner co-ordination sphere of the metal ions are replaced by basic donor atoms of the ligand molecules. The extraction of U(VI) by tri-*n*-butyl phosphate (TBP) from nitric acid medium [21] is an example of the solvation mechanism and is represented as follows:

$$UO_2{}^{2+}{}_{aq} + 2NO_3{}^{-}{}_{aq} + 2TBP_{org} \leftrightarrow UO_2(NO_3)_2.2TBP_{org} \qquad (1.10)$$

1.5.1.2 Chelation mechanism

In this case*,* ligands having more than one donor sites (e.g. β diketones) can coordinate simultaneously to form 5-6 member stable rings. The example of this is the extraction of Pu(IV) by 2-thenoyltrifluoroacetone (HTTA) in benzene [22].

$$Pu^{4+}{}_{aq} + 4HTTA_{org} \leftrightarrow [Pu(TTA)_4]_{org} + 4H^{+}{}_{aq} \qquad (1.11)$$

1.5.1.3 Ion-pair extraction mechanism

This type of extraction proceeds with the formation of neutral ion-pair species between the cationic metal bearing species and anionic bulky counter anion or anionic metal bearing species and an organic cation, for example protonated form of an amine. Acidic ligands such as sulphonic acids, carboxylic acids and organophosphoric acids provide anions by liberating protons which then complexed with the metal cation to form ion-pair. On the other hand, basic ligands provide cations which complex with aqueous anion metal complex to form ion-pair. The best examples of basic extractants are quaternary ammonium salts such as Aliquat 336 which extracts metal ions such as UO_2^{2+} from hydrochloric acid medium as given by the following equation.

$$UO_2^{2+}{}_{aq} + 3Cl^-_{aq} + (R)_3R'\ NCl_{org} \leftrightarrow ((R)_3R'\ N)^+(UO_2Cl_3)^-_{org} + Cl^-_{aq} \qquad (1.12)$$

1.5.1.4 Synergistic extraction

Synergism refers to the phenomenon where the extraction of metal ions in the presence of two or more extractants is more than that expected from the sum of the extraction employing the individual extractants. Well known example of synergistic extraction is the extraction of Pu(IV) from nitric acid medium by a mixture of HTTA and tri-*n*-octyl phosphine oxide (TOPO) in benzene [23].

1.5.2 Chromatographic techniques

Ion exchange and extraction chromatographic techniques are also adopted for the separation of metal ions. Though, high separation efficiency and generation of lesser amounts of organic liquid waste make these techniques attractive, slow rate of separation limits the chromatography based techniques. Ion-exchange materials, normally in the form of beads, are made from water insoluble polymers. The surface of the polymer beads has suitably developed pores with specific structure in which the extractant or the binder can be encapsulated. The extractant / binder have exchange sites where the metal ions are exchanged with the cations (such as H^+ ions) or their anionic complexes with the anions in the resin and hence the technique is named as ion-exchange. Column properties are influenced by the particle size of the ion exchanger. In extraction chromatographic resins, the extractant molecules are trapped inside the polymer matrix by chemical or physical means. Extraction chromatographic techniques are generally much more selective than the ion exchange techniques as it also imparts the selectivity due to the presence of specific extractants.

1.5.3 Criteria for selection of extractants

The factors respossible for selecting or designing a particular extractant for the separation of metal ions for industrial applications are as follows [24]

1. High solubility in paraffinic solvents (non-polar solvents)
2. Low solubility in the aqueous phase
3. Non-volatility, non-toxicity and non-inflammability
4. High complexation ability with the metal ions of interest
5. High solubility of the metal-ligand complex in the organic phase, i.e. high metal loading capacity in the organic phase
6. Ease of stripping of metal ions from the organic phase
7. Reasonably high selectivity for the metal ion of interest over the other unwanted metal ions present in the aqueous solution
8. Optimum viscosity for ease of flow and optimum interfacial tension (IFT) to enable a faster rate of phase disengagement
9. Ease of regeneration of the extractant for recycling

10. High resistance to radiolytic and chemical degradation during operation
11. Ease of synthesis / availability at a reasonable cost

1.6 REPROCESSING OF SPENT NUCLEAR FUEL

Reprocessing of the spent nuclear fuel is mandatory for not only to restrict radio-toxic effects of the fission / activation products, but also for the recovery of valuable fissile materials to sustain the future nuclear energy programme. During the reprocessing of the spent nuclear fuel, the unutilized uranium and the plutonium generated through activation are recovered in the hydrometallurgical process leaving behind highly radioactive liquid waste solution known as the high level waste (HLW). A brief mention about the reprocessing of the spent fuel by PUREX process is presented here.

1.6.1 PUREX process

The Plutonium Uranium Reduction Extraction (PUREX) process is employed for the reprocessing of the spent nuclear fuel throughout the world [25]. It involves the selective co-extraction of the hexavalent uranyl ion and the tetravalent plutonium ion from the spend fuel dissolved in 3-4 M HNO_3 using 30% tri-*n*-butyl phosphate (TBP) in *n*-dodecane. Pu is preferentially stripped back from loaded organic phase by conversion of Pu^{4+} to Pu^{3+} while 0.1 M HNO_3 was found to be useful for the quantitative recovery of U from the loaded TBP phase. The challenges remain in managing the highly radio toxic effluent containing trivalent (Am and Cm) and pentavalent (Np) minor actinides along with the fission products.

1.6.2 Partitioning and transmutation

Several countries worldwide are currently exploring the strategy of P&T (Partitioning and Transmutation), which aims to reduce the radiotoxicity of the waste by the co-extraction of minor actinides and lanthanides (Partitioning) from HLW solution (concentrated form of the effluent generated from the PUREX process) followed by transmutation of the minor actinides in dedicated facilities yielding shorter-lived or more stable elements. A typical schematic view of the partitioning of waste by solvent extraction is presented in **Fig. 1.6**, where U, Pu, and Np are partitioned in the PUREX process. In the DIAMEX (DIAMide EXtraction) process, actinides and lanthanides are co-extracted from the bulk of the HLW containing corrosion and fission products. Finally, the actinides and lanthanides are mutually separated in the SANEX (Selective ActiNide EXtraction) process.

The actinides and lanthanides are *f* - block elements and found to possess similar chemical and physical properties [26 - 28]

I. Both are considered as hard acids as per the Pearson classification [29].Their interactions with inorganic and organic ligands are, therefore, predominantly determined by electrostatic and steric factors.
II. The trivalent cations have the same electronic configuration within each group (apart from the filling of the *f* shell) and almost similar ionic radii.
III. Both exist predominantly in their trivalent oxidation states in aqueous acidic solutions.
IV. Both have a similar hydration number.

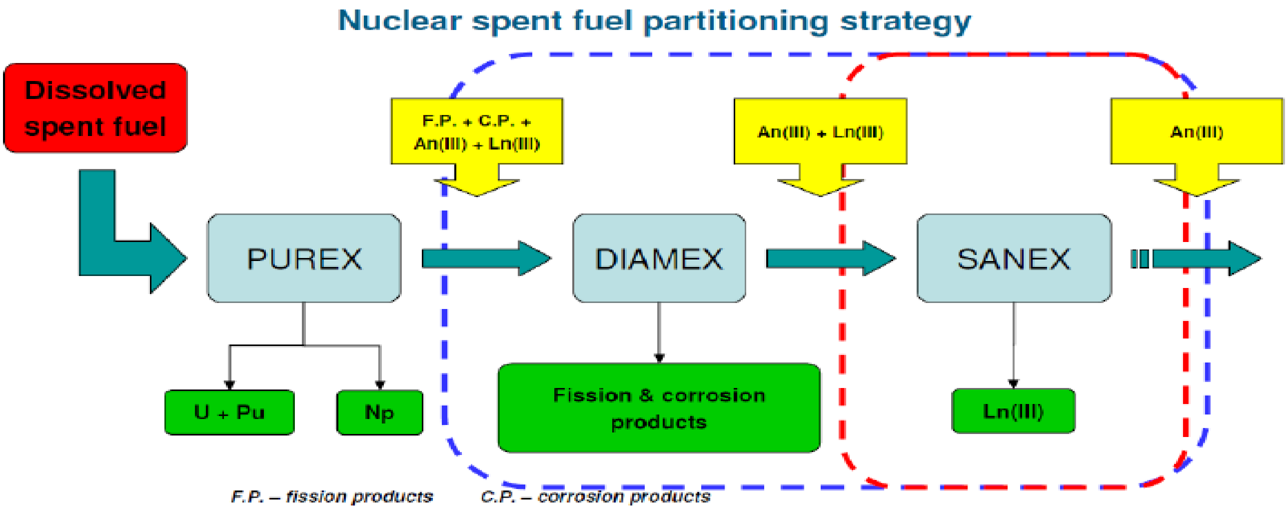

Fig. 1.6: Schematic view of the partitioning of waste by solvent extraction

1.6.3 Actinide/lanthanide separation

Although both actinides and lanthanides are considered to be hard acids according to Pearson's HSAB theory, the higher spatial expansion of the 5*f* orbitals of the actinides with respect to the 4*f* orbitals of the lanthanide opens up possibilities to discriminate them through their relative hardness. It has been postulated that an increased covalent nature in the interaction of An^{3+} with soft donor atoms and/or changes in coordination geometries account for these effects [30-32]. Therefore, ligands containig soft donor atoms (e.g. S, N) may allow subtle discrimination between An(III) and Ln(III) via differences in the metal-ligand complex coordination, such as differences in binding, stoichiometry, affinity and structure.

Due to the large concentration of the lanthanides present in the spent fuel and their high neutron absorption cross section, the actinides must be separated from the lanthanides for subsequent transmutation in a dedicated facility. Until now there is no process known that can selectively separate individual actinides from spent fuel directly. In the processes developed over the recent years the lanthanides and actinides are co-extracted followed by their mutual group separations. The separation of An^{3+} can be achieved either by selective extraction into the organic phase or by selective complexation in the aqueous phase. Most of the processes described in the literature extract the An(III) + Ln(III) containing solution issued from a first step process, which has separated the An(III) + Ln(III) fraction from a highly active PUREX [33] raffinate. The examples of such first step processes are TRUEX [34, 35] (TRans Uraniun EXtraction), TRPO [36] (TRialkylPhosphine Oxide), DIAMEX [37] (DIAMide EXtraction) and DIDPA [38] (DiIsoDecyl Phosphoric Acid). The second step processes are SANEX (Selective ActiNide EXtraction), ALINA [39] (Actinide-Lanthanide INtergroup separation from Acidic media), and some processes involving nitrogen containing polydentate ligands. The separation of actinides by complexing in the aqueous phase is achieved by processes like TALSPEAK [40] (Trivalent Actinide Lanthanide Separations by Phosphorus-reagent Extraction from Aqueous Komplexes) and Innovative SANEX [41].

1.6.3.1 Organophosphorus ligands

Trialkylphosphine oxides have been used for the removal of transuranic elements (TRU) from the radioactive waste. Based on trialkylphosphine oxides, the TRPO process was developed in China [36]. The bidentate carbamoyl phosphonates were for the first time described for the extraction of actinides and lanthanides in the 1960s [42,43]. Several derivatives of CH_2-bridged organophosphorus ligands, e.g the bidentate neutral organophosphorus compounds (BNOPCs) [44,45] diphenyl(diisobutylcarbamoylmethyl)phosphine oxide ($Ph_2{}^iBu_2$-CMPO) [46,47] and octyl(phenyl)-*N,N*-diisobutylcarbamoylmethyl phosphine oxide (OPh^iBu_2CMPO) (**Fig.1.7**)

[48,49] have been extensively studied for the extraction of various actinides and lanthanides. The TRUEX process was developed in the 1980s, which used a mixture of CMPO and TBP [50-51] allowing all minor actinides and lanthanides to be extracted from moderate concentrations of HNO_3.

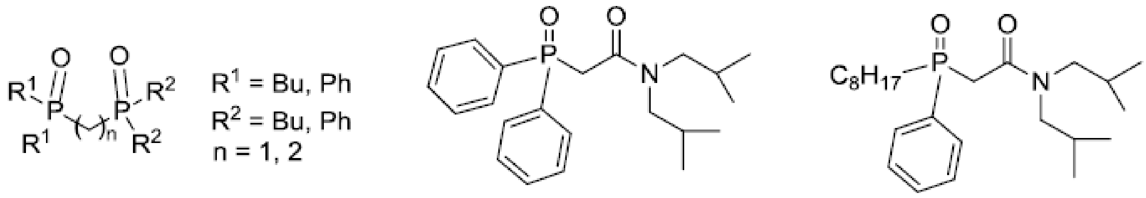

BNOPCs   Ph$_2$Bu$_2$-CMPO   OPh^{i}Bu$_2$CMPO

Fig.1.7: Structural formulae of different organo-phosphorus ligands

1.6.3.2 Malonamides

The malonamides, which are bidentate oxygen donor ligands, are used for the extraction of An^{3+} and Ln^{3+} from the HLW since the 1980s [52]. These extractants are completely incinerable and the amount of secondary waste produced can be significantly reduced compared to phosphorus-containing ligands. Extensive studies involving structural modifications [53-57] led to the DIAMEX process. Initially, *N*,*N*′ -dimethyl-*N*,*N*′ -dibutyltetradecylmalonamide (DMDBTDMA) was considered to be the best malonamide for the DIAMEX process. Subsequently, *N*,*N*′ -dimethyl-*N*,*N*′ -dioctyl-2-(2-hexyloxyethyl)malonamide (DMDOHEMA) was found to be a superior extractant than DMDBTDMA (**Fig.1.8**). The extraction efficiency of Eu^{3+} using bicyclic malonamides was found to increase 10^7 times than that of the linear homologue [58].

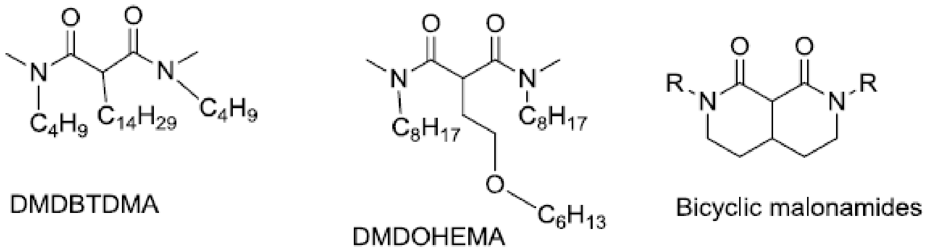

Fig.1.8: Structural furmulae of different malonamide ligands

1.6.3.3 Diglycolamides

Since malonamides have a weak binding efficiency towards actinide/lanthanide metal ions, relatively high extractant concentrations are required. During the late 1990s, Sasaki and Choppin showed that diglycolamides have better extraction properties towards actinides from acidic waste solutions than malonamides [59, 60]. Extensive extraction studies have been carried out in the last two decades using this class of extractants [61-64]. Diglycolamide (DGA) derivatives with varying chain lengths on the amidic nitrogen have been synthesized and *N,N,N′,N′*-tetraoctyl diglycolamide (TODGA) (**Fig. 1.9(a)**) was found to be the most suitable extractants in terms of extraction, solubility in aliphatic solvents, and stability. The nature of the *N*-substituents of diglycolamide (DGA) compounds plays an important role in the metal ion extraction.

The polarity of the organic diluents plays an important role in the extraction using DGAs. The D_M values decrease in the order *n*-octanol ~*n*-dodecane > dichloromethane > toluene > chloroform, persumably because the oxygen donor atoms of the DGAs interact with aromatic and halogenated diluents [65,66]. TODGA has a tendency to form a third phase in aliphatic solvents such as *n*-dodecane, particularly at high metal and HNO_3 concentrations [66].

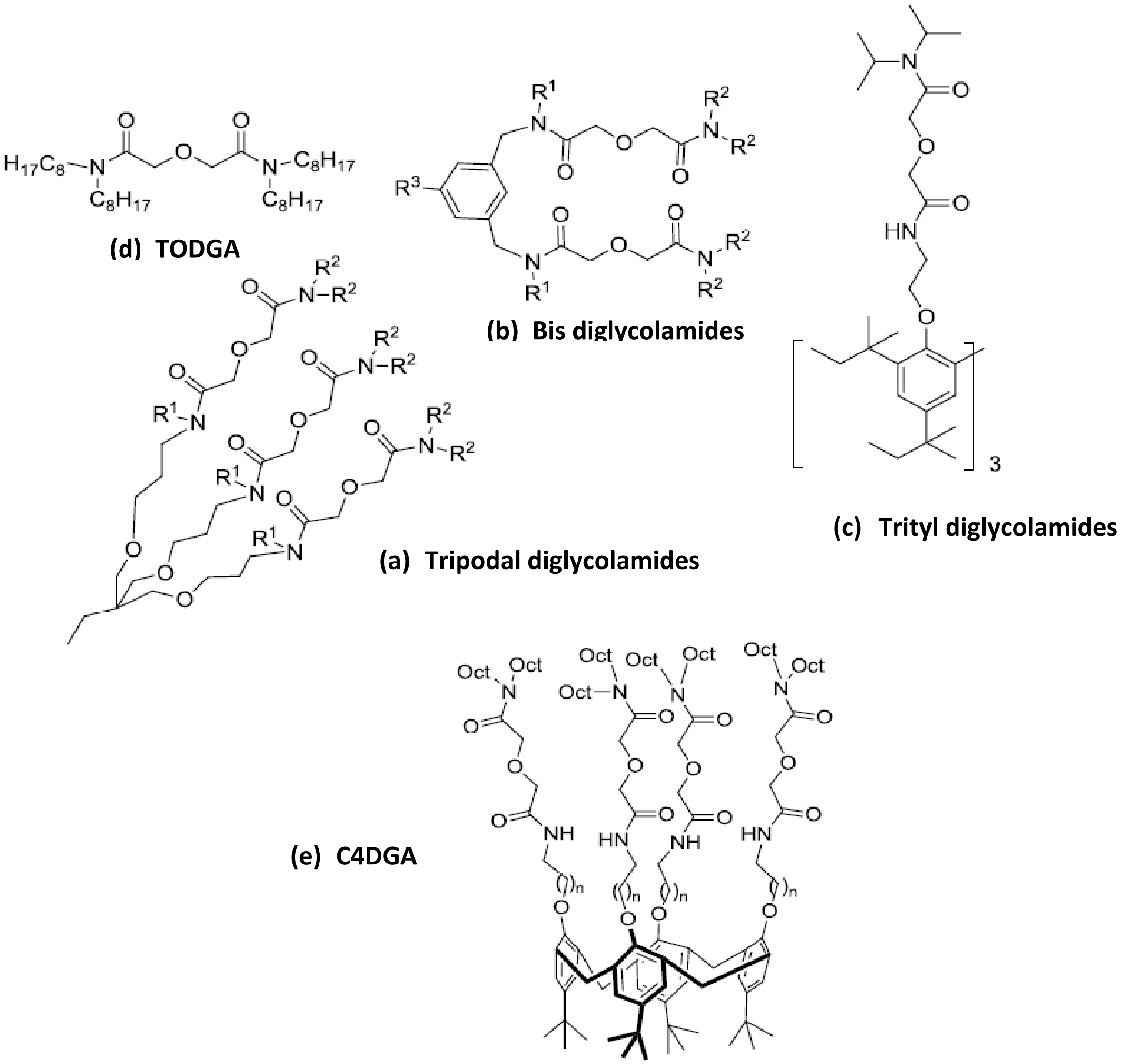

(d) TODGA

(b) Bis diglycolamides

(c) Trityl diglycolamides

(a) Tripodal diglycolamides

(e) C4DGA

Fig. 1.9: Structural formulae of DGA based ligands

Bis diglycolamides (**Fig. 1.9(b)**) bearing various substituents on the nitrogen atoms of diglycolamides showed a decrease in the *D* value compared to the simple DGAs [67]. However, the $SF_{\mathrm{Eu/Am}}$ values were generally higher for bisdiglycolamides compared to the simple diglycolamides. DGA on the trityl platform (trityl DGA) has a better separation factor for Eu^{3+} over Am^{3+}. The DGA functional groups preorganized at the C-pivot tripodal platform tripodal diglycolamides (**Fig. 1.9(c)**) , showed to be very efficient extractants for Am^{3+} and Eu^{3+} with up to five times higher relative extraction ability for Eu^{3+} [68]. TODGA has been preorganized on the triphenoxymethane (also referred to as trityl) platform (trityl diglycolamides) (**Fig. 1.9(d)**) [69,70]. Four TODGA molecules appended on a calix[4]arene (C4DGA) platform (**Fig. 1.9(e)**) was also reported to extract Am^{3+} and Eu^{3+} very efficiently [71].

1.7 APPLICATION OF RTILS IN NUCLEAR FUEL CYCLE

In the recent past, room temperature ionic liquids (RTIL) have been receiving increasing attention for possible applications in the area of nuclear fuel reprocessing and waste management [72-74]. RTILs are compounds composed fully of dissociated ions and melt at temperatures lower than 373K [75,76]. Typical examples of cation-anion combinations for making RTILs are shown in **Fig. 1.10**. The RTILs have many attractive properties such as insignificant vapor pressure, ability to dissolve a wide range of organic and inorganic compounds, wide electrochemical window, and tunability of properties by suitable combination of cation and anion, etc. Consequently, there has been a significant increase in the studies related to the use of RTILs in aqueous and non-aqueous reprocessing applications. Essentially, RTILs are investigated as possible substitute to the molecular diluent in solvent extraction procedures and as an alternative to high temperature molten salts in non-aqueous reprocessing applications. Some of the striking features of RTILs that make them promising for even nuclear fuel cycle application are listed below.

I. The selectivity of the target metal ion can be easily manipulated by the change of cation-anion combinations of RTIL diluent, rather than redesigning the structure of the extractant.

II. Presence of ionic diluent in organic phase facilitates a new mode of recovery of metals by direct electrodeposition from the extracted phase.

III. Ionic liquids can be functionalized with organic moieties for task specific applications.

IV. RTILs can be designed to be completely incinerable, which would simplify the management of spent organic waste.

V. Due to negligible vapor pressure of RTILs, the fire hazards are significantly reduced.

In addition, unusual extraction of metal ions has been observed when traditional extractants are used in RTIL based diluents. Broadly, the application of RTILs in nuclear fuel cycle can be categorized into three types

a. RTIL as diluents
b. Functionalized or Task specific ionic liquids (TSIL)
c. RTILs with strongly co-ordinating ions.

1.7.1 RTILs as diluents

A systematic study on the extraction of UO_2^{2+} from nitric acid medium by a solution of TBP in [C_4mimPF_6] or [C_4mim][NTf_2] was reported by Giridhar et al. [77,78] and a comparison was made with molecular diluents like *n*-dodecane. For RTILs, an initial decrease in D_U with increase in the concentration of nitric acid was attributed to the predominance of a cation exchange mechanism in the lower acidity range followed by predominance of a solvation mechanism in the higher acidity range (**Fig 1.11**). The extraction of Pu^{4+} from nitric acid medium by CMPO in [C_8mim][PF_6] was proposed to be the cation exchange of $[Pu(NO_3)(CMPO)_x]^{+3}$ ion with $[C_8mim]^+$ ion of ionic liquid phase [79].

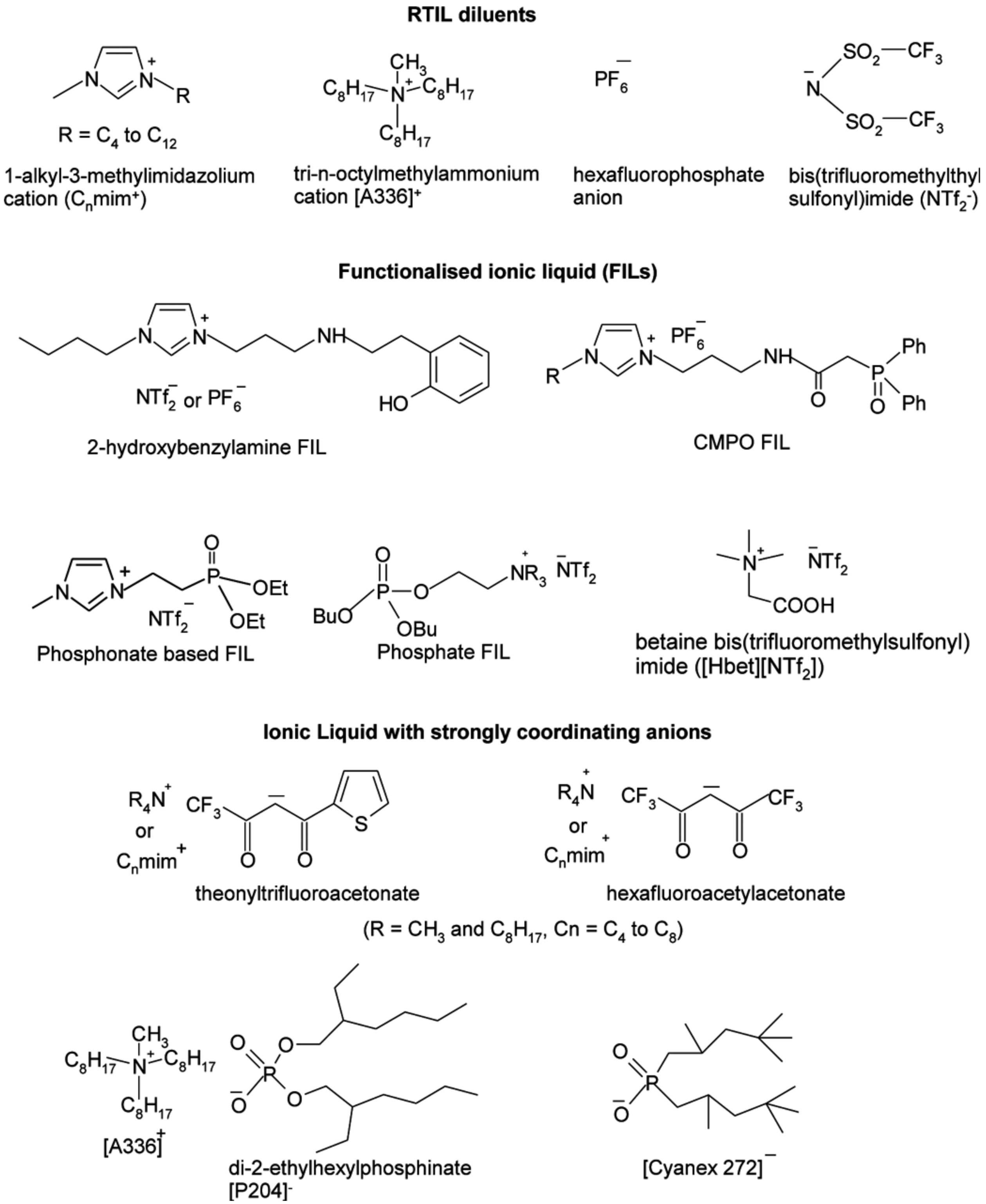

Fig. 1.10: Structural formulae of different room temperature ionic liquids

Similarly, the extraction of Pu(IV) in DC18C6 in [C_4mim][PF_6] (or [C_6mim][PF_6]) was also dominated by cation exchange mechanism involving $Pu(CE)(NO_3)_2^{2+}$ species [80]. A preliminary investigation on extraction of f-block elements using 0.1 M CMPO + 1.0 M TBP in [C_4mim][PF_6] was reported by Visser et al. [81]. The distribution ratios of Am^{3+}, Pu^{4+}, Th^{4+} and UO_2^{2+} were found to be an order higher in RTIL than those obtained in *n*-dodecane under similar conditions. Nakashima et al. [82] have subsequently studied the extraction of trivalent lanthanides by the solvent containing CMPO in [C_4mim][PF_6]. The liquid–liquid extraction of lanthanides (Ln^{3+}) from aqueous medium by a solution of TODGA in [$C_n$mim][NTf_2] (n = 2,4,6) was investigated by several groups [83, 84]. Dai et al. [85] and subsequently Visser et al. [86] attempted to separate Cs^+ and Sr^{2+} ions from aqueous medium using a solution of crown ether in imidazolium based ionic liquids

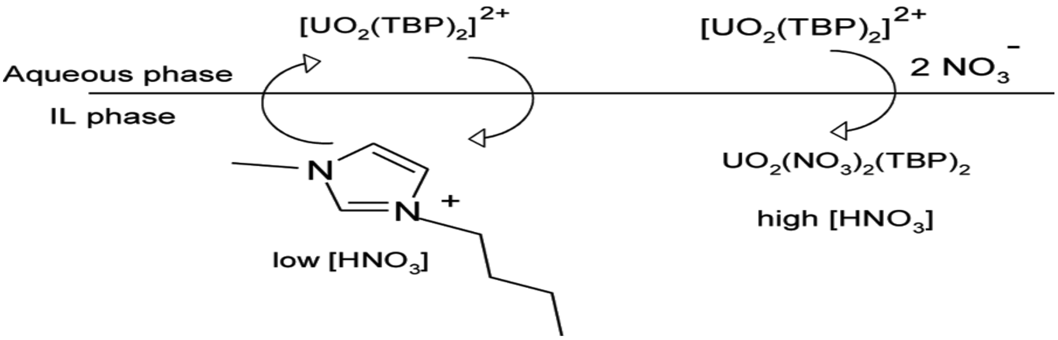

Fig. 1.11: Schematic of extraction mechanism during UO_2^{2+} extraction by TBP

1.7.2 Functionalized / Task specific ionic liquids (TSIL)

The cationic or anionic part of the room temperature ionic liquid tethered covalently with organic functionalities, which can perform specific applications are known as functionalized ionic liquids (FILs) or task specific ionic liquids (TSILs). Due to the presence of the functional group, the resultant TSIL is expected to show the properties of both ionic liquid and organic functionality. The extraction behavior of Hg^{2+} and Cd^{2+} using thio-urea functionalized ionic liquids as a function of various parameters was one of the earliest work reported in the literature by Visser et al. [87] while the synthesis of 2-hydroxybenzylamine TSIL and the extraction of Am^{3+} from aqueous medium was reported by Ouadi et al. [88, 89]. Luo et al. [90] reported the synthesis of imidazolium based ionic liquids functionalized with monoaza-crown ether for the extraction of Cs^+ and Sr^{2+} from aqueous solutions. CMPO functionalized TSIL impregnated on polymer supports also showed good extraction of Pu^{4+}, Am^{3+}, Eu^{3+} and UO_2^{2+} from HNO_3 medium [91].

1.7.3 RTILs with strongly coordinating anions

Recently, ionic liquids with strongly coordinating anions [92] are becoming popular in addition to the TSILs. Usually, the conjugate base of the acids such as phosphate, phosphonate, diketonate, etc., act as anions. The advantages of such ionic liquids over TSILs are simple method of preparation, higher loading of metals, and miscibility with non-polar diluents such as toluene, etc. These properties are very useful for some types of applications. Sun et al. [93] studied the solvent extraction of Eu^{3+} using a bi-functional ionic liquid extractant associated with phosphonate, phosphinate, or carboxylate as the anion and $[A336]^+$ as cation.

Employing RTILs in place of the inorganic chloride media for non aqueous reprocessing would lead to the operation of the entire process at near ambient conditions. Furthermore, the cation and anion combination of organic salt can be tuned to obtain a completely incinerable electrolyte, which makes the management of spent electrolyte easy.

1.8 Objectives

Unlike conventional ligands like CMPO, DMDBTDMA etc., where the extraction efficiency of different oxidation states of the actinides depend on their ionic potential, the formation of reverse miceller aggrigates by four TODGA molecules in molecular diluents like dodecane is reported to be responsible for the extra ordinarily high extraction efficiency of trivalent actinides over tetravalent and hexavalent actinides. Therefore four diglycolamide moieties appended on a molecular platform, Calix[4] arene can show some interesting extraction behavior of actinides. As we have mentioned earlier that the formation of aggregates highly depends on the nature of the medium, ionic liquid will be an interesting choice of organic media for the extraction studies.

On view of the above fact, it is clear that a combination of diglycolamide functionalized ligands in RTILs would be interesting for extraction of actinides. The main objectives of the present study are

I. Conventional extractants in RTILs reported by show very high extraction efficiency and separation behavior of target metal ions as compared to that in molecular diluents. Therefore, it is thought to be interesting to study the extraction / separation behavior of actinides by using newly synthesized multiple – DGA-functionalized ligands in RTILs. It was also thought of our intersect to study the extraction efficiency of different oxidation states of actinides and their separation behavior between themselves and with respect to long lived fission products in terms of separation factors. Changes in diluents from molecular solvents like dodecane to RTILs can lead to change in extraction mechanism of metal ion. So it was also thought of interest to understand the mechanism of metal ion extraction whether it is 'ion exchange' or 'solvation'. Stripping of metal ion form RTILs is one of the challenges faced by separation chemist, so, it was also thought to study the back extraction of actinides from loaded RTIL phase.

II. To design a successful separation procedure, it is essential to understand the inside of the complexation, kinetics and thermodynamics associated with the extraction procedure. In this context, it is very interesting to study the metal – ligand stoichiometry, nature of bonding, amount of covalence between metal – ligand bond, symmetry of the complex, perturbation of actinide – oxygen bond on complexation of actinyl ion etc. Whether a complex is inner sphere / outer sphere; conformational changes of the ligands due to complexation (which is of significance when macromolecules are used), spontaneity of a separation process etc. keep signature on the thermodynamic parameters like change in Gibb's free energy, change in enthalpy, change in entropy etc. Therefore, it was also thought of interest to evaluate the thermodynamic parameters associated with the extraction.

III. Task specific ionic liquids or functionalized ionic liquids (TSILs) and have many advantages over the solvent systems containing an extractant in an IL. Apart from the compatibility of extractants and diluents molecules, the functional groups appended onto RTIL can impart a particular reactivity pattern, enhancing its capacity for interaction with specific metal ions, thereby improving the selectivity enormously. Therefore, it was thought of our interest to study the extraction behavior, selectivity, extraction mechanism, and bonding, nature and symmetry in metal – ligand complex etc of DGA based TSILs.

IV. Finally, the central idea of developing a solvent system for 'actinide partitioning' is its successful application in preferentially extraction of target metal ions from HLW solution. It is also required to know the extraction behavior of the concomitatnt metal ions present in HLW solution. For the long term application of the solvent system for actinide extraction, one needs to understand the radiolytic degradation behaviour which can answer queries on the sustainability and recycling possibilities. It is also very interesting to identify the radicals and the products generated during the irradiation of the solvent systems and responsible for detoriation of the performance of the solvent systems.

V. ^{90}Sr ($T_{1/2}$ ~ 28.5 years) is one of the most important fission products present in high-level waste (HLW) solution generated during the reprocessing of spent nuclear fuel. The separation of long-lived ^{90}Sr from HLW prior to vitrification is helpful not only in reducing the volume of the disposable waste but also in reducing the risk of matrix deformation caused by the generated heat. So it is required to develop RTIL based solvent system for selective separation of Sr^{2+}

CHAPTER - 2

Experimental

2.1 MATERIALS

2.1.1. Radiotracers

The radiotracers, ^{241}Am, Pu (mainly ^{239}Pu), and ^{233}U tracers were used from laboratory stock solutions and BRIT after purification prior to their use by ion-exchange methods as reported earlier [94]. ^{239}Np was obtained by irradiating natural U in a nuclear reactor at a neutron flux of 10^{13} n/cm^2/s followed by separation according to a method reported previously [95]. ^{85,89}Sr, ^{137}Cs and ^{152,154}Eu tracer were procured from Board of Radiation and Isotope Technology (BRIT), Mumbai, and their radiochemical purity was assured by gamma spectrometry employing high resolution HPGe detector. The experiments were carried out with <1% counting statistics errors.

2.1.2. Ionic liquids

Room temperature ionic liquid (RTIL) such as 1-butyl-3-methyl-imidazolium hexafluorophosphate ([C_4mim][PF_6]), 1-hexyl-3-methyl-imidazolium hexafluorophosphate ([C_6mim][PF_6]) and 1-octyl-3-methyl-imidazolium hexafluoro phosphate ([C_8mim][PF_6]); 1-butyl-3-methylimidazolium bis[(trifluoromethyl)sulphonyl] imide ([C_4mim][NTf_2]), 1-hexyl-3-methyl-imidazolium bis[(trifluoromethyl)-sulphonyl] imide ([C_6mim][NTf_2]) and 1-octyl-3-methyl-imidazolium bis[(trifluoromethyl)sulphonyl] imide([C_8mim][NTf_2]) with purities > 99% were procured from Iolitec, Germany and were used as obtained.

2.1.3. Solvents and materials

Chloroform (Merck, Germany), *n*-dodecane (Lancaster, UK), 1-octanol (Fluka, Switzerland), 2- nitrophenyloctylether (NPOE) (Aldrich, USA), methylisobutyl ketone (MIBK, Merck, Germany) and nitrobenzene (Fluka, Switzerland) were procured at > 99% purity, and were used as obtained. Phenyltrifluoromethylsulphone (PTMS, also known as FS-13 [96]) was synthesized as reported previously [97]. All other reagents used in this study were of AR grade and were used as received. Suprapur nitric acid (Merck, Germany) was used for preparing the aqueous feed solutions for the solvent extraction studies and the final strength of the dilute acid solutions was determined by acid–base titration using standard NaOH solution and phenolphthalein (Merck) as indicator. EDTA (ethylenediamine- N,N,N',N'-tetraacetic acid), DTPA (diethylenetriamine-N,N,N' ,N'' ,N''-pentaacetic acid), and guanidine carbonate were obtained from Alfa Aeser, USA, while formic acid, hydrazine hydrate, and citric acid were procured from SD Fine Chem, Mumbai. All other reagents used in this study were of AR grade.

2.1.4. Extractants

2.1.4.1 TODGA

TODGA (*N,N,N',N'*-tetraoctyl diglycolamide) was obtained from Thermax Ltd, Pune, India. The extractant was characterized by NMR, HPLC and GC-MS while all other novel extractants like C4DGAs (diglycolamide-functionalized calix[4]arenes), T-DGA (tripodal diglycolamide), DGA-TSILs (diglycolamide-functionalized task specific ionic liquids) and CMPO-TSIL (carbamoylmethyl phosphine oxide-functionalized task specific ionic liquids) were synthesized at University of Twente, The Netherlands.

2.1.4.2 C4DGAs

2.1.4.2.1 Lower rim functionalized C4DGA

The brief scheme for the synthesis of C4DGAs with different spacer length is summarized in **Fig 2.1**. Two tetra-DGA-calixarenes, with a C2 and C3 spacer between the calixarene platform and the DGA, were prepared by reaction of cone tetrakis(aminoalkoxy)calix[4]arenes with *p*-nitrophenol-activated DGA. The detailed synthetic steps, experimental conditions etc. are described elsewhere [71]. The compounds were characterized by NMR and mass spectroscopy. The purity of the compounds was checked by standard physicochemical methods.

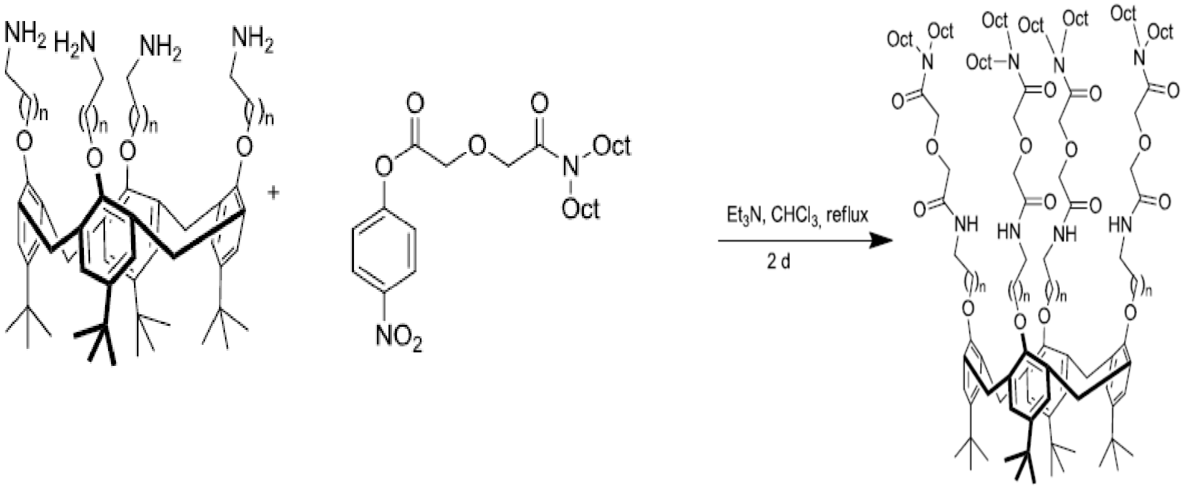

Fig. 2.1: Synthesis scheme for the preparation of C4DGA with different spacer length

It was anticipated that the introduction of alkyl group at the amide nitrogen atom close to the calixarene platform would force the amide oxygens to point inwards to avoid steric crowding, thereby, preorganizing the molecule and consequently influencing its extraction efficiency. Therefore, three different Calix-DGAs were prepared with *n*-propyl, 3-pentyl and *n*-

octyl groups, respectively, introduced at the amide nitrogen atom (**Fig 2.2**). The starting tetrakis(alkylaminoalkoxy)calix[4]arenes were prepared by the reaction of cone tetrakis(aminoalkoxy)calix[4]arenes with propionyl and octanoyl chloride, respectively followed by reduction of the amide carbonyl groups with $LiAlH_4$. The corresponding 3-pentyl-substituted derivative was synthesized by reductive amination. Tetrakis(aminopropoxy)calixarene was reacted with 3-pentanone in THF using ti(iso-propoxide) as a catalyst, followed by *in situ* reduction of the formed imine by $NaBH_4$. In a manner similar to that described above, they were further reacted with p-nitrophenol-activated DGA to convert them into the tetra-DGA-calix[4]arenes. Electrospray mass spectroscopy (ESI-MS) and NMR spectroscopy were used to characterize the ligands. The detailed synthesis procedure is described elsewhere [71].

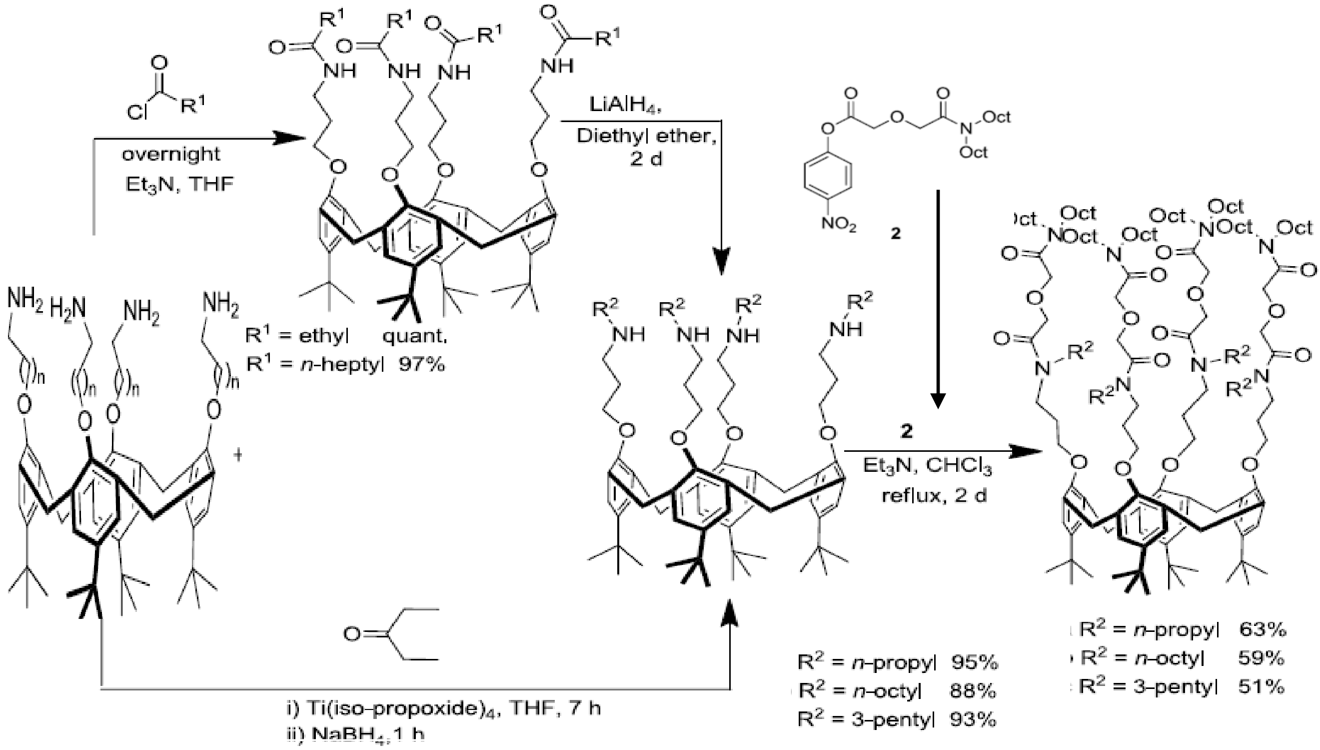

Fig. 2.2: Synthesis scheme for the preparation of C4DGA with different alkyl substituent

2.1.4.2.2 *Both rim functionalized C4DGA*

Ligands bearing DGA moieties on both rims of the calix[4]arene scaffold was synthesized using a two-step procedure involving first cleavage of the phthalimide groups by hydrazine followed by reduction of the nitro moieties, using Raney Ni, as a catalyst and was further reacted with p-nitrophenol-activated DGA to yield both rim functionalized C4DGA (**Fig. 2.3**). The detailed synthesis procedure is described elsewhere [71].

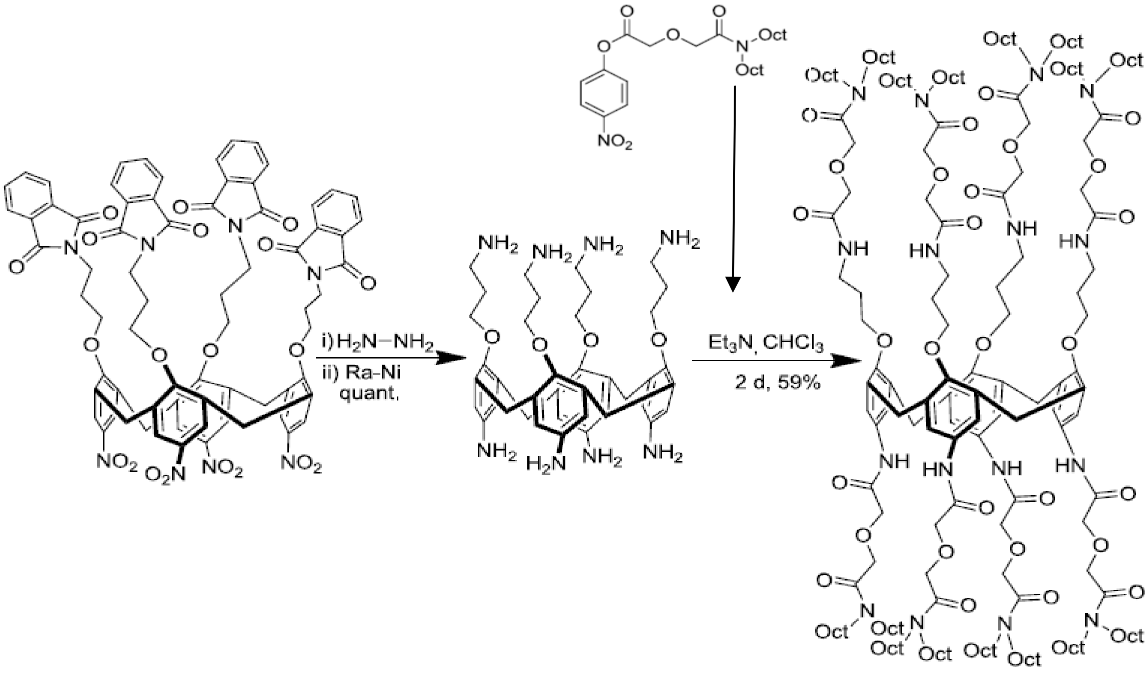

Fig. 2.3: Synthesis scheme for the preparation of both rim functionalized C4DGA

2.1.4.2.3 *Upper rim functionalized C4DGA*

Upper rim C4DGA was prepared by the reaction of tetrabutoxycalix[4]arene tetraamine with *p*-nitrophenol-activated DGA (**Fig 2.4**). The ESI-MS and ^{1}H NMR spectrum confirmed the preparation of the target molecules i.e. upper rim functionalized C4DGA. The detail synthesis procedure has been described elsewhere [71].

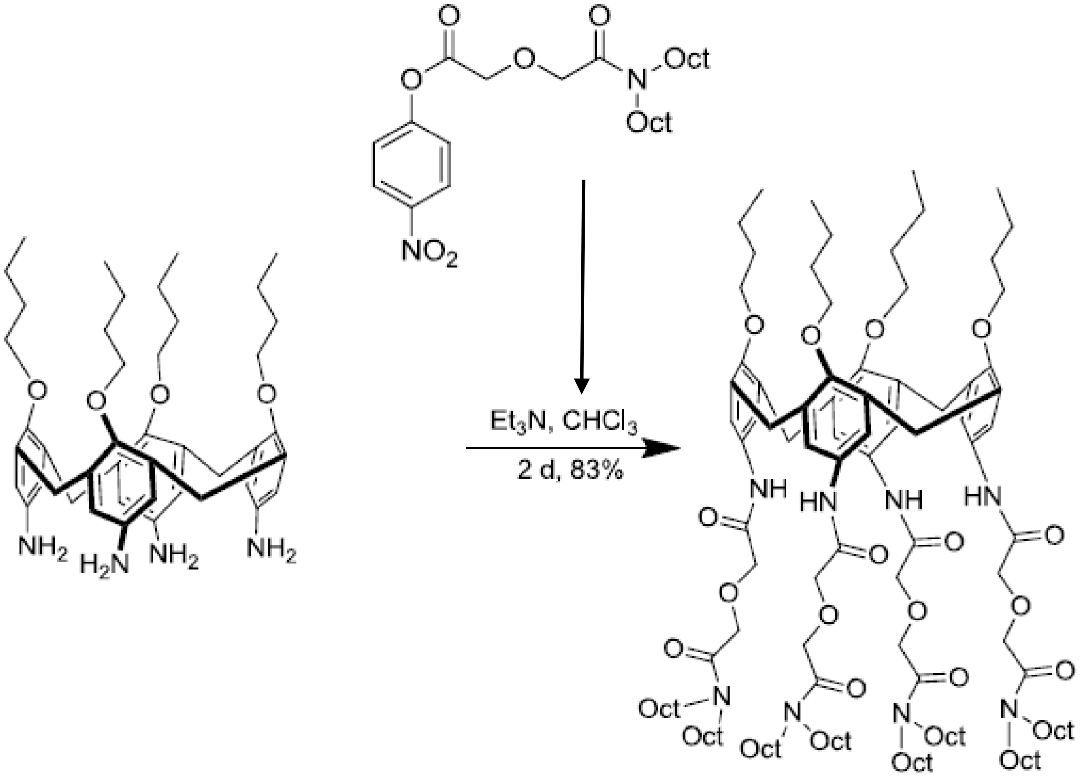

Fig. 2.4: Synthesis scheme for the preparation of upper rim C4DGA

2.1.4.3 T-DGA

The detailed synthetic scheme of the tripodal diglycolamide T-DGA was reported by Jan´czewsk et al. [68]. A brief description is given as follows (**Fig 2.5)**. A mixture of *p*-nitrophenol activated DGA and triethylamine in chloroform was refluxed for 2 days. The crude reaction mixture was successively washed with 2 M NaOH solution, 1 M HCl, and water. The organic layer was concentrated under reduced pressure and the crude product was purified by column chromatography to afford T-DGA as oil.

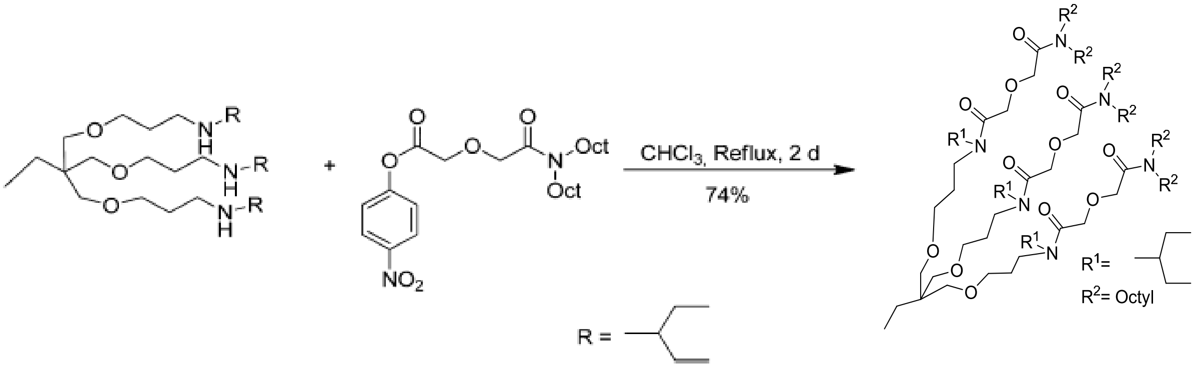

Fig. 2.5: Synthesis scheme for the preparation of T-DGA (tripodal diglycolamide)

2.1.4.4 DGA-TSIL

Commercially available 3-(1*H*-imidazol- 1-yl)propan-1-amine (**1**) was treated with the known 2-(2-(dioctylamino)-2-oxoethoxy)acetic acid (**2**) in chloroform using *N*,*N'*-dicyclohexylcarbodiimide (DCC) and 1-hydroxybenzotriazole (HOBT) as coupling agent to get imidazole-diglycolamide **3**. Compound **3** was further reacted with *n*-butyl bromide in acetonitrile for 2.5 days to give ionic liquid **4** having bromide as the counter-anion. The bromide counter-anion of **4** was exchanged with either hexafluorophosphate or bis(trifluoromethane)sulfonamide by treating with the corresponding sodium and lithium salts, to give TSILs **5** and **6**, respectively **(Fig 2.6)**. The products obtained in each step were characterized by NMR and high resolution electro spray mass spectrometry.

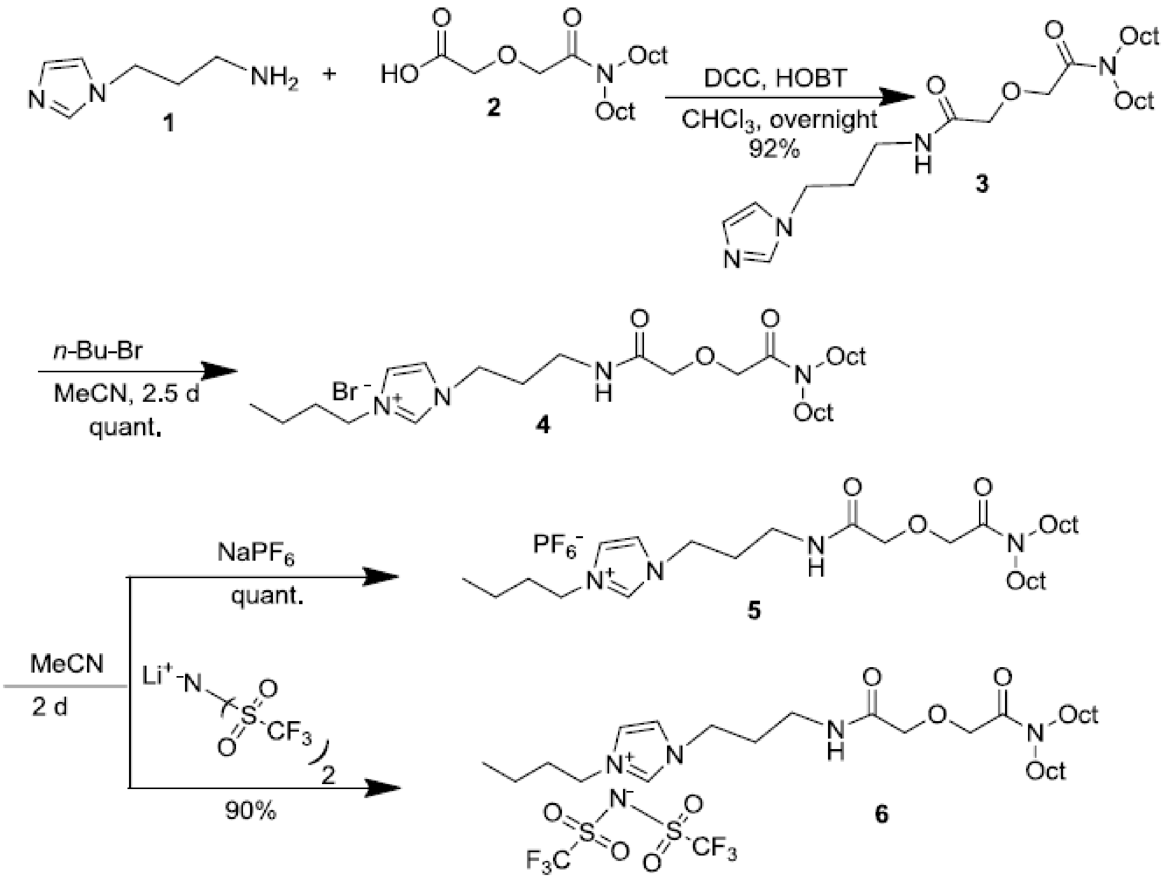

Fig. 2.6: Synthesis scheme for the preparation of DGA-TSILs

2.1.4.5 CMPO-TSIL

CMPO-TSILs were synthesized in two steps by reaction of diphenyl phosphite with ethyl bromoacetate and subsequent reaction of the formed product with 3-(1H-imidazol- 1-yl)propan-1-amine, was reacted with *n*-dodecyl bromide in refluxing acetonitrile to afford ionic liquid. The bromide counter-anion in was exchanged with either hexafluorophosphate or bis(trifluoromethane)sulfonamide by treating with the corresponding sodium and lithium salts, to give CMPO-TSILs (**Fig 2.7**). ^{1}H NMR spectra and the high resolution ESI-MS were used to characterize the CMPO-TSILs.

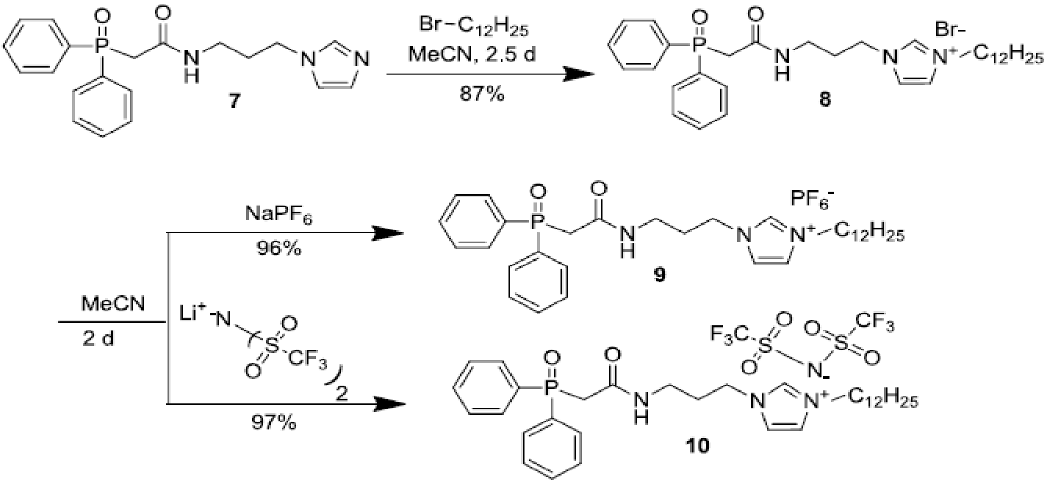

Fig. 2.7: Synthetic scheme for the preparation of CMPO-TSIL

2.1.4.6 Substituted crown ether

Dicyclohexano-18-crown-6 (DCH18C6) and 4, 4' (5')-di-*tert*-butyldicyclohexano-18-crown-6 (DTBCH18C6) were procured from Fulka, Switzerland with > 97% purity and used as such.

2.2 METHODS AND INSTRUMENTS

2.2.1 Distribution studies

The distribution studies were carried out by equilibrating 1 mL of the organic phase solution with an equal volume of the requisite aqueous phase containing the radiotracers at a particular concentration of HNO_3 in Pyrex tubes in a thermostated water bath at 25 ± 0.1 ˚C for about 3 h, which was optimized by an experiment with varying equilibration time. For the temperature variation studies, the tubes were equilibrated at varying temperatures in the range of 20 – 40 ˚C. The distribution ratio of the metal ions (D_M) was defined as the ratio of the activity per unit volume in the ionic liquid phase to that in the aqueous phase. As the ionic liquid phases were of reasonably higher viscosity than the aqueous phases, sampling errors may be significant. Therefore, the D_M values in the ionic liquid phase were determined by the difference of the initial and final counts in the aqueous phase as follows:

$$D_M = (C_i - C_f) / (C_f) \tag{2.1}$$

where, C_i and C_f are the initial and final concentrations of the metal ion, respectively. All experiments were carried out in duplicate and the precision of the experimental data points was within ±5%.

2.2.2 Stripping studies

Stripping studies were carried out in a manner similar to the forward extraction studies with the difference that the activity loaded organic phases were equilibrated with an equal volume of the aqueous phase containing either 0.05 M DTPA/EDTA in 1 M guanidine carbonate or a buffer mixture containing 0.1 M citric acid + 0.4 M formic acid + 0.4 M hydrazine hydrate.

2.2.3 Actinide tracer solutions

The studies involving Am, U, and Pu were carried out using about 10^{-7}, 10^{-5}, and 10^{-6} M concentrations of the respective metal ions, while the concentration of Np was at the tracer level ($<10^{-10}$ M). After equilibration, the tubes were centrifuged followed by phase separation and assayed radiometrically. The valency of Pu was adjusted to the +4 state by using a few drops of 1 X 10^{-2} M $NaNO_2$, which was checked by the TTA extraction method [98]. On the other hand, Pu was oxidized to the +6 state by the use of AgO followed by mild warming under an IR lamp. The Np valency state was adjusted to the +4 state by ferrous sulphamate and hydroxylamine hydrochloride, while NpO_2^{2+} was prepared using potassium dichromate [99].

2.2.4 Inductively coupled plasma atomic emission spectroscopic (ICP-AES) studies

Standard solutions for rare earth and other common impurity elements were prepared from CertiPUR® ICP multi standard solutions (E-Merck, Darmstadt, Germany) after dilution with 0.5 M HNO_3. Suprapur HNO_3 and quartz double distilled water were used for making 0.5 M HNO_3. Multi-point standardization was carried out using 0.5 M HNO_3 as lower standard and 0.05 -1000 µg/mL of the corresponding elemental standard as higher standards for each line after proper peak search. Thus, the calibration curves obtained for the best analytical lines of each analytes were used for the determination of the analytes in the samples.

2.2.5 Thermostated water bath used for maintaining constant temperature

All the solvent extraction experiments were carried out in a thermostated water bath (**Fig 2.8)** with temperature control. Generally, all the experiments were carried out at 30 ± 1°C.

Fig. 2.8: Photograph of the thermostated water bath used in the present study

2.2.6 Liquid scintillation counter

Liquid scintillation counter is the most widely used detector for quantitative analysis of α and β emitters. Nearly 100% detection efficiency of this detector for α emission is of great advantage and as low as few Bq of alpha activity can be assayed with good precision. A scintillator is a material that luminesces in a suitable wavelength region when ionizing radiation interacts with it. Interaction of charged particles with the scintillator results in the emission of photons and the intensity of the emitted light is a quantitative measure of the incident radiation. The photomultiplier tube (PMT) which produces signal representative of primary radiation then collects the light emitted from scintillator. In cases where scintillator emits photons in the UV region, a wavelength shifter is added to the scintillator to shift emitted light wavelength to visible region. Liquid scintillation counter is used to get gross alpha or beta activity in a given radioactive sample.

Radionuclides such as ^{239}Pu and ^{233}U were assayed by liquid scintillation counting (Hidex, Finland) using Ultima Gold scintillator cocktail (Sisco Research Laboratory, Mumbai). Each sample was counted for sufficient time to get around 10,000 counts to restrict the statistical error.

2.2.7 NaI (Tl) scintillation counter

In the present work, a 3''x 3'' well type NaI (Tl) detector coupled with a multi-channel analyzer has been used for gamma ray counting (**Fig. 2.9**). Nearly 100% efficiency for moderate energy photons in a well type detector is a key feature of this detector. Sodium iodide doped with 0.1-0.2% of thallium, is the most widely used inorganic scintillator for quantitative analysis of the γ ray emitting radionuclides. NaI is an attractive material of choice because the high atomic number (Z=53) of iodine ensures that photoelectric absorption will be an important interaction process. The band gap of NaI crystal is 5-6 eV. When ionizing radiation falls on the detector, its energy is used up for the excitation of electrons from the valance band either to the conduction band or for ionization of atom. Generally, the de-excitation leads to the emission of photons in the UV region, as the band gap is large. To shift the emitted photon in the visible region, an activator impurity Tl (having intermediate level conduction band) is doped in the NaI crystal. It is enclosed in Al, which also acts as an internal reflector. The resolution of NaI (Tl) detector is about 7% at 662KeV.

A suitable aliquot of the desired analyte solution taken in a glass counting tube (1 cm dia) was placed in the sample holder port of the detector coupled with PMT and associated electronics. Each sample was counted for sufficient time to get around 10000 counts to restrict statistical counting error.

Fig. 2.9: Close view of the sample holder port of NaI(Tl) scintillation counter

2.2.8 Inductively coupled plasma atomic emission spectrometer

The analytical experiments were carried out using computer controlled, high resolution, simultaneous atomic emission spectrometer (Spectro Arcos, Germany) with ICP and DC Arc as excitation sources and a charged coupled device (CCD) as detector.

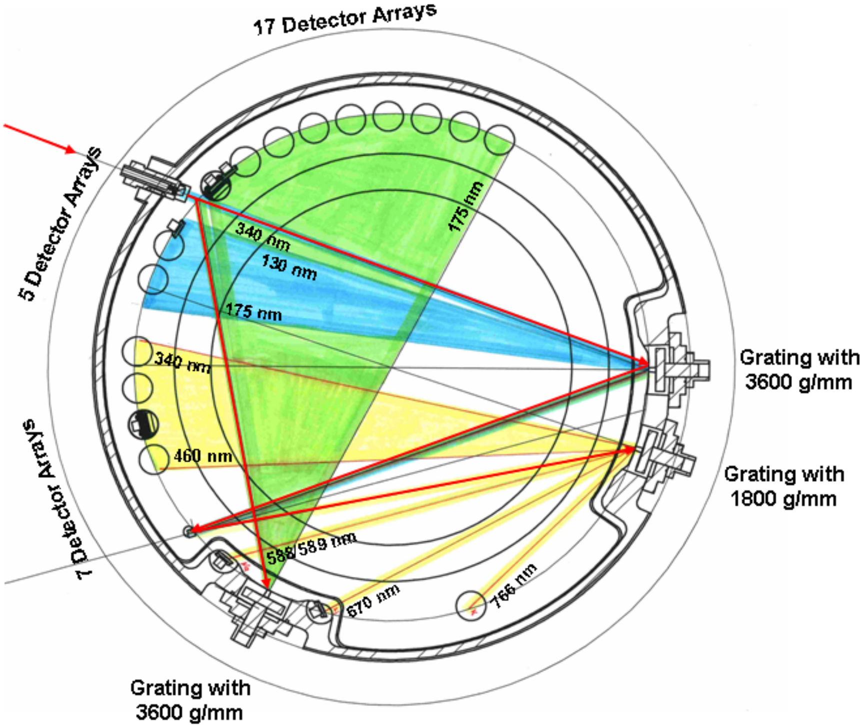

Fig. 2.10: Cross sectional view of the array of pixels in CCD based detector

The instrumental specification and experimental parameters are summarized in **Table 2.1**. The detector system, consisting of linear arrays of CCD detectors (3648 pixels/array), thermally stabilized together with an optical system, provides the ability to choose the alternate analytical lines. **Fig. 2.10** is showing the cross sectional view of the detector.

Table 2.1: Specifications and operating conditions of ICP-AES

Instrumental specification	
Optical design	Paschen-Runge mounting, Circular design
Focal length	750 mm
Grating	Holographic
Groove density	1800 grooves/mm (1), 3600 grooves/mm (2)
Wave length range	130-800 nm
Entrance slit width	15 microns
Resolution (FWHM)	0.01 nm from 130-450nm, 0.02 nm from 450-800nm
Thermal regulation	Controlled to 30 ± 1°C
Frequency	27.12 MHz
Pump	Dual channel peristaltic pump
Detector	Linear arrays of CCD (3648 pixels/array)
Nebulizer	Concentric nebulizer with cyclonic spray chamber
ICP-torch	Demountable, radial viewing
Operating condition	
Coolant flow	6 L/min
Auxiliary flow	0.6 L/min
Total time of measurement	28 s
Pump speed	30 Rpm
RF power out put	0.8 – 1.5 kW
Input power	230 V AC

2.2.9 EPR Studies

EPR studies were carried out using a Bruker-EMX (EMM1843) spectrometer (**Fig 2.11)** at X-band frequency operated at 9.5 GHz with 100 kHz field modulation (instrumental parameters are given in ESI). The ‘g’ values were evaluated relative to a small single crystal of BDPA (1,3–bisdiphenylene–2-phenylallyl) with g = 2.0028 and a line width of 0.63 G. BDPA is an ideal sample for calibrating the phase and the field modulation amplitude of the single channel of the spectrometer. The viscous samples were transferred to a quartz tube. The sample tubes were degassed to remove O_2 and N_2 and then the sample tubes were sealed. These tubes were irradiated at liquid nitrogen temperature (77 K) to quench all the radicals generated during irradiation. The various ESR parameters for the different radicals were determined precisely from the calculated spectra by simulation using the Bruker SIMFONIA program based on the perturbation theory.

The theoretical ESR signals were calculated using the spin Hamiltonian parameter (H) as per the following equation:

$$H = \beta H_j S_j g_j \tag{2.1}$$

where, *j* is the component along one of the axes x, y, or z, *H* is the applied field, *S* is the total spin of the electron, *g* is the g factor, and *β* is the Bohr magneton. In the SBO samples, EPR signals were simulated by generating 9000 random orientations of the magnetic field and by summing the corresponding 9000 absorption signals. The final signal was obtained by performing a convolution (Gaussian or Lorentzian line shape) of each transition line adding all contributions and calculating the first derivative of the signal. The line width of each component was optimized in order to obtain a best fit between the simulated and the experimental data.

Temperature variation studies were done on a Bruker variable temperature accessory Eurotherm BVT-2000.

Fig. 2.11: Photograph of the EPR spectrometer used in the present study

2.2.10 Luminescence studies

Emission and excitation spectra were recorded on an Edinburgh F-900 fluorescence spectrometer (**Fig 2.12**) in the 200–750 nm region with a Xe lamp as the excitation source, M-300 monochromators, and a Peltier cooled photomultiplier tube as detector. The acquisition and analysis of the data were carried out by F-900 software supplied by Edinburgh Analytical Instruments, UK. Sample was taken in a quartz tube and kept inside the sample holder for measurement.

Fig. 2.12: Photograph of the fluorescence spectrometer used in the present study

Fluorescence spectroscopy is primarily concerned with electronic and vibrational states. Generally, the species being examined has a ground electronic state (a low energy state) of interest, and an excited electronic state of higher energy. Within each of these electronic states there are various vibrational states. In fluorescence spectroscopy, the species is first excited, by absorbing a photon, from its ground electronic state to one of the various vibrational states in the excited electronic state. Collisions with other molecules cause the excited molecule to lose vibrational energy until it reaches the lowest vibrational state of the excited electronic state.

The molecule then drops down to one of the various vibrational levels of the ground electronic state again, emitting a photon in the process. As molecules may drop down into any of several vibrational levels in the ground state, the emitted photons will have different energies, and thus frequencies. Therefore, by analysing the different frequencies of light emitted in fluorescent spectroscopy, along with their relative intensities, the structure of the different vibrational levels can be determined. For atomic species, the process is similar; however, since atomic species do not have vibrational energy levels, the emitted photons are often at the same wavelength as the incident radiation. This process of re-emitting the absorbed photon is "resonance fluorescence" and while it is characteristic of atomic fluorescence, is seen in molecular fluorescence as well.

2.2.11 Radiolytic degradation studies

The radiolytic degradation studies were carried out by irradiating the solvent used for the extraction/ separation studies by a ^{60}Co gamma irradiator **(Fig. 2.13)** with a dose rate of 2.4 kGy/h. For EPR measurements, the irradiation studies were carried out in a continuous manner and the tube containing the solvent was frozen in order to retain the free radicals for detection by EPR spectroscopy.

Fig. 2.13: Photograph of the gamma irradiator with ^{60}Co source used in the present study

CHAPTER - 3

Evaluations of diglycolamide based systems in room temperature ionic liquid for extraction of actinides

Extractants such as CMPO (carbamoyl methyl phosphine oxide), malonamide, TRPO (trialkyl phosphine oxide), DIDPA (diisodecyl phosphoric acid) and DGA (diglycolamide) are well known for the extraction of trivalent actinides from moderately acidic medium [36,37,66, 100,101]. Use of CMPO leads to the generation of large amounts of secondary waste, while malonamide-based extractants are prone to third phase formation [102]. In this context diglycolamide-based extractants are found to be environmentally benign and do not form third phase under suitable conditions. Among the diglycolamide-based extractants, TODGA (N,N,N′,N′-tetraoctyl diglycolamide) was found to be one of the most promising extractants for the separation of trivalent actinides from moderately acidic aqueous feed [58,103] Further, a recent study has indicated that a mixture of CyMe$_4$BTP (2,6-bis(5,5,8,8-tetramethyl-5,6,7,8-tetrahydrobenzo[1,2,4]triazin-3-yl) pyridine) and TODGA can be used for direct extraction of the trivalent actinides which is termed as 1-cycle SANEX (selective actinide extraction) process [104].

It has been reported that the extraction mechanism with TODGA involves reverse micelle formation with four TODGA molecules [105], which results in unusually high distribution coefficients for trivalent actinide ions such as Am(III) and Cm(III) as compared to the tetra- and hexavalent actinide ions [103]. The usual trend of extraction for actinide ions with analogous extractants such as CMPO, malonamides, etc., is that tetravalent ions are more extracted than the hexavalent ions, which in turn are more extracted than the trivalent actinide ions. On the other hand, the trend observed in case of TODGA is $M^{3+} > M^{4+} >> MO_2^{2+}$. As diluents have a very important role in the formation of reverse micelles, the extraction trends and also the species extracted vary significantly with the nature of the diluent. To exclude the effect of the diluent, the ligating sites can be appended onto a molecular platform. Since four diglycolamide molecules are required for the reverse micelle formation, calix[4]arene is considered as the ideal platform or scaffold. It is known that calixarenes appended with actinide specific ligating sites such as CMPO give rise to more efficient metal ion binding and extraction based on a co-operative complexation mechanism [106]. Similarly, diglycolamide functional groups preorganized at the C-pivot and trialkylphenyl platforms showed good extraction efficiencies of Eu^{3+} and Am^{3+} [68]. In addition, the performance of a tripodal diglycolamide in solvent extraction and supported liquid membrane studies was evaluated for actinide ion extraction [107]. However, very little work has been reported thus far dealing with the diglycolamide-functionalized calixarenes.

Room temperature ionic liquids (RTILs) have generated increasing interest as alternative diluent medium in synthesis [108–111], separation [81,112–115] and electrochemistry [116,117] as a result of their unique chemical and physical properties [118-122]. These solvents exhibit several properties that make them attractive as a potential basis for ‘green’ separation processes which include negligible vapour pressure, a wide liquid range, non flammable nature, tunable viscosity and miscibility and good thermal and radiation stability. Even minor structural variations, either in cationic or anionic moieties, can produce significant changes in their physicochemical properties [123]. This tunability is obviously offering vast opportunities for the design of ionic liquid-based separation systems, and also poses formidable challenges to separation scientists. Significant studies have been reported on the extraction of Sr^{2+} from acidic nitrate media by dicyclohexano-18-crown-6 [124], uranyl ion by a CMPO–TBP (tri-n-butyl phosphate) mixture [125], Ag^{+} by calix[4]arenes [126] and Eu^{3+} by 2-thenoyltrifluoroacetone (TTA) from a perchlorate acid medium [127] by various water immiscible N,N′-dialkyl imidazolium- based ionic liquids. Odinets et al. synthesized a novel class of functionalized ionic liquids with grafted CMPO moieties for the recovery of actinides and rare earth elements [91]. Attempts were also made to understand the mechanism of metal ion transfer and complexation of metal ions in ionic liquids [73,74,128]. Recent reports deal with the use of TODGA for the extraction of alkali metal, alkaline earth metal and lanthanide ions with room temperature ionic liquids as the diluents [129,130]. The structures of the ligands used in this Chapter are as follows.

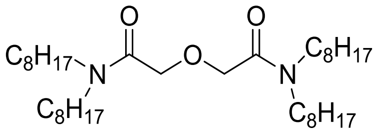

TODGA

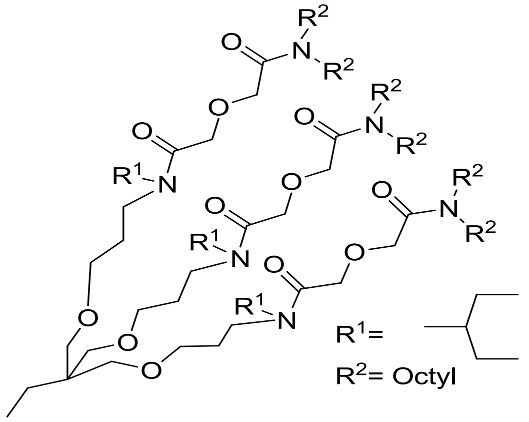

T-DGA

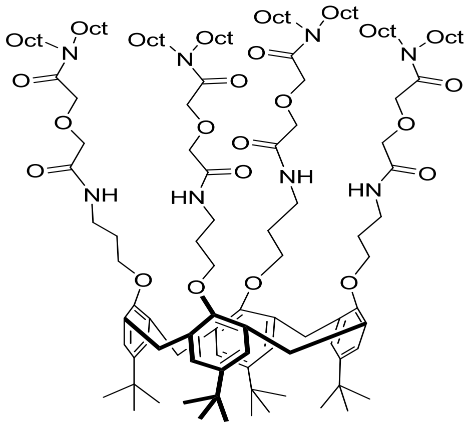

C4DGA

Fig. 3.1: Structures of multiple diglycolamide functionalized ligands used in Chapter 3

3.1. Evaluation of multiple diglycolamide-functionalized ligands in room temperature ionic liquid for extraction of actinides

The present work deals with the extraction of Am(III) from acidic feeds using TODGA in three commercially available room temperature ionic liquids, viz. $[C_4mim][PF_6]$, $[C_6mim][PF_6]$ and $[C_8mim][PF_6]$ (C_nmim^+ = 1-alkyl-3-methylimidazolium). Extraction of Am (III) was also carried out using a calix[4]arene-tetradiglycolamide ligand (abbreviated hence forth as C4DGA) in $[C_8mim][PF_6]$, which displayed a reasonably good solubility of the extractant, favourable kinetics of extraction and reasonably high distribution ratio values. The stoichiometry of the complexes was determined for both the TODGA–RTIL as well as the C4DGA–RTIL extraction systems. The thermodynamic parameters, such as the change in enthalpy, entropy and Gibb's free energy during the extraction of the complexes, were also calculated for both the ligands. Finally, selective extraction of Am^{3+} from UO_2^{2+} and Pu^{4+} was observed when the C4DGA–RTIL extraction system was used leading to possible separation of Am from radioactive wastes containing U, Pu and Am for possible applications in neutron sources, smoke detectors, etc.

3.1.1 Extraction efficiency of Am^{3+} using TODGA-RTIL solvent system

The room temperature ionic liquids used in the present study did not extract Am(III) in the absence of TODGA (**Table 3.1**). Similar behaviour was reported by Shimojo et al. [129] in their studies on lanthanide extraction using a different set of ionic liquids. In the presence of TODGA as the extractant, however, a sharp increase in the D_M-values was observed. The distribution ratio values obtained with 0.01 M TODGA in RTILs are significantly higher than those obtained with TODGA in *n*-dodecane as the organic phase (< 0.1). Similar enhancements in the distribution ratio values were reported with RTILs for Sr(II) extraction using crown ethers

[85,86], for Cs(I) extraction using calix-crown ligands [130-132] and for actinide extraction using a CMPO and TBP mixture. The extractability of Am(III) in the ionic liquids with TODGA as the extractant was found to be [C_4mim][PF_6] > [C_8mim][PF_6] > [C_6mim][PF_6]. Shimojo et al., on the other hand, have shown that the extraction of Eu(III) with TODGA decreased with increase of the alkyl chain length [129]. They have also reported that 10^{-4} M TODGA is capable of extracting Eu(III), a trivalent lanthanide ion of comparable ionic radius as Am(III), when the aqueous phase acidity was 0.01 M. In the present study, a distribution ratio value of ~2500 was obtained for Am(III) with 0.01 M TODGA in [C_4mim][PF_6] from a feed containing 0.01 M HNO_3, which is significantly lower than that reported by Shimojo et al. for Eu(III). Higher extraction of Eu(III) as compared to Am(III) has been reported previously using TODGA as the extractant [62,103].

Table 3.1: D_{Am} values without and with 0.01 M TODGA, time to attain equilibrium D_{Am} values, and physical parameters of the ionic liquids

RTIL	Equilibrium D_{Am} No TODGA	Equilibrium D_{Am} 0.01 M TODGA	Time to attain equilibrium (min)	Dynamic viscosity (mPa. s)	Density (g cm^{-3})
[C_4mim][PF_6]	<0.01	102	60	250.9	1.37
[C_6mim][PF_6]	<0.01	34	60	308.5	1.29
[C_8mim][PF_6]	<0.01	74	180	694.2	1.235

3.1.2 Extraction kinetics

In order to get information on the attainment of the extraction equilibrium, the extraction kinetics was investigated. The kinetics of Am(III) extraction was reported to be fast when TODGA in *n*-dodecane was used as the solvent system [103]. In the present study, the Am(III) extraction kinetics was studied from a 3 M HNO_3 feed solution using 0.01 M TODGA in $[C_n\text{mim}][PF_6]$ with an organic to aqueous volume ratio of 1. The ligand concentration was kept at 1 x 10^{-2} M, which is about 10 times lower than the usual concentration employed for actinide ion extraction in the n-dodecane system. **Fig. 3.2(a)** represents the extraction kinetics of americium with TODGA into $[C_n\text{mim}][PF_6]$. In case of $[C_4\text{mim}][PF_6]$, a sharp increase in the D_{Am} values was observed up to 60 min, beyond which a plateau was observed with a distribution ratio of ~ 100. Similar observations were made in case of $[C_6\text{mim}][PF_6]$ where the D_{Am} value increased with the equilibration time followed by a plateau beyond 60 min with a consistent D_{Am}-value of ~ 35. On the other hand, for $[C_8\text{mim}][PF_6]$, the D_{Am} value increased gradually up to 180 min, followed by a plateau with a D_{Am} value of ~ 70 showing the slowest kinetics among the three RTILs. The observed slower kinetics in all the cases as compared to conventional diluents like *n*-dodecane can be attributed to the high viscosity of the ionic liquids. **Table 3.1** lists the dynamic viscosity data which indicates that $[C_8\text{mim}][PF_6]$ is almost as viscous as the other two RTILs. As a consequence, $[C_8\text{mim}][PF_6]$ showed the slowest kinetics among the three RTILs investigated, though the butyl and the hexyl derivatives exhibited nearly similar extraction kinetics. The Am(III) extraction kinetics was also studied using 1.0 x 10^{-3} M C4DGA in $[C_8\text{mim}][PF_6]$ (**Fig. 3.2(b)**) under identical feed conditions. The concentration of C4DGA was kept 10 times lower than that employed with TODGA as the extractant due to the fact that four diglycolamide moieties are present in C4DGA to make it a superior extractant than TODGA.

The distribution ratio of Am(III) increased sharply up to 180 minutes with a D_{Am} value of about 700 followed by a plateau. Though the viscosity of the resulting organic phase is comparable with that used with TODGA, the slower kinetics may also be due to the conformational rigidity of the C4DGA ligand. Extraction of lanthanides (including Eu^{3+}) by TODGA in RTIL was also extensively studied by Shimojo et al [83].

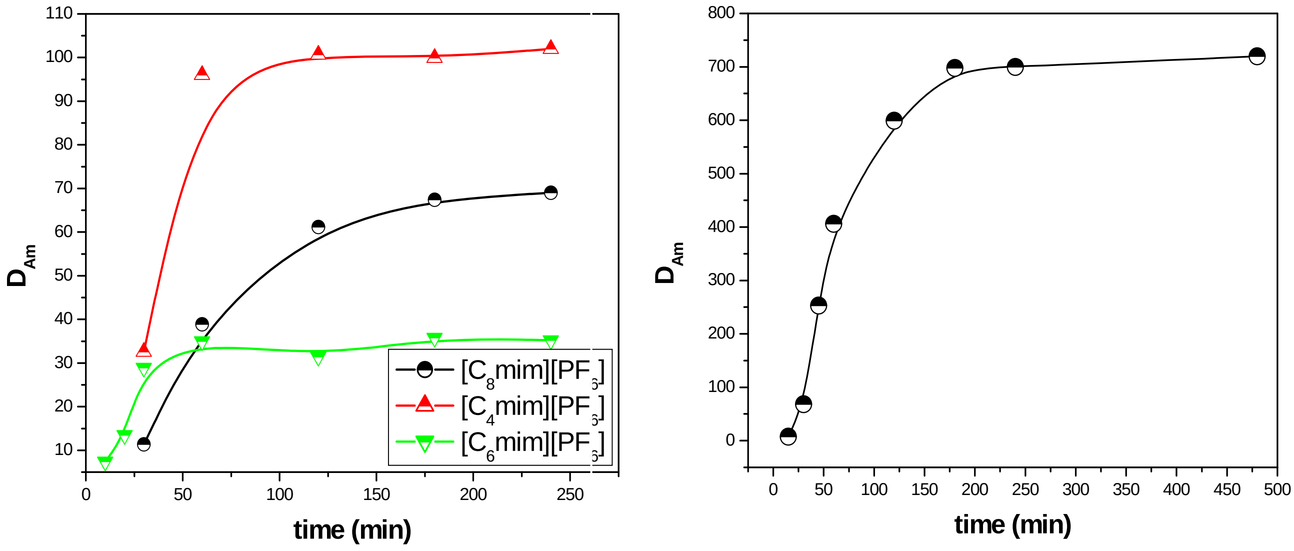

(a) **(b)**

Fig. 3.2: Extraction kinetics of americium from 3 M HNO_3 feed into (**a**) 1.0 x 10^{-2} M TODGA in $[C_nmim][PF_6]$ (n = 4, 6, 8) and (**b**) 1.0 x 10^{-3} M C4DGA in $[C_8mim][PF_6]$

3.1.3 Effect of the number of ligating sites and a substituent on the calix[4]arene

The effect of the number of ligating sites and a substituent on the calix[4]arene extractant was also investigated using $[C_8mim][PF_6]$ as the diluent. For comparison purpose, the concentration of the calix-2DGA (abbreviated as C2DGA and C2DGA-Bu [133]) ligands was taken as 5 x 10^{-4} M and the results of Am(III) extraction from 3 M HNO_3 feed solutions are listed in **Table 3.2**. The equilibration time was fixed at 3 h, similar to that used for the C4DGA as mentioned above. The results showed a significantly lower extraction of Am(III) with the C2DGA compounds, clearly indicating that the C4DGA is far more effective for metal ion extraction. This is in line with observations reported on the extraction behaviour of the three calix[4]arene DGA compounds in *n*-dodecane as the organic diluents [133].

Table 3.2: Extraction of Am(III) with the diglycolamide-functionalized calix[4]arenes from 3 M HNO_3 using 5 x 10^{-4} M extractant in $[C_8mim][PF_6]$

Extractant	D_{Am}
C4DGA	194 ± 2
C2DGA	0.69 ± 0.02
C2DGA-Bu	0.23 ± 0.06

3.1.4 Effect of the feed acidity

Fig. 3.3(a) shows the dependence of the distribution ratio values of Am(III) using 0.01 M TODGA with the change in the feed nitric acid concentration. For all the RTILs, an increase in the feed nitric acid concentration led to a decrease in the Am(III) distribution ratio values. Though a sharp fall was observed in the lower acidity region, plateau like profiles were noticed at higher acidities (beyond 3 M HNO_3). Similar to the trend mentioned above, the highest D_{Am} value (~2500) was obtained at 0.01 M HNO_3 with $[C_4mim][PF_6]$ as the diluent, while the lowest D_{Am} value (~1100) was obtained under identical conditions with $[C_6mim][PF_6]$ as the diluent. A drastic decrease in the D_{Am}-value was observed in the latter case by changing the feed acidity from 1.0 x 10^{-2} M HNO_3 (D_{Am} = 1100) to 2 M HNO_3 (D_{Am} = 58) followed by a moderate decrease in the D_{Am} value with a further increase of the feed acidity. A similar trend was noticed in case of [C_8mim][PF_6] as the diluent, where the D_{Am} value decreased from ~2090 (1.0 x 10^{-2} M HNO_3) to 240 (1.0 M HNO_3), followed by a moderate decrease upon further increase of the feed acidity. The variation of the D_{Am} values with the feed acidity was studied using 7 × 10^{-4} M C4DGA in [C_8mim][PF_6] as the organic phase with a phase ratio of 1 : 1. The equilibration time was kept at 3 h to ensure complete attainment of equilibrium. Also in this case, the D_{Am} values decreased with increasing aqueous phase acidity (**Fig. 3.3(b)**). The D_{Am} value was found to be > 1800 at 1.0 x 10^{-2} M HNO_3, which decreased drastically up to 1.0 M HNO_3 with a D_{Am} value of ~340 with much lower subsequent decrease upon further increase in the aqueous phase acid concentration.

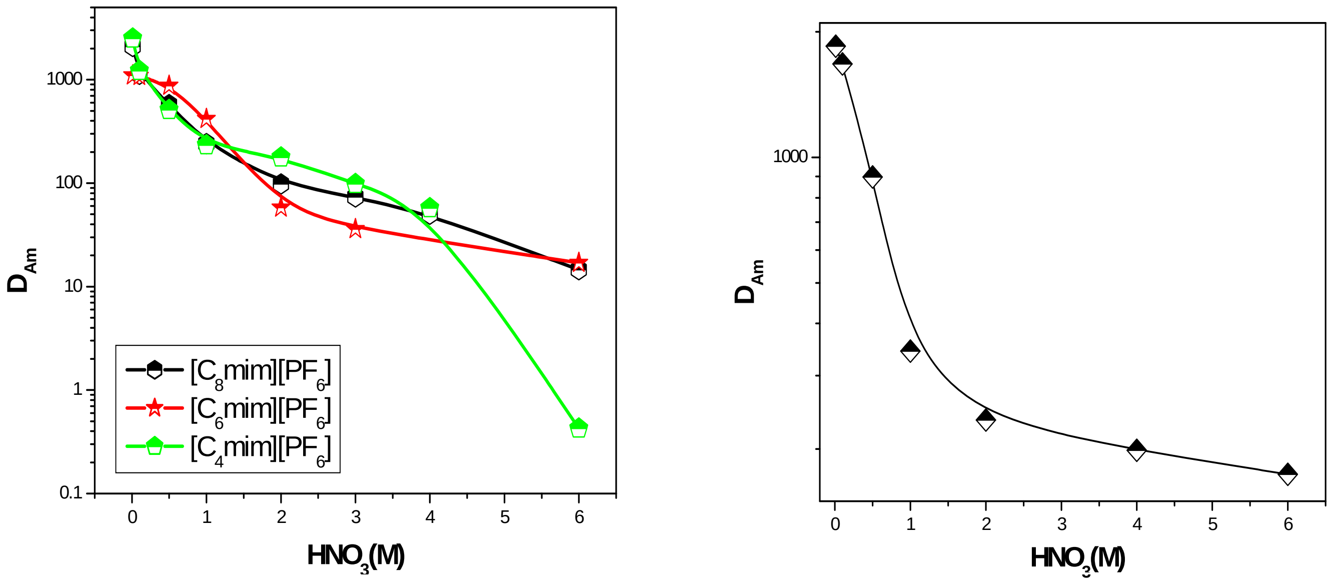

(a) **(b)**

Fig. 3.3: Extraction behavior of americium from different feed acidities into (**a**) 1.0 x 10^{-2} M TODGA in [$C_n$mim][PF_6] (n = 4, 6, 8) and (**b**) 7 x 10^{-4} M C4DGA in [C_8mim][PF_6]

The decrease in the D_{Am} values with increasing feed acidity is entirely opposite to the trend observed with the extraction of actinides with diglycolamide extractants such as TODGA in diluents like *n*-dodecane. The extraction profiles obtained in the present study indicate that the extraction mechanism is not ion-pair type as in case of the conventional diluents such as *n*-dodecane. On the contrary, an ion-exchange mechanism is responsible for the extraction of Am(III) from nitric acid feed to the ionic liquid phase. At higher acidity, the H^+ ions compete with the metal ions in the ion-exchange process resulting in substantially lower D_{Am} values. Extraction of nitric acid was investigated by equilibrating the ionic liquid solutions with 3 M HNO_3 and the results suggested 7.3%, 8.1% and 8.6% extraction of the acid using the *n*-butyl, *n*-hexyl and *n*-octyl derivatives of the ionic liquids using 1.0×10^{-2} M TODGA as the extractant.

3.1.5 Effect of the DGA ligand concentration

The extraction of Am(III) with varying TODGA concentration was also investigated in the three RTILs and the results are presented in **Fig. 3.4(a)**. An increase in Am(III) extraction with increasing TODGA concentration in the ionic liquids was observed. This indicates that the extracted species contains one or more TODGA molecule(s). A similar increase in Am(III) extraction was observed with C4DGA in $[C_8mim][PF_6]$ as the diluent (**Fig. 3.4(b)**). Shimojo et al. reported a similar trend in the extraction of lanthanide ions with TODGA in ionic liquids [129]. It was of interest to understand the nature of the extracted species and the number of TODGA molecules associated with this.

In view of the above observations, the extraction of Am(III) using TODGA in ionic liquids can be best represented by an ion exchange mechanism as per the following equation,

$$Am^{3+}_{aq} + nTODGA_{IL} + 3C_nmim^{+}_{IL} = Am\,(TODGA)_n{}^{3+}_{IL} + 3C_nmim^{+}_{aq} \qquad (3.1)$$

where, species with the subscripts 'aq' and 'IL' refer to those in the aqueous and the ionic liquid phases, respectively. A strong influence of hydrogen ion on Am(III) extraction can be explained on the basis of a competing equilibrium reaction as follows:

$$H^{+}_{aq} + TODGA_{IL} + C_nmim^{+}_{IL} = H.\,TODGA^{+}_{IL} + C_nmim^{+}_{aq} \qquad (3.2)$$

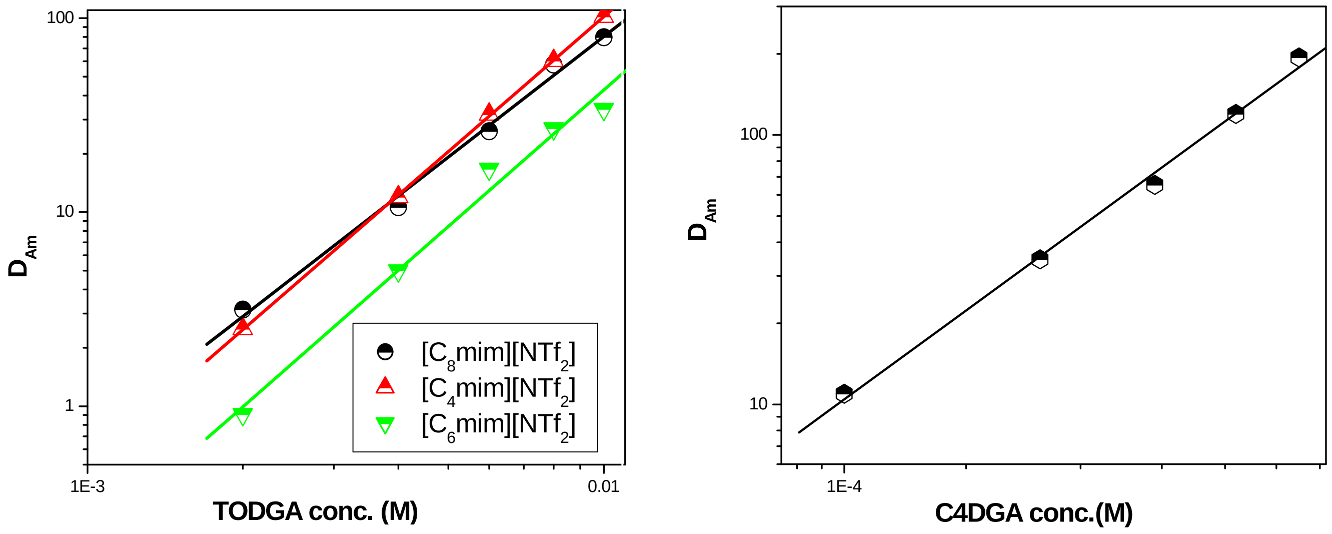

(a) **(b)**

Fig. 3.4: D_{Am} at varying (**a**) TODGA concentrations from 3 M HNO_3 feed into [$C_n$mim][PF_6] (n = 4, 6, 8) and (**b**) C4DGA concentrations from 3 M HNO_3 feed into [C_8mim][PF_6]

Formation of adducts of TODGA with nitric acid is well reported [103] and could be attributed to be the reason for a sharp decrease in the D_{Am} values with increasing acidity. In case of molecular diluents like *n*-dodecane, though $HNO_3{\cdot}TODGA$ adduct also gets extracted, the effect of decreasing D_{Am} with acidity leading to a plateau is seen only at higher acidities [103]. On the other hand, the increasing extraction with increasing acidity seen at lower acidities is due to increasing nitrate ion concentration (nitrate ion is part of the extracted species).

In case of room temperature ionic liquids, the decrease in D_{Am} with increasing acid concentration is seen in the entire range of acidity (**Fig. 3.4**) which corroborates the fact that the extracted species does not contain nitrate ion and the ion-exchange mechanism as indicated above is prevailing. A similar ion-exchange extraction mechanism was reported for the extraction of lanthanide ions using TODGA [131]. If D_{Am} is the distribution ratio, P_{Cnmim+} represents the partition coefficient of the ionic liquid and K_{Am} the equilibrium constant for the extraction of Am(III), then it can be written that

$$K_{Am} = ([Am(TODGA)_n{}^{3+}]_{IL}\ [C_nmim^+]_{aq}{}^3)\ /\ ([Am^{3+}]_{aq}\ [TODGA]_{IL}{}^n\ \ [C_nmim^+]_{IL}{}^3) \quad (3.3)$$

Or, substituting D_{Am} for the term $[Am(TODGA)_n{}^{3+}]_{IL}\ /[Am^{3+}]_{aq}$ one obtains

$$K_{Am} = D_{Am} / ([TODGA]^n{}_{IL}\ .\ P_{Cnmim+} \qquad (3.4)$$

Taking the logarithm and rearranging:

$$\log D_{Am} = \log K_{Am} + \log P_{Cnmim+} + n \log [TODGA] \qquad (3.5)$$

A plot of log D_{Am} vs. the concentration of TODGA or C4DGA should result in straight lines with a slope ‘n’, i.e. the number of TODGA or C4DGA molecules associated with the complex formed during the extraction and the intercept represents log K_{Am} + log P_{Cnmim+}. On the basis of eqn (3.5), a slope analysis was conducted as a function of the equilibrium concentration of a ligand in $[C_nmim][PF_6]$ (n = 4, 6, 8) and used to determine the fundamental stoichiometry of the Am(III) – diglycolamide complex formed in 3 M HNO_3 feed. **Fig. 3.4(a)** represents the variation in the log D_{Am} value with the TODGA concentration. The straight line plots of log D_{Am} vs log [TODGA] have slope values of 2.23 ± 0.07, 2.29 ± 0.06 and 2.02 ± 0.07 where $[C_4mim][PF_6]$, $[C_6mim][PF_6]$ and $[C_8mim][PF_6]$ were used as diluents, respectively. Fractional slope values (**Fig. 3.4(a)**) indicated extraction of mixed species of 1 : 2 as well as 1 : 3 M: L compositions. Extraction of mixed species has previously been reported in case of molecular diluents [62,103]. However, Shimojo et al., reported extracted species with 1 : 3 stoichiometry for lanthanide ion extraction using $[C_nmim][NTf_2]$ as the ionic liquid medium [129]. The extraction of Am(III) with TODGA can thus be expressed as

$$Am^{3+}_{aq} + xTODGA_{IL} + 3C_nmim^{+}_{IL} = Am[TODGA]_x{}^{3+}_{IL} + 3C_nmim^{+}_{aq} \qquad (3.6)$$

A similar study was carried out to determine the stoichiometry of the complex formed by americium with C4DGA in $[C_8mim][PF_6]$. The log D_{Am} vs. log[C4DGA] plot (**Fig. 3.4(b)**) yielded a slope value of 1.8 indicating the extraction both ML and ML_2 type of species from 3 M HNO_3 with the latter being present predominantly in the ionic liquid phase. However, this is rather unusual in view of the large coordination number feasible with the 1:2 (M:L) species with 24 coordinating atoms present around the metal ion. Earlier studies involving a tripodal diglycolamide ligand has also shown complexes with rather high coordination number [107]. The extraction of Am (III) with C4DGA can be represented by the following equilibrium reaction as:

$$Am^{3+}_{aq} + 2C4DGA_{IL} + 3C_nmim^{+}_{IL} = Am[C4DGA]_2{}^{3+}_{IL} + 3C_nmim^{+}_{aq} \qquad (3.7)$$

For a particular range of ligand concentration the ratio $[C_n\text{mim}^+]_{IL}$ / $[C_n\text{mim}^+]_{aq}$ can be regarded as constant (the aqueous phase is saturated with $[C_n\text{mim}][PF_6]$ salt) and, therefore, the conditional extraction constant K'_{Am} can be given as:

$$K'_{Am} = [Am\cdot L_2{}^{3+}]_{IL} / [Am^{3+}]_{aq} [L]_{IL}{}^2 \tag{3.8}$$

where, L represents the extractant (TODGA or C4DGA when the two ligand molecules are assumed to be present in the extracted species). Substituting D_{Am} for the term $[Am\cdot L_2{}^{3+}]_{IL}$ / $[Am^{3+}]_{aq}$, one obtains

$$K'_{Am} = D_{Am} / [L]_{IL}{}^2 \tag{3.9}$$

$$\log D_{Am} = \log K'_{Am} + 2 \log[L]_{IL} \tag{3.10}$$

The K'_{Am} value is calculated from the intercept of a plot of log D vs. log $[\text{TODGA}]_{IL}$ at a constant nitric acid concentration. K'_{Am} was calculated for Am(II) extraction by TODGA in $[C_n\text{mim}][PF_6]$ (n = 4, 6, 8) and by C4DGA in $[C_8\text{mim}][PF_6]$. The complex formation equilibrium in an ionic liquid can be described by the following equations.

$$Am^{3+}{}_{IL} + 2L_{IL} = [Am \cdot L_2]^{3+}{}_{IL} \tag{3.11}$$

$$K_{form} = [Am \cdot L_2{}^{3+}]_{IL} / [Am^{3+}]_{IL} [L]_{IL}{}^2 \tag{3.12}$$

$$K_{form} = K'_{Am} [Am^{3+}]_{aq} / [Am^{3+}]_{IL} \tag{3.13}$$

$$K_{form} = K'_{Am} / P_{Am} \tag{3.14}$$

where P_{Am} is the partition coefficient of Am^{3+} in ionic liquids defined as the ratio of $[Am^{3+}]_{IL}$ to $[Am^{3+}]_{aq}$. **Table 3.3** lists the extraction constants (K'_{Am}) of Am(III) with TODGA as well as

C4DGA in [$C_n$mim][PF_6]. As indicated in **Table 3.1**, the P_{Am} values are <0.01 suggesting that the K_{form} values are approximately two orders of magnitude higher as compared to the extraction constants. The acid uptake for TODGA and C4DGA in [C_8mim][NTf_2] was found to be 7% and 11%, respectively. The extraction of HNO_3 by pure RTIL, TBP-RTIL and other RTIL based solvent systems was reported in the literature [78, 141, 154]

Table 3.3: Extraction (K'_{Am}) constants of Am(III) from 3 M HNO_3 at 298 K

Ligand	Diluent	Log K'_{Am}
1 x 10^{-2} M TODGA	[C_4mim][PF_6]	6.45 ± 0.18
	[C_6mim][PF_6]	6.24 ± 0.13
	[C_8mim][PF_6]	5.92 ± 0.17
5 x 10^{-4} M C4DGA	[C_8mim][PF_6]	8.26 ± 0.15

3.1.6 Determination of thermodynamic parameters

The effect of temperature on the extraction of americium from 3 M HNO_3 by 1.0 x 10^{-2} M TODGA or 5 x 10^{-4} M C4DGA into [C_8mim][PF_6] was studied as this RTIL gave reasonably high distribution coefficient values with faster extraction kinetics. The distribution ratio of Am(III) either with TODGA (**Fig. 3.5(a)**) or with C4DGA (**Fig. 3.5(b)**) was found to decrease with increasing temperature, indicating the extraction process to be exothermic. The change in enthalpy (ΔH) during the complexation can be calculated by using the Van't Hoff equation:

$$\Delta H = -2.303\ R\ \Delta \log D / \Delta(1/T) \qquad (3.15)$$

A plot of log D vs. 1/T gives a straight line with a slope of $-\Delta H/2.303\ R$, while the change in Gibb's free energy (ΔG) can be calculated from the following equation

$$\Delta G = - 2.303\ RT \log K'_{Am} \tag{3.16}$$

The change in entropy (ΔS) at a particular temperature can be calculated using the equation

$$\Delta G = \Delta H - T\Delta S \tag{3.17}$$

The thermodynamic parameters calculated for the two extraction systems are summarized in **Table 3.4**. The ΔH values, calculated from the slope of the log D vs. 1/T plot, are −71.61 kJ mol^{-1} and −86.93 kJ mol^{-1}, respectively, for TODGA and C4DGA using $[C_8mim][PF_6]$ as the diluent. The overall enthalpy change during extraction (ΔH) is a sum of the contribution due to dehydration of the metal ion (ΔH_1), formation of the complex (ΔH_2), and the partitioning of the complex species into the organic phase (ΔH_3). The favourable ΔH in C4DGA over TODGA can be mainly attributed to the contributions from ΔH_2 and ΔH_3. Due to the pre-organized structure and higher lypophilicity of C4DGA, ΔH_2 and ΔH_3 values for C4DGA complexes are suggested to be larger than those of respective TODGA complexes.

The ΔG calculated from eqn (3.17) shows that the extraction of Am(III) by C4DGA ($\Delta G = -46.53$ kJ mol^{-1}) is thermodynamically more favoured than that by TODGA ($\Delta G = -34.63$ kJ mol^{-1}), which is also reflected in their D_{Am} values. On the other hand, the negative entropy change in case of TODGA ($\Delta S = -123$ J mol^{-1}) as well as C4DGA ($\Delta S = -135$ J mol^{-1}) can be attributed to the loss of rotational entropy of the ligands during complexation.

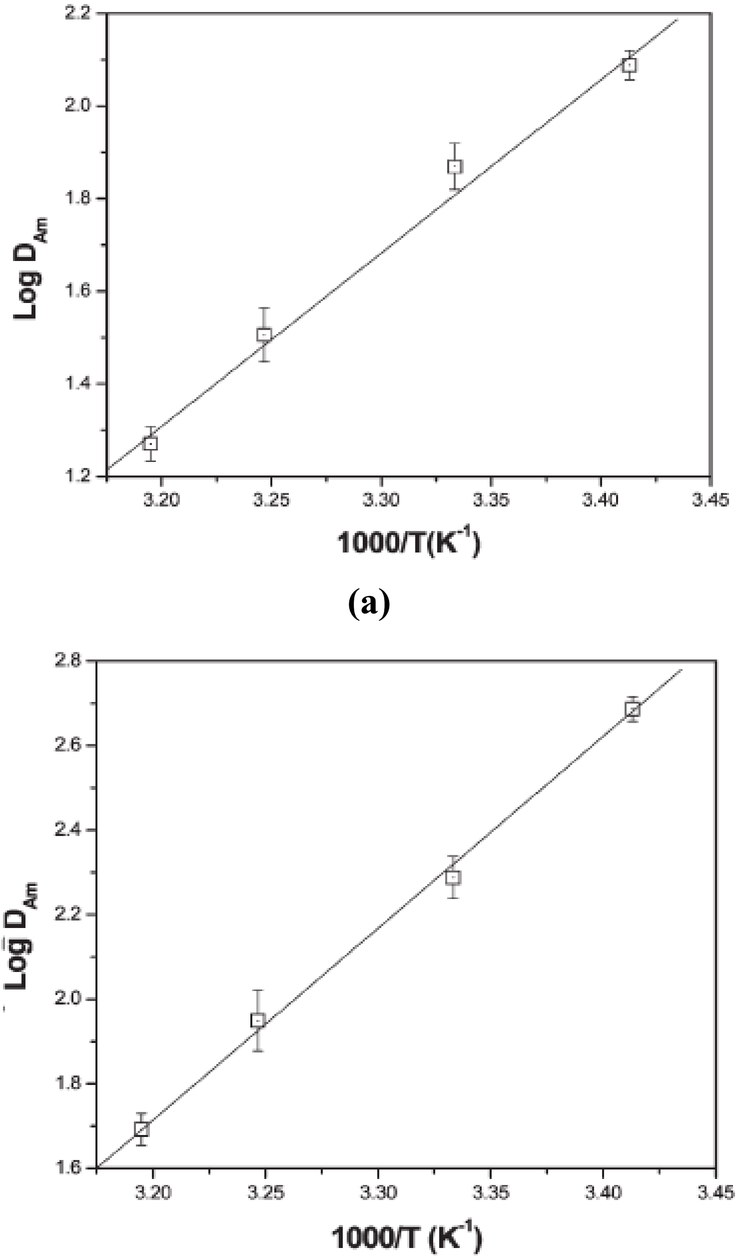

(a)

(b)

Fig. 3.5: Variation in distribution ratio of americium at (**a**) different temperatures from 3 M HNO_3 feed using 1.0 x 10^{-2} M TODGA in [C_8mim][PF_6] and (**b**) different temperatures from 3 M HNO_3 feed using 5 x 10^{-4} M C4DGA in [C_8mim][PF_6]

Table 3.4: Thermodynamic parameters (ΔG, ΔH and ΔS) of americium extraction from 3 M HNO_3 using TODGA/C4DGA in $[C_8mim][PF_6]$ at 300 K

Ligand	ΔG (kJ mol^{-1})	ΔH (kJ mol^{-1})	ΔS (J mol^{-1} K^{-1})
1.0 x 10^{-2} M TODGA	−34.64	−71.61	−123
5.0 x 10^{-4} M C4DGA	−46.53	−86.93	−135

3.1.7 Extraction of actinides

Solvent extraction studies of several other actinide ions such as UO_2^{2+}, Np^{4+}, Pu^{4+}, and PuO_2^{2+} were carried out and the results are listed in **Table 3.5**. As most radioactive wastes consist of long lived fission product nuclides such as ^{90}Sr ($t_{1/2}$: 28.5 y) and ^{137}Cs ($t_{1/2}$: 30.1 y), distribution data of Sr (II) and Cs (I) obtained using 1 x 10^{-2} M TODGA and 5 x 10^{-4} M C4DGA in $[C_8mim][PF_6]$ from 3 M HNO_3 feed solutions are also included in **Table 3.5**. It is interesting to note that the D values for Am(III), Np(IV), and Pu(IV) are significantly higher compared to those obtained with other metal ions, viz. PuO_2^{2+}, UO_2^{2+}, Cs^+ and Sr^{2+}, indicating the effectiveness of TODGA in RTIL for selective actinide ion extraction.

Table 3.5: Distribution data of actinides and fission products from 3 M HNO_3 feed solutions using TODGA and C4DGA as the extractant in $[C_8mim][PF_6]$ as the diluents

	Distribution coefficient values using DGA extractants	
Metal ion	TODGA	C4DGA
Am^{3+}	75	194
Pu^{4+}	30.7	20.6
PuO_2^{2+}	1.19	0.64
UO_2^{2+}	0.52	0.19
Np^{4+}	3.92	7.46
Sr^{2+}	0.024	0.017
Cs^{+}	0.12	0.15

Interestingly, the D_{Am} values with C4DGA are much higher than those obtained with TODGA, while the D values for U(VI) and Pu(VI) are significantly lower with C4DGA than with TODGA. The low extraction of U and Pu in the hexavalent oxidation state though not very surprising, may be based on the unusual coordination geometry of the actinyl ion and the strain associated with complex formation using the ligand. The separation factor values (defined as the ratio of the distribution ratio values of the concerned metal ions) were determined for the metal ions Am–U and Am–Pu in both extractants, viz. TODGA and C4DGA, in $[C_8mim][PF_6]$ as well as *n*-dodecane (the conventional diluents used for metal ion separations, especially actinide separations) and the results are listed in **Table 3.6**. It was interesting to note that the ionic liquid medium showed an unusually high enhancement in the separation factor values of the metal ions as compared to *n*-dodecane. Moreover, C4DGA was found to be a superior extractant from the actinide separation point of view as well. Finally, the combination of C4DGA in [C_8mim][PF_6] results in a highly efficient separation system for Am(III) extraction (**Table 3.6**).

Table 3.6: Comparative separation behaviour in the ionic liquid ([C_8mim][PF_6]) and conventional diluent with TODGA and C4DGA

Solvent system	SF_{AmU} (D_{Am}/D_U)	SF_{AmPu} (D_{Am}/D_{Pu})
TODGA – *n*-dodecane[a]	132	25
TODGA – [C_8mim][PF_6][a]	144	63
C4DGA – *n*-dodecane[b]	45	173
C4DGA – [C_8mim][PF_6][b]	1021	303

Note: [a] 1.0×10^{-2} M TODGA was used. [b] 5.0×10^{-4} M C4DGA was used.

3.1.8 Selective Am(III) extraction from waste

These results are encouraging and can be applied for the selective extraction of Am from radioactive wastes containing Am, U and Pu (usually present in high level radioactive wastes or PUREX process raffinates). A synthetic sample containing U (^{233}U tracer was used as a surrogate due to the very long half life of natural U), Pu and Am in 3 M HNO_3 was subjected to treatment with AgO, followed by extraction with 5×10^{-4} M C4DGA in [C_8mim][PF_6]. The alpha spectra of the aqueous phase before and after the extraction are presented in **Fig. 3.6**. Complete extraction of Am with almost no uptake of U and Pu is clearly demonstrated by this study suggesting that selective Am recovery from high level waste can be performed using C4DGA in RTIL. This is of interest due to its use as a neutron source (Am–Be source) or in smoke detectors.

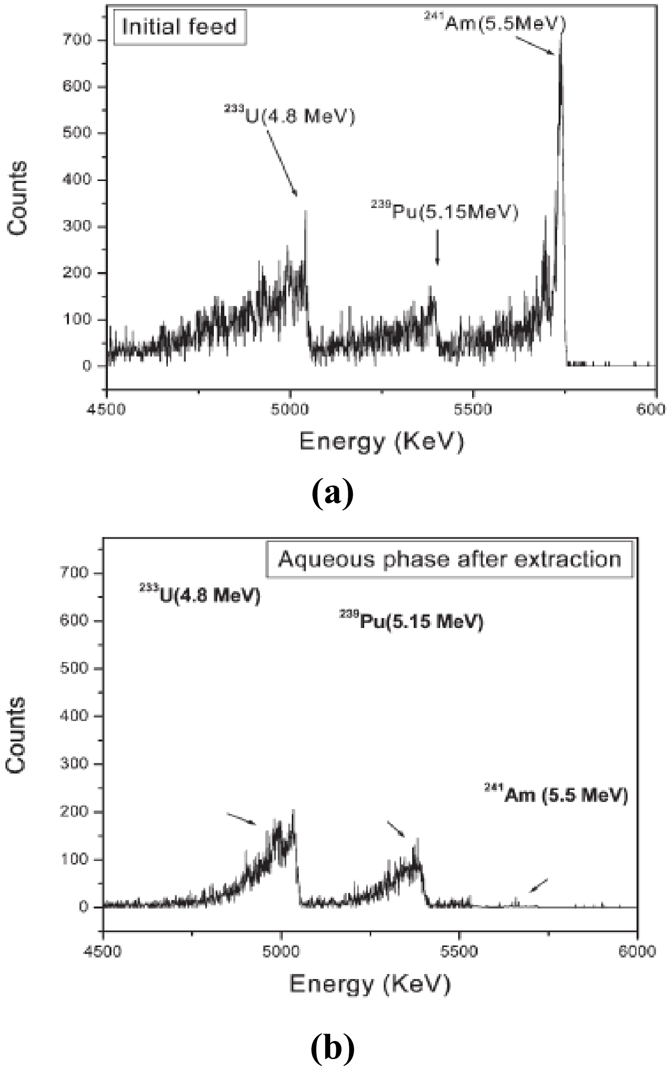

Fig. 3.6: Alpha spectra of the aqueous feed solution (3 M HNO_3): (**a**) before and (**b**) after extraction using 5 x 10^{-4} M C4DGA in $[C_8mim][PF_6]$

3.2. Extraction of Am(III) using novel solvent systems containing a tripodal diglycolamide ligand in room temperature ionic liquids

Diglycolamide extractants, such as N,N,N',N'-tetra-*n*-octyl diglycolamide (TODGA) have been found to be significantly more effective for minor actinide partitioning as compared to CMPO and several counter-current test runs have been carried out using ‘hot’ radioactive waste solutions [134,135]. On the other hand, functionalized diglycolamides were found to be more efficient than TODGA and a tripodal diglycolamide (T-DGA) has shown unique actinide extraction properties [68,107]. Usually, the dielectric constant of the diluent decides the number of extractant molecules being associated in the extracted species [62,136]. With TODGA as the extractant, the number of extractant molecules in the extracted species vary from 2 for nitrobenzene (dielectric constant of 35.6 [137]) to 4 for *n*-dodecane (dielectric constant of 2.012 [137]) for Am (III) bearing extracted species [62,136]. The objective of using the tripodal diglycolamide extractant is to discount this diluent dependent metal ion extraction and to enable the formation of large organophilic complexes with high distribution ratio values in any diluent system. Furthermore, in view of the improved extraction and separation behaviour of room temperature ionic liquids, it was of interest to carry out actinide extractions using T-DGA in ionic liquids.

The present work deals with the extraction of Am(III) from acidic feed solutions using a tripodal diglycolamide (T-DGA) in three commercially available room temperature ionic liquids, viz. [C_4mim][NTf_2], [C_6mim][NTf_2] and [C_8mim][NTf_2]. The extraction data are compared with those obtained with TODGA which has been used in several process test runs. In addition to the effects of equilibration time and feed acidity, the stoichiometry of the complexes, the thermodynamic parameters, and the radiolytic stability are also studied.

Though no extraction of Am(III) was noticed with RTIL alone (D_{Am} < 0.01), in the absence of the extractants TODGA or T-DGA, a sharp increase in the D_M values was observed when a small amount (about 1.0 x 10^{-3} M) of the extractant was added to the ionic liquid phase. With comparable concentrations of the extractants, the D_M values obtained with RTILs were significantly higher than those obtained with molecular diluents in the organic phase [107]. This is in line with the observations made by Nakashima et al. [82], during their studies on lanthanide extraction using CMPO dissolved in RTILs.

They have also reported that ionic liquids with NTf_2^- counter anions extracted the metal ions more efficiently as compared to those with PF_6^- counter anions. The extraction data for Am(III) are listed in **Table 3.7** with the three ionic liquids, viz. [C_4mim][NTf_2], [C_6mim][NTf_2] and [C_8mim][NTf_2] and 1.0 x 10^{-3} M concentration of both the extractants. For comparison purposes, D_{Am} values in molecular diluents, viz. *n*-dodecane and an *n*-dodecane/*iso*-decanol mixture (95% *n*-dodecane + 5% *iso*-decanol) are also included in **Table 3.7**. As reported in the literature, T-DGA has limited solubility in *n*-dodecane alone and is fairly soluble in the diluent mixture, *n*-dodecane and iso-decanol (95% *n*-dodecane + 5% *iso*-decanol) [107]. The observed trend of Am(III) extraction in T-DGA is [C_4mim][NTf_2] > [C_6mim][NTf_2] > [C_8mim][NTf_2], which is similar to that reported in several systems such as the extraction of Am^{3+} and UO_2^{2+} using CMPO and TODGA as the extractants, respectively [138,139]. Apparently, the relatively higher aqueous solubility of the butyl form of the ionic liquid was responsible for the higher metal ion extraction as will be discussed below.

Table 3.7: Distribution data of Am(III) using 1.0 x 10^{-3} M TODGA and T-DGA in room temperature ionic liquids from aqueous nitric acid feed solutions

	D_{Am} with T-DGA				D_{Am} with TODGA			
$[HNO_3]$, M	$[C_4mim][NTf_2]$	$[C_6mim][NTf_2]$	$[C_8mim][NTf_2]$	*n*-dodecane*	$[C_4mim][NTf_2]$	$[C_6mim][NTf_2]$	$[C_8mim][NTf_2]$	*n*-dodecane
3	0.6	0.2	0.17	30.1	0.25	0.13	0.12	0.003
0.5	91.1	32	3	0.05	0.76	0.29	0.22	0.002
1 x 10^{-2}	1518	161	105	0.02	208	27.9	26.2	5.0 x 10^{-4}

Note: D_{Am} values in the absence of the extractants were typically ~0.01 in all the three ionic liquids; * Containing 5% *iso*-decanol

3.2.1 Extraction kinetics

Though extraction kinetics is an important parameter in all liquid–liquid extraction studies, it requires great significance in studies involving ionic liquids as these diluents invariably have higher viscosities as compared to the molecular diluents. The extraction kinetics of Am(III) was studied from a feed solution containing 1.0 x 10^{-3} M T-DGA in $[C_n\text{mim}][\text{NTf}_2]$. **Fig. 3.7** represents the extraction kinetics data up to a period of 4 h, within which, complete attainment of the equilibrium was seen for all the three RTILs. The rate of attainment of equilibrium follows the trend: $[C_4\text{mimNTf}_2] > [C_6\text{mim}][\text{NTf}_2] \sim [C_8\text{mim}][\text{NTf}_2]$, suggesting that while 1 h is sufficient for the butyl derivative, 2 h are required for both the *n*-hexyl and *n*-octyl derivatives of the ionic liquids. The observed slower kinetics in all cases as compared to the conventional diluents like *n*-dodecane can be attributed to the high viscosity of the ionic liquids. The attainment of the equilibrium was the slowest with $[C_8\text{mim}][\text{NTf}_2]$, while the extraction kinetics was much faster with $[C_4\text{mim}][\text{NTf}_2]$. Though the attainment of the equilibrium with $[C_6\text{mim}][\text{NTf}_2]$ as the diluent should be in between those observed with $[C_4\text{mim}][\text{NTf}_2]$ and $[C_8\text{mim}][\text{NTf}_2]$, the results indicated an Am(III) extraction kinetics with $[C_6\text{mim}][\text{NTf}_2]$ similar to that of $[C_8\text{mim}][\text{NTf}_2]$.

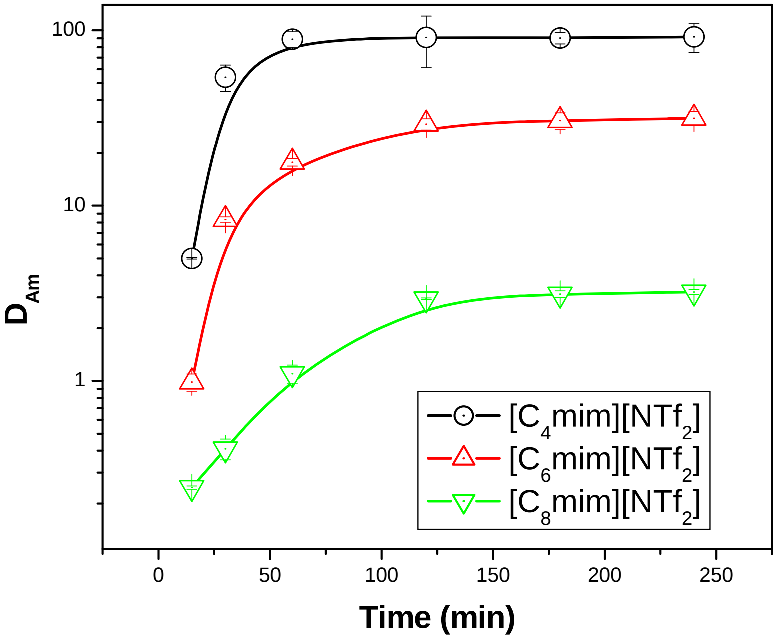

Fig. 3.7: Extraction kinetics of Am from 0.5 M HNO_3 feed into 1.0 x 10^{-3} M T-DGA in $[C_nmim][NTf_2]$ (n = 4, 6, 8)

3.2.2 Relative extraction and separation behaviour

Apart from the Am^{3+} ion, the extraction of several actinide ions viz., UO_2^{2+} and Pu^{4+} was also investigated using 0.5 M HNO_3 as the aqueous feed and 1.0 x 10^{-3} M T-DGA in the ionic liquids as the extractant; the results are listed in **Table 3.8**. Distribution ratio data for some important fission product elements were also determined under identical experimental conditions. The results are included in the table for comparison purposes, the extraction trend being $Eu^{3+} > Am^{3+} > Pu^{4+} > UO_2^{2+} \sim Sr^{2+} > Cs^{+}$. The extractability trend for the elements is similar to that reported with the T-DGA–*n*-dodecane–*iso*-decanol system [107]. The relative extraction behaviour of Am^{3+} vis-a`-vis that of Sr^{2+} and UO_2^{2+} is interesting when compared to those observed with the analogous TODGA–*n*-dodecane system [140].

Table 3.8: Comparative extraction data of actinides and fission product elements using 1.0×10^{-3} M T-DGA in different ionic liquids. Feed: 0.5 M HNO_3

Metal ion	$[C_4mim][NTf_2]$	$[C_6mim][NTf_2]$	$[C_8mim][NTf_2]$
Am(III)	91.1	32.6	3.1
Pu(IV)	30	16.9	1.4
U(VI)	0.24	0.23	0.06
Cs(I)	0.12	0.04	0.01
Sr(II)	0.27	0.12	0.02
Eu(III)	219	64.0	12.7

The separation factor values are listed in **Table 3.9**. Though Sr^{2+} extraction with TODGA– *n*-dodecane system was about 50%, the S.F. (separation factor is defined as D_{Am}/D_{Sr}) value was as high as 302 (**Table 3.9**). On the other hand, the D_{Sr} (0.02) as well as the S.F. (1.08×10^4) values were reported to be favourable for Sr decontamination in T-DGA in *n*-dodecane–*iso*-decanol. It is clearly seen from **Table 3.9** that U decontamination is significantly higher with T-DGA as the extractant, while ionic liquids are less effective than the molecular diluents (*n*-dodecane–*iso*-decanol mixture). On the other hand, a higher U decontamination was observed in T-DGA + ionic liquid solvent systems as compared to the TODGA in *n*-dodecane system. This indicates that the decontamination is due to T-DGA and not due to the ionic liquid, which is the opposite of the trend shown with the C4DGA extractant. For Pu and Eu decontamination, the results are not very favourable and hence are not discussed here (**Table 3.9**).

Table 3.9: Separation factors of Am(III) with respect to other actinides and fission products using T-DGA (1.0×10^{-3} M) in various room temperature ionic liquids. Feed: 0.5 M HNO_3

Extraction system	Separation factors			
	Am(III)/U(VI)	Am(III)/Pu(IV)	Am(III)/Eu(III)	Am(III)/Sr(II)
T-DGA in $[C_4mim][NTf_2]$	380	3.04	0.42	337
T-DGA in $[C_6mim][NTf_2]$	142	1.93	0.51	272
T-DGA in $[C_8mim][NTf_2]$	51.7	2.21	0.24	155
TODGA in *n*-dodecane	28.9	--	1.04	302
T-DGA in *n*-dodecane + *iso*-decanol	895	1.48	--	1.0×10^4

3.2.3 Effect of the feed acidity

Usually, for solvating type extractants, such as TBP, CMPO and TODGA, the extraction of the metal ion increases with increasing the feed acidity, which is based on an increase in the counter anion concentration which helps in the formation of neutral extractable species as per eqn (3.18):

$$M^{n+} + nNO_3^- + mL_{(o)} \leftrightarrow M(NO_3)_n \,.\, mL_{(o)} \qquad (3.18)$$

where, species with the subscript '(o)' indicate those present in the organic phase, while those without any subscript indicate species in the aqueous phase. Though this trend has invariably been observed in molecular diluents such as *n*-dodecane [68], an entirely different trend, i.e., decrease in the metal ion extraction with increasing aqueous feed acidity has been reported in ionic liquids as the diluent due to a ion-exchange mechanism [141], as indicated in eqn (3.19) (subscript ''IL'' means species in ionic liquidphase):

$$Am^{3+} + nT\text{-}DGAIL + 3C_nmim^+_{IL} \leftrightarrow [Am\,(T\text{-}DGA)_n]\,^{3+}_{IL} + 3C_nmim^+ \qquad (3.19)$$

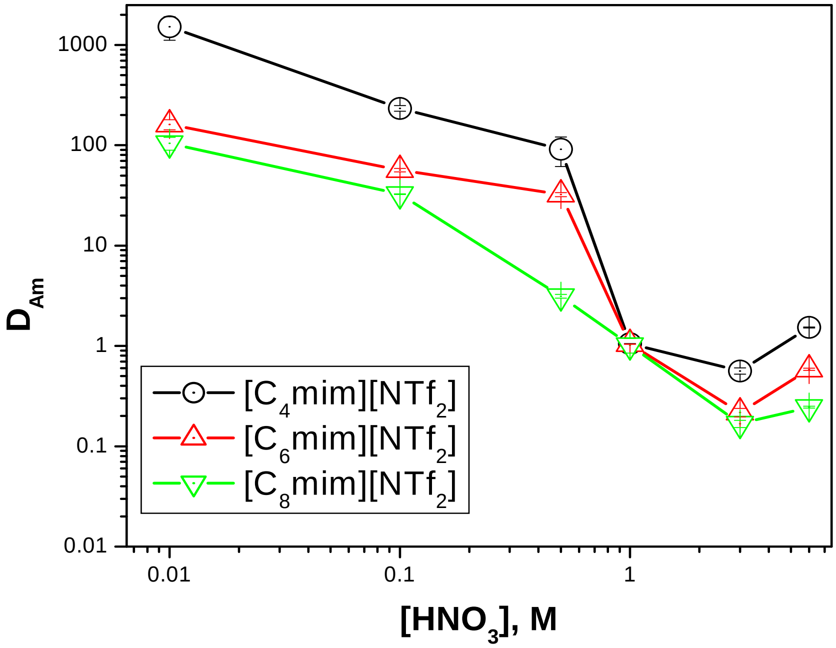

Fig. 3.8: Extraction behavior of Am from different feed acidities into 1.0 x 10^{-3} M T-DGA in $[C_nmim][NTf_2]$ (n = 4, 6, 8) after 3 h of equilibration

As discussed above, eqn (3.19) suggests that a higher solubility of the $[C_nmim^+]$ part of the ionic liquid will result in higher metal ion extraction. **Fig. 3.8** shows the dependence of the distribution ratio of Am(III) with the change in the feed nitric acid concentration for the ionic liquid solvents containing 1.0 x 10^{-3} M T-DGA. It is clear that an increase in the feed nitric acid concentration led to a decrease in the D_M values in the acidity range of 0.01 to 3 M, beyond which a slight increase was noticed. The decrease was less significant for $[C_6mim][NTf_2]$ and $[C_8mim][NTf_2]$ where the D_{Am} values decreased by about 600 – 700 times as compared to about 2700 times when $[C_4mim][PF_6]$ was used as the ionic liquid (**Fig. 3.8**). The extraction profiles obtained in the present study indicate that the extraction mechanism is not the same as that in the case of conventional molecular diluents such as *n*-dodecane and an ion-exchange mechanism is responsible for the extraction of Am(III) to the ionic liquid phase. The ion-exchange mechanism also gets credence from the fact that the extraction of Am(III) increased with decreasing carbon chain length of the RTIL. The decrease in D_{Am} values with n values (solubility of C_nmim^+ in aqueous phase decreases with increase in n values due to more hydrophobic nature) and with the addition of C_nmim^+ in aqueous phase confirmed the 'cation exchange' mechanism is operating in the extraction [49, 73]. As shown in **Fig. 3.8**, there is a marginal increase in the D_{Am} values for all the three ionic liquids beyond 3 M HNO_3. This can be attributed to a solvation mechanism with nitrate ion participation as described previously for a crown ether based extraction system [118].

3.2.4 Effect of T-DGA concentration

In order to get an idea on the nature of the extracted species, the extraction of Am(III) with varying T-DGA concentrations was investigated using all the three RTILs from the aqueous feed solutions (0.1 M HNO_3). The results, presented in **Fig. 3.9**, show an increase in Am(III) extraction with increasing T-DGA concentration for all the three ionic liquids. The slope values of the plots are close to 1 (1.17 ± 0.05 for [C_4mim][NTf_2]; 1.13 ± 0.02 for [C_6mim][NTf_2]; and 1.05 ± 0.04 for [C_8mim][NTf_2]) suggesting that one T-DGA unit is present in the extracted species, which is in sharp contrast to the extracted species found in the molecular diluents containing 95% *n*-dodecane + 5% *iso*-decanol mixture [107]. It is well known that a lower number of ligands may be present in the extracted species with the increasing dielectric constant of the diluents [137]. On the other hand, higher metal ion extraction has been reported with diluents of high dielectric constant even though lesser number of ligand molecules are associated in the extracted complexed species as compared to those with low dielectric constant diluents. In view of this, it is expected that the relatively high dielectric constant of the ionic liquids [142] as compared to the molecular solvents used, would prevent the participation of a second T-DGA unit, which would otherwise lead to 'stereochemical crowding'.

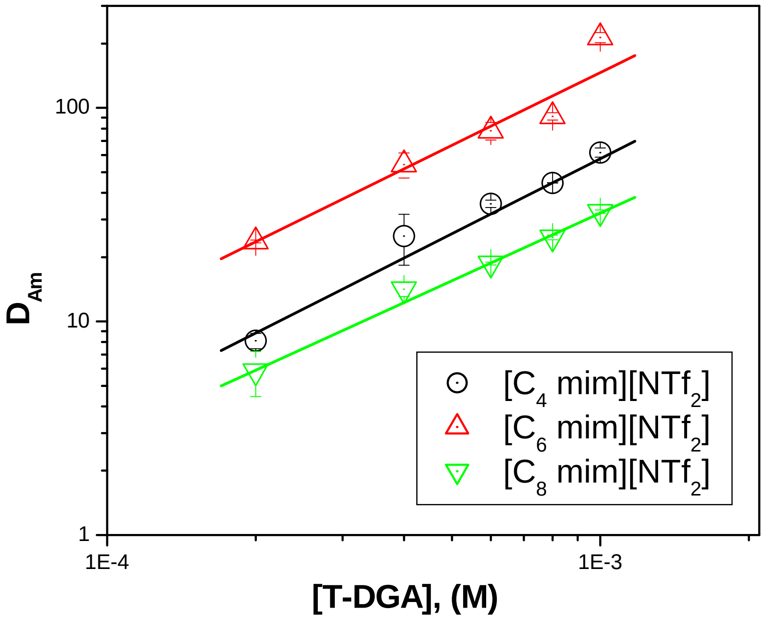

Fig. 3.9: Dependence of Am(III) extraction on varying T-DGA concentrations from

0.5 M HNO_3 feed into $[C_nmim][NTf_2]$ (n = 4, 6, 8)

3.2.5 Stripping studies

With room temperature ionic liquids, the stripping of the metal ions from the ionic liquid phase is one of the major challenges. Usually, with studies involving diglycolamide extractants such as TODGA, the extraction is carried out at higher acidity (3–6 M HNO_3), while the stripping is done at lower acidity (pH - 2.0). However, with ionic liquids as the diluent the D values at pH - 2.0 are very high, which do not decrease significantly with increasing the aqueous phase acidity resulting in ineffective stripping. Nakashima et al. [82], have employed 0.05 M DTPA + 1 M guanidine carbonate, 0.05 M EDTA + 1 M guanidine carbonate and a buffer mixture comprising of 0.1 M citric acid + 0.4 M formic acid + 0.4 M hydrazine hydrate for the effective stripping of rare earth metal ions from ionic liquid extracts. These solutions were employed in the present study for the stripping of Am (III) from the T-DGA in $[C_4mim][NTf_2]$ extracts.

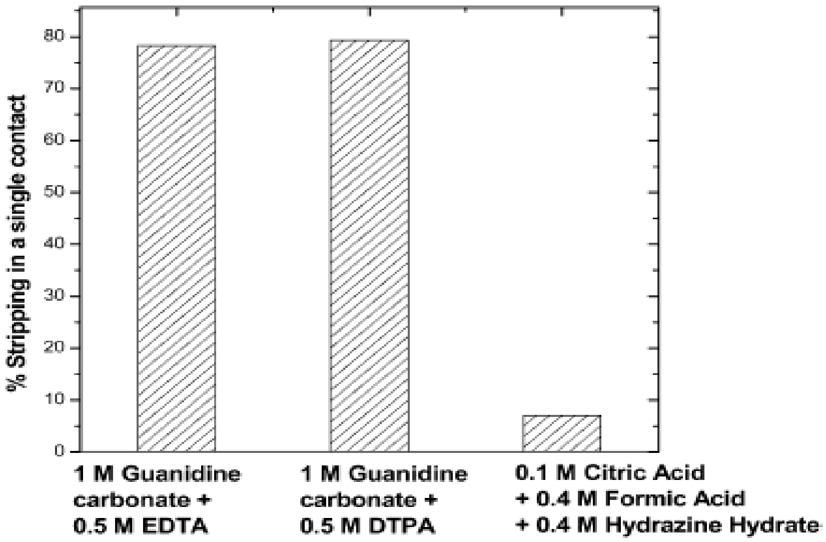

Fig. 3.10: Stripping behaviour of Am(III) from an extract made using 1.0×10^{-3} M T-DGA in $[C_4mim][NTf_2]$

The results are shown in **Fig. 3.10**, which suggest that EDTA and DTPA solutions in 1 M guanidine carbonate are effective as strippant where close to 80% stripping of Am was observed in a single stage. On the other hand, the buffer mixture was not very effective as a strippant as only < 10% stripping was obtained in a single step. The results are encouraging as > 99% stripping of Am(III) is possible using the complexing agents in three stages.

3.2.6 Determination of thermodynamic parameters

With T-DGA as the extractant, significant stereochemical ordering is required during the complexation reaction. The thermodynamic parameters were determined to throw light on the nature of the complexation. Temperature variation studies on Am(III) extraction were carried out from 0.5 M HNO_3 using 1.0 x 10^{-3} M T-DGA in the three RTILs being studied. The Van't Hoff plots (Van't Hoff equation (3.15)) for the distribution ratio data as a function of temperature are presented in **Fig. 3.11**. The change in enthalpy (ΔH) during the complexation was calculated by using the Van't Hoff equation. The slope (ΔH/2.303 R) values of the log D vs. 1/T plots are listed in **Table 3.10**. The Gibb's free energy (ΔG) and the entropy change (ΔS) at a particular temperature were calculated and the thermodynamic parameters are listed in **Table 3.10**. The ΔH values are similar in all the three ionic liquids. Furthermore, the extraction reactions were found to be exothermic in nature. This is possibly due to the large amount of heat required to remove the inner-sphere water molecules of the hydrated metal ion, which is nearly compensated by the strong complexation with the polydentate T-DGA ligand. The complete removal of the inner-sphere water molecules is understood from the very high positive entropy values. Overall, the reactions are spontaneous with large ΔG values. It is quite clear that larger distribution coefficient values in the RTIL system as compared to the molecular diluents resulted in higher extraction constants (log K_{ex}, **Table 3.10**) which are responsible for the large negative ΔG values.

Table 3.10: Extraction data and thermodynamic parameters (ΔG, ΔH and ΔS) of Am(III) extraction from 0.5 M HNO_3 using T-DGA in various room temperature ionic liquids at 300 K

Extractant	Ionic liquid	D_{Am}	Log K_{ex}	ΔG (kJ mol^{-1})	ΔH (kJ mol^{-1})	ΔS (J mol^{-1} K^{-1})
T-DGA	$[C_4mim][NTf_2]$	91	5.56	-31.9	20.6	550
	$[C_6mim][NTf_2]$	32	5.27	-30.3	20.5	450
	$[C_8mim][NTf_2]$	3	4.66	-26.8	20.5	440

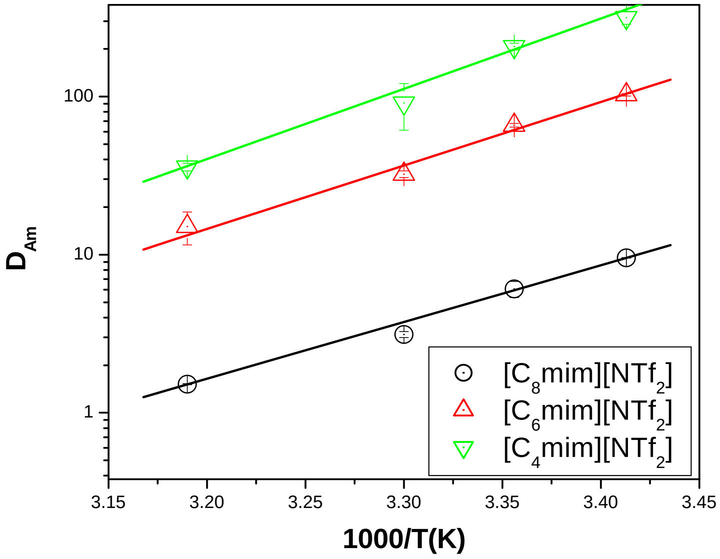

Fig. 3.11: Variation in distribution ratio of Am(III) at different temperatures from 0.5 M HNO_3 feed using 1.0 x 10^{-3} M T-DGA in $[C_nmim][NTf_2]$ (n = 4, 6, 8) after 3 h equilibration.

3.2.7 Radiolytic degradation

A recycling option in process applications for radioactive waste treatment requires that the solvent system should have adequate radiation stability. **Fig. 3.12** shows the changes in the D_{Am} values as a function of the absorbed radiation dose (gamma ray) up to a maximum of 1000 kGy. Interestingly, the decrease in the D_{Am} values was insignificant when the solvents were exposed to a 500 kGy dose for all the three ionic liquids. However, an appreciable decrease in the D_{Am} values was seen when the solvents were exposed to a 1000 kGy radiation dose. It was interesting to note that the D_{Am} value of 91.2 with 1.0 x 10^{-3}M T-DGA in [C_4mim][NTf_2] decreased to 37 when the solvent was irradiated up to a 1000 kGy dose. This decrease is little over 60%, which means that T-DGA is far more stable than a Cs-selective calix-crown extractant containing the same ionic liquid ([C_4mim][NTf_2]) where the decrease was > 95% even for an absorbed dose of 550 kGy [143]. Though the very poor irradiation stability of the Cs-selective solvent system was attributed to the degradation of the ionic liquid leading to acidic products, a similar effect might have affected the D_{Am} values in the present system as well, which is shown by the sharp dependence of the Am(III) extraction on the aqueous phase acidity. On the other hand, Allen et al. [144], have reported that the radiation stability of the ionic liquids is higher than that of diluents like *n*-dodecane, due to the presence of aromatic groups such as the imidazolium group. The radiation stability of solutions of T-DGA in ionic liquids is far higher compared to that of TODGA in a molecular solvent, where the degradation was > 95% for an absorbed dose of 1000 kGy [145]. The amazingly high stability of the solvent system containing T-DGA [C_4mim][NTf_2] may be attributed to the high viscosity of the ionic liquid system (leading to recombination of the free radicals) as compared to the TODGA in *n*-dodecane solvent system. Similar high radiolytic stability of T2EHDGA (a branched homolog of TODGA) was seen when undiluted extractant was irradiated, which can also be attributed to the recombination of the radicals in a viscous medium. These results, together with the very high extraction and effective stripping, suggest that the solvent containing T-DGA in [C_4mim][NTf_2] may be used as a possible 'green' alternative for actinide partitioning instead of TODGA–*n*-dodecane based solvents.

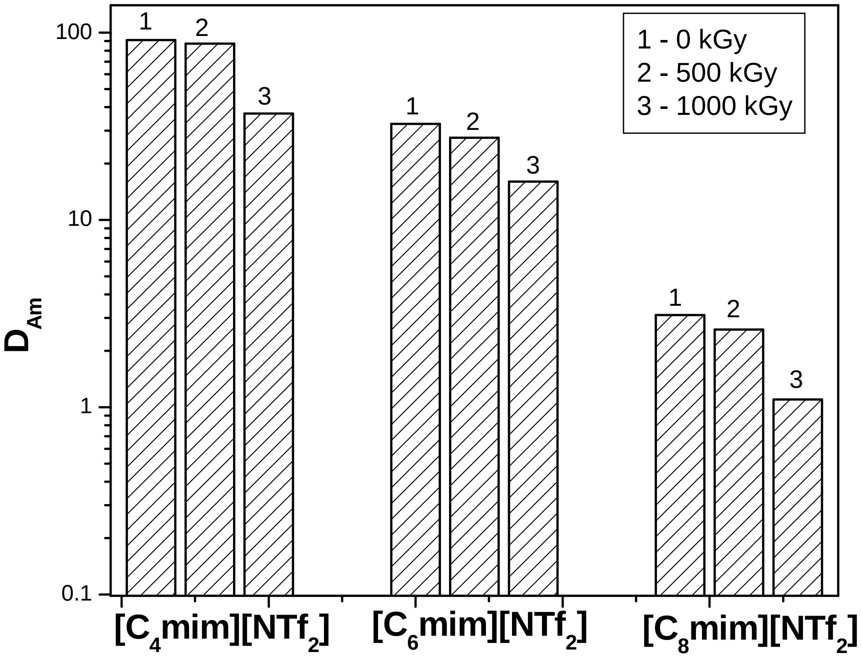

Fig. 3.12: Effect of absorbed dose on the extraction of Am(III) from 0.5 M HNO_3 using 1.0×10^{-3} M T-DGA solutions in [$C_n$mim][NTf_2] (n = 4, 6, 8)

3.2.8 Laser induced fluorescence studies

Though the nature of the extracted species was determined by slope analysis from T-DGA concentration variation studies, further evidence was obtained by time resolved laser fluorescence spectroscopy (TRLFS) using the Eu^{3+} – T-DGA complexes. In view of the similarities in the chemical properties of the trivalent actinides and lanthanides, Eu^{3+} was taken as the surrogate of Am^{3+} and the results of the Eu^{3+} luminescence studies can be extended for the Am^{3+} system as well. Luminescence spectroscopic investigations on the Eu^{3+} aqueous complex and Eu^{3+} – T-DGA complex (both containing 1.0 x 10^{-3} M Eu^{3+}) showed interesting behaviour as the intensity of the characteristics peaks at 617 nm ($^5D_0 \rightarrow {}^7F_2$ hyper sensitive transition, electric dipole), 592 nm ($^5D_0 \rightarrow {}^7F_1$ transition, magnetic dipole), and at 690 nm ($^5D_0 \rightarrow {}^7F_4$ transition, electric dipole, sensitive to Eu^{3+} environment) increased significantly (the former by more than 100 times) when T-DGA was added in an acetonitrile–water mixture as the solvating medium (**Fig. 3.13**). The acetonitrile – water mixture (5: 1) contained dilute nitric acid to prevent hydrolysis of Eu^{3+}. Further, an extract containing the Eu^{3+} – T-DGA complex in [C_4mim][NTf_2] also showed a similar increase in the emission intensities suggesting similarity between the complexes in both the acetonitrile – water mixture and the ionic liquid medium. The mode of complexation was studied by TRLFS, where the presence of inner - sphere water molecules or the lack of them would be reflected in the lifetime of the $^5D_0$ emitting level of the Eu^{3+} – T-DGA complex. It is well known that the luminescence lifetime depends on several radiative (independent of the environment) and non-radiative decay processes and that the number of inner-sphere water molecules is determined by the lifetime of the $^5D_0$ emitting level of Eu^{3+} [146, 147]. Un-complexed Eu^{3+} has nine water molecules in its primary co-ordination sphere. In the presence of nitric acid in the aqueous phase, some nitrate complexation is expected, which can decrease the number of water molecules in the inner hydration sphere, which is also reflected by an increase of the emission lifetime. Furthermore, with a decreasing number of water molecules in the primary hydration sphere, which results in the addition of the T-DGA ligand, the lifetime should show an increasing trend. The fluorescence decay profiles of Eu^{3+} and Eu^{3+} – T-DGA both in the acetonitrile – water mixture and the extract containing the Eu^{3+} – T-DGA complex in $[C_4mim][NTf_2]$ point to the presence of a single complexed species with 1 : 1 stoichiometry in all cases. The lifetime data are presented in **Table 3.11**. The number of water molecules was calculated from the lifetime (τ) using equation 3.20 [148].

$$N_{H2O} = (1.06 / \tau) - 0.19 \tag{3.20}$$

The lifetime of Eu^{3+} in the absence of T-DGA was found to be 0.155 ms, which increased to about 2.5 ms in the presence of the complexing extractant. It has been reported that the Eu^{3+} aqueous ion has a lifetime of 114 ms, which increases in the presence of nitric acid, apparently due to the replacement of some inner-sphere water molecules by the nitrate ions [149]. The appearance of an additional peak at 617 nm indicates a strong interaction with the DGA moieties of T-DGA similar to that observed with the C4DGA ligands which will be discussed in a subsequent Chapter. In case of the extract containing the Eu^{3+} – T-DGA complex in $[C_4mim][NTf_2]$, a similar pattern was observed with a lifetime of 2.5 ms. However, the intensity of the split lines at 617 nm was found to change significantly indicating very strong complex formation with the DGA moieties of T-DGA with practically no inner-sphere water molecules. Comparable lifetimes for extracts made from both 0.01 M and 0.5 M HNO_3 suggested extraction of similar 'inclusion' complex species, in which all the water molecules are replaced by the coordinating sites of the DGA groups.

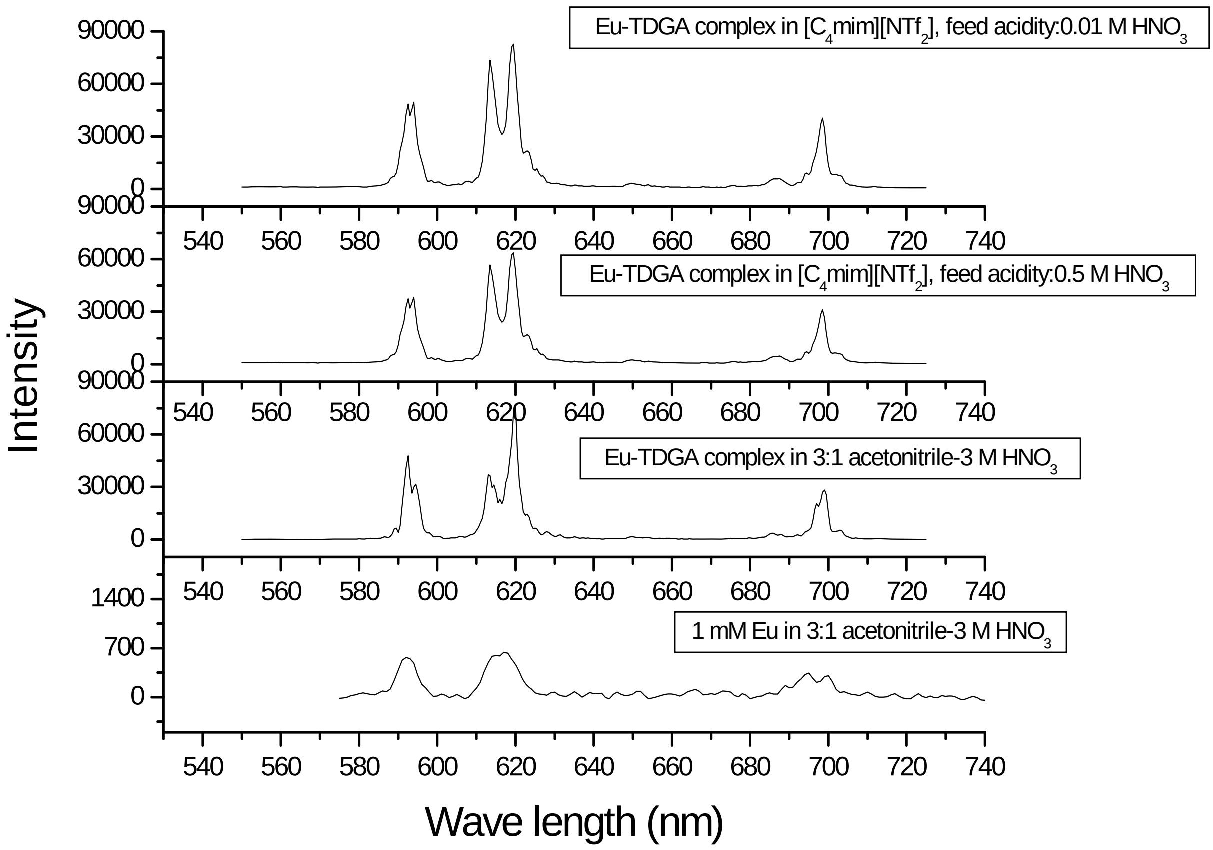

Fig. 3.13: Emission spectra of Eu^{3+} (1.0 x 10^{-3} M) in the absence and presence of T-DGA in acetonitrile : water (5 : 1) and those of the Eu^{3+}–T-DGA extract in $[C_4mim][NTf_2]$ obtained from different feed acidities

Table 3.11: Time resolved laser induced fluorescence spectroscopy data for Eu^{3+} (1.0 x 10^{-3} M) under varying experimental conditions in the absence and presence of T-DGA

Sample	Lifetime (ms)	Inference
Eu in ACN-3 M HNO_3	0.15	6 water; 3 nitrate
Eu – T-DGA complex in ACN–3 M HNO_3	2.28	No inner-sphere water
Eu – T-DGA complex in [C_4mim][NTf_2], feed acidity 0.5 M HNO_3	2.25	No inner-sphere water
Eu – T-DGA complex in [C_4mim][NTf_2], feed acidity 0.01 M HNO_3	2.25	No inner-sphere water

3.3 Electrochemical studies on the complexation of Eu(III) with TODGA in [C_6mimBr]

Stripping of the metal ion from the ionic liquid phase is one of the major challenges which can be addressed by carrying out electro deposition of metal ion from the ionic liquid phase. Therefore, it is of relevance to study the redox behavior of Eu in ionic liquid. Besides use of ionic liquid as the medium in electrochemical studies, is of interest because of their properties such as, large potential window, wide liquid range, high degree of solubility of different organic and inorganic moieties etc. Therefore, an attempt was made to understand the electro chemical behavior of Eu^{3+} in RTIL. The kinetics and the thermodynamics of Eu^{3+}/Eu^{2+} redox behaviour were investigated in the present study. Since cyclic voltametry can probe the local environment around metal ion, efforts were put to understand the complexation of Eu^{3+} with TODGA in RTIL. TODGA being one of the promising extractants for actinide partitioning, it was of interest to understand its complexation behaviour with Eu^{3+}. In the present study, cyclic voltametry was used as a tool to determine the stoichiometry of the Eu^{3+}-TODGA complex, kinetics of the complexation and the formation constant of the complex.

3.3.1 Electrochemical window of [C_6mim][Br]

The cyclic voltammogram (CV) of the bare RTIL ([C_6mim][Br]) suggested that the electrochemical window is ~ 2.0V with the cathodic limit at -1.45 V and the anodic limit at 0.55 V (vs. Ag/AgCl as given above). The presence of water is known to shorten the electrochemical window. Accordingly, the RTIL was vacuum dried to get the window to the miximum extent. These limits are almost comparable to those reported for an analogous system, e.g. [C_4mim][Cl] [150].

3.3.2 Determination of diffusion coefficient of Eu(III)

The cyclic voltamogram (CV) of Eu(III) at temperature 298 K, at a scan rate of 0.1 V/sec. consists of a cathodic wave occurring at a peak potential of -0.362 V (vs. Ag/AgCl) which can be attributed to the reduction of Eu(III) to Eu(II). It can be seen that unlike in an earlier report, which employed [C_4mim][Cl] [150], there was no pre-wave / post wave for Eu(III) which ruled out any adsorption current. **Fig. 3.14** shows the CV of Eu(III) at different temperatures. **Table 3.12** lists the cathodic peak potential (E_p^c) along with anodic peak potential (E_p^a) and the formal potentials $(E_p^c+E_p^a)/2$ at various temperature. The formal potentials were comparable to those obtained in similar systems [150].

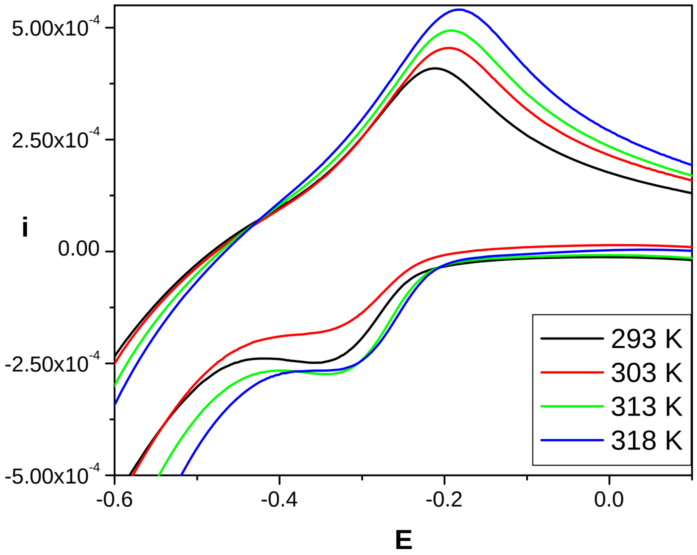

Fig.3.14: Cyclic voltamogram of Eu^{3+} at different temperatures obtained with a scan rate of 0.1 V/s in [C_6mim][Br]

Table 3.12: Cathodic, anodic and formal potentials for Eu^{3+} at different temperatures along with diffusion coefficients and activation energies in [C_6mim][Br]

Metal ion	T(K)	E_p^a(V)	E_p^c(V)	$E^0 = (E_p^c+E_p^a)/2$(V)	$D_o^* \times 10^8$/cm^{2}s^{-1}	E_a(kJ mol^{-1})
Eu	293	-0.213	-0.362	-0.287	2.99	39.34
	303	-0.201	0.358	-0.279	3.08	
	308	-0.196	-0.354	-0.275	6.40	
	313	-0.193	-0.35	-0.271	8.40	
	318	-0.181	-0.347	-0.264	10.3	

Fig. 3.15 gives the cyclic voltammograms for Eu(III) (100 mM) as a function of scan rate at T = 298 K. A general trend was found at all temperatures. The cathodic and anodic peak potentials show a marginal shift with the scan rate. The peak shifts at low scan rates (0.025 - 0.15 V/s) (**Fig. 3.16** shows the extent of shifts in the cathodic peak potentials) suggested that the redox processes of these metal ions were quasi-reversible or involved irreversible charge transfer. Thus, assuming that these processes in the RTIL are controlled by both diffusion and charge transfer kinetics, the appropriate relationship between the cathodic diffusion peak current [$(i_p^c)_{diff}$] and scan rate for a irreversible / quasi-reversible system [150] can be given below.

$$(i_p^c)_{diff} = 0.496\, nFAC_o^* \sqrt{D_o^*}\, (\alpha n_\alpha F\nu/RT)^{1/2} \tag{3.21}$$

where,

A = Electrode area in cm^2 (= 1.68 cm^2)

C_o^* = The concentration of the corresponding metal ion in mol.cm^{-3}

D_o^* = The diffusion coefficient in cm^2s^{-1}

F = Faraday constant

n = The number of exchanged electrons (1 for Eu)

ν = Potential sweep rate in Vs^{-1}

α = The charge transfer coefficient

n_α = The number of electron transferred in the rate determining step

T = Absolute temperature in K

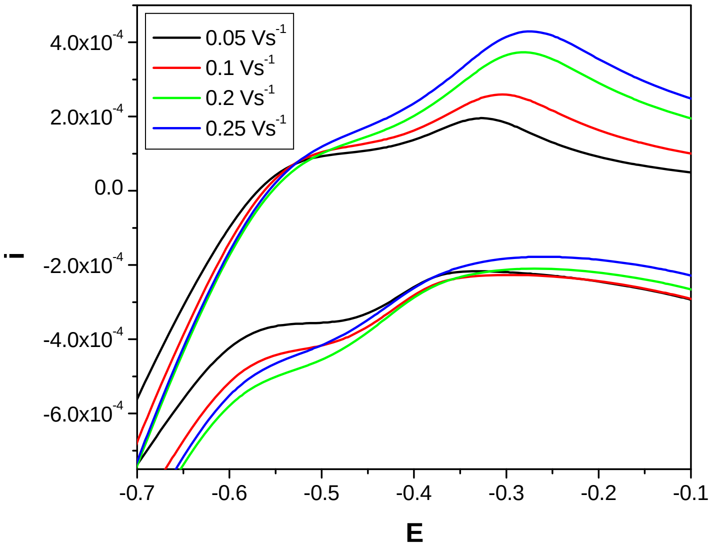

Fig. 3.15: Cyclic voltamograms of Eu^{3+} as a function of the scan rates at 298 K

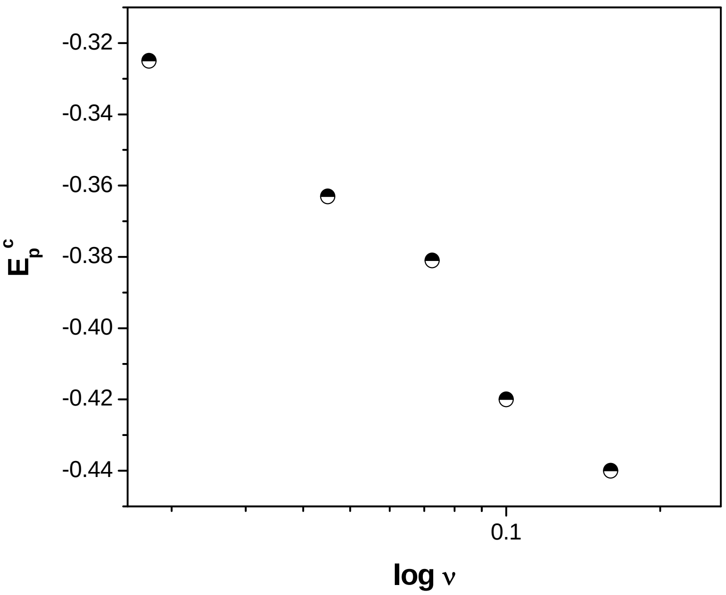

Fig.3.16: Dependencies of cathodic peak potentials on scan rate for the reduction of Eu^{3+} in $[C_6mim][Br]$

If this relation was valid, cathodic peak current $(i_p^c)_{diff}$ vs $\nu^{1/2}$ should give a straight line with a slope value of $0.496\ nFAC_0^*\sqrt{D_0^*}\ (\alpha n_\alpha F/RT)^{1/2}$. The diffusion coefficient (D_o^*) can be calculated from the slope value with the αn_α obtained from the following equation

$$E_p^c - E_p^c{}_{1/2} = 1.857RT/\ \alpha n_\alpha F \qquad (3.22)$$

Fig 3.17 shows the straight line plots of $\nu^{1/2}$ vs. i_p^c for Eu(III) indicating that the equation (3.21) is valid in the present system. The non-zero intercepts of the straight line plots can be attributed to non - Faradaic current. The D_o^* values computed from the slopes at different temperatures are listed in **Table 3.12**. The increase in the diffusion coefficient with increasing temperature is attributed to the apparent decrease in the viscosities of the medium at higher temperatures. **Table 3.13** gives a comparison of D_o^* values obtained in the present case for Eu^{3+} ion with those reported in the literature and found to be in the same range.

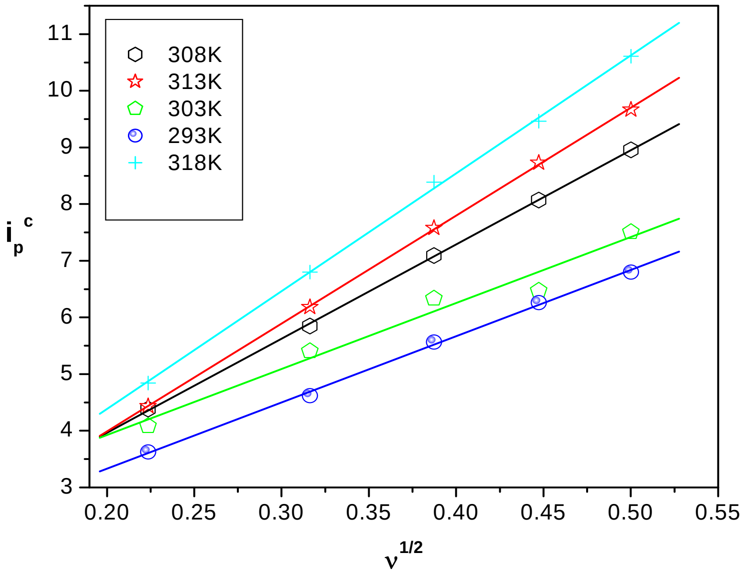

Fig. 3.17: Plots of $\nu^{1/2}$ vs. i_p^c of Eu^{3+} at different temperatures

The cyclic voltammograms of Eu at varying concentrations of the metal ion, recorded at 298 K were represented in **Fig. 3.18** which indicated increase in diffusion peak current $(i^c_p)_{diff}$ with increasing metal ion concentration.

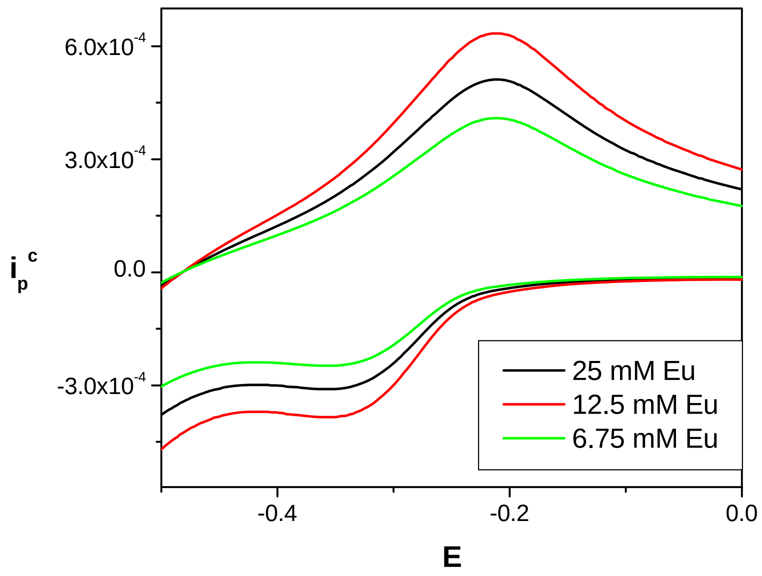

Fig. 3.18: Cyclic voltammograms of Eu^{3+} as a function of metal ion concentration at 300 K and scan rate 0.1 Vs^{-1}

Table 3.13: Comparison of distribution coefficients (D_0^*) and activation energies (E_a) in literature by cyclic voltametry

Metal ion	Medium	T(K)	D_0^* x10^8/cm^{2}s^{-1}	E_a(kJmol^{-1})	Reference
Eu^{3+} / Eu^{2+}	[C_6mim][Br]	318	10.3 x 10^{-8}	39.3	present work
	[BMPy][NTf_2]	323	5.3 x 10^{-8}	29.5	Ref [151]
	[C_4mim][Cl]	343	4.9 x 10^{-8}	54.5	Ref [150]

3.3.3 Determination of activation energy and thermodynamic parameters

The activation energy for the diffusion of the metal ion can be related to the diffusion coefficient through the Arrhenius equation,

$$D_o^* = A \exp(-E_a/RT) \tag{3.23}$$

where, A is pre-exponential factor and E_a is the corresponding activation energy. Therefore, a plot of ln D_o^* vs 1/T should give a straight line as shown in **Fig. 3.19** with a slope of ($-E_a/R$) from which E_a for the diffusion of metal ion is deduced and listed in **Table 3.13**. The activation energies of the diffusion of Eu^{3+} was found to be 39.3 kJ/mol while Jagadeeswara Rao et al. [150] reported the same for the diffusion of Eu^{3+} as 54.5 kJ/mol in [C_4mim][Cl].

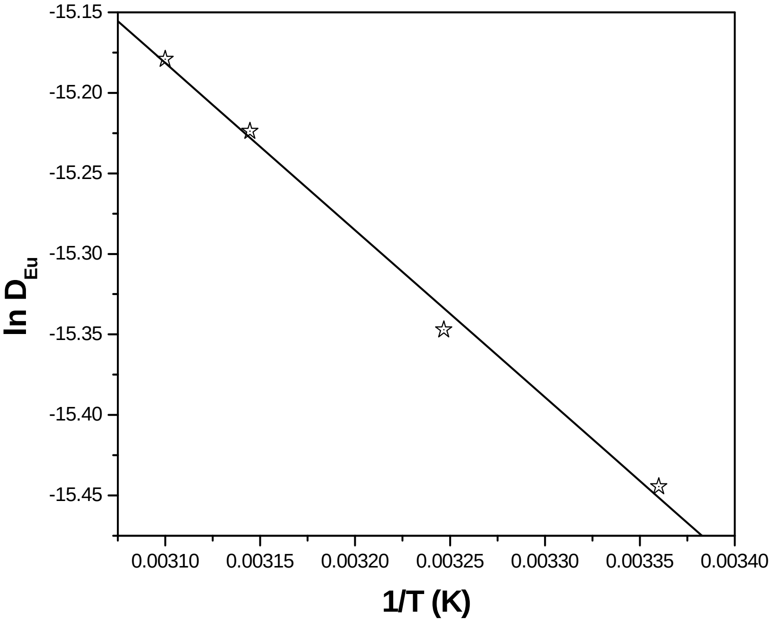

Fig. 3.19: Arrhenius plot for the diffusion of Eu^{3+} in [C_6mim][Br]

The trivalent lanthanide ion undergoes reduction in [C_6mim][Br] according to the following equation

$$2EuBr_3 \rightarrow 2EuBr_2 + Br_2 \quad (3.24)$$

The cathodic and anodic peak potentials are related to the apparent standard potential, $E^{0*}_{ox/red}$ by the following equations

$$E_p^c = E^{0*}_{ox/red} - 1.11\ RT/nF - RT/nF\ \ln(\sqrt{D_{ox}}/\ \sqrt{D_{red}}) \quad (3.25)$$

$$E_a^c = E^{0*}_{ox/red} + 1.11\ RT/nF - RT/nF\ \ln(\sqrt{D_{ox}}/\ \sqrt{D_{red}}) \quad (3.26)$$

$$\text{where, } E^{0*}_{ox/red} = E^{0}_{ox/red} + RT/nF\ \ln\ (\gamma_{ox}/\ \gamma_{red}) \quad (3.27)$$

where, $E^{0}_{ox/red}$ and γ represent the standard potential and activity coefficient, respectively. The reduction reaction involves 'n' electron transfer, the apparent standard potential, $E^{0*}_{ox/red}$ determined using the equation (3.28) is plotted against T in **Fig. 3.20**. It is observed that $E^{0*}_{ox/red}$ increases with an increase in the temperature.

$$E^{0*}_{ox/red} = (E_p^a+E_p^c)/\ 2 + RT/nF\ \ln(\sqrt{D_{ox}}/\ \sqrt{D_{red}}) \quad (3.28)$$

From the linear regression of the experimental data, the $E^{0*}_{ox/red}$ values are related to the temperature by the following expression

$$E^{0*}_{Eu3+/Eu2+} = -0.5534 + 9 \times 10^{-4}\ T \quad (3.29)$$

The standard Gibb's energy for the reactions can be determined using equation (10) with the assumption that the solution is dilute and the activity coefficients are unity.

$$\Delta G^0 = -nF\,E^{0*}_{ox/red} \qquad (3.30)$$

where, $E^{0*}_{ox/red}$ is the apparent standard potential of the metal ion oxidation. The expression for standard Gibb's energy of the reactions (ΔG^0) as a function of temperature can be expressed as

$$\Delta G^0\,(EuBr_3) = -106.82 + 0.175\,T \qquad (3.31)$$

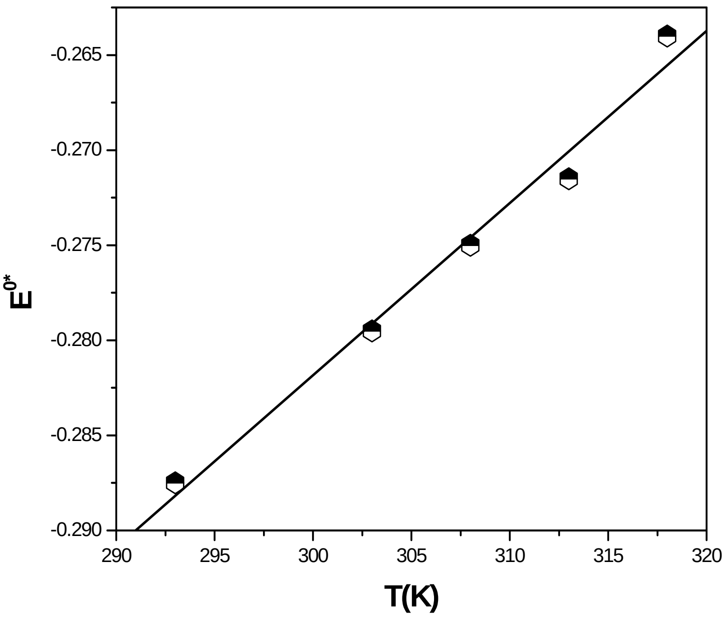

Fig. 3.20: Plot of E^0* vs T(K) for the reduction of $Eu^{3+} \rightarrow Eu^{2+}$ using 100 mM in [C_6mim][Br]

Comparing equations (3.31) and (3.32) the enthalpy and the entropy of the redox reactions can be evaluated.

$$\Delta G^0 = \Delta H^0 - T\Delta S^0 \qquad (3.32)$$

Since ΔH^0 values are all negative, the reactions can be considered as exothermic, and ΔS^0 values too are negative indicating that the reactions involved a decrease in the entropy chage. Bromine being a gas having higher disorder reacts with the other reactants leading to the formation of a less disordered bromide compound.

3.3.4 Complexation with TODGA

By the addition of appropriate aliquots of 100 mM TODGA the i_p^c was found to decrease and followed a time profile [**Fig.3.21**]. Thus, the rate of change of i_p^c can be indicative of the kinetics of complexation. It was found to follow an exponential decay characteristic of first order reaction. The slow kinetics of the complexation can be attributed to the high viscosity coefficient of the medium. The kinetics of the complexation of Eu^{3+} by TODGA in [C_6mim][Br] after fitting the data, can be expressed by the following equation

$$i_p^c = 0.669 + 0.218 \exp(-\tau/30.083) \qquad (3.33)$$

The pseudo-first order rate constant for the complexation reaction (= 1/30.083) was determined as 5.5×10^{-4} s^{-1}. The i_p^c was also found to decrease with subsequent addition of TODGA into the electrochemical cell. A plot of i_p^c vs volume of added TODGA was plotted [**Fig. 3.22**] wherein the inflection point represents the complete formation of the Eu(III) - TODGA complex and the stoichiometry of the complex was calculated from the inflection point and was found to be 1:1. The complex formation constant of the metal ligand complex was calculated from the following equation [152]

$$(i_p{}^c{}_o - i_p{}^c) / i_p{}^c = K_f\,[\mathrm{TODGA}] \qquad (3.34)$$

where, K_f = formation constant of Eu^{3+}- TODGA complex, $i_p{}^c{}_o$ = oxidation current of Eu^{3+} in the absence of TODGA, $i_p{}^c$ = oxidation current of Eu^{3+} in the presence of TODGA, [TODGA] = concentration of added TODGA in solution.

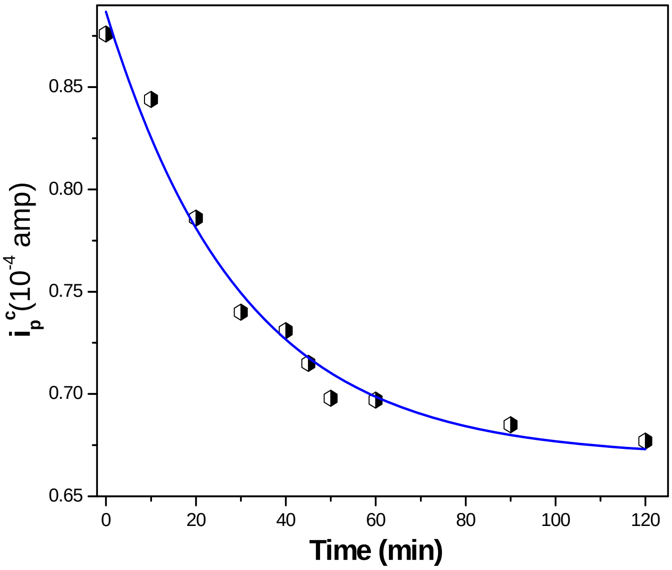

Fig. 3.21: Eu^{3+}-TODGA complexation kinetics in $[C_6mim][Br]$; Scan rate: 0.1 V/s; Temp: 25ºC.

The 'conditional' formation constant was determined to be 3.31 x 10^8 M^{-1}. In another similar study, Pathak et al. [149] reported log K_f for the 1:3 complex as 14.6 in ethanol and water medium by time resolved fluorescence spectroscopy (TRFS). In another study [74] using the analogous TMDGA (tetramethyl diglycolamide) as complexing agent, the log K_f for Nd(III) 1:1

complex formation was reproted as 2.84. Interaction of diluents with ligand molecule and the interaction of metal ion with the ligand molecule are responsible for the observed stoichiometry of the metal ligand complex in a particular medium. In ionic liquid, due to more interaction of the ligand molecule with ionic liquid diluent, chances of ligand agreegation is less and as a result, less number of ligand molecules were found to be involved in complex formation with a stoichiometry of 1:1.

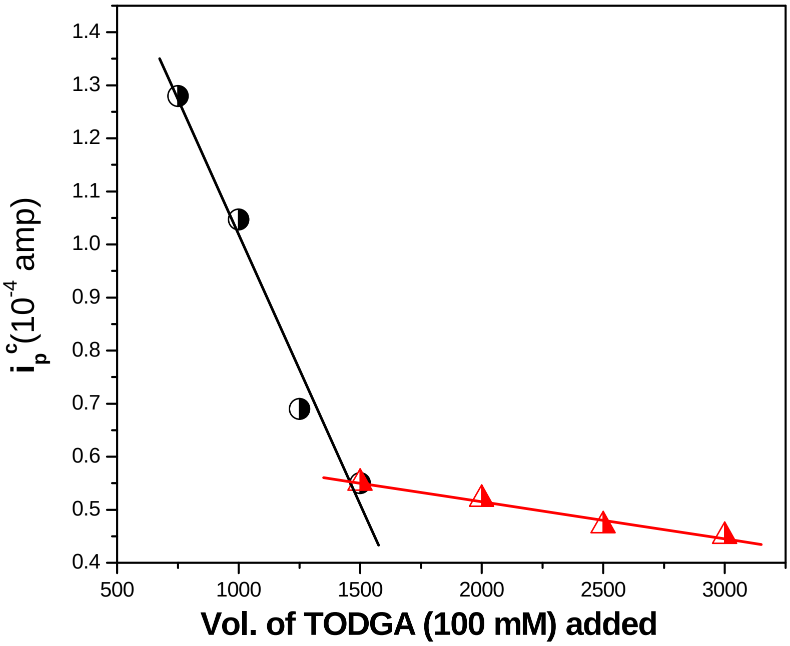

Fig. 3.22: Plot of reduction peak current (i_P^C) vs. volume of TODGA added, at 25° C and scan rate 0.1 V/s Determination of stoichiometry of Eu^{3+}-TODGA complex in [C_6mim][Br] for the determination of stoichiometry of Eu^{3+}-TODGA complex in [C_6mim][Br]

3.4 Summary

From the above studies, it can be concluded that extraction of Am(III) can be considerably enhanced when diglycolamide (DGA) extractants such as TODGA or C4DGA are used. in room temperature ionic liquids instead of the conventional *n*-dodecane as the diluent. The unusually high extraction of Am(III) can be attributed to the unique ion-exchange extraction mechanism in the RTIL medium, while the high viscosity of the RTILs is responsible for the slower extraction kinetics. Am(III) can be selectively extracted from a mixture containing U(VI), Pu(IV) and Pu(VI), and Am(III) by adjusting the oxidation state of Pu to +6. The large negative entropy changes observed during the thermodynamic studies, point to the formation of ordered extracted complexes with both TODGA as well as C4DGA, possibly without the liberation of the inner-sphere water molecules, indicating outer sphere interactions. The analytical significance of this work lies in the exceptionally high separation factors obtained and this can be applied for the selective extraction of Am(III) from acidic waste samples. Moreover, Am(III) can be selectively recovered from high level waste and can find application.

The solvent extraction studies of Am(III) using T-DGA in various room temperature ionic liquids clearly demonstrated that the ionic liquid medium extracts the metal ions more efficiently as compared to the molecular diluents such as *n*-dodecane. Furthermore, the tripodal diglycolamide T-DGA is a far superior extractant as compared to TODGA. It extracts Am(III) from acidic feed solutions with the butyl derivative being the most efficient ionic liquid. The extracted species follow an ion-exchange mechanism at lower acidities and possibly by a solvation mechanism at higher acidities. Though the extraction of the tetravalent actinide ion was lower as compared to the trivalent lanthanide and actinide ions (both Eu(III) and Am(III) were highly extracted), the extraction of the hexavalent actinyl ion was rather insignificant. The extracted species was a 1 : 1complex formed between Am(III) and T-DGA with no inner – sphere water molecules, which was confirmed by the TRLFS studies using the analogous Eu (III) complexes. The stripping results were very encouraging with the possibility of > 99% stripping after three stages when a complexing agent such as EDTA or DTPA was used in guanidine carbonate. The thermodynamics of the extraction indicated a highly entropy driven reaction, suggesting the removal of a large number of water molecules from the inner-coordination sphere. Radiolytic stability studies showed a significantly higher stability of the ionic liquid solvent systems as compared to those reported previously in the literature, which may lead to possible long term recycling options. This also makes the proposed solvent system a viable 'green' alternative to the TODGA based solvent systems with molecular diluents.

Cyclic voltammogram of Eu(III) was recorded in a hydrophilic RTIL, [C_6mim][Br] which has a moderately large electrochemical window of ~1.8 V. The aqueous reference electrode, Ag/AgCl gave reproducible results. The diffusion coefficient for Eu was found to be 3.08×10^{8} cm^2s^{-1} at 303 K while the activation energy for the conversion of $Eu^{3+} \rightarrow Eu^{2+}$ was 39.3 kJ mol^{-1} and quasi-reversible in nature. In addition, thermodynamic parameters such as Gibbs free energy, enthalpy and entropy and activation energies of the redox reactions were computed. A systematic study was carried out to understand the complexation Eu^{3+} with TODGA in [C_6mim][Br] which showed slow first order kinetics. The slower kinetics can be attributed to the high viscosity of the medium. Eu^{3+} forms 1:1 complex with TODGA in [C_6mim][Br] with a formation constant of 3.31×10^{8} M^{-1} while the rate constant of the complexation was evaluated as 5.5×10^{-4} s^{-1}

CHAPTER - 4

Studies on the effect of ligand structure of C4DGA on actinide ion extraction into RTIL

In Chapter-3, a diglycolamide functionalized calixarene (C4DGA) has been used for actinide ion extraction into ionic liquid medium. It was needed to understand the role of the nature of the substituents in the C4DGA molecules on the general extraction/separation behavior of actinides. Apart from this, the extraction mechanism, species involved for extraction, their kinetics and thermodynamic parameters involved are likely to vary in ionic liquid media which may play significant role in the extraction and the separation properties of metal ions. Finally, on the basis of these studies the C4DGA based solvent systems in ionic liquids are evaluated for nuclear waste remediation using simulated high level waste. The structures of different C4DGA ligands used in this Chapter are shown below.

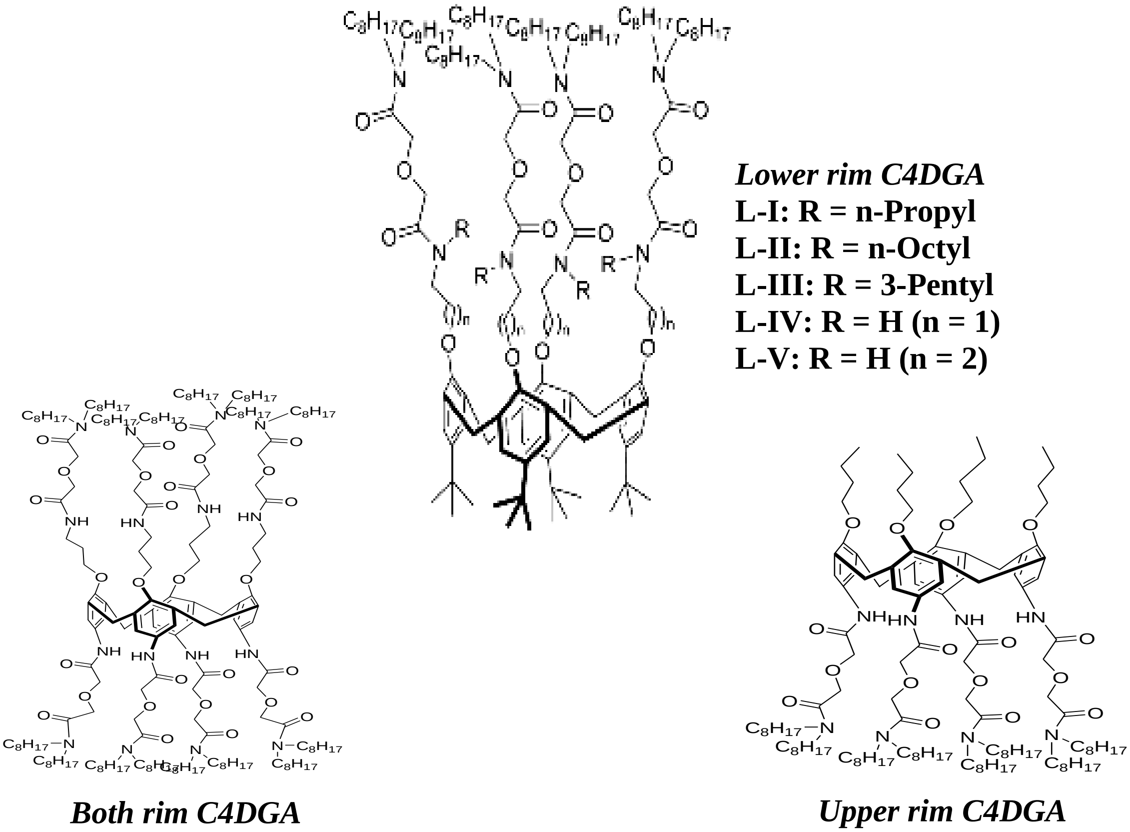

Lower rim C4DGA
L-I: R = n-Propyl
L-II: R = n-Octyl
L-III: R = 3-Pentyl
L-IV: R = H (n = 1)
L-V: R = H (n = 2)

Both rim C4DGA
L-VI

Upper rim C4DGA
L-VII

Fig. 4.1: Structures of the C4DGA ligands used in Chapter-4

4.1 Extraction profile of Americium at different feed acidities

A systematic study was carried out to understand the extraction behavior of americium at different feed acidities using the diglycolamide-functionalized calixarenes, L-I−L-IV, in [C_8mim][NTf_2]. As shown in (**Figure 4.2(a)**), the D_{Am} values decrease sharply with HNO3 concentration up to 0.5 M HNO_3 followed by a moderate decrease. Similar to diglycolamide extractants like TODGA, the C4DGAs can form an adduct of the type C4DGA·HNO_3 at higher acidities, suggesting that the H^+ ion competes with the metal ion, and hence Am(III) extraction decreased with increasing feed acidity, suggesting an ion exchange mechanism given by equation (4.1)

$$Am^{3+}_{aq} + nC4DGA_{IL} + 3C_8mim^+_{IL} = Am[C4DGA]_n{}^{3+}_{IL} + 3C_8mim^+_{aq} \qquad (4.1)$$

where, the species with the subscripts ‘aq’ and ‘IL’ refer to those in the aqueous phase and in the RTIL phases, respectively. A strong influence of H^+ ion on the Am(III) extraction can be explained on the basis of a competing equilibrium reaction given as follows:

$$H^+_{aq} + C4DGA_{IL} + C_nmim^+_{IL} = H.C4DGA^+_{IL} + C_nmim^+_{aq} \qquad (4.2)$$

Other than the influence of equation (4.2) on lowering the Am(III) extraction with increased acidity, nitrate ion complexation can also play a significant role, especially at higher nitric acid concentrations, leading to the formation of neutral salvation type complexes which can lead to increase metal ion extraction. At 0.01 M HNO_3 the distribution ratios of Am(III) for C4DGA ligands follow the order, L-IV(12400) > L-III (8850) > L-II (650) > L-I (290), while at 0.5 M HNO_3 the order becomes L-IV (750) > L-I (10) > L-III (0.40) ~ L-II (0.50). L-IV with a spacer chain containing two carbon atoms is a better extractant in comparison to L-V with a longer spacer chain (3 C atoms). On the other hand, an opposite trend was observed with molecular diluents as has been reported previously [71]. A plausible explanation for this behavior may be based on the preorganized structure of the ligands. It seems that the ligands with lower spacer length can impart certain amount of rigidity to the pendent arms (due to lower flexibility) leading to a relatively more preorganized structure. Therefore, L-V, with longer spacer length can give rise to a pre-organized structure which explains its lower complexation tendency in ionic liquid medium. It is expected that at lower feed acidity (0.01 M HNO_3), the ligating ability of the carbonyl oxygen will be enhanced if the adjacent amidic nitrogen atom contains any group having a +I (inductive) effect. Since the +I effect of the substituents follow the trend, *3*-pentyl > *n*-octyl > *n*-propyl, the electron density on the concerning amidic nitrogen atoms will follow the same order. As a consequence, the extraction efficiencies follow the same order, namely, L-III > L-II > L-I. This trend changes at comparatively higher feed acidities where the amidic nitrogen is protonated and becomes pyramidal and only steric factors are of interest. As a consequence, at 0.5 M HNO_3, the least sterically crowded ligand (L-I) was the most efficient of the four C4DGAs, while L-III, containing four 3-pentyl groups showed the least complexing ability. Since at 0.5 M HNO_3, L-I and L-IV showed good extraction efficiencies for Am(III), this condition and these ligands were used for further studies.

Studies on the extraction profiles of Am(III) with different rim functionalized C4DGA revealed that remarkable acidity independent high extraction efficiency was observed for both-rim DGA functionalized calix[4]arene (L-VI) ligand in ionic liquid medium. Comparative extraction data for Am(III) were obtained with the three C4DGA extractants and the results are shown in **Fig. 4.2(b)**. The D_{Am} values at 0.01 M HNO_3 were nearly comparable for L-VI and L-V, while that with L-VII was about 3 orders of magnitude lower. This can be attributed to higher stereochemical strain arising during the complexation of the wide rim-functionalized C4DGA with the metal ion. Furthermore, the shorter spacer length in L-VII could lead to less effective metal ion complexing, which was also observed with narrow rim functionalized ligands with a spacer length of 2 as compared to those with a spacer length of 3 [71]. It was further of interest that, while there was a sharp fall in the D_{Am} value with increasing acidity with both L-V and L-VII, an opposite trend was seen in case of L-VI. This is in sharp contrast to the reported behavior in molecular diluents where the D_{Am} value with L-V was higher as compared to that with L-VI [71]. This is of great significance as an entirely different mechanism appeared to be responsible for the extraction of metal ions with L-VI. Though the presence of DGA groups on both rims of L-VI makes it a strong complexing agent, it is difficult to visualize how the metal ion can possibly coordinate with all the donor atoms at the same time with a coordination number of 16 or 24 (if the etheric 'O' atom is to coordinate). On the other hand, it may be suggested that the metal ion binds to the DGA groups attached to only one side of the calix[4]arene, while the other side is either uncoordinated or complexed with the hydrogen ion. Complexes of hydrogen ion with macrocyclic ligands are not uncommon [153]. The insignificant change in the extractability of the metal ion in the entire acidity range in case of L-VI is of utmost importance, as the metal ion can be extracted from almost any acidity doing away with the feed adjustment step, which is one of the prerequisites in many separation processes. Such exceptional extraction properties of an extractant in ionic liquid medium are reported for the first time. The extraction profiles of Am^{3+} using L-I, L-II, L-V, L-VI and L-VII in $[C_8mim][NTf_2]$ from SHLW (at varying HNO_3 concentration) showed similar trend as seen with tracer studies involving Am(III) but with decrease in D_{Am} values (**Fig. 4.2(c)**).

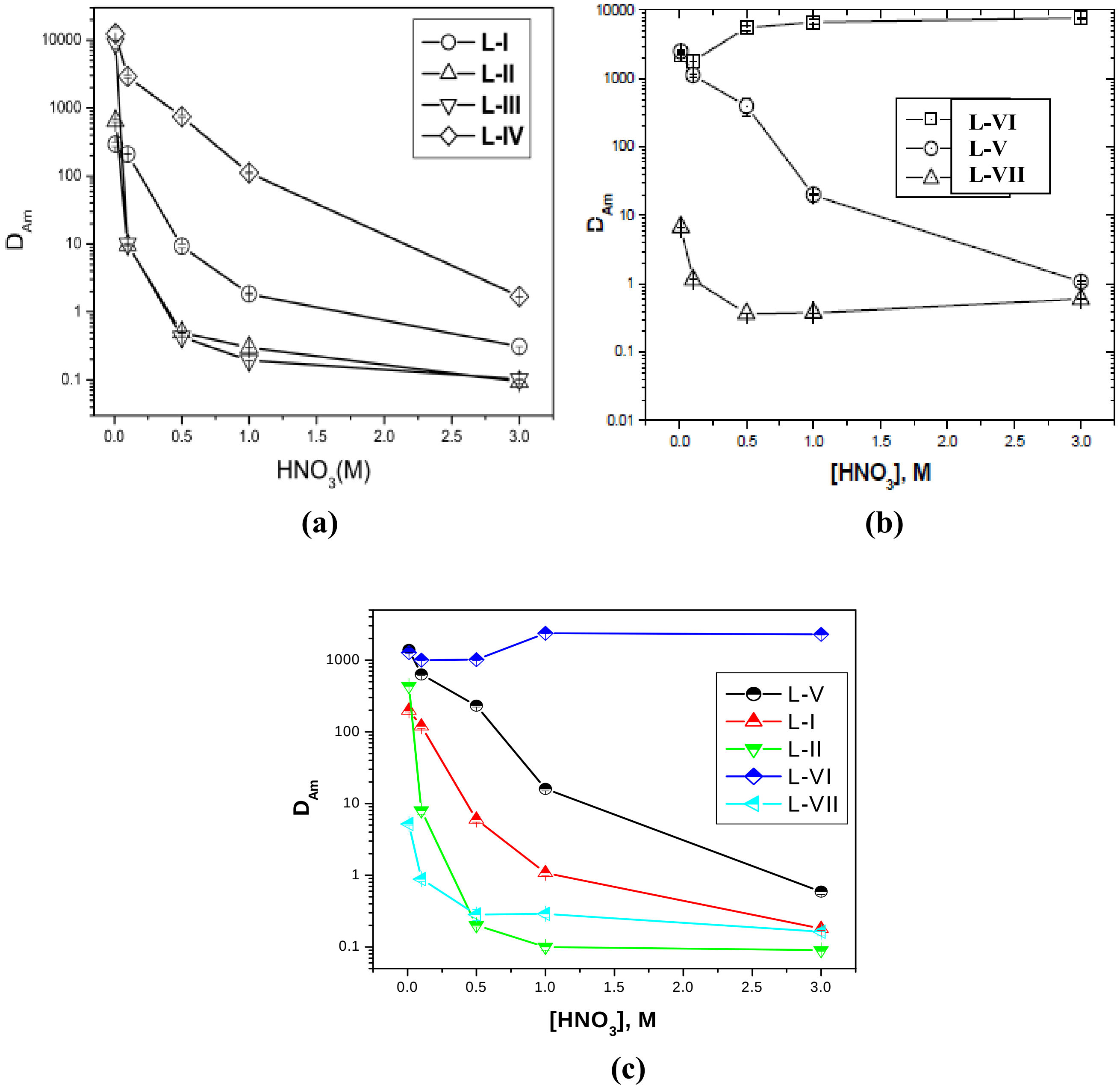

(a) **(b)**

(c)

Fig. 4.2: Extraction profiles of Am^{3+} from different aqueous phase acidities using (**a**) structurally modified C4DGA ligands; (**b**) different rim functionalized C4DGA ligands; (**c**) different C4DGA ligands under SHLW condition. Equilibration time: 2 h; C4DGA concentration: 5.0 x 10^{-4} M; Diluent: $[C_8mim][NTf_2]$.

4.2 Extraction kinetics of Am(III)

Extraction kinetics studies were carried out using the above mentioned C4DGA ligands in ionic liquid. In view of the high viscosity of the RTILs, it was expected that the mass transfer rate will be slower and consequently, the equilibrium would be attained at a relatively longer time than those observed with common molecular diluents. The distribution ratios of americium in [C_8mim][NTf_2] increased with increasing equilibration time up to 120 min, while a plateau was observed afterwards (**Fig. 4.3**). A similar observation of slow extraction kinetics was also found for the extraction of Am(III) into [C_8mim][NTf_2] by T-DGA (Chapter III). Although L-IV and L-V have different spacer lengths, the time required to attain equilibrium is nearly the same in both cases. This suggested that the re-orientation during complexation from the free ligand structure has a minimum barrier. The slow attainment of equilibrium is mainly attributed to the viscosity effect of the diluents, which is responsible for the slow mass transfer rates. The extraction kinetics of Am(III) was studied from a feed solution containing 0.5 M HNO_3 and using 5.0 x 10^{-4} M concentrations of L-I – L-VI in [C_8mim][NTf_2]. On the other hand, the extraction kinetics of L-VII was studied at 0.01 M HNO_3, due to the low D_{Am} values in 0.5 M HNO_3. **Fig. 4.3(a)** gives data on the extraction kinetics of Am(III) using structurally modified C4DGAs, while **Fig. 4.3(b)** presented the same using different rim functionalized C4DGAs in [C_8mim][NTf_2]. As shown in **Fig 4.3(c)**, the time required to attain equilibrium was about 60 - 180 minutes for the extraction of Am(III) from SHLW at different temperatures using L-I, L-II, L-V, L-VI and L-VII in [C_8mim][NTf_2]. It was observed that for different C4DGAs, the time required to attain equilibrium at a particular temperature is comparable to those with the SHLW feeds. This suggests that the nature of diluent is responsible for the slow attaininment of equilibrium.

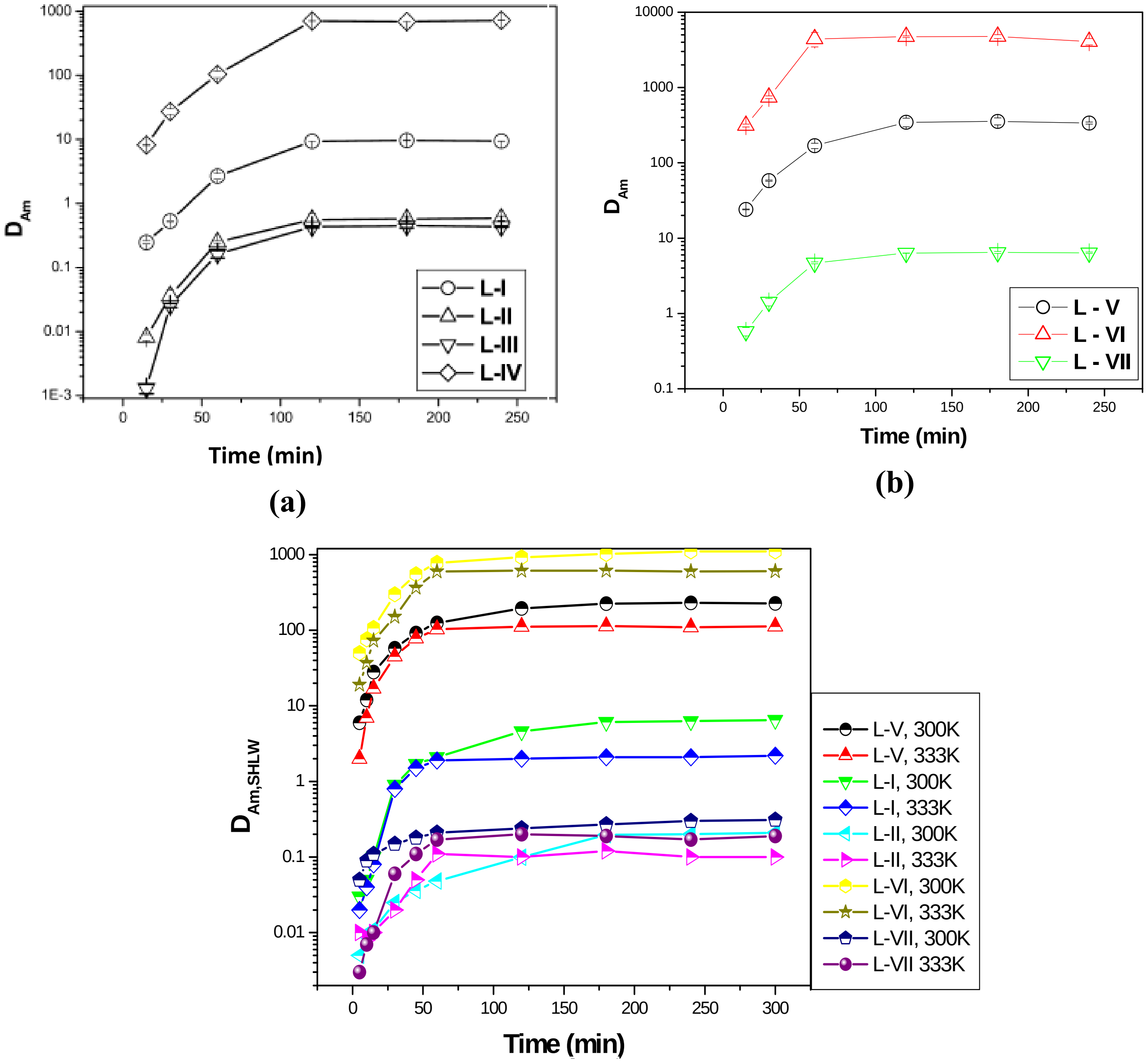

(a)

(b)

(c)

Fig. 4.3: Extraction kinetics for Am(III) (**a**) using structurally modified C4DGAs; (**b**) using different rim functionalized C4DGAs; (**c**) from SHLW using different C4DGAs. Ligand concentration: 5 x10^{-4} M. Diluent: [C_8mim][NTf_2]. Feed acidity: 0.5 M HNO_3 for L-I – L-VI, 0.01 M HNO_3 for L-VII.

It was decided to carry out the kinetics of extraction studies at 60˚C (most HLW solutions are at 40-60°C due to the decay heat of the radio-nuclides) and it was interesting to observe lesser time was needed to attain equilibrium at higher temperature. This may be attributed to lower viscosity of the solvent systems (**Table 4.1**). Apparently, this will help the extraction of minor actinides while dealing with actual high level wastes.

Table 4.1: Correlation of the time to attain equilibrium D_{Am} values with temperature and viscosity for Am(III) using different C4DGAs from SHLW. Ligand concentration: 5.0×10^{-4} M. Diluent: $[C_8mim][NTf_2]$

Ligand	D_{Am}	T (K)	Dynamic viscosity (mPa.s)	Time needed for attaining equilibrium (min)
L-V	225	300	73	180
	113	333	16*	60
L-I	6.5	300	73	180
	2.2	333	16*	50
L-II	0.21	300	73	200
	0.1	333	16*	60
L-VII	0.31	300	73	180
	0.19	333	16*	60
L-VI	1105	300	73	200
	603	333	16*	120

Note: *Data taken from ref. [154]

4. 3 Extraction of actinides, fission products and other elements co-extracted from SHLW

Apart from the Am^{3+} ion, the extraction of other actinide ions (UO_2^{2+}, Pu^{4+}, PuO_2^{2+}), important fission products (Cs^+, Sr^{2+}) and other elements co-extracted from SHLW were also investigated using 5.0 x 10^{-4} M C4DGAs in [C_8mim][NTf_2]. The results showed the trend: $Eu^{3+} > Am^{3+} > Pu^{4+} > UO_2{}^{2+} > Sr^{2+} > Cs^+$ (**Table 4.2)**, which was found to be similar to that reported for the T-DGA in both *n*-dodecane - *iso*-decanol system [107] as well as in ionic liquids (Chapter 3). The higher extraction efficiency for the trivalent lanthanide ion, Eu^{3+}, in comparison to the trivalent actinide ion, Am^{3+}, can be attributed to the hard-hard interaction of the former metal ion with the oxygen atoms of the extractant molecules. It is interesting to note that L-I has higher relative extraction of Eu^{3+} vs Am^{3+} than L-IV, which can be utilized for lanthanide-actinide separation, a relevant step in the high level waste remediation through the "Partitioning and Transmutation" strategy [26,106]. The lower distribution ratio values of hexa- and tetravalent actinide ions, as compared to the trivalent ones, are in line with previous studies with analogous ligands [62]. The separation factor (SF) values for Am(III) with respect to UO_2^{2+}, Cs(I), Sr(II), Pu(IV), and PuO_2^{2+} are 130, 1040, 470, 3.2, and 90, respectively with L-I in [C_8mim][NTf_2], which increased enormously to 4670, 13120, 4990, 130, and 4160, respectively, for L-IV in [C_8mim][NTf_2]. It can be inferred that L-IV is not only a better ligand with respect to the higher extraction efficiency of americium; it also shows a significantly favorable separation behavior. This may have applications in the separation of actinides from high level waste. Typically, the HLW solution contains about 10^{-4} M Am, implying the solvent system should contain about 10^{-3} M C4DGA ligand. The ligand inventory can, therefore, be significantly lower than the other reported solvent systems for actinide partitioning making the C4DGA based separations not only cost-effective but also holds promise for significant reduction in the secondary waste volumes.

On the other hand, the distribution ratio values of the trivalent actinide / lanthanide ions are about 2 orders of magnitude higher with L-VI in the RTIL medium, suggesting interesting separation possibilities. This enhancement can be attributed to the preorganization effect of the DGA-functionalized calix[4]arenes. This effect resulted in very high D_M values for Am(III) and Sr(II) and partly for Pu(IV) (in case of L-VI), while an opposite trend was seen with the remaining metal ions, *viz*. U(VI), Pu(VI), and Cs(I). In literature [155], a S.F.(Am/Sr) value of about 100 was reported when 0.1 M TODGA in *n*-dodecane was used in the acidity range of 1-2 M HNO_3. However, it increased remarkably to >3000 in ionic liquid medium. The very high separation factors can lead to effective decontamination of the trivalent minor actinide (Am and Cm) products from the accompanying metal ions.

An attempt was made to understand the extraction behavior of the other metal ions present in high level waste (HLW) using these ionic liquid based solvent systems. The aqueous phases after extraction experiments were analyzed by ICP-AES technique. The analytical data revealed that Na, K, Pd, Fe, Sr, Mn, Pd, Ce, Ru and Ba remain un-extracted by all the systems. Y, La, Sm, Y, Pr, Nd, Zr and Mo were found to be extracted into the organic phase. All other metal ions were found to be extracted partially and to different extent by different C4DGA – RTIL systems. On the basis of the analytical data, L-V and L-I were found to have better performance towards actinide partitioning. The analytical results are listed in **Table 4.3**.

Table 4.2: Comparative extraction data of actinides and fission product elements using C4DGAs in [C_8mim][NTf_2]

Metal ion	L-I	L-IV	L-V	L-VI	SF $_{\text{L-I}}$ $^{\#}$	SF $_{\text{L-IV}}$ $^{\#}$	SF$_{\text{L-V}}$ $^{\#}$	SF$_{\text{L-VI}}$ $^{\#}$
$D_{Am(III)}$	9.34	748	397	5500				
$D_{U(VI)}$	0.07	0.16	0.41	0.19	1.3 x 10^2	4.6 x 10^3	9.6 x 10^2	2.9 x 10^4
$D_{Eu(III)}$	143	897	561	7000	0.065	0.85	0.71	0.79
$D_{Cs(I)}$	0.01	0.06	0.08	0.09	1038	1.3 x 10^4	4963	6.2 x 10^4
$D_{Sr(II)}$	0.02	0.15	0.15	0.18	467	4.9 x 10^3	2.6 x 10^3	3.1 x 10^4
$D_{Pu(IV)}$	2.88	5.62	6.17	62	3.24	133	64.3	89
$D_{Pu(VI)}$	0.1	0.18	0.6	0.26	93.4	4.1 10^3	6.6 x 10^2	2.1 x 10^4

Note: Ligand concentration: 5.0 x 10^{-4} M. Equilibration time: 3 h. feed acidity: 0.5 M HNO_3. Diluent: [C_8mim][NTf_2]. $^{\#}$ SF means the separation factor values of Am(III) with respect to other metal ions, i.e., SF = D_{Am}/D_M.

Table 4.3: Analytical results obtained by ICP-AES technique after single contact of SHLW (0.5 M HNO_3) by different C4DGAs into [C_8mim][NTf_2]

Metal ion	SHLW (gL^{-1})	L-I (gL^{-1})	L-II (gL^{-1})	L-V (gL^{-1})	L-VI (gL^{-1})	L-VII (gL^{-1})
Na	5.9 ± 0.07	5.8 ± 0.05	5.6 ± 0.06	5.4 ± 0.01	5.9 ± 0.01	5.5 ± 0.09
K	0.20 ± 0.01	0.17± 0.02	0.12 ± 0.007	0.073 ± 0.005	0.11 ± 0.003	0.120 ± 0.0001
Cr	0.13 ± 0.01	0.09 ± 0.01	0.035 ± 0.0004	0.075 ± 0.001	0.036 ± 0.0001	0.081 ± 0.0002
Mn	0.50 ± 0.02	0.45 ± 0.06	0.48 ± 0.0005	0.5 ± 0.06	0.47 ± 0.0004	0.047 ± 0.0001
Fe	0.86 ± 0.03	0.84 ± 0.04	0. 8 ± 0.0007	0.89 ± 0.008	0.86 ± 0.0001	0.87 ± 0.0003
Sr	0.03 ± 0.001	0.021 ± 0.001	0.022 ± 0.0006	0.029 ± 0.002	0.029 ± 0.0004	0.030 ± 0.0002
Ru	0.03 ± 0.003	0.026 ± 0.001	0.025 ± 0.0001	0.022 ± 0.001	0.02 2± 0.0001	0.027 ± 0.0003
Pd	0.01 ± 0.002	0.01 ± 0.001	0.01 ± 0.003	0.011 ± 0.001	0.01 ± 0.002	0.020 ± 0.0002
Mo	0.16 ± 0.02	0.007 ± 0.001	0.009 ± 0.0001	0.008 ± 0.0004	0.009 ± 0.0004	0.005 ± 0.0002
Ba	0.06 ± 0.001	0.054 ± 0.001	0.057 ± 0.0001	0.05 ± 0.006	0.058 ± 0.0001	0.06 ± 0.0005
Y	0.06 ± 0.002	0.001 ± 0.003	0.016 ± 0.0004	0.004 ± 0.0007	0.008 ± 0.0005	0.002 ± 0.0003
La	0.08 ± 0.02	0.02 ± 0.003	0.028 ±0.0007	0.016 ± 0.0001	0.019 ± 0.0002	0.019± 0.0001
Zr	0.07 ± 0.003	0.032 ± 0.002	0.021 ± 0.0004	0.070 ± 0.007	0.011 ± 0.0004	0.052 ± 0.0001
Nd	0.11 ± 0.003	0.03 ± 0.001	0.031 ± 0.0005	0.039 ± 0.0004	0.035 ± 0.0001	0.023 ± 0.0002
Sm	0.08 ± 0.005	0.041 ± 0.003	0.042 ± 0.0001	0.048 ± 0.0001	0.044 ± 0.0001	0.034 ± 0.001
Ce	0.06 ± 0.003	0.051 ± 0.002	0.052 ± 0.0003	0.053 ± 0.004	0.052 ± 0.0001	0.054 ± 0.0003
Pr	0.09 ± 0.002	0.039 ± 0.001	0.042 ± 0.0002	0.027 ± 0.0001	0.028 ± 0.0001	0.035 ± 0.0001

4. 4 Ligand concentration variation studies

The nature of the extracted species, from available literature on analogous extraction systems, has been indicated in equation (4. 1). However, the number of C4DGA molecules involved in the metal ion extraction can be easily found out by slope analysis method by carrying out Am (III) extraction studies at varying C4DGA concentrations at a fixed HNO_3 concentration. From equation (4.1), the two-phase extraction equilibrium constant (K_{ex}) can be expressed as

$$K_{ex} = ([Am(C4DGA)_n{}^{3+}{}_{IL}]\,[C_8mim^+]^3{}_{aq})/\,([Am^{3+}]_{aq}[C4DGA]^n{}_{IL}[C_8mim^+]^3{}_{IL}) \qquad (4.3)$$

$$K_{ex} = (D_{Am}[C_8mim^+]^3{}_{aq})/([C4DGA]^n{}_{IL}\,[C_8mim^+]^3{}_{IL}) \qquad (4.4)$$

$$(K_{ex}.[C_8mim^+]^3{}_{IL})/[C_8mim^+]^3{}_{aq} = D_{Am}/[C4DGA]^n{}_{IL} = K'_{ex} \qquad (4.5)$$

where K'_{ex} is the conditional extraction constant. Taking the logarithm and rearranging, one obtains

$$\log D_{Am} = \log K'_{ex} + n \log [C4DGA]_{IL} \qquad (4.6)$$

The ligand concentration variation studies were carried out using L-I − L-VII in $[C_8mim][NTf_2]$ from aqueous feed solutions of 0.5 M HNO_3 for L-I, L-IV, L-V and L-VI, 0.1 M HNO_3 for L-II and L-III and 0.01 M HNO_3 for L-VII, while the equilibration time was kept as 2 h. The lower acidity for L-II, L-III and L-VII was required to obtain measurable D_{Am} values. The log D_{Am} vs log [C4DGA], plots presented in **Fig. 4.4(a) & (b),** showed linear increase in Am(III) extraction with increasing C4DGA concentrations. As per equation (4.6), the log D_{Am} vs log $[C4DGA]_{IL}$ plots should give a straight line with a slope value of n, the number of ligand molecules associated with the metal ion, and the intercept as log K'_{ex}. The slope values were found to be very close to 1 for all C4DGA extractants indicating the stoichiometry of the extracted complex as 1:1. The slopes of the log D vs log[C4DGA] plots and the conditional extraction constant values are listed in **Table 4.4**. The complex formation equilibrium in the ionic liquid medium can be presented by the following equations

$$Am^{3+}_{aq} + C4DGA_{IL} = Am\,[C4DGA]^{3+}_{IL} \tag{4.7}$$

The complex formation constant (K_{form}) can be expressed as

$$K_{form} = [Am(C4DGA)^{3+}]_{IL}/[Am^{3+}]_{IL}[C4DGA]_{IL} \tag{4.8}$$

$$K_{form} = (K'_{ex}[Am^{3+}]_{aq})/[Am^{3+}]_{IL} \tag{4.9}$$

$$K_{form} = K'_{ex}/P_{Am} \tag{4.10}$$

where, P_{Am} is the partition coefficient of Am^{3+} defined as the ratio of the Am^{3+} concentration in the ionic liquid phase to that in the aqueous phase, which was determined to be 1.09×10^{-2}. The K_{form} values are calculated from equation (4.10) and are listed in **Table 4.4** along with the K'_{ex} values. K_{AmL} values were found to be nearly comparable for L-VI and L-V, indicating an almost similar mode of complex formation (**Table 4.4**). The K_{AmL} value of L-VII is 2 orders of magnitude lower, which is reflected in the lower extraction constant. This also supports our assumption that similar to L-V, only four DGA moieties of L-VI may be binding with Am^{3+}.

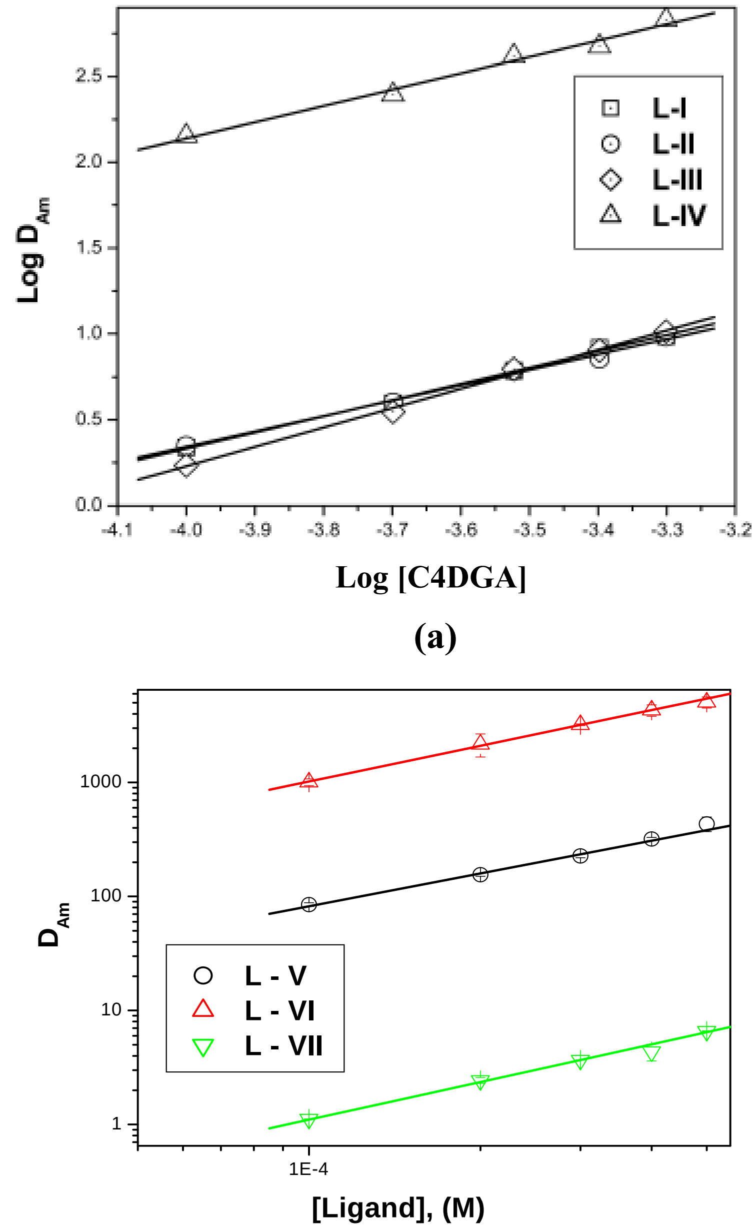

(a)

(b)

Fig. 4.4: Effect of ligand concentration on the distribution ratio of Am^{3+} using **(a)** different structurally modified C4DGAs; **(b)** different rim functionalized C4DGAs. Aqueous phase: 0.5 M HNO_3 for L-I, L-IV, L-V and L-VI, 0.1 M HNO_3 for L-II and L-III and 0.01 M for L-VII. Diluent: $[C_8mim][NTf_2]$. Equilibration time: 2 h. T = 300 K.

Table 4.4: Formation constants (K_{AmL}) and conditional extraction constants (K_{ex}) for Am(III) with C4DGA ligands

Ligand	Aq. Phase	slope	intercept	K'_{ex}	K_{form}
L-I	0.5 M HNO_3	0.94	4.11	1.29×10^4	1.18×10^7
L-II	0.1 M HNO_3	0.89	3.92	8.32×10^3	7.63×10^6
L-III	0.1 M HNO_3	1.13	4.74	5.50×10^4	5.04×10^7
L-IV	0.5 M HNO_3	0.95	5.94	8.71×10^5	7.99×10^8
L-V	0.5 M HNO_3	1.02	7.17 ± 0.12	1.48×10^7	1.35×10^9
L-VI	0.5 M HNO_3	0.97	6.74 ± 0.07	5.50×10^6	5.01×10^8
L-VII	0.01 M HNO_3	0.89	4.27 ± 0.10	1.86×10^4	1.70×10^6

Note: Equilibration time: 3 h. Diluent: $[C_8mim][NTf_2]$. Partition coefficient of Am^{3+} in $[C_8mim][NTf_2]$: 1.09×10^{-2}.

4.5 Effect of Eu loading on extraction efficiency

The above results have indicated that the rare earth ions present in SHLW are favourably extracted by the solvent systems containing L-I, L-II and L-V. However, it was required to understand the loading effects by their presence taking a single rare earth element (such as Eu(III)) as a surrogate which is required for quantification purpose. Therefore, a systematic study was carried out to understand the effect of Eu loading on the extraction efficiency of Eu(III) (by measuring the partitioning of ^{152,154}Eu radiotracer). As shown in **Fig 4.5**, maximum D_{Eu} values were obtained for tracer concentration for all the C4DGA ligands. For L-I, the distribution ratio values decrease gradually with Eu loading in aqueous phase throughout the observed concentration range of Eu. For L-II to L-V, a gradual decrease of D_{Eu} was observed up to 10 µg/mL of Eu while a more drastic decrease in D_{Eu} values was seen at Eu carrier concentrations larger than 10 µg/mL. The decrease in the D_{Eu} values is attributed to the loading effect which implies that with increase in the metal ion concentration in the aqueous phase, the free ligand concentration in the ionic liquid phase decreases. Consequently, the distribution ratio values were found to decrease.

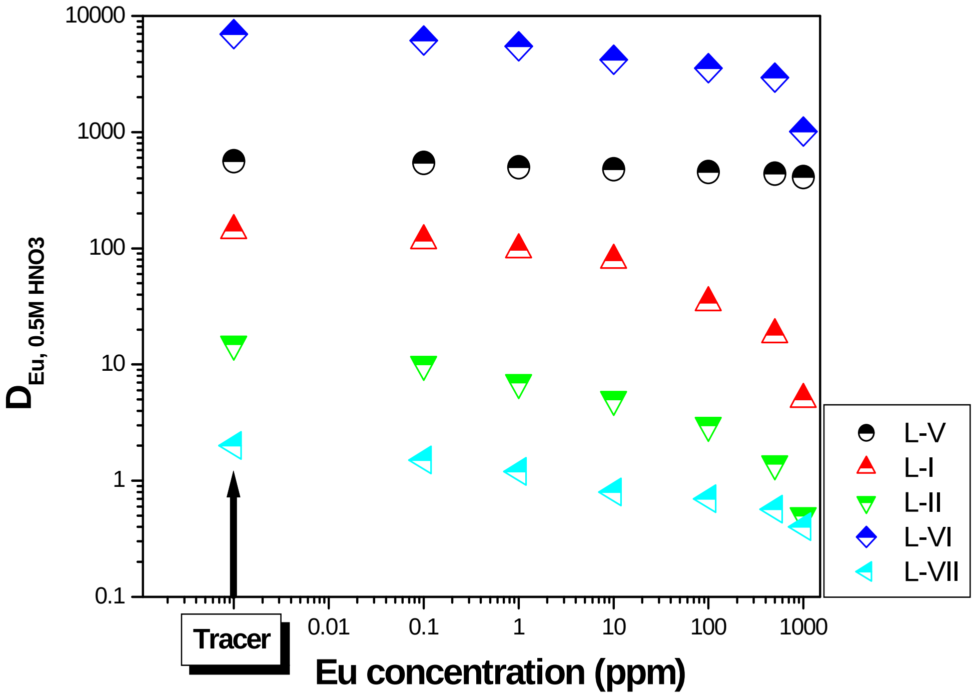

Fig. 4.5: Effect of Eu loading on extraction efficiency of Eu^{3+}. Equilibration time 3 h, Feed: 0.5 M HNO_3, T=300 K

4.6 Determination of thermodynamic parameters

In C4DGA ligands, diglycolamide moieties are anchored on a calix[4]arene molecular platform to create a pre-organized structure to favor complexation with trivalent lanthanides and actinides. The stereo-chemical configuration of the calixarenes may also play a role in the complexation. C4DGAs may lead to a disordered 'flip out' structure due to repulsions between the electron cloud of the 'O' atoms present in the DGA moieties. Therefore, a great deal of stereochemical ordering may be required upon metal ion complexation. As the conformational changes upon metal ion complex formation are linked to entropy changes, thermodynamic studies were carried out. The metal ion extraction data at varying temperatures were used to calculate the thermodynamic parameters, which were subsequently used to understand the complexation of americium with the C4DGAs in [C_8mim][NTf_2] (**Table 4.5**). The D_{Am} values decreased with increasing temperature (**Fig. 4.6(a) & (b)**), indicating the complexation to be exothermic in nature. The change in the Gibb's free energy for the complexation of Am^{3+} with L-IV in [C_8mim][NTf_2] is more negative than that observed for L-I, L-II, and L-III, which reveals that the complex formation of L-IV is thermodynamically more favorable than that of the other ligands. These are in the same line as the K_{form} data reported in **Table 4.4**. The overall enthalpy change during the extraction of Am^{3+} by a C4DGA in [C_8mim][NTf_2] is the sum of three main factors: i) change of enthalpy due to the dehydration of the metal ion (ΔH_1), ii) change in enthalpy due to the complex formation (ΔH_2), and iii) partitioning of the metal ligand complex into the RTIL phase (ΔH_3). In the present study, the contributions of ΔH_1 and ΔH_2 are identical as it primarily involves the interaction of Am (III) with the amidic carbonyl oxygen. The longer spacer length and the n-propyl group on the amidic nitrogen atom make the L-I metal complex more lipophilic than that of L-IV and hence more energy will be released during the dissolution of the Am(III) - L-I complex into the RTIL phase than in case of the Am(III) - L-IV complex, which is reflected in the overall enthalpy change (ΔH) of the extraction. The enthalpy changes for L-I, L-II, and L-III are nearly comparable, while that of L-IV is less negative, suggesting a relatively weaker interaction with this ligand. The overall entropy change for the extraction is negative for all the four extractants, although more negative for L-III and less negative for L-IV. The net entropy changes can be attributed to conformational changes taking place during complexation. Since the spacer of L-I is longer than that of L-IV, the C−C bond rotation will be more restricted for L-I, which is reflected in the entropy changes upon complexation.

Fig. 4.6(c) presented the variation of D_{Am} from SHLW as a function of temperature using C4DGAs in [C_8mim][NTf_2]. ΔH values for different C4DGAs were found to follow the order L-I (-28.91 kJmol^{-1}) > L-II (-18.38 kJmol^{-1}) > L-V (-17.62 kJmol^{-1}) > L-VI (-15.70 kJmol^{-1}) > L-VII (-12.06 kJmol^{-1}). It was interesting to note that the enthalpy changes are far less negative as compared to those with feeds containing only dilute HNO_3. In case of SHLW solutions, the presence of large number of cations and anions decrease the water activity significantly and it is expected that the metal ion dehydration could be more facile suggesting less positive ΔH values for the dehydration reaction. This should be reflected in more negative ΔH values. However, less negative ΔH values [**Table 4.5**] suggest factors other than this, such as competitive complexation with other metal ions may be contributing to result in the significantly less negative enthalpy change values.

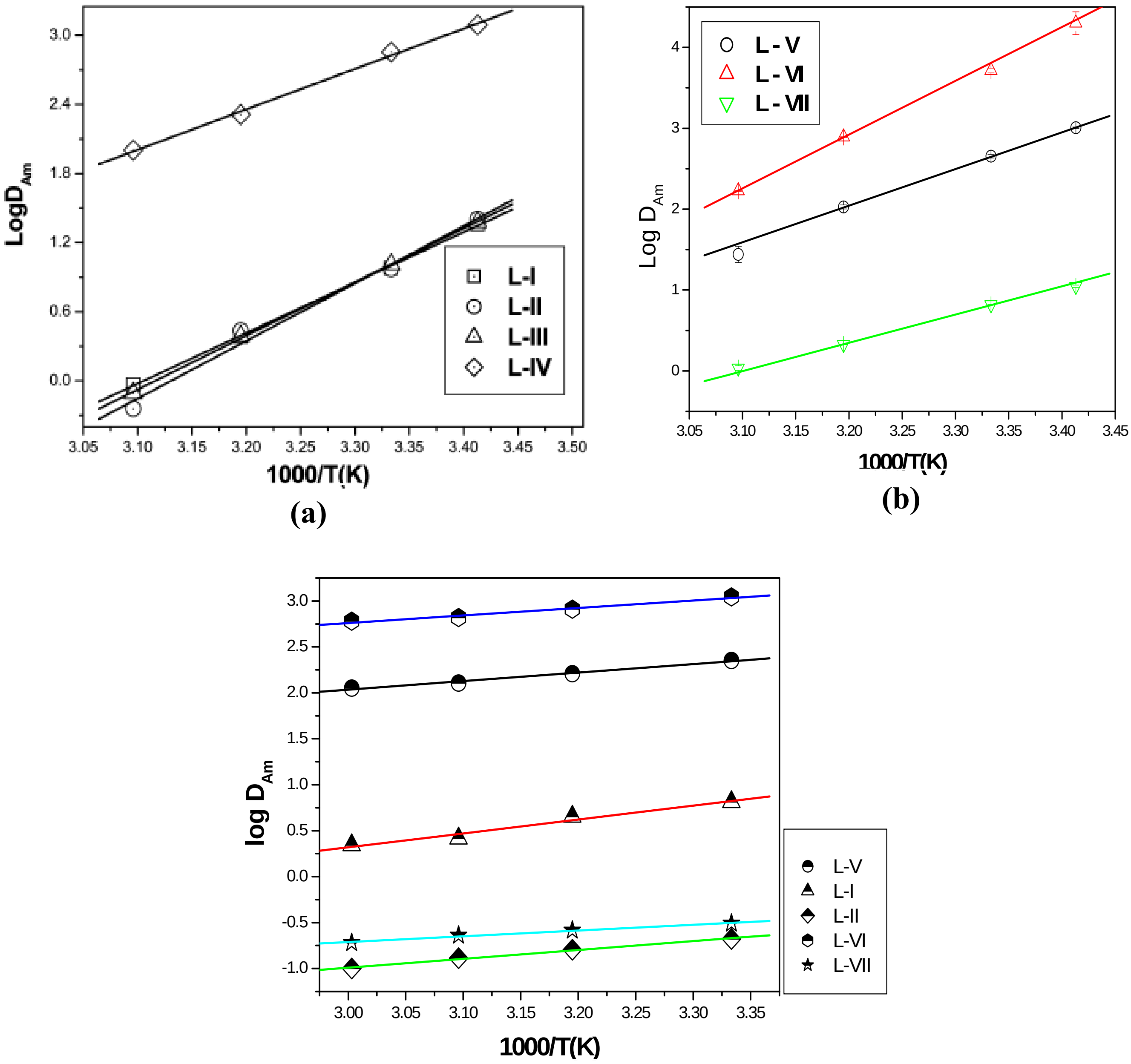

(a)

(b)

(c)

Fig 4.6: Effect of temperature on the extraction of Am(III) using (**a**) structurally modified C4DGAs; (**b**) different rim functionalized C4DGAs; (**c**) C4DGAs from SHLW. Diluent: [C$_8$mim][NTf$_2$], Equilibration time: 3 h. C4DGA conc. 5 x 10^{-4} M. Aq. Phase acidity: 0.5 M HNO$_3$.

Table 4.5: Thermodynamic parameters for the extraction of Am^{3+} using C4DGAs in RTIL

Ligand	ΔG ($kJmol^{-1}$)	ΔH($kJmol^{-1}$)	ΔS($Jmol^{-1}K^{-1}$)
L-I	-23.6	-84.1 (-28.9)	-201
L-II	-22.5	-95.7 (-18.4)	-244
L-III	-27.2	-89.3	-388
L-IV	-34.1	-67.2	-110
L-V	-40.9	-123 (-17.6)	-274
L-VI	-38.5	-93.3 (-15.7)	-202
L-VII	-24.4	-62.2 (-12.1)	-126

Note: Data inside the parenthesis is for Am^{3+} extraction from SHLW. Aqueous phase: 0.5 M HNO_3 (for L-I L-IV, L-V, L-VI), 0.1 M HNO_3 (for L-II and L-III) and 0.01 M HNO_3 (for L-VII); organic phase: 5.0×10^{-4} M C4DGA in $[C_8mim][NTf_2]$; equilibration time: 2 h.

4.7 Stripping Studies

Stripping of a metal ion from an ionic liquid phase has always been a challenging task because of the very high distribution ratio values at lower acidities and reasonably good extraction at higher acidities. Though the back extraction of the metal ion is possible at higher acidities, such as 3 M HNO_3 with two of the ligands (L-II and L-III), it may be difficult for the other two (L-I and L-IV). Therefore, complexing agents were employed for this purpose with amazingly good results [82,156] In the present study, the stripping of Am^{3+} was performed by employing three strippants, namely, (i) 0.05 M DTPA + 1 M guanidine carbonate, (ii) 0.05 M EDTA + 1 M guanidine carbonate, and (iii) a buffer mixture containing 0.4 M formic acid + 0.4

M hydrazine hydrate + 0.2 M citric acid; the results are summarized in **Table 4.6**. The results indicated that though near quantitative stripping took place with both complexing agents in a single contact (at a volume ratio of 1:1), the buffer mixture was not quite efficient. The stripping data are quite encouraging and suggest that the solvent system can be regenerated and reused for further metal ion extraction. Chemical degradation of the ligands were found to be negligible, though long-term use can have transfer of the ionic liquid into the aqueous phase requiring development of alternative diglycolamide-functionalized ionic liquids. The results suggested that from L-VI, which showed acid independent remarkably high extraction values for Am^{3+} in ionic liquids, quantitative stripping of trivalent actinide was possible.

Table 4.6: Stripping of Am(III) from C4DGAs in RTIL

Ligand	Strippant	% stripping in single contact
L-I	Guanidine carbonate + EDTA	99.3
	Guanidine carbonate + DTPA	99.6
	citric acid + formic acid+ hydrazine hydrate	78.3
L-IV	Guanidine carbonate + EDTA	99.2
	Guanidine carbonate + DTPA	98.9
	citric acid + formic acid+ hydrazine hydrate	99.3
L-V	Guanidine carbonate + EDTA	99.6
	Guanidine carbonate + DTPA	99.3
	citric acid + formic acid+ hydrazine hydrate	46.6
L-VI	Guanidine carbonate + EDTA	99.6
	Guanidine carbonate + DTPA	99.8
	citric acid + formic acid+ hydrazine hydrate	73.6

Note: Ligand concentration: 5×10^{-4} M, Diluent: [C_8mim][NTf_2], Feed acidity : 0.5 M HNO_3, T: 300 K, Equilibration time: 30 min, EDTA/ DTPA: 0.05 M, Guanidine carbonate: 1 M, Formic acid / Hydrazine hydrate: 0.4 M, Citric acid: 0.2 M

4.8 Radiolytic stability of the solvent systems

Though the C4DGA ligands are highly promising for actinide ion extraction, their actual use for actinide ion separation requires their prolonged reusability, which means their good radiolytic stability. This is because all actinide ions emit high LET (linear energy transfer) alpha particles, which can cause significant radiolytic damage. However, as exposure to the equivalent dose of γ radiation can show similar effect, it was decided to carry out the radiolytic degradation studies using a ^{60}Co irradiator (vide supra). A systematic study, carried out to investigate the radiolytic stability of the C4DGAs in [C_8mim][NTf_2], indicated that after exposing the organic phase to 500 kGy of the absorbed gamma dose, the extraction efficiency becomes 72%, 49%, 69%, and 72% of the original D_{Am} values (with the unirradiated ligand solution) with L-I, L-II, L-III, and L-IV, respectively, which after exposure to 1000 kGy decreased to 50%, 35%, 50%, and 46%, respectively of the original values (**Fig. 4.7(a)**). However, the degradation was most pronounced with L-VII. L-VI exhibited a significantly high resistance to radiolytic degradation as only 7% lowering in D_{Am} value was noticed after exposure to 500 kGy, which, however, sharply dropped to 37% upon an absorbed dose of 1000 kGy. On the other hand, L-V showed a medium stability against radiolytic damage. The results shown in **Fig. 4.7(b)** suggest that L-VI has a great potential for the extraction of actinides from radioactive waste streams as it can be easily recycled and even after exposure to a significantly large radiation dose, the solvent can be recycled for a long time thereby reducing the process costs. The present results are very significant, since several solvent systems in ionic liquid medium are reported to have poor radiation stability [157,158]. Also, in view of the relatively large D_{Am} values obtained with the solvent systems in ionic liquids, the % extraction data is not significantly affected even after exposure up to 1000 kGy.

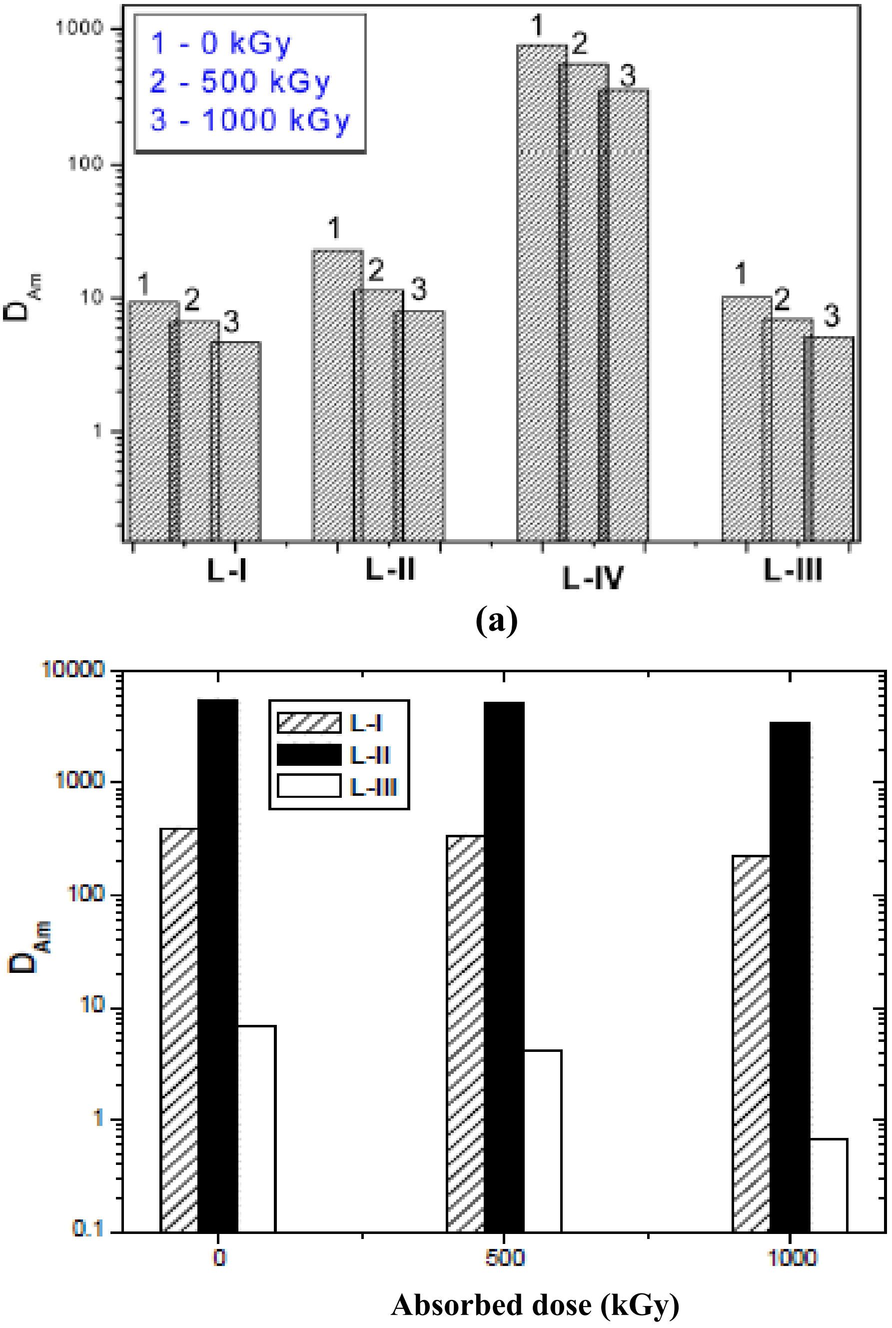

(a)

(b)

Fig 4.7: Effect of absorbed dose on the distribution ratio of Am^{3+} into 5.0 x 10^{-4} M C4DGAs in $[C_8mim][NTf_2]$. Aqueous phase: 0.5 M HNO_3 (for L-I, L-IV, L-V, L-VI), 0.1 M HNO_3 (for L-II and L-III) and 0.01 M HNO_3 (for L-VII); equilibration time: 2 h.

4.9 Studies on the complexation of Eu(III) with C4DGA ligands by luminescence spectroscopy

The structure of the metal-ligand complexes needs to be analyzed to understand the nature of the bonding in the ionic liquid-based solvents. However, in view of the difficulty in obtaining single crystals, as an alternative, spectroscopic technique is applied. This study deals with the characterization of Eu^{3+}-C4DGA complexes in the ionic liquid $[C_8mim][NTf_2]$ using time resolved laser induced fluorescence spectroscopy (TRLFS). Eu^{3+}, with luminescence properties, has been used as a surrogate of Am^{3+} to study the complexation with the different C4DGA ligands.

In addition to the effect of the medium, the role of structural modification of the C4DGA ligands, viz. alkyl substituents at the amidic nitrogen atom, spacer length (between the calix[4]arene platform and the ligating sites) and different rim functionalized C4DGAs, on the luminescence properties of Eu^{3+} and the complexation nature were also investigated. Judd - Ofelt parameters, i.e. Ω_2, Ω_4, which indicate the measure of covalency of the bond between the metal ion and the ligating atoms in a metal-ligand complex and the long range effect, respectively [159-164], were calculated for all complexes and correlated with the steric hindrance around the ligating sites. The radiative and non-radiative lifetimes, branching ratios, the number of water molecules in the primary coordination sphere of the Eu^{3+} ion, and the probabilities of the observed transitions were also calculated. For comparison purpose, similar studies were also carried out using TODGA and T-DGA (Chapter 3).

4.9.1 Local environment around Eu^{3+} ion

Emission spectroscopy is one of the important tools to probe the local environment around metal ions. The emission profiles of all the Eu^{3+}-C4DGA complexes in $[C_8mim][NTf_2]$ appear to be similar with one peak at 593 nm (assigned to the $^5D_0 \rightarrow {}^7F_1$ transition), two peaks at 614 and 619 nm (due to the $^5D_0 \rightarrow {}^7F_2$ transitions), three peaks at 686, 698, and 701.5 nm (attributed to the $^5D_0 \rightarrow {}^7F_4$ transitions) (**Fig. 4.8(a) and (b)**). The high intensity of the peaks due to the $^5D_0 \rightarrow {}^7F_2$ transitions revealed that there is low symmetry around the Eu^{3+} ion. The asymmetric factor, which is the signature of asymmetry around the Eu^{3+} ion with respect to inversion, was calculated using the following equation: [165]

$$A = I(^5D_0 \rightarrow {}^7F_2) / I(^5D_0 \rightarrow {}^7F_1) \qquad (4.11)$$

where, A is termed as the asymmetry factor, $I(^5D_0 \rightarrow {}^7F_2)$ and $I(^5D_0 \rightarrow {}^7F_1)$ being the intensities of the corresponding transitions. $^5D_0 \rightarrow {}^7F_1$ transitions being magnetic-dipole transitions, $I(^5D_0 \rightarrow {}^7F_1)$ is independent of the ligand field. The $^5D_0 \rightarrow {}^7F_2$ transition being a hypersensitive electric-dipole transition, its intensity is hypersensitive to the ligand field. The asymmetric factor values for the ligands follow the trend: L-VII > L-V > L-VI > T-DGA > L-IV > L-II > TODGA > L-I > L-III for the complexes in $[C_8mim][NTf_2]$ (**Table 4.7**), while the trend in the 5:1 acetonitrile-water mixture follows the order: L-II > L-I > L-V ~ L-III > T-DGA (**Table 4.7**). In general, relatively higher asymmetry factors were obtained for the metal-ligand complexes in the 5:1 acetonitrile-water mixture than in $[C_8mim][NTf_2]$. A comparative study was carried out to understand the effect of medium on the photo physical properties of the complex. **Fig 4.8(c)** represented the emission spectra of different Eu – C4DGA complexes in a mixture of water:

acetonitrile (1:5). The complexes in [C_8mim][NTf_2] are more symmetric with respect to the inversion symmetry. The increase in intensity upon complexation may be due to the relaxation of the selection rule originating from the overlap of the metal ion orbital with that of the ligand. Number of water molecules present in the primary co-ordination sphere of the Eu^{3+} was calculated from the lifetime (τ) using equation (4.12) [166].

$$N_{H2O} = (1.06/\tau) - 0.19 \qquad (4.12)$$

The results suggested absence of inner sphere water molecules in the complexes except for the Eu^{3+}- L-VII complex which contained five water molecules. Life times beyond 1.2 ms suggested that there is no non-radiative transition through the OH group, while the variation in the life times indicated that some other route is responsible for the non-radioactive decay. The life times of the Eu^{3+} complex having C4DGA ligands with an NH group (L-V and L-IV) are smaller than those of the ligands with alkyl-substituted nitrogen atoms (L-I, L-II, and L-III) in case of the Eu^{3+} complexes in ionic liquid, indicating that in the first case there are some additional non-radiative pathways to depopulate the $^5D_0$ level.

Fig. 4.9 represents a schematic route for the determination of the symmetry point group around Eu^{3+} from the splitting of the transitions [167]. Four sets of peaks due to the $^5D_0 \rightarrow {}^7F_0$, $^5D_0 \rightarrow {}^7F_1$, $^5D_0 \rightarrow {}^7F_2$, and $^5D_0 \rightarrow {}^7F_4$ transitions for the Eu^{3+} - L-I complex are shown in **Fig. 4.10(a)**. Though the $^5D_0 \rightarrow {}^7F_{0,}$ $^5D_0 \rightarrow {}^7F_2$ and $^5D_0 \rightarrow {}^7F_4$ transitions with the expected single peak at 579 nm, two peaks at 613 nm and 618 nm, and four peaks at 686 nm, 696 nm, 698 nm and 701.5 nm, respectively are easily identified, the peaks from $^5D_0 \rightarrow {}^7F_1$ transitions are not clearly identified as they are merged. A careful Gaussian deconvolution of the bands gives the $^5D_0 \rightarrow {}^7F_1$ bands with two lines. The spectral assignments for the other complex systems are shown in **Fig.s 4.10(b)-4.10(j)**. The above number of peaks corresponding to the specified transitions indicates that in all cases, the local symmetry around Eu^{3+} is C_{4V} (**Fig. 4.10**). A similar observation was found for all analogous complexes in the acetonitrile-water (5:1) mixture. In C_{4V} symmetry, the C_4 axis will pass through Eu^{3+} and the point where two diagonals of the molecular plane intersect. Out of four σ_vs, two will cut the molecular plane without touching the carbonyl group, while the other two will cut the carbonyls. Both sets of σ_vs will contain the C_4 axis. The strain generated due to the pre-organization of four DGA units to achieve C_{4V} geometry will be compensated by the formation of eight coordinated bonds (two carbonyl oxygen atoms from each DGA moiety) from the carbonyl oxygen to Eu^{3+}. The coordination number of Eu^{3+} in such a complex should be eight (from C4GDA), which is similar to the complex of Am^{3+} with TODGA in *n*-dodecane as $Am(TODGA)_4^{3+}$ [103]. From the splitting pattern, the symmetry around Eu^{3+} was found to be C_{2V} for the Eu^{3+}-T-DGA complex in both $[C_4mim][NTf_2]$ and the acetonitrile – water (5:1) mixture, whereas the local symmetry of Eu^{3+}-TODGA complex in $[C_4mim][NTf_2]$ was found to be C_{4V}. The splitting pattern of the emission spectra of Eu^{3+}-L-VII suggested the symmetry to be C_1, C_2, or C_S.

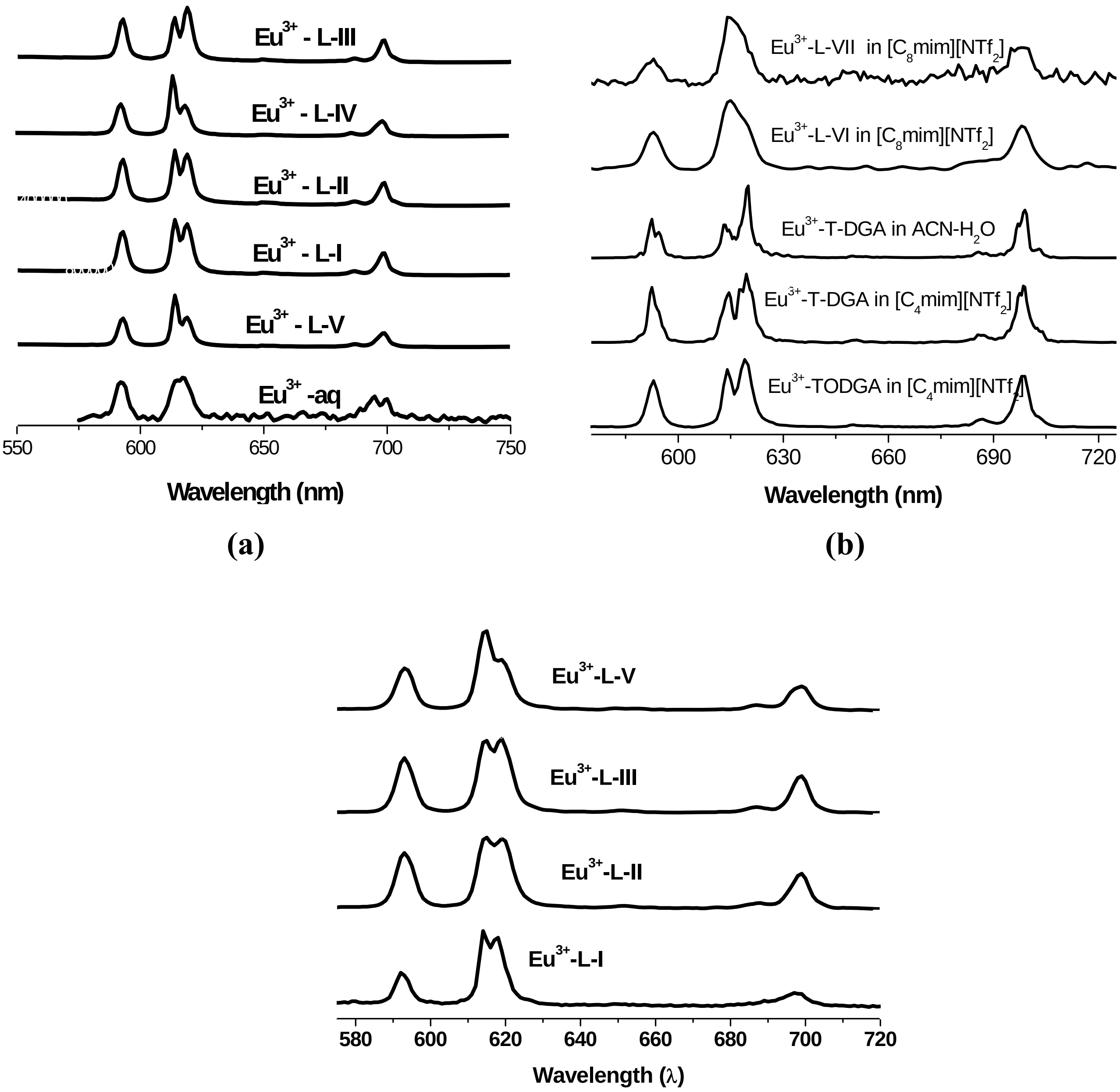

(a) (b)

(c)

Fig. 4.8: Fluorescence spectra of (**a**) Eu^{3+} complexes of different structurally modified C4DGAs in [C$_8$mim][NTf$_2$]; (**b**) Eu^{3+} complexes of different rim functionalized C4DGAs in [C$_8$mim][NTf$_2$];(**c**) Eu^{3+} complexes of different structurally modified C4DGAs in acetonitrile – water mixture (5:1)

Table 4.7: Determination of photo-physical properties of Eu^{3+} - C4DGA complexes

Complex	Lifetime (μs)	$N(H_2O)$	A	τ_R (s)	τ_{NR} (s)	η	β_1	β_2	β_4	A_{md}	A_{2ed}	A_{4ed}
Eu^{3+} - L-I*	1869 ± 19	0	1.9	214	320	0.4	0.20	0.50	0.30	42.65	106.0	63.3
Eu^{3+} -L-II*	2082 ± 21	0	2.08	214	266	0.5	0.20	0.49	0.30	42.6	105.0	65.0
Eu^{3+} - L-III*	2119 ± 21	0	1.54	213	259	0.5	0.20	0.49	0.30	42.5	107.0	64.6
Eu^{3+} - L-IV*	1544 ± 15	0	2.12	225	420	0.4	0.19	0.51	0.29	42.5	115.0	64.4
Eu^{3+} - L-V*	1522 ± 15	0	2.73	226	431	0.3	0.19	0.52	0.28	42.6	117.0	64.4
Eu^{3+}- L-VI*	1522 ± 13	0	2.41	268	465	0.4	0.18	0.48	0.30	42.6	112.0	71.6
Eu^{3+}- L-VII*	210 ± 6	5	2.86	349	4412	0.1	0.18	0.48	0.31	42.7	146.0	111.0
Eu^{3+}- TODGA*	2171 ± 16	0	1.98	224	280	0.4	0.19	0.48	0.30	42.6	107.0	67.0
Eu^{3+}- T-DGA*	2251 ± 16	0	2.34	219	225	0.5	0.20	0.47	0.31	42.8	102.0	68.4
Eu^{3+}-L-I**	2096 ± 21	0	2.75	188	288	0.4	0.19	0.49	0.32	34.95	94.7	58.6
Eu^{3+}-L-II**	1689 ± 17	0	2.63	189	401	0.3	0.18	0.50	0.31	34.95	94.7	58.6
Eu^{3+}-L-III**	2720 ± 27	0	2.65	186	181	0.5	0.19	0.48	0.32	34.97	89.8	60.3
Eu^{3+}-L-V**	1695 ± 17	0	2.69	187	402	0.3	0.19	0.50	0.30	34.96	94.2	55.9
Eu^{3+}- T-DGA**	2282 ± 13	0	2.51	231	206	0.5	0.19	0.48	0.30	42.81	111.0	69.7

Note: * Refers to the complexes in $[C_8mim][NTf_2]$, ** refers to the complexes in acetonitrile – water (5:1)

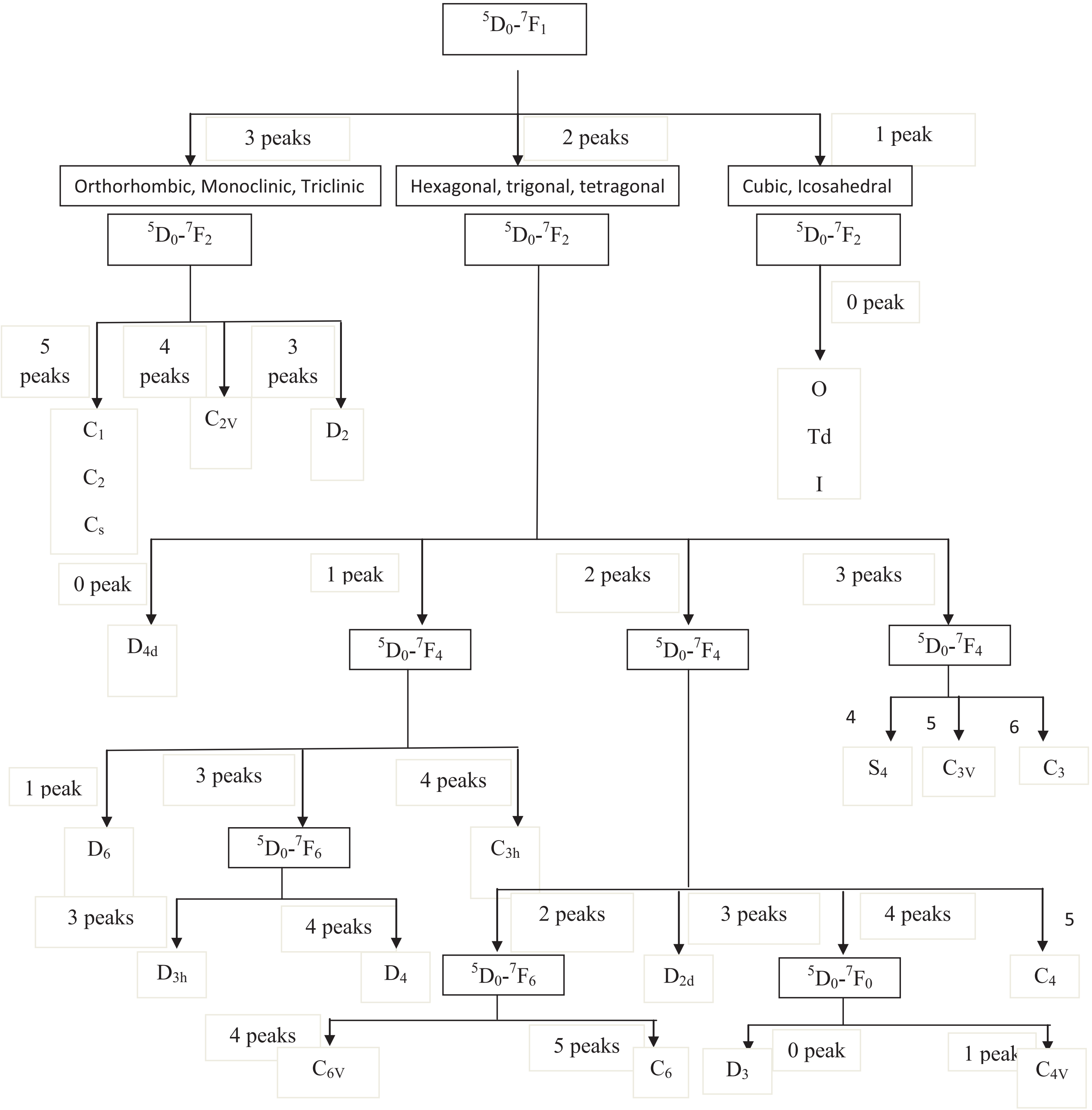

Fig. 4.9: Scheme for point group determination of the luminescent Eu^{3+} ion.

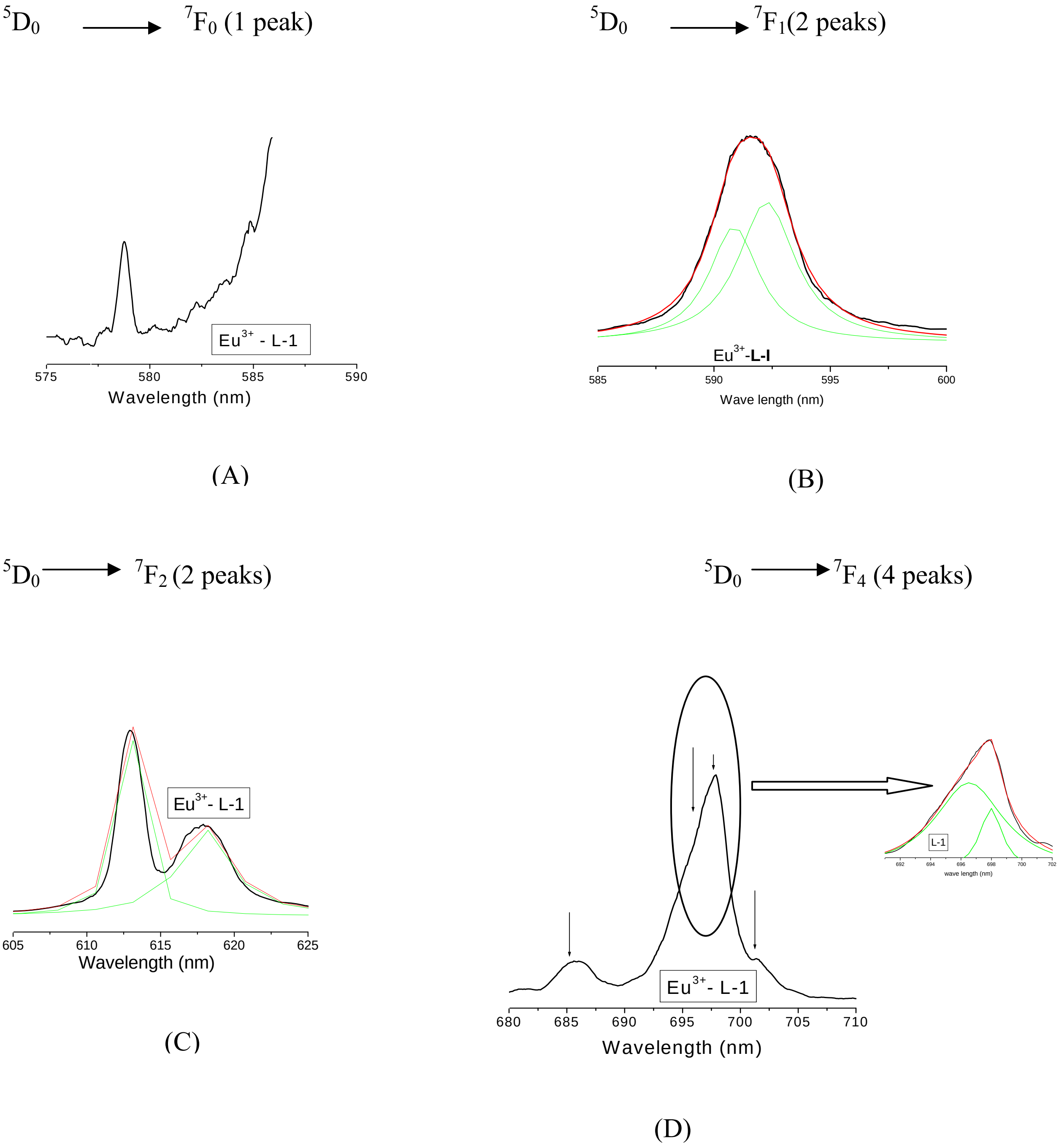

$^5D_0 \longrightarrow {}^7F_0$ (1 peak)

$^5D_0 \longrightarrow {}^7F_1$(2 peaks)

$^5D_0 \longrightarrow {}^7F_2$ (2 peaks)

$^5D_0 \longrightarrow {}^7F_4$ (4 peaks)

Eu^{3+}-L-I complex in [C$_8$mim][NTf$_2$]: (A) $^5D_0 \rightarrow {}^7F_0$, (B) $^5D_0 \rightarrow {}^7F_1$, (C) $^5D_0 \rightarrow {}^7F_2$ and (D) $^5D_0 \rightarrow {}^7F_4$ transitions

(a)

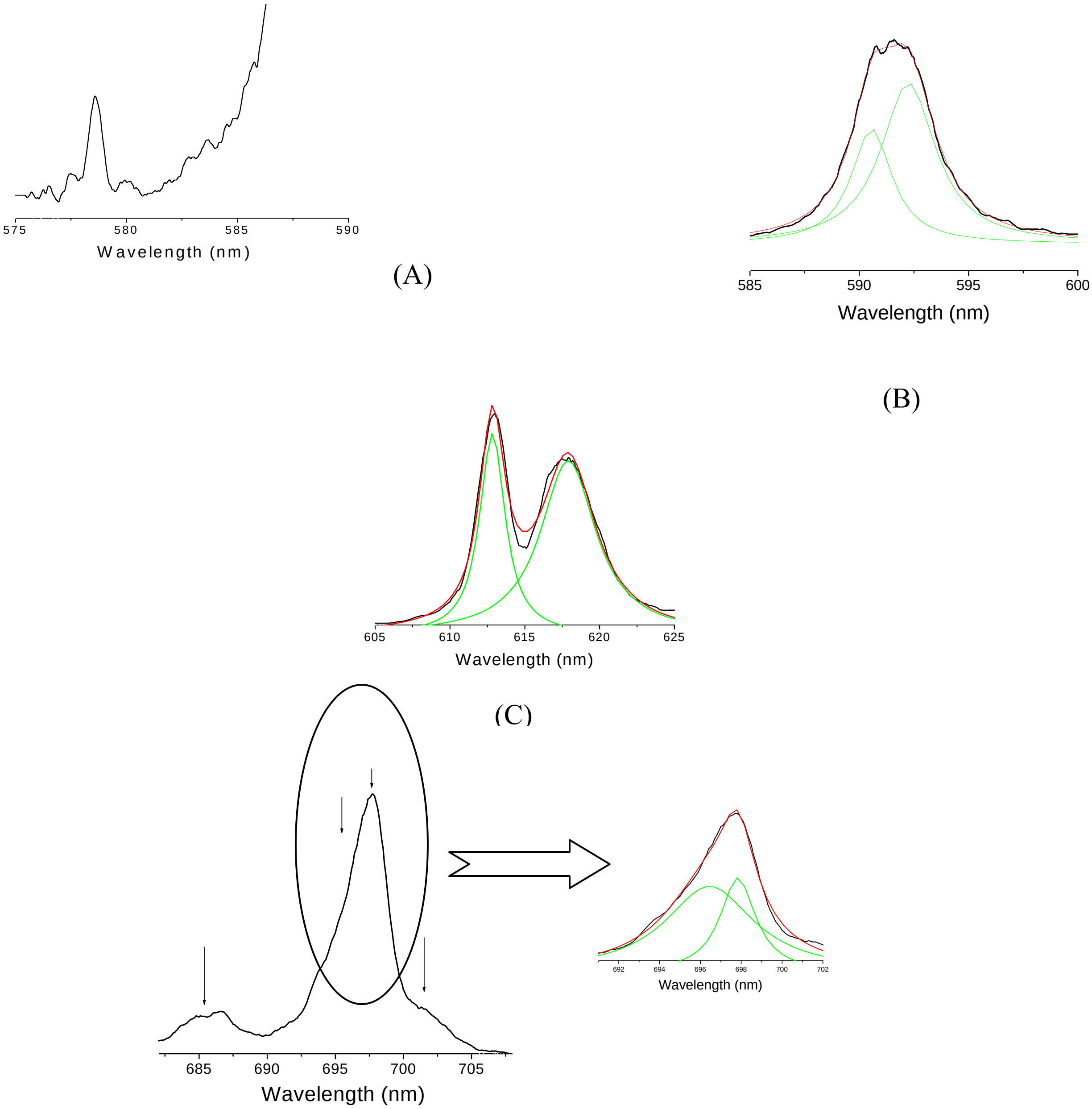

(A)

(B)

(C)

(D)

Eu^{3+}-L-II complex in [C$_8$mim][NTf$_2$]: (A) $^5D_0\rightarrow{}^7F_0$, (B) $^5D_0$-$^7F_1$, (C) $^5D_0\rightarrow{}^7F_2$ and (D) $^5D_0\rightarrow{}^7F_4$ transitions

(b)

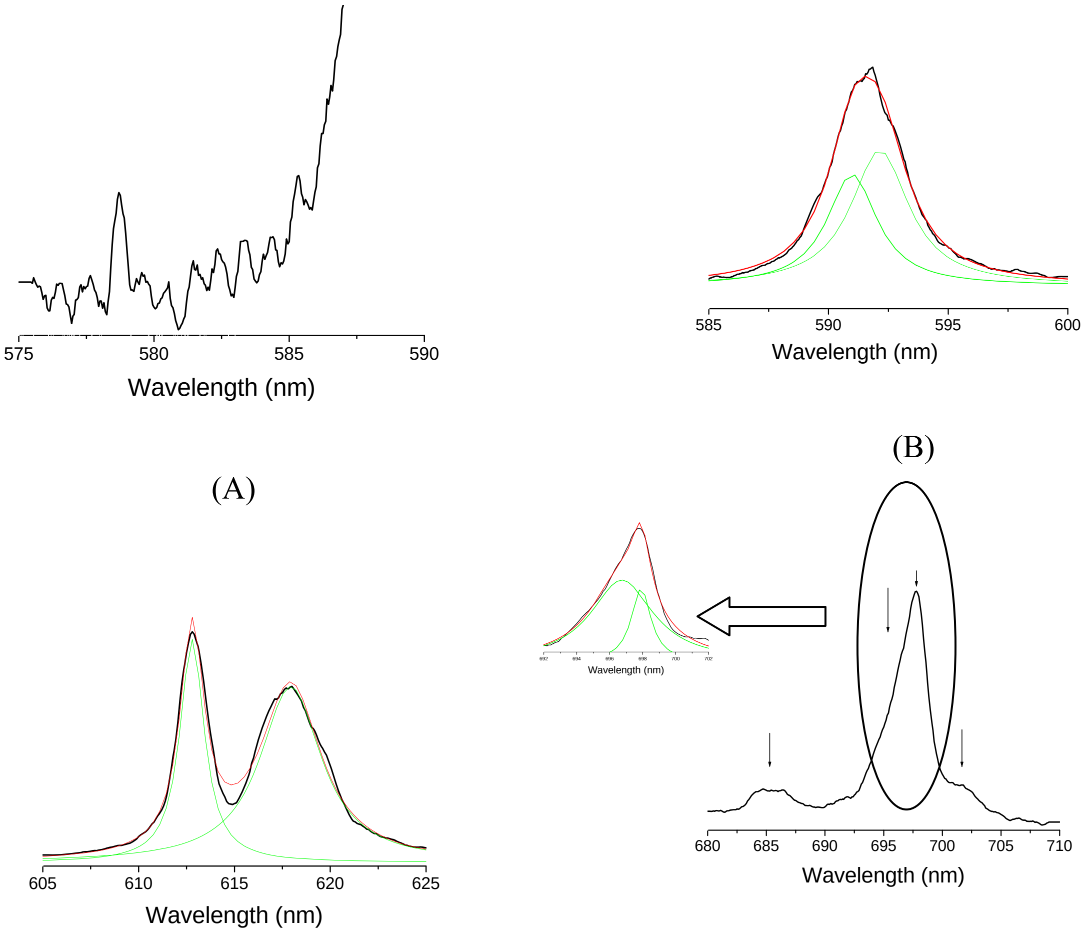

(A)

(B)

(C)

(D)

Eu^{3+}-L-III complex in [C$_8$mim][NTf$_2$]: (A) $^5D_0 \rightarrow ^7F_0$, (B) $^5D_0 \rightarrow ^7F_1$, (C) $^5D_0 \rightarrow ^7F_2$ and (D) $^5D_0 \rightarrow ^7F_4$ transitions

(c)

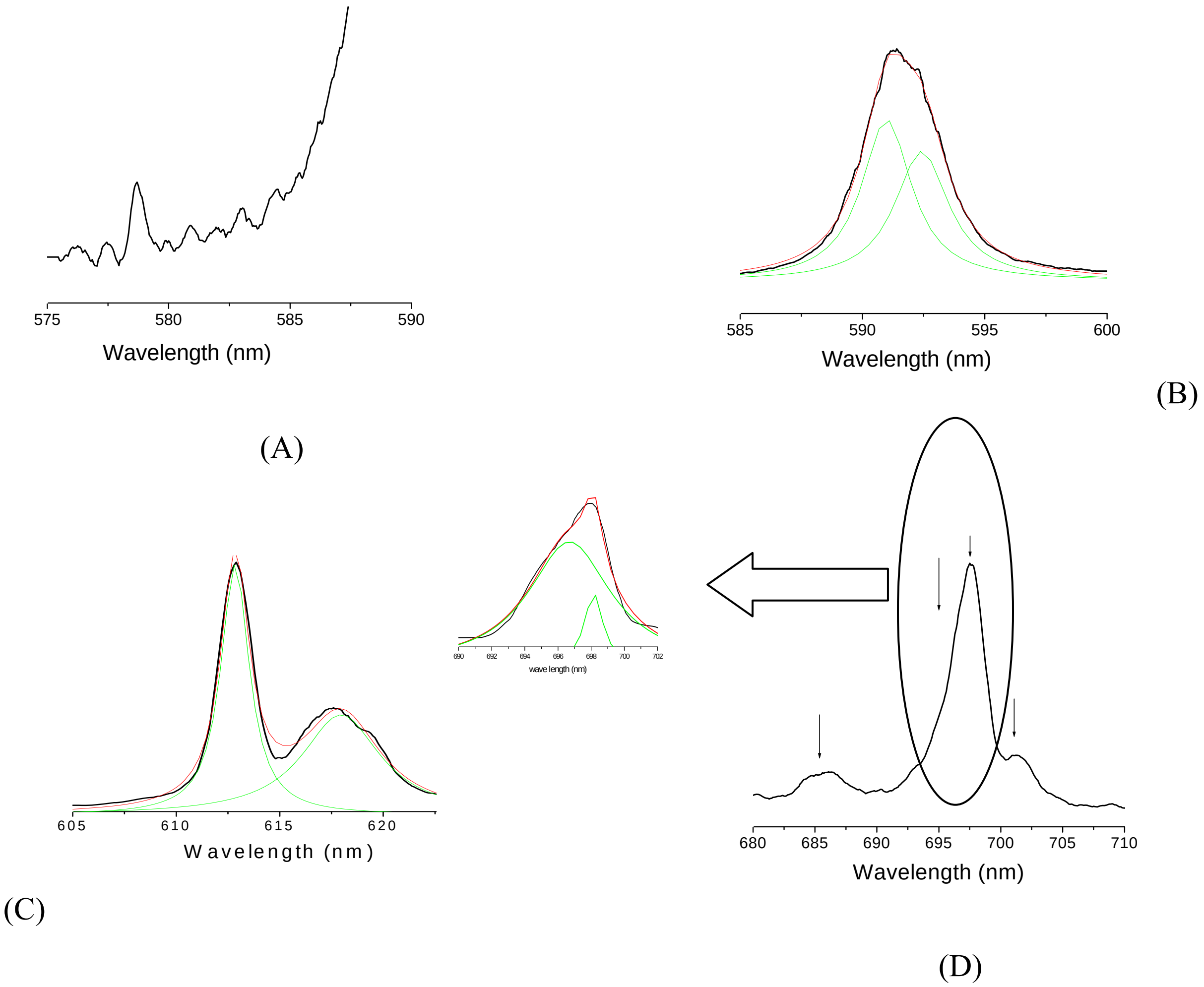

Eu^{3+}-L-IV complex in [C$_8$mim][NTf$_2$]: (A) $^5D_0 \rightarrow ^7F_0$, (B) $^5D_0 \rightarrow ^7F_1$, (C) $^5D_0 \rightarrow ^7F_2$ and (D) $^5D_0 \rightarrow ^7F_4$ transitions

(d)

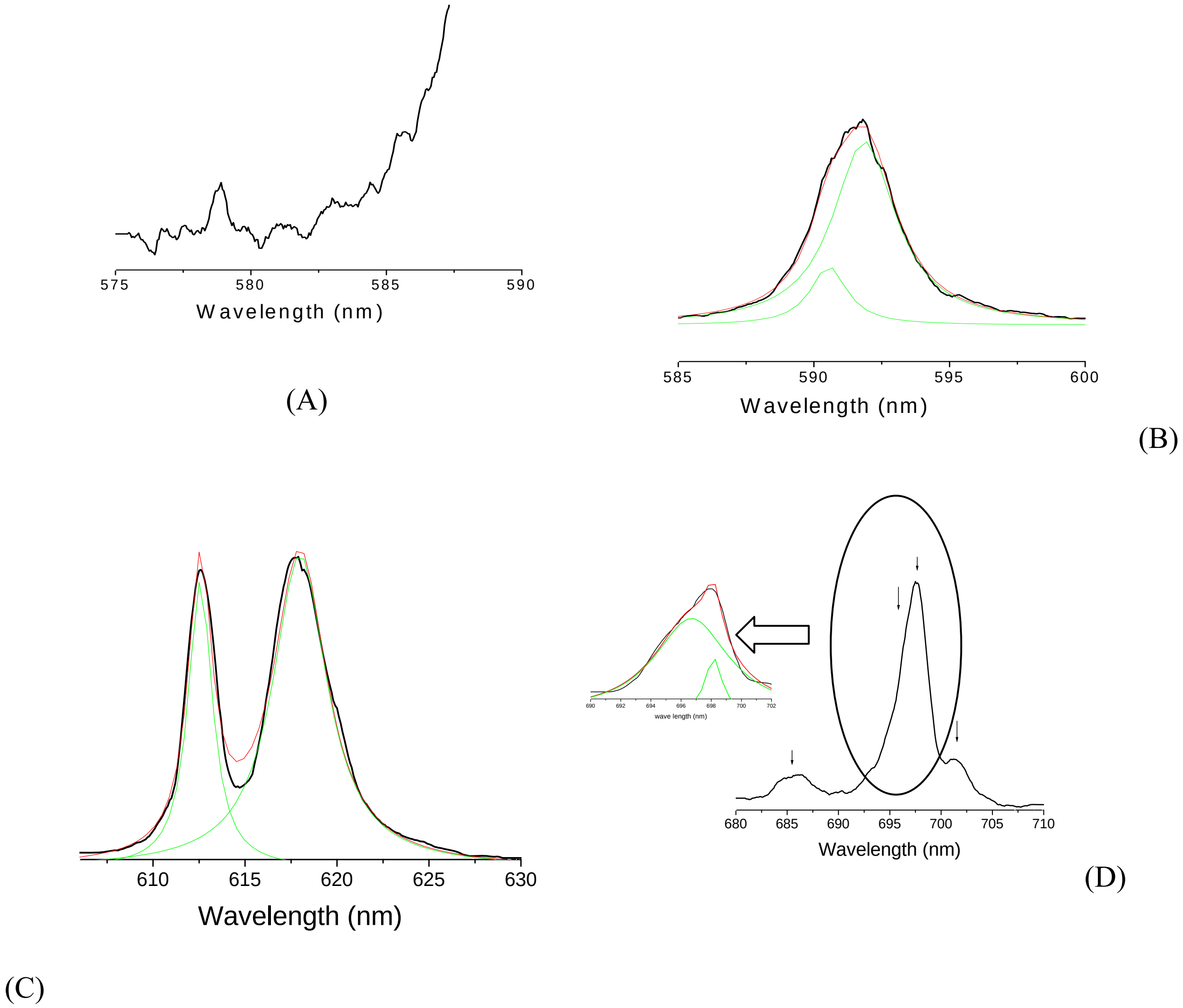

Eu^{3+}-L-V complex in [C$_8$mim][NTf$_2$]: (A) $^5D_0 \rightarrow {}^7F_0$, (B) $^5D_0 \rightarrow {}^7F_1$, (C) $^5D_0 \rightarrow {}^7F_2$ and (D) $^5D_0 \rightarrow {}^7F_4$ transitions

(e)

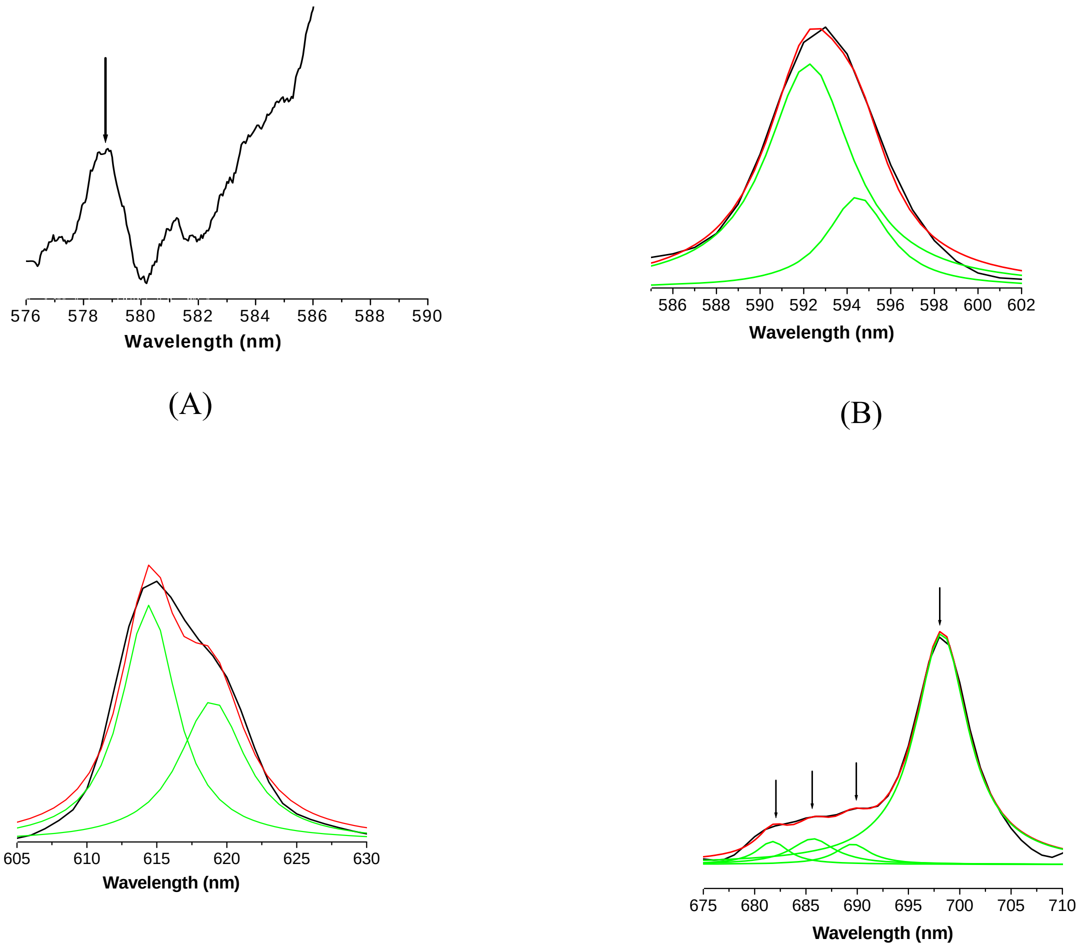

(A)

(B)

(C)

(D)

Eu^{3+}-L-VI complex in [C$_8$mim][NTf$_2$]: (A) – $^5D_0 \rightarrow {}^7F_0$ transition – 1 peak, (B) – $^5D_0 \rightarrow {}^7F_1$ transition – 2 peaks, (C) - $^5D_0 \rightarrow {}^7F_2$ transition – 2 peaks, (D) – $^5D_0 \rightarrow {}^7F_4$ transition – 4 peaks, C$_{4V}$ symmetry

(f)

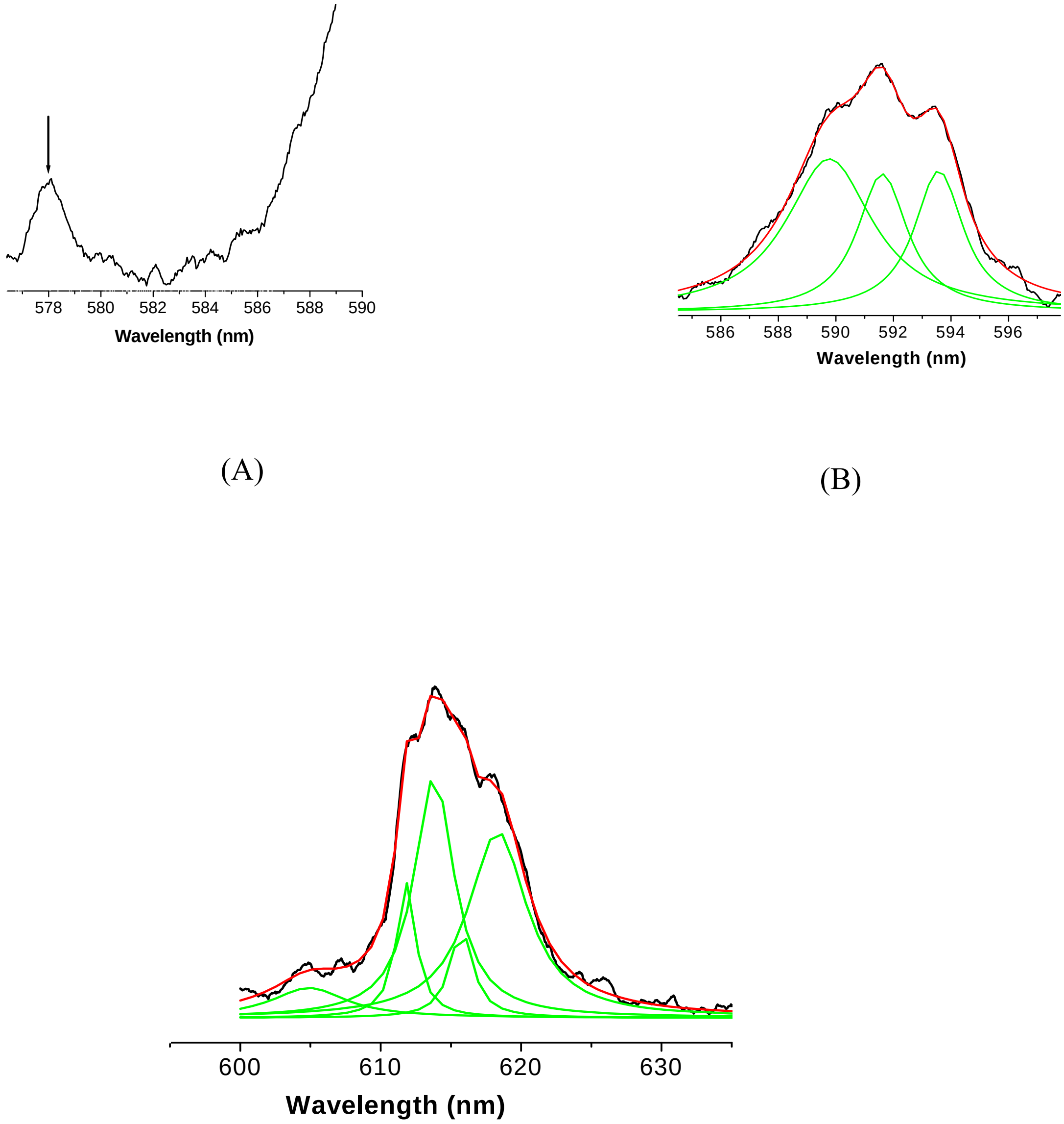

(A)

(B)

(C)

Eu^{3+}-L-VII complex in [C$_8$mim][NTf$_2$]: (A) – $^5D_0 \rightarrow {}^7F_0$ transition – 1 peak, (B) – $^5D_0 \rightarrow {}^7F_1$ transition – 3 peaks, **(**C) **-** $^5D_0 \rightarrow {}^7F_2$ transition – 5 peaks, C$_1$, C$_2$, C$_S$ symmetry

(g)

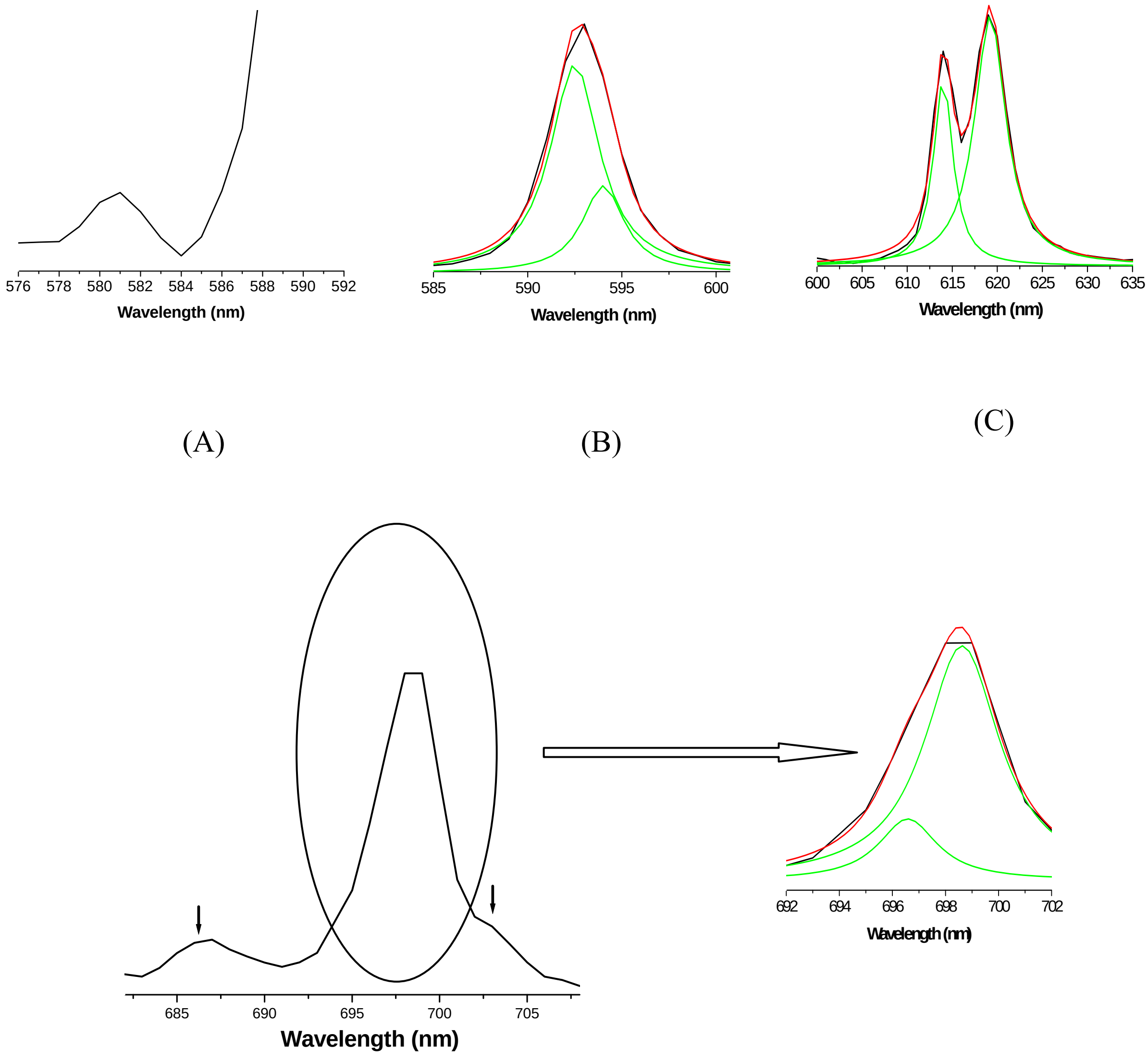

(A)

(B)

(C)

(D)

Eu^{3+}-TODGA complex in [C$_4$mim][NTf$_2$]: (A) – $^5D_0 \rightarrow {}^7F_0$ transition – 1 peak, (B) – $^5D_0 \rightarrow {}^7F_1$ transition – 2 peaks, (C) - $^5D_0 \rightarrow {}^7F_2$ transition – 2 peaks, (D) – $^5D_0 \rightarrow {}^7F_4$ transition – 4 peaks, C_{4V} symmetry

(h)

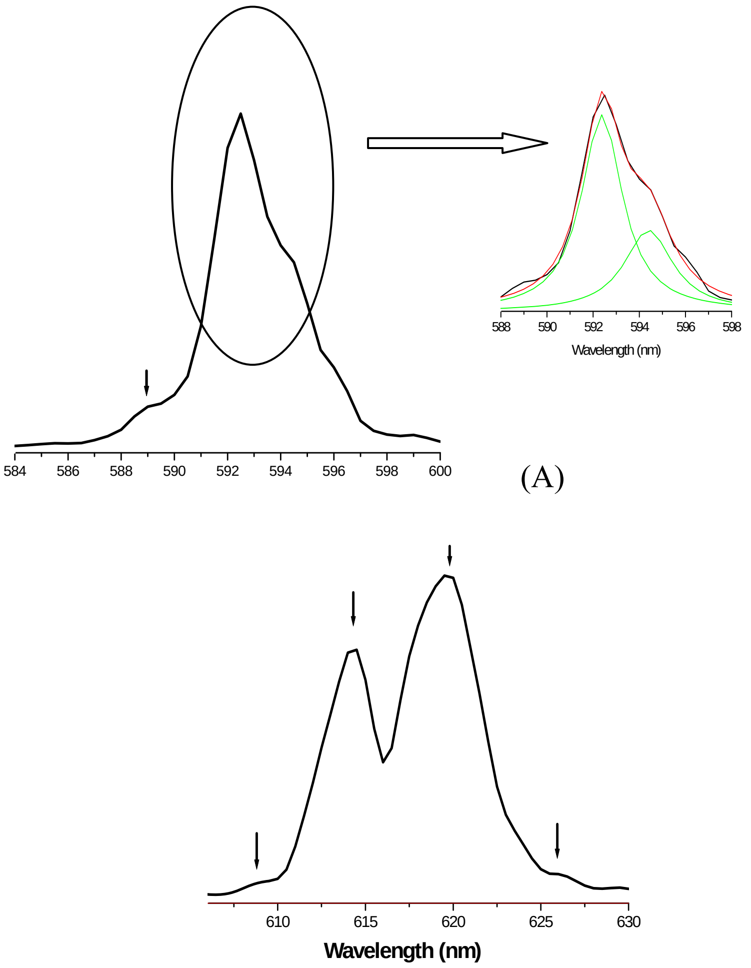

(A)

(B)

Eu^{3+}-T-D-GA complex in [C$_4$mim][NTf$_2$]: (A) – $^5D_0 \rightarrow {}^7F_1$ transition – 3 peaks, (B) – $^5D_0 \rightarrow {}^7F_2$ transition – 4 peaks, C_{2V} symmetry

(i)

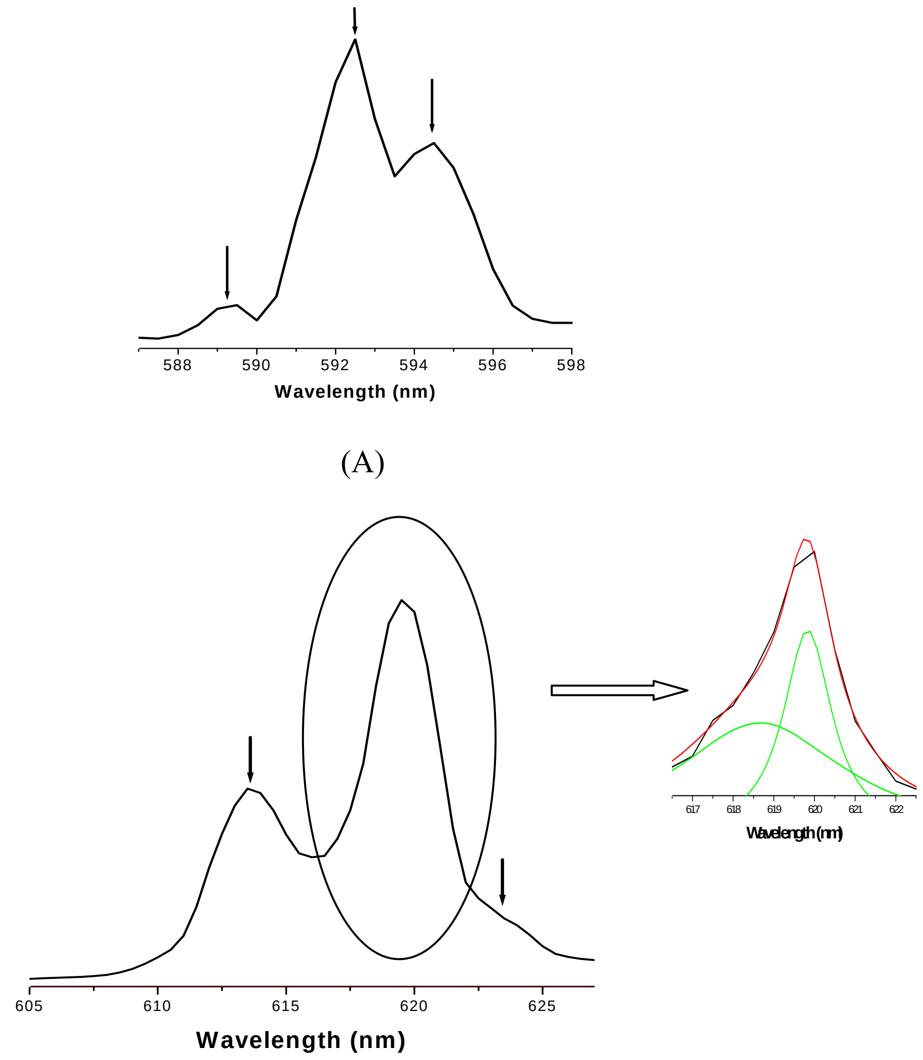

(A)

(B)

Eu^{3+}-T-DGA complex in acetonitrile – water mixture: (A) – $^5D_0 \rightarrow {}^7F_1$ transition – 3 peaks, (B) – $^5D_0 \rightarrow {}^7F_2$ transition – 4 peaks, C_{2V} symmetry

(j)

Fig. 4.10: Splitting pattern of the emission profiles of (**a**) Eu^{3+}-L-I in RTIL; (**b**) Eu^{3+}-L-II in RTIL; (**c**) Eu^{3+}-L-III in RTIL; (**d**) Eu^{3+}-L-IV in RTIL; (**e**) Eu^{3+}-L-V in RTIL; (**f**) Eu^{3+}-L-VI in RTIL; (**g**) Eu^{3+}-L-VII in RTIL; (**h**) Eu^{3+}-TODGA in RTIL; (**i**) Eu^{3+}-T-DGA in RTIL; (**j**) Eu^{3+}-T-DGA in acetonitrile - water

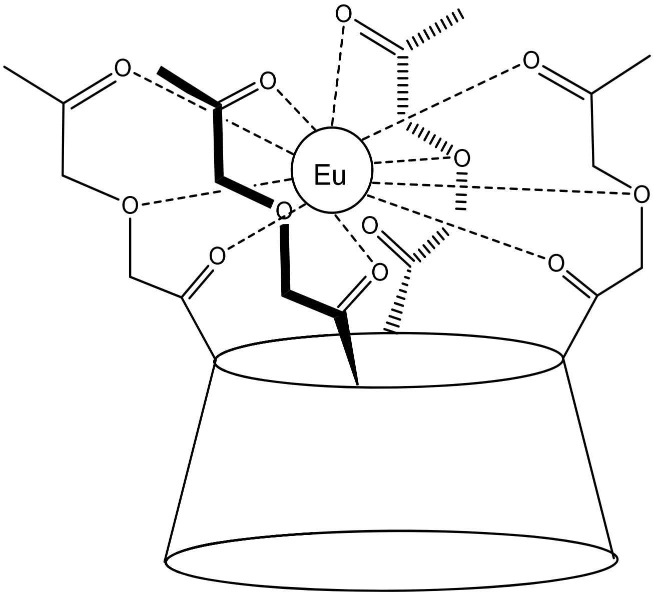

Fig. 4.11: Schematic representation of Eu^{3+}-C4DGA complex with C_{4v} symmetry

4.9.2 Line broadening effect

Since all experiments were carried out in solution, broadening of the spectra was observed, which points to the continuous motion of the complexes in the medium. With increase in the viscosity of the medium, the motion gets restricted and the emission profile becomes sharper. In the present case, a marginal sharpening in the line width of the Eu^{3+}-C4DGA complexes in $[C_8mim][NTf_2]$ (which has relatively higher viscosity value) was observed compared to that in the acetonitrile –water (5:1) mixture (**Fig. 4.12**).

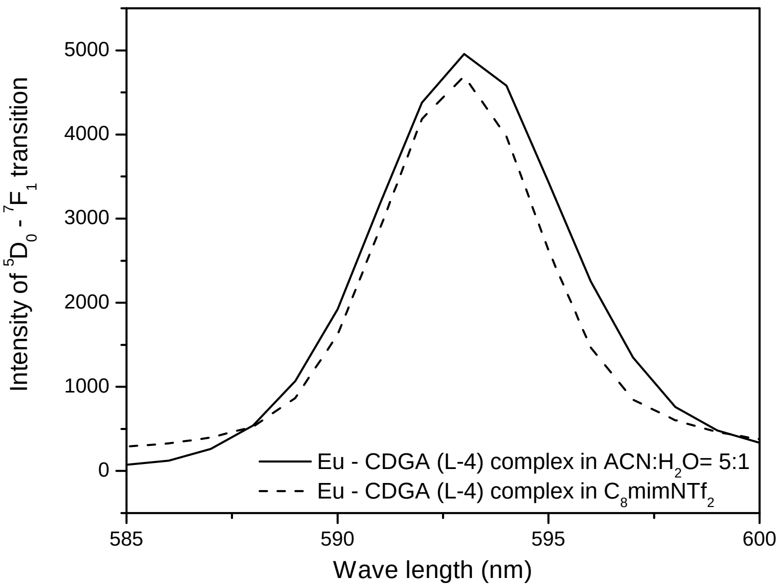

Fig. 4.12: Line broadening in different media: effect of viscosity

4.9.3 Calculation of J-O parameters

Judd–Ofelt intensity parameters are essential indicators in judging the radiative potential of rare earth ions complexed in a host, which are usually derived from the absorption spectrum. However, owing to the special energy level structure of Eu^{3+}, they can be calculated from the emission spectrum. The transitions of Eu^{3+} from $^5D_0$ to ^7F_J (J = 2, 4, 6) are electronic-dipole allowed and the spontaneous emission probability A_{ed} from initial manifold ψ to terminal manifold ψ' is given by equation (4.13): [82,156]

$$A_{ed} = 64\pi^4 e^2 \nu^3\, n(n^2 + 2)^2 / (3h(2J + 1))\ 9)\ \Sigma\, \Omega_\lambda\, |<\psi||U^\lambda||\psi'>|^2 \qquad (4.13)$$

where, h is the Planck constant, e is the electron charge, n is the refractive index, J is the total angular momentum of the excited state, and ν is the wavenumber of a transition. Ω_λ are the Judd–Ofelt parameters. The term $|<\psi||U^\lambda||\psi'>|^2$ is the square of the matrix elements of the tensor operator, which connects ψ to the final state ψ' and is considered to be independent of the host matrix.

The $^5D_0 \rightarrow {}^7F_1$ of Eu^{3+} ions is a magnetic-dipole transition and the spontaneous emission probability of the magnetic-dipole transition A_{md} [82,156] is given as

$$A_{md} = 64\pi^4 \nu^3 n^3 S_{md} / 3h\,(2J+1) \qquad (4.14)$$

where, S_{md} is the magnetic-dipole line strength (constant and independent of the medium). Due to selection rules and the unique nature of the transition intensities of Eu^{3+} ions, each of the $|<\psi||U^\lambda||\psi'>|^2$ values decide the intensities of the transitions, since the remaining two are zero. Thus, the Ω_λ value can be determined from the ratios of the intensities of $^5D_0 \rightarrow {}^7F_{2\ 4,\ 6}$ transitions to those of the $^5D_0 \rightarrow {}^7F_1$ transitions as follows:

$$\int IJ(\nu)d\nu / \int I_{md}(\nu)\, d\nu = A_J/A_{md} = 64\pi^4 e^2 \nu^3 / 3h(2J+1) \text{ x } n(n^2+2)^2/9A_{md}\, \Omega_\lambda\, |<\psi||U^\lambda||\psi'>|^2 \qquad (4.15)$$

The derived Ω_2 and Ω_4 parameters are listed in **Table 4.8**. The Ω_6 intensity parameter was not determined, because the $^5D_0 \rightarrow {}^7F_6$ emission in this system could not be detected and recorded. Judd–Ofelt intensity parameters reflect the local structure and bonding in the vicinity of the rare earth ions [156]. For example, Ω_2 exhibits the dependence on the covalency between the Eu^{3+} ion and the ligand donor atoms and gives information about the asymmetry of its local environment. In $[C_8mim][NTf_2]$, the Ω_2 values follow the order Eu^{3+}-L-V > Eu^{3+}-L-IV > Eu^{3+}-L-III > Eu^{3+}-L-I > Eu^{3+}-L-II and as a consequence, the covalency of the metal–ligand bond follows the same trend. As a matter of fact, the bond distance will show an increasing trend which can be attributed to the steric hindrance at the amidic N atoms. In case of ligands L-I, L-III, and L-II, the size of the substituents on N increases from *n*-propyl to *iso*-pentyl to *n*-octyl, and as a result, the approach of the metal ion towards the ligating sites is hindered. Hence, the bond length between the Eu^{3+} ion and the ligand increases leading to a decrease in the covalency of the bond and a concomitant decrease in Ω_2. The Ω_2 of L-IV is smaller than that of L-V, probably because of its shorter spacer length (2 vs 3 carbon atoms) causing steric hindrance of the calix[4]arene ring. In the acetonitrile-water (5:1) mixture, a similar order of the Ω_2 values indicates no significant difference in the covalent character of the Eu^{3+}-C4DGA bonds and the bond lengths are also of the same order. The very low Ω_2 value of Eu^{3+}-aquo ion suggests its higher ionic nature than the Eu^{3+} complexes. Ω_4, which is a measure of long range ordering, was found to be similar for all Eu^{3+}-C4DGA complexes in $[C_8mim][NTf_2]$, while those in the acetonitrile-water (5:1) mixture are higher and follow the trend: Eu^{3+}-L-III > Eu^{3+}-L-I > Eu^{3+}-L-II > Eu^{3+}-L-V.

Comparison of different rim functionalized C4DGAs with different DGA functionalized ligands in RTIL revealed that the Ω_2 (**Table 4.8**) values followed the trend, L-VII (in $[C_8mim][NTf_2]$) > L-VI (in $[C_8mim][NTf_2]$) > T-DGA (in ACN-H_2O) > TODGA (in $[C_4mim][NTf_2]$) > T-DGA (in $[C_4mim][NTf_2]$) > $Eu^{3+}{}_{aq}$. The variation of Ω_2 reflected by the hypersensitivity of the $^5D_0 \rightarrow {}^7F_2$ transition can be related to the variation in covalency of Eu^{3+}-O bond. The large value of Ω_2 for Eu^{3+}-C4DGA complex suggests an enhanced covalency and strengthening of Eu^{3+}-O bond i.e., higher bond energy and shorter bond length. The lowest value of Ω_2 for Eu^{3+}_{aq} system can be attributed to lowest covalence of Eu^{3+}-O bond. Due to the pre-organized structure of C4DGAs (L-VI and L-VII) compared to TODGA, the bond length is shorter for the complexes of L-VI and L-VII while two bulky T-DGA ligands in Eu^{3+}-T-DGA complex in ionic liquid restricts the bond length between Eu^{3+} and oxygen atom.

For all the complexes, the values of Ω_2 are found to be less than that of Ω_4, which is a measure of long range ordering and found to follow the trend: L-VII ($[C_8mim][NTf_2]$) > > L-VI ($[C_8mim][NTf_2]$) > T-DGA (ACN-H_2O mixture) > T-DGA ($[C_4mim][NTf_2]$) > TODGA > Eu^{3+}_{aq}.

4.9.4 Radiative properties of Eu^{3+}-C4DGA complexes

The Judd–Ofelt parameters were used to calculate important radiative properties such as transition probabilities, branching ratios, and lifetimes for the excited states of the Eu^{3+} ions in the Eu^{3+}-C4DGA complexes in both $[C_8mim][NTf_2]$ and in the acetonitrile–water (5:1) mixture. The radiative transition probability A for a transition $\psi J \rightarrow \psi' J'$ was calculated from equation (4.16): [82,156]

$$A(\psi J, \psi' J') = A_{ed} + A_{md} \tag{4.16}$$

The predicted radiative lifetime τ_{rad} of an excited state in terms of A_T, the total radiative transition probability of an excited state, is given by

$$\tau_{rad}(\psi J) = 1/A_T\,(\psi J) \tag{4.17}$$

Table 4.8: Determination of J.O. parameters for Eu^{3+} - DGA complexes

System	Ω_2 (x 10^{20})	Ω_4(x 10^{20})	Ref No
Eu^{3+}- CDGA L-I in $[C_8mim][NTf_2]$	4.09	4.95	Present study
Eu^{3+}- CDGA L-II in $[C_8mim][NTf_2]$	4.03	5.11	Present study
Eu^{3+}- CDGA L-III in $[C_8mim][NTf_2]$	4.12	5.06	Present study
Eu^{3+}- CDGA L-IV in $[C_8mim][NTf_2]$	4.42	5.04	Present study
Eu^{3+}- CDGA L-V in $[C_8mim][NTf_2]$	4.48	5.07	Present study
Eu^{3+}- L-VI in $[C_8mim][NTf_2]$	4.32	5.49	Present study
Eu^{3+}- L-VII in $[C_8mim][NTf_2]$	5.58	9.09	Present study
Eu^{3+}-TODGA in $[C_4mim][NTf_2]$	4.13	5.23	Present study
Eu^{3+}-T-DGA in $[C_4mim][NTf_2]$	3.97	5.35	Present study
Eu^{3+}- CDGA L-V in ACN-H_2O	4.38	5.36	Present study
Eu^{3+}- CDGA L-I in ACN-H_2O	4.32	5.67	Present study
Eu^{3+}- CDGA L-II in ACN-H_2O	4.43	5.57	Present study
Eu^{3+}- CDGA L-V in ACN-H_2O	4.34	5.76	Present study
Eu^{3+}-T-DGA in ACN-H_2O	4.30	5.44	Present study
Eu^{3+} (aquo)	1.62	3.87	[168]
Eu^{3+}- Dipicolinic acid (1:1)	3.35	4.83	[168]
$Eu(TTA)_3phen$	13.87	0.33	[169]
$Eu(TTA)_3phen$(0.10)-PMO	24.81	0.83	[169]
Euphen(0.10)-PMO	7.09	0.37	[169]
Eu-DBM	10.97	1.47	[170]
Eu-DBM-Si	14.11	2.17	[170]
$Eu(TTA)_2(Phen)(H_2O)$	14.7	1.46	[171]
$Eu(TTA)_2$(Phen)(AA)	14.5	0.87	[171]
$Eu(TTA)_2$(Phen)(MA)	13.7	0.83	[171]

The branching ratio β corresponding to the emission from an excited level to its lower levels is described as

$$\beta(\psi J) = A(\psi J, \psi'J')/A_T(\psi J) \tag{4.18}$$

The spontaneous transition probability of the electric-dipole transition A_{ed} and the magnetic-dipole transition A_{md}, the total transition probability A_T, the emission branching ratio β, the radiative and non-radiative lifetime τ_{rad} and τ_{nonrad}, and the quantum efficiency (η) of the Eu^{3+}-C4DGA complexes are presented in **Tables 4.7**. The branching ratio follows the order $\beta_2 > \beta_4 > \beta_1$. Neither structural modifications of the C4DGA ligands nor the medium in which the Eu^{3+}-C4DGA complexes are formed, have a significant effect on the branching ratio values. The probability of the electric-dipole transitions are higher than the magnetic-dipole transitions for all Eu^{3+}-C4DGA complexes both in $[C_8mim][NTf_2]$ and in the acetonitrile-water (5:1) mixture. In general, both transition probabilities (A_{md}, A_{2ed}, A_{4ed}) are higher in $[C_8mim][NTf_2]$ than in the acetonitrile-H_2O (5:1) mixtures indicating more mixing of the metal orbital (f) with that of the ligand. The transition probability of the electric-dipole transition of $^5D_0 \rightarrow {}^7F_2$ is three times more than the magnetic-dipole transition probability and twice that of the electric-dipole transition of $^5D_0 \rightarrow {}^7F_4$. It was also noticed that substituents on the amidic nitrogen atoms increase the quantum efficiency as it decreases the additional non-radiative path for de-excitation.

Comparison of different rim functionalized C4DGA ligands with different DGA functionalized ligands in RTILs revealed that the non radiative transition life time (τ_{NR}) was found to follow the trend for the ligands L-VII in $[C_8mim][NTf_2]$ > L-VI in $[C_8mim][NTf_2]$ > TODGA > T-DGA in $[C_4mim][NTf_2]$ > T-DGA in ACN-H_2O mixture, while an opposite trend was observed for their quantum efficiency values (η). Presence of H_2O molecules in the primary co-ordination sphere of Eu^{3+}-L-VII complex provides additional pathways of non radiative transitions while other europium complexes with no water molecules in their primary co-ordination spheres differed significantly with respect to their non-radiative lifetime suggesting the influence of other parameters in their lifetime. Medium can also play significant role (as seen in the case of Eu^{3+}-T-DGA complex) in determining the non radiative lifetime even though medium is not directly present in primary coordination sphere of Eu^{3+}. For all the complexes, the magnetic and electric dipole transitions probabilities behaved in the fashion of $A_{2ed} > A_{4ed} > A_{md}$. Though there are significant differences in the electric dipole transition values from complex to complex, the constancy of magnetic dipole transitions established the fact that there is no perturbation of magnetic dipole transitions by the crystal field. The radiative and non-radiative life times, branching ratio of different transitions, quantum efficiency, probability of electric dipole and magnetic dipole transition etc. are summarized in **Table 4.7**.

4.10 Understanding the role of organic diluent on actinide ion extraction using a both rim functionalized C4DGA (L-VI)

Zhu et al. [64], have reported unusual size selective extraction of main group elements with TODGA in *n*-dodecane as the extracting solvent which was attributed to the size selective extraction of metal ions with ionic size of about 100 pm for the divalent ions while for the tri- and tetravalent ions exceptionally high D values were seen for the metal ions with ionic sizes of 87–113 and 83–94 pm, respectively. Jensen et al. [105] carried out small angle neutron scattering (SANS) studies with TODGA solutions equilibrated with varying concentrations of nitric acid to suggest that the size selective extraction behaviour could be due to a reverse micelle formation at nitric acid concentrations beyond 0.7 M and aggregates containing four TODGA molecules were reported at 3 M HNO_3. Subsequent studies on actinide ion extraction in the presence of phase modifiers such as DHOA [103] (dihexyloctanamide) or *iso*-decanol [172] indicated lowering of the D values which was attributed to the instability of the aggregates in a solvent system of higher polarity. These observations indicate that the diluents play a very significant role in the extraction of metal ions; especially the actinide ions using DGA based extractants. Several studies were carried out to understand the role of organic diluents on metal ion extraction using DGA extractants. Sasaki et al. [62] studied the extraction of Am^{3+} and Eu^{3+} using 0.1 M TODGA in about 11 diluents from 1 M HNO_3 and observed very high extraction of the metal ions (D values >500) in polar diluents such as nitrobenzene, 1-octanol and ethyl acetate. However, similar high D values were also observed with hexane and *n*-dodecane. They have observed much lower metal ion extraction with aromatic or halogenated solvents which was attributed to their tendency to react with the donor oxygen of diglycolamide thereby reducing the effective ligand concentration drastically. Similar observations were made by Ansari et al. [103] and Panja et al. [136] in subsequent studies.

In a series of separate studies involving ionic liquids as the diluent, we observed that the both-rim DGA-functionalized calix[4]arene showed unusual acid concentration independent actinide extraction while showing unprecedented high extractability of Am^{3+}. This prompted us to investigate thoroughly the both-rim DGA-functionalized calix[4]arene (L-VI) for actinide ion extraction. It was also decided to carry out such studies with different diluents to see the possible effects of the solvent medium on the metal ion extraction. Studies were also carried out as a function of the aqueous phase nitric acid concentration. The nature of the extracted species in different diluents was ascertained from slope analysis method by carrying out solvent extraction studies at varying concentrations of the C4DGA ligand (L-VI). Finally, temperature variation studies were also carried out at a fixed ligand concentration and fixed aqueous phase acidity.

4.10.1 Effect of organic diluent media on americium extraction

The extraction of metal ions into the organic phase is basically a net result of three independent steps, viz. a) partitioning of the extractant from the organic phase to the aqueous phase, b) complex formation between the metal ion and the extractant in the aqueous phase, c) partitioning of the complex from the aqueous phase in to the organic phase. Out of these, steps a) and c) involve the properties of diluent and hence any enhancement in the extraction should be linked to the diluent characteristics. Interaction of the diluents with the ligating atoms of the extractant decides the availability of free ligand for complexation of the metal ion and is the reason given by Sasaki et al., for the poor extraction of Am^{3+} by TODGA in chloro or aromatic solvents [62]. Compared to TODGA, C4DGA ligands (both L-VI and L-VII) have rather complex architecture of the pendent arms and the complexation and de-complexation reactions may involve significant reorientation / configurational changes in the pendent arms to position the coordinating atoms in an 'endo' configuration to bond with the metal ion. This may lead to significant slow kinetics of extraction of the metal ions. Another factor, though of lesser significance is the viscosity of the diluent medium which decides the mass transfer rates. The results of the kinetics of extraction of Am^{3+} using the L-VI ligand in various diluents such as, chloroform, *n*-dodecane, *1*-octanol, *2*-ntrophenyloctyl ether (NPOE), FS-13 (phenyl trifluoromethylsulphone), hexone or methyl *iso*-butyl ketone (MIBK) and nitrobenzene are presented in **Fig. 4.13**. The extraction rates were slower as anticipated and about 15-20 minutes were needed to attain equilibrium while only 5 minutes were needed to reach equilibrium with TODGA (in *n*-dodecane).

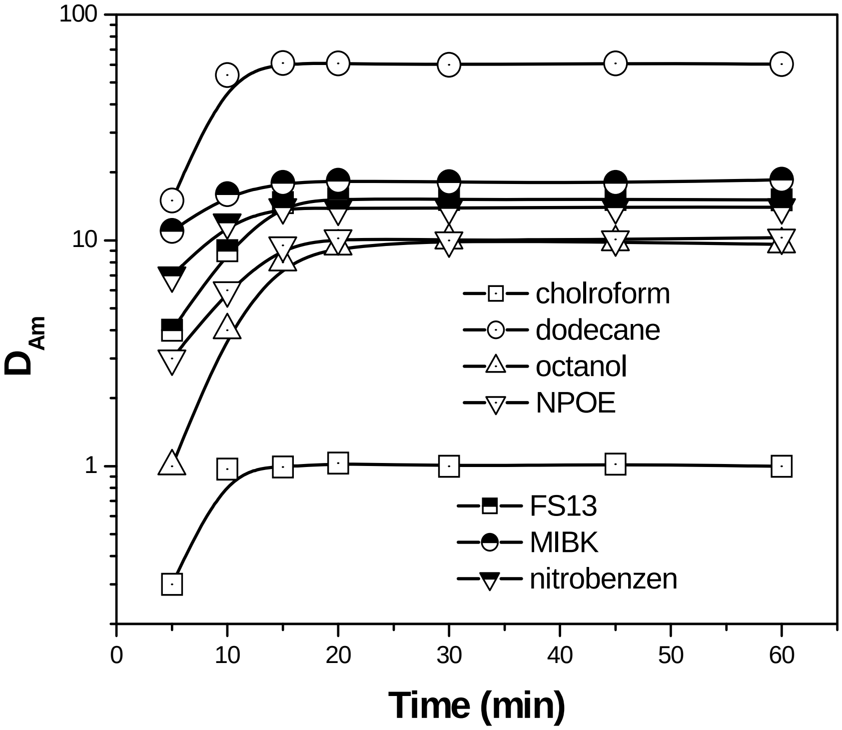

Fig. 4.13: Extraction kinetics data using 1.0 x 10^{-3} M C4DGA (L-VI). Aqueous phase: 3 M HNO_3

It is generally believed that charge neutralized complexes will be stabilized in a non-polar diluent while a charge separated complex will be stabilized in a polar diluent. This has been the reason for the use of polar diluents for the extraction of metal ions which follow an ion-pair mechanism. **Table 4.9** lists the D_{Am} values using L-VI as the extractant in several diluents. For comparison purpose, the distribution ratio data obtained with TODGA and L-V are also listed in the table. At 3 M HNO_3 the distribution ratio data of Am(III) in a given diluent were found to follow the trend: *n*-Dodecane > MIBK > FS-13 > Nitrobenzene > NPOE > 1-Octanol >

Chloroform. Surprisingly, while nitrobenzene as the diluent yielded significantly higher D_{Am} values as compared to *n*-dodecane for both TODGA and L-V, an opposite trend was seen with L-VI. While TODGA in 1-octanol extracted Am(III) by about 2.5 times higher as compared to the case where *n*-dodecane was used as the diluent, the later diluent resulted in > 6 times higher Am(III) extraction as compared to 1-octanol in the present study. We have tried to correlate the D_{Am} values with the dielectric constant of the medium (**Fig. 4.14**) which showed a rough linear correlation with four of the seven diluents used in the present study. While MIBK and 1-octanol deviated from the straight-line plot marginally, *n*-dodecane was significantly above the line.

Table 4.9: Extraction of Am^{3+} in various diluents using TODGA, L-V and L-VI

Diluent	Dielectric constant[a]	D_{Am}		
		TODGA[b]	L-V[c]	L-VI[d]
n-Dodecane	2.00	30	9.83	61[e]
Chloroform	4.81	0.12	1.87	1.04
1-Octanol	10.3	81	--	9.6
NPOE	23.1	--	5.78	10.1
FS-13	34	--	--	15.2
MIBK	13.1	--	8.52	18.6
Nitrobenzene	34.8	220	252	13.9

Note: [a]: Data taken from ref. [173]; [b]: Data taken from ref. [62], aq. phase: 1 M HNO_3, org. phase: 0.1 M TODGA; [c]: Data taken from ref. [174], aq. phase: 3 M HNO_3, org. phase: 1.1×10^{-3} M L-V; [d]: Present work, aq. phase: 3 M HNO_3; org. phase: 1.0×10^{-3} M L-VI ; e: 5% *iso*-Decanol was added as the phase modifier

Shmidt and coworkers introduced the empirical diluent parameter (DP) as a "universal constant" characterizing the diluent and can be expressed by the empirical correlation formula [175,176]

$$\text{Log D} = K + a.DP \qquad (4.19)$$

where, D is the distribution ratio of the metal ion while ‘K’ and ‘a’ are constants characteristic of the extraction system. DP was obtained from distribution measurements of trace amounts of $ZnCl_2$ extracted from aqueous 0.16 M hydrochloric acid using 0.047 M tri-*n*-octylamine hydrochloride in the diluent, relative to the value with benzene.

$$DP = \log D - \log D \text{ (in benzene)} \qquad (4.20)$$

Fig. 4.15 represents the plot of log D *vs* DP (calculated for some of the common diluents by Shimdt and available in the literature) showing similar correlation as expected by equation (4.19). Data for PTMS is not included in the figure as the DP value for the diluent is not available. However, for NPOE, we have included the DP value of analogous ether diluents [175]. Chloroform is found to be an exception of the above study as indicated by Schmidt et al. [176]. Marcus [175] also attempted to correlate the diluents parameter with the Hildebrand’s solubility parameter through an empirical relation as given below:

$$DP = -(10.61 \pm 0.93) + (0.241 \pm 0.026)\, E_T + (0.217 \pm 0.077)\, \delta \qquad (4.21)$$

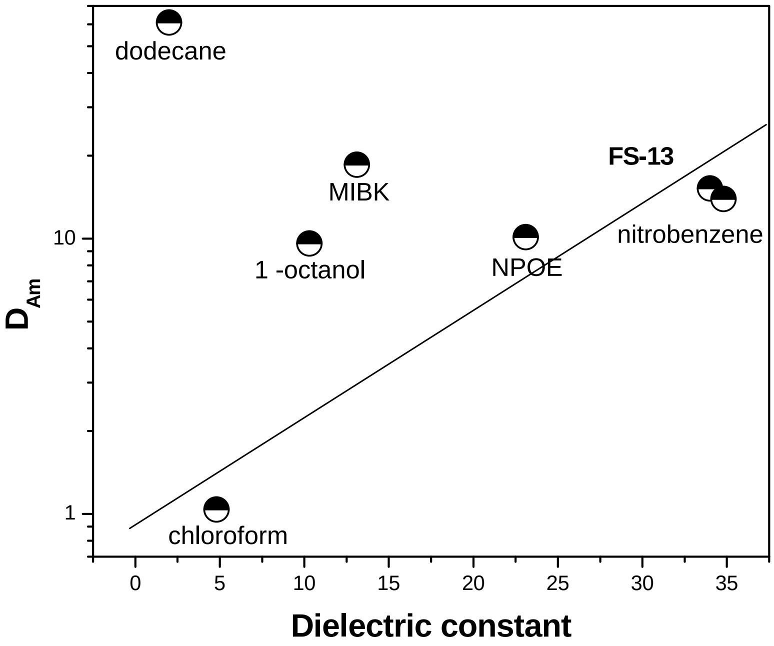

Fig. 4.14: Correlation of D values of americium with the dielectric constants of the diluents using 1.0 x 10^{-3} M concentration of L-VI

where, E_T represents the polarity (it combines in some manner the Lewis acid and Lewis base properties) while δ is Hildebrand's solubility parameter which describes the cohesiveness of a solvent. Using the DP value obtained by Marcus from the above correlation (eq.(4.21)), log D was plotted as a function of DP (**Fig. 4.15**). It also revealed linear correlation as the D values decreased with increasing DP, while chloroform did not fall in the line as indicated above.

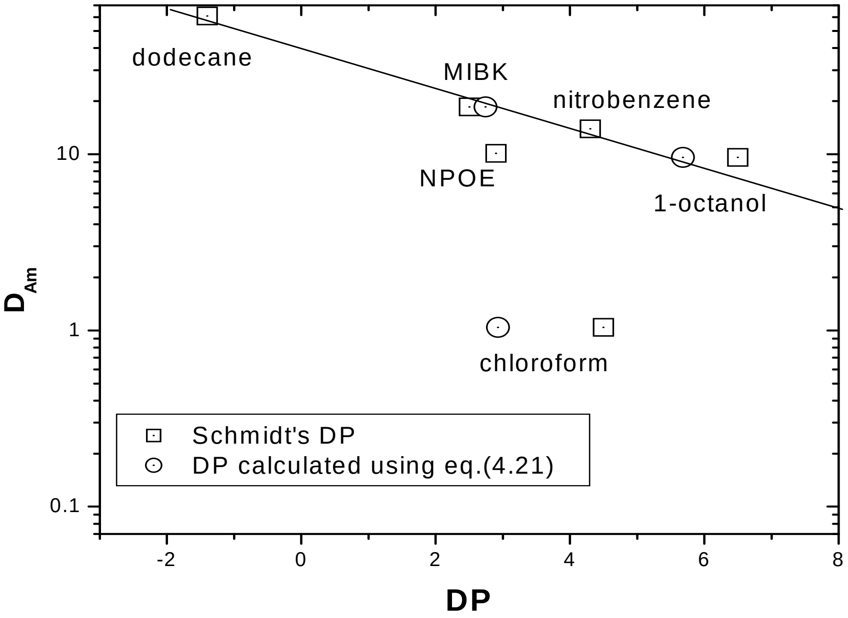

Fig. 4.15: Correlation of D_{Am} values with the diluent parameter reported by Schmidt and those calculated by Marcus (ref. [175]) using 1.0 x 10^{-3} M L-VI

The mechanism of extraction has been difficult to predict based on several competing factors. The high D values obtained with TODGA (**Table 4.9**) can be attributed to the extra hydrophobicity of the complex in a reverse micellar extraction mechanism [62]. However, in view of very low concentration of the DGA-functionalized calixarene ligand used for Am^{3+} extraction (in the present study and as reported in ref [177]), such mechanism may be ruled out. One possibility could be the favourable orientation of the DGA moieties present in the L-V or L-VI ligands in the medium of low polarity which can facilitate higher extraction of the metal ion.

The lowest D_{Am} in chloroform can be attributed to the ligand - diluent interaction through hydrogen bonding [178,179]. There could also be interaction of 1-octanol with the donor groups of the L-VI ligand possibly through H-bonding which is manifested in the lowering of the expected D_{Am} value. However, in view of the high polarity of the diluent [180], the D_{Am} values are seen to be higher than the expected lowering on the basis of the H-bonding interactions. In case of NPOE, due to the proximity of the electron withdrawing nitro group (-I and –R effect), it is likely to develop δ+ charge on etheric oxygen which may interact with the diglycolamide molecules to decrease the availability of ligand molecules for metal ion interaction. The above fact was seen by the decrease in the D_{Am} value in NPOE compared to that in FS-13 and nitrobenzene.

4.10.2 Separation behaviour

The diglycolamide extractants have the unique feature of poor extraction of UO_2^{2+} and Sr^{2+}, two of the important constituents of the high level waste (HLW), making these ligands achieve good decontamination factors (DF) for Am^{3+} separation. With DGA-functionalized calix[4]arenes, the DF values have been reported to be higher due to large enhancement in the D_{Am} values with almost no change in the D_U and D_{Sr} values as compared to those obtained with TODGA [69]. The distribution ratio values of Am^{3+}, UO_2^{2+} and Sr^{2+} were determined from feed acidity 3 M HNO_3 and 0.01 M HNO_3 using L-VI as the extractant in different diluents and the results are listed in **Table 4.10**. At 0.01 M HNO_3, the distribution ratio of all the three metal ions in all the diluents were found to be very low which can be attributed to the lower concentration of nitrate ion for the formation of metal DGA nitrate complex. The separation factor (S.F.) values, defined as the ratio of D_{Am} and D_M (where M = U or Sr) are also listed in the table. The distribution ratio values for U (D_U) in the diluents followed the trend: *n*-dodecane > FS-13 > MIBK > 1-octanol > chloroform > nitrobenzene > NPOE.

Table 4.10: Separation data for Am^{3+}, UO_2^{2+} and Sr^{2+} from nitric acid feeds using 1.0×10^{-3} M L-VI in different organic diluents

Medium	Feed acidity (M)	D_{Am}	D_U	S.F. (D_{Am}/D_U)	D_{Sr}	S.F. (D_{Am}/D_{Sr})
Chloroform	3	1.04	0.48	2	0.01	100
	0.01	0.005	0.01	0.45	< 0.0001	>39
95% *n*-Dodecane + 5% *iso*-decanol	3	60.96	8.27	7	2	30
	0.01	0.15	0.05	3	0.003	48
1-Octanol	3	9.60	1.21	8	0.4	24
	0.01	0.02	0.01	1	0.002	9
NPOE	3	10.12	0.04	236	0.005	2024
	0.01	0.02	0.01	4	< 0.0001	>204
FS-13	3	15.22	3.08	5	0.4	38
	0.01	0.06	0.03	2	< 0.0001	>649
MIBK	3	18.57	2.47	8	0.3	62
	0.01	0.02	0.02	1	< 0.0001	>210
Nitrobenzene	3	13.94	0.28	50	0.05	279
	0.01	0.20	0.002	113	0.001	202

Though distribution ratio of americium is highest in *n*-dodecane – *iso*-decanol mixture, the distribution ratios of uranium as well as Sr^{2+} are also high. So, *n*-dodecane can be used for the simultaneous extraction of these three metal ions. On the other hand, most efficient decontamination from U was observed from 3 M HNO_3 with NPOE as the diluent while nitrobenzene can be an effective diluent for 1.0 x 10^{-2} M HNO_3 as the feed. The distribution ratio values of Sr^{2+} in the diluents followed the trend: *n*-dodecane > FS-13 ~ 1-octanol ~ MIBK while practically there was no extraction of Sr^{2+} into the organic phase when chloroform, nitrobenzene and NPOE were used as diluents. For Am – Sr separation also, NPOE is found to be the most efficient diluent with S.F. values in excess of 2000. Other diluents like FS-13 and nitrobenzene can also be used for effective separation of Sr^{2+} from Am^{3+}.

4.10.3 Extraction of Am at different feed acidities

The solvation mechanism, operative for the extraction of actinide ions using neutral extractants, suggests an increase in metal ion extraction with increasing nitric acid concentration till interaction of ligand molecules with the acid affect the D values. The D_{Am} values were found to increase with increasing feed acidity up to 3 M HNO_3 beyond which a plateau was observed (**Fig. 4.16**). Up to 3 M HNO_3, with increasing nitric acid concentration, a resultant increase in nitrate ion concentration occurs which favours the formation of americium – L-VI complex in different media as indicated by equation (4.22), where ‘n’ is the number of ligand molecules associated with the Am(III) ion.

$$Am^{3+}_{aq} + n\ L\text{-}VI_{org} + 3NO_3^-{}_{aq} \leftrightarrow Am(L\text{-}VI)_n{\cdot}3NO_{3,org} \qquad (4.22)$$

where, the subscripts, ‘aq’ and ‘org’ refer to the species in the aqueous and the organic phases, respectively. The plateau beyond 3 M HNO_3 is attributed to a concomitant increase in the concentration of hydrogen ion which competes for the ligating sites (as per eq. (4.23)), thereby affecting the metal ion distribution ratio values from any further increase.

$$H^{+}_{aq} + m\ L\text{-}VI_{org} + NO_3^{-}{}_{aq} \leftrightarrow HNO_3 \cdot m\ L\text{-}VI_{org} \quad (4.23)$$

where, 'm' is the number of extractant molecules associated in the ligand – acid adduct. In equations (4.22) and (4.23), though more than one extractant molecules (n > 1; m > 1) are theoretically possible to be present in the extracted species, the large number of DGA moieties present in the L-VI molecule prompted us to believe that not more than one unit of extractant may be present in the extracted species.

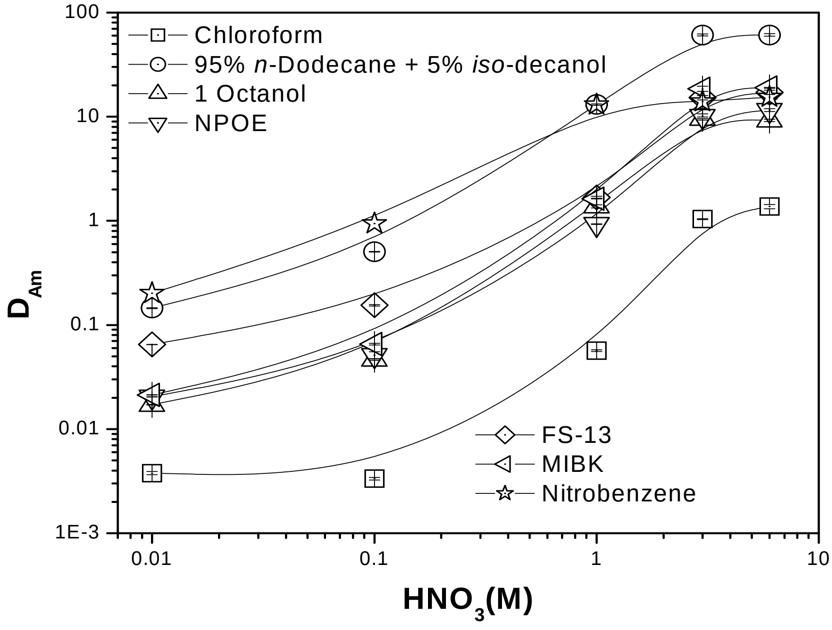

Fig 4.16: Extraction profiles of americium using 1.0 x 10^{-3} M L-VI in different media from

4.10.4 Nature of the extracted species

Fig. 4.17 gives the log – log plots of D_{Am} *vs* [L-VI] which are straight lines with the slope values close to 1 indicating that one molecule of L-VI is associated in the extracted species. The conditional extraction constant (K'_{ex}) can be calculated from the intercept which follow the order, K'_{ex} (*n*-dodecane) > K'_{ex} (MIBK) > K'_{ex} (1-octanol) > K'_{ex} (FS-13) > K'_{ex} (nitrobenzene) > K'_{ex} (NPOE) >> K'_{ex} (chloroform) (**Table 4.11**). These results are in the same line as those observed for C4DGA ligands (L-VI) for most of the diluents [177]. The possibility of 1:2 complexes is ruled out in view of very high stereochemical constraints with L-VI containing eight DGA moieties.

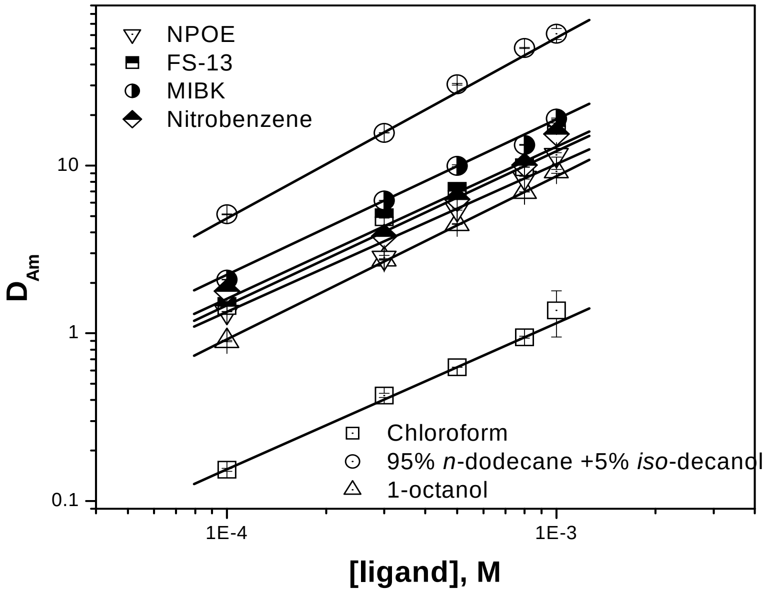

Fig. 4.17: Effect of ligand concentration on the distribution ratio of americium

Table 4.11: Determination of extraction constants from slope ratio method

Medium	Slope	Log K_{ex}
Chloroform	0.87 ± 0.011	0.46
n-Dodecane – *iso*-decanol mixture	1.07 ± 0.004	95.49
1-Octanol	0.97 ± 0.003	7.08
NPOE	0.88 ± 0.005	4.36
FS-13	0.92 ± 0.001	6.92
MIBK	0.92 ± 0.003	11.22
Nitrobenzene	0.91 ± 0.084	6.76

In order to obtain the thermodynamic parameters, the distribution ratio values were measured at varying temperatures. The distribution ratio values of Am^{3+} obtained at different diluent media were found to decrease with increasing temperature indicating that the extraction process is exothermic in nature (**Fig. 4.18**). The thermodynamic parameters are listed in **Table 4.12** which suggest that the extraction of Am^{3+} by L-VI in all the diluents appears to be spontaneous. The change in enthalpy of the metal ion extraction in different diluents followed the order, nitrobenzene > *n*-dodecane > FS-13 > MIBK > chloroform > NPOE > octanol while the change in entropy followed the order, *n*-dodecane >> MIBK > octanol > NPOE > FS-13 > chloroform > nitrobenzene.

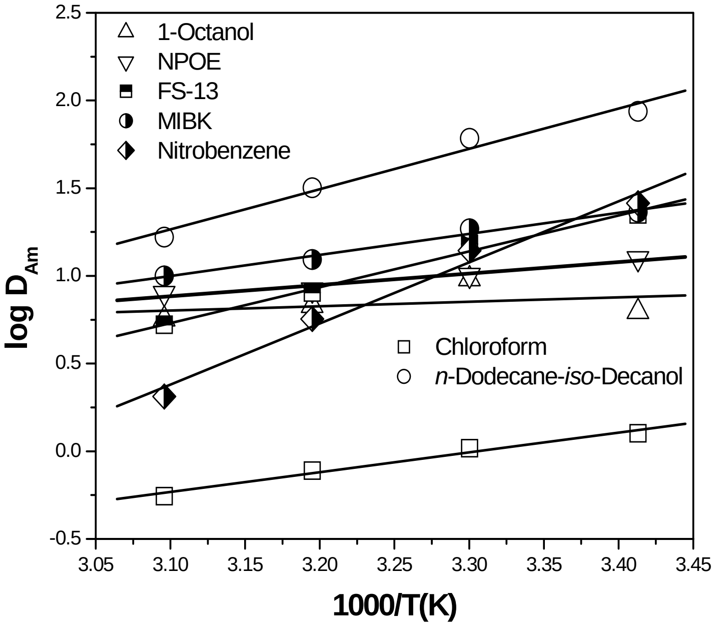

Fig. 4.18: Effect of temperature on Am(III) extraction. Aqueous phase: 3 M HNO_3; Organic phase: 1 x 10^{-3} M L-VI in the given diluents

As previously mentioned, the overall change in the enthalpy is dependent on three main factors, viz. i) enthalpy required to dehydrate the metal ion (ΔH_1), ii) enthalpy released during formation of the metal – ligand complex (ΔH_2) and iii) partitioning of the metal-ligand complex into the diluents phase (ΔH_3) which in many cases involves the destruction of an ordered diluent structure. In the present case, the first two factors will be same for all the cases. The properties of the diluents only contribute significantly in case of ΔH_3. Increase in entropy due to the extraction can be explained based on an increased disorder due to the release of the solvent molecules during complexation while in case of chloroform and nitrobenzene the overall entropy decreases. Large positive entropy values obtained in case of 1-octanol and NPOE may be attributed to the complexation reaction resulting in breaking of an highly ordered H-bonded structure of the solvent systems.

Table 4.12: Thermodynamic parameters experimentally determined from the Am(III) extraction studies carried out using L-VI (1.0 x 10^{-3} M) in different diluents at varying temperature

Medium	ΔG (kJ/mol)	ΔH (kJ/mol)	ΔS (J/K/mol)
Chloroform	-15.3	- 21.6	-21.0
n-Dodecane – *iso*-Decanol	-28.6	- 43.9	-51.1
1-Octanol	-22.1	- 4.79	57.6
NPOE	-20.9	- 12.5	28.3
FS-13	-22.1	- 39.1	-56.9
MIBK	-23.3	- 23.0	0.94
Nitrobenzene	-22.0	- 66.6	-149

4.11 Summary

The above studies involving the diglycolamide-functionalized calix[4]arenes in [C_8mim][NTf_2] lead to the following important conclusions. A decrease in the distribution ratio of americium with increasing aqueous phase acidity was attributed to an ion exchange mechanism in all cases. A remarkable acid concentration independent Am(III) extraction was observed using L-VI in RTIL. Because of the higher viscosity of the ionic liquid in comparison to the molecular diluents [142, 181], 2 h were required to reach equilibrium D values. The ligand with a short spacer was found to be a better extractant in comparison to its analog with a longer spacer probably because of the better pre-organization of the diglycolamide moieties on the calixarene platform as a result of restricted C−C single bond rotation. At lower feed acidity, the coordinating ability of the carbonyl oxygen was enhanced because of the electron density on the amidic nitrogen atom to which a group with a +I effect is attached, while at comparatively higher feed acidity the steric crowding around the coordinating group plays a significant role. Both ligands form complexes with 1:1 stoichiometry. A time-resolved fluorescence study confirmed the strong interaction of the metal ion with the C4DGA ligands in $[C_8mim][NTf_2]$ as single species without inner sphere water molecules. Radiolytic stability studies indicated that the extraction efficiencies of L-I and L-IV are not significantly affected up to 500 kGy of absorbed dose. The the extraction efficiency of the C4DGAs in $[C_8mim][NTf_2]$ was found to follow the trend: $Eu^{3+} > Am^{3+} > Pu^{4+} > PuO_2^{2+} > UO_2^{2+} > Sr^{2+} > Cs^{+}$. And finally, metal - C4DGA complex formation is thermodynamically favorable and the overall extraction process is exothermic in nature with a decrease in the overall entropy of the system.

Diluents play a very important in the extraction of the metal ions not only with simple DGA ligands such as TODGA, but also with complex molecules such as L-VI. *n*-Dodecane has shown favourable extraction of not only Am(III), but also metal ions such as UO_2^{2+} and Sr(II). The separation factor values were found to be favourable in NPOE as the diluent. The acid concentration dependence of metal ion extraction was mainly due to nitrate ion concentration in the aqueous phase while the saturation in the D values was due to competing extraction by the hydronium ion. The extracted species has shown extraction of 1:1 species into the organic phase and the reaction has been found to be spontaneous. The exceptional extraction behaviour of the L-VI ligand as seen in room temperature ionic liquids was not to be seen in the molecular diluents.

CHAPTER- 5

Studies involving Task specific ionic liquid (TSIL) for the separation of actinides

Due to their negligible vapour pressure, high thermal stability, and high ionic conductivity, room temperature ionic liquids (ILs) have been evaluated as future 'green' alternatives to the molecular diluents [111-114]. The applications of ionic liquid based solvent systems for actinide extraction have been reviewed recently [154,182-183]. Out of the ILs, those appended with specific extractant functional groups have been termed as Task Specific Ionic Liquids (TSILs) or functionalized ionic liquids (FILs) and have many advantages over the solvent systems containing the analogous extractant in an IL [184,185]. One of the major advantages of TSILs includes alleviation of problems associated with finding extractant molecules that remain exclusively in the IL phase under all process conditions. Furthermore, the functional groups appended onto the IL can impart a particular reactivity pattern to the IL, enhancing its capacity for interaction with specific metal ions, thereby improving the selectivity enormously. Some of the recent reports involve TSILs containing ligands specific for actinide ion extractions, especially from acidic feed conditions, which have potential applications in radioactive waste remediation [88,89]. Out of the various TSILs tested for actinide ion extraction, there are very few reports on CMPO-functionalized IL [91]. To the best of our knowledge, there is no report dealing with DGA (diglycolamide)-based TSIL. As solvents containing CMPO in ionic liquids were found to be much inferior extractants [138,186] as compared to those containing DGA extractants in IL [136,139], it was of interest to evaluate diglycolamide-based task specific ionic liquids (DGA-TSILs) for actinide extraction. The present study deals with their synthesis and extraction behavior from acidic feed solutions. Their extraction behaviour towards actinide ions such as Am^{3+}, Pu^{4+}, Np^{4+}, and UO_2^{2+} and fission product ions such as Eu^{3+}, Sr^{2+}, and Cs^{+} was compared with that of TODGA, a widely studied DGA-based extractant [134,187], in both molecular diluent and analogous IL diluents. In order to have insight into the extraction mechanism, the nature of the extracted species was determined from by the conventional analysis method and also by time resolved laser induced fluorescence studies. Stripping and radiolytic degradation studies were carried out for possible applications of these DGA-TSILs in ‘actinide partitioning’ with recycling options. A comparative study was also carried out to understand the extraction behavior of Np(IV) and Np(VI) with CMPO-functionalized ionic liquid as well as DGA-TSIL in a more detailed manner. Structures of the TSILs used in this chapter are as follows

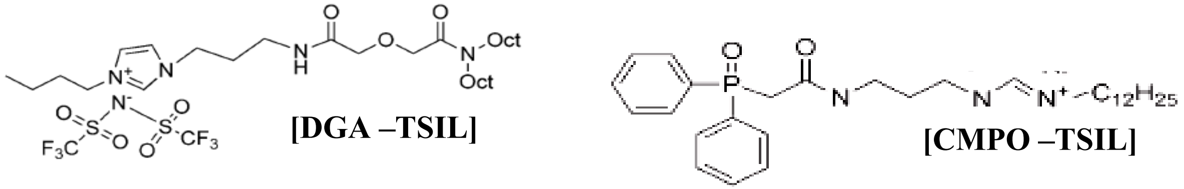

Fig. 5.1: Structures of TSILs used in Chapter-5

5.1 The kinetics for the extraction of Am^{3+} with [DGA-TSIL][X] (where, X = NTf_2 and PF_6)

The time required to attain equilibrium D values was found to be much higher (about 6 h, **Fig. 5.1**) in case of the two DGA-TSILs as compared to the TODGA-IL solvent systems (Chapter 3), which can be attributed to the very high viscosity of the TSILs [142,181]. In order to discount the effect of the viscosity with the neat TSILs, solutions of [DGA-TSIL][NTf_2] and [DGA-TSIL][PF_6] were used after appropriate dilution in [C_4mim][NTf_2] and [C_4mim][PF_6], respectively for the extraction kinetics studies. The results are included in **Fig. 5.2** which indicate a sharp decrease in the time required to attain equilibrium D_{Am} values (from > 6 h in case of undiluted TSILs to about 1 h with the diluted TSILs) corroborating the viscosity effect as the reason for the slow extraction kinetics with neat TSILs as suggested above. Similar examples of diluting a TSIL in IL diluents have been reported in the literature [184]. In view of the lower viscosity of [C_4mim][PF_6] and [C_4mim][NTf_2] as compared to [C_8mim][PF_6] and [C_8mim][NTf_2], the butyl derivatives of the ionic liquids were used for making the dilutions [188].

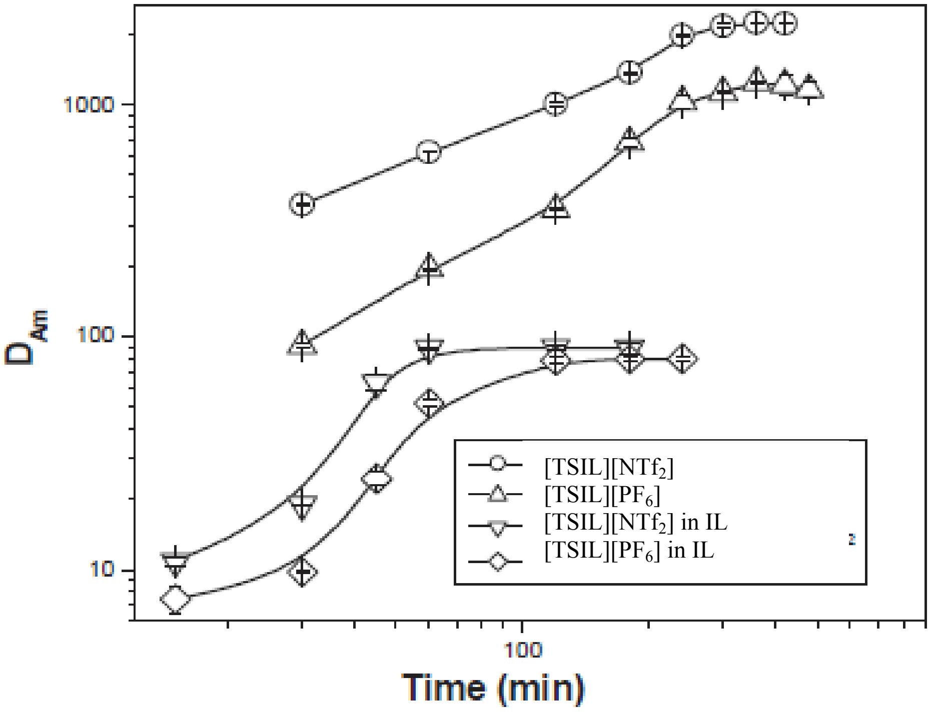

Fig. 5.2: Am^{3+} extraction profiles as a function of equilibration time for the [DGA-TSIL][NTf_2] and [DGA-TSIL][PF_6] and the diluted solution in [C_4mim][NTf_2] and [C_4mim][PF_6] respectively.

5.2 Effects of feed acidity on the extraction properties of metal ions

Fig 5.3(a) showed the extraction profiles of Am^{3+} with [DGA-TSIL][NTf_2] and [DGA-TSIL][PF_6]. The decreasing trend of D_{Am} with increasing feed acidity suggested predominance of cation exchange mechanism. With pure [DGA-TSIL][NTf_2] and [DGA-TSIL][PF_6], as C_4mim^+ is a part of the complexing entity, there is no chance of it getting partitioned into the aqueous phase, because of the much increased lipophilicity due to the presence of two octyl groups. Hence, the possible extraction mechanism can be given as:

$$Am^{3+}_{aq} + n[DGA\text{-}TSIL]^+_{IL} \leftrightarrow [Am\ (DGA\text{-}TSIL)_n]^{(3+n)+}_{IL} \qquad (5.1)$$

Further, with DGA-TSIL in an ionic liquid ([C_4mim][X]) as the diluent, the extraction mechanism can be presented as:

$$Am^{3+}_{aq} + 3C_4mim^+_{IL} + n[DGA\text{-}TSIL]^+_{IL} \leftrightarrow Am\ (DGA\text{-}TSIL)_n{}^{(3+n)+}_{IL} + 3C_4mim^+_{aq} \qquad (5.2)$$

The distribution ratio values of the actinide metal ions in different oxidation states (such as +3, +4 and +6) were also found to follow similar trend with feed acidity (**Fig. 5.3(b)**). It was also observed that Zr(IV), Pd(II), Y(III), La(III), Ce(IV), Pr(III), Nd(III), and Sm(III) were co-extracted along with minor actinides like americium. Except for Zr, prevalence of the cation exchange mechanism was also observed for these metal ions (**Fig. 5.3(c)**). Furthermore, there was acid transfer into the ionic liquid phase during the extraction of metal ions [**Fig. 5.3(d)**]. As a consequence, at higher feed acidity there is a competition between metal ions and H^+ ions for extraction into the organic phase, which is reflected in the decreasing trend of the D_M values at higher feed acidity.

$$H^+_{aq} + m[DGA\text{-}TSIL]^+_{IL} + C_4mim^+_{IL} = H\ [DGA\text{-}TSIL]^{(m+1)+}_{m;IL} + C_4mim^+_{aq} \qquad (5.3)$$

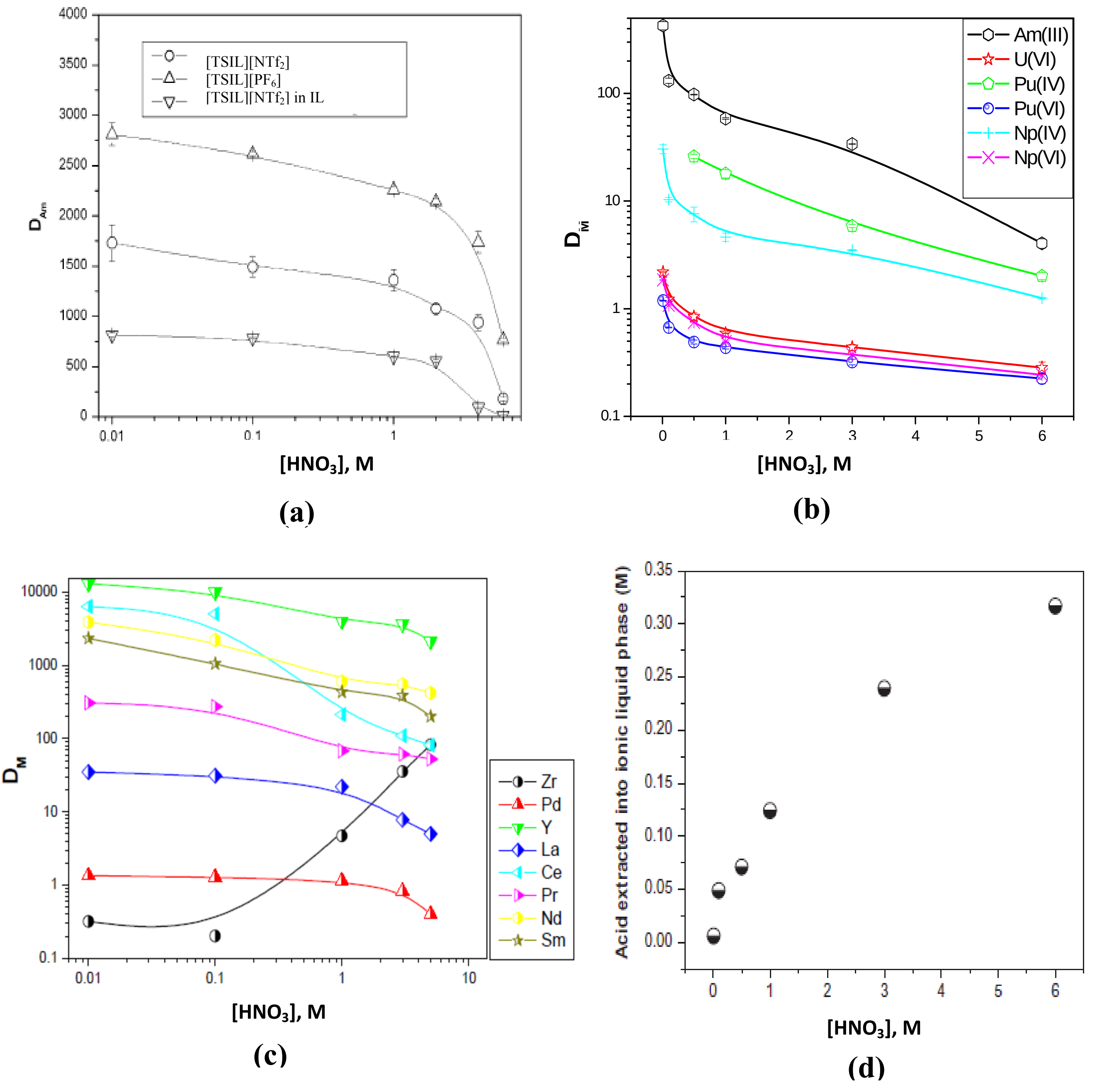

(a) **(b)**

(c) **(d)**

Fig. 5.3: Extraction profiles of **(a)** Am(III) using [DGA-TSIL][X] (where, X = PF_6 and NTf_2); (**b**) different actinide ions; (**c**) metal ions extracted from SHLW into 3.6 x 10^{-2} M [DGA-TSIL][NTf_2] in [C_4mim][NTf_2]; (**d**) Acid uptake in the organic phase as a function of the feed acidity using 3.6 x 10^{-2} M [DGA-TSIL][NTf_2] in [C_4mim][NTf_2]

5.3 Effect of Eu loading in the aqueous phase on its distribution ratio value

Most of the literature on the extraction of actinide ions deals with the distribution ratio values of the metal ions obtained with the radiotracers only. However, due to the higher concentration of the analytes and the presence of other concomitant metal ions in actual solutions, these data are not very relevant. Therefore, it is essential to study the effect of different metal ion concentrations in the aqueous phase on its distribution ratio. The distribution ratio of Eu^{3+} was found to decrease with increasing Eu loading in the aqueous phase, which can be attributed to the decrease in availability of free ligand for extraction [**Fig. 5.4(a)**].

The distribution ratio of Eu at tracer level was 470, which decreased to 200 when the feed was changed to SHLW, in which the total rare earth concentration (equivalent to Eu^{3+}) is about 500 µg/mL. It further decreased to 160 when the Eu concentration in the aqueous feed was 1000 µg/mL. The plot of log D_{Eu} vs log [Eu^{3+}] can be fitted by a polynomial equation [**Fig. 5.4(b)**]. Using eq. (5.4) the distribution ratio of Eu^{3+} can be calculated for any concentration of Eu^{3+} from 3 M HNO_3 feed into the ionic liquid phase containing the DGA-TSIL.

$$\text{Log } D_{Eu} = 2.593 - 0.084 \log [\text{Eu}] - 0.012 (\log [\text{Eu}])^2 \tag{5.4}$$

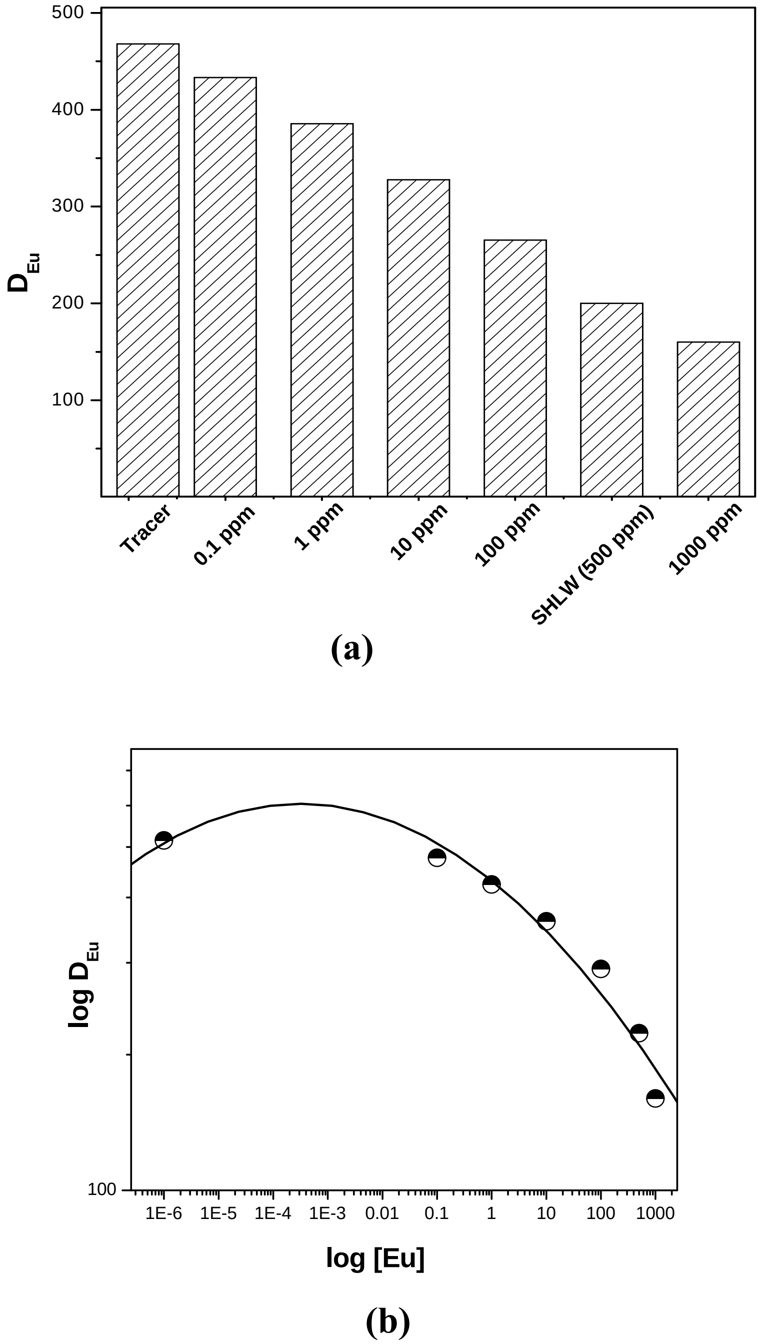

Fig. 5.4: Effect of Eu loading on its distribution ratio value into ionic liquid phase containing 3.6×10^{-2} M DGA-TSIL in $[C_4mim][NTf_2]$

5.4 Determination of the nature of complexes formed by task specific ionic liquids

The relative extractability of the actinide ions also depends on the nature of the extracted species and its overall organophilicity, which depends in turn on factors such as the number of extractant molecules and the number of associated water molecules (both inner- sphere and outer-sphere). In order to determine the metal–ligand stoichiometry in the complex, slope analysis experiments were carried out. An increase in the D_M values upon increasing the ligand concentration primarily suggests that the ligand molecule is directly taking part in the extraction process (**Fig. 5.4**). The extraction constant (K_{ex}) of the separation process can be expressed as follows:

$$K_{ex} = ([M(TSIL)_m]^{n+}{}_{IL} [C_4mim^+]^n{}_{aq}) / ([M^{n+}]_{aq} [TSIL]^m{}_{IL} [C_4mim^+]^n{}_{IL}) \qquad (5.5)$$

Substituting the value of D_M in Eq. (5.6) one obtains

$$K_{ex} = (D_M[C_4mim^+]^n{}_{aq}) / ([TSIL]^m{}_{IL} [C_4mim^+]^n{}_{IL}) \qquad (5.6)$$

The conditional extraction constant (K'_{ex}) can be obtained from the equation as follows:

$$K_{ex}([C_4mim^+]^n{}_{IL}/ [C_4mim^+]^n{}_{aq}) = D_M/ [TSIL]^m{}_{IL} = K'_{ex} \qquad (5.7)$$

Taking the logarithm one obtains

$$\log D_M = \log K'_{ex} + n \log [TSIL]_{IL} \qquad (5.8)$$

A plot of log D_M vs log $[TSIL]_{IL}$ should yield a straight line with a slope of 'n', the number of ligand molecule associated with the metal ion, and the intercept of log K'_{ex}. The complex formation equilibria in an ionic liquid can be described by the following equation:

$$M^{n+}_{IL} + TSIL_{IL} = M\,[TSIL]^{n+}_{IL} \qquad (5.9)$$

The complex formation constant (K_{form}) can be expressed as

$$K_{form} = [M(TSIL)^{n+}]_{IL} / ([M^{n+}]_{IL}[TSIL]_{IL}) \qquad (5.10)$$

$$K_{form} = K'_{ex}[M^{n+}]_{aq} / [M^{n+}]_{IL} \qquad (5.11)$$

$$K_{form} = K'_{ex} / P_M \qquad (5.12)$$

where, P_M is the partition coefficient of the particular actinide ion (M^{n+}) defined as the ratio of the metal ion (M^{n+}) concentration in the ionic liquid phase to that in the aqueous phase. It may be noted further that the P_M values refer to the extraction of metal ions into the pure RTILs in the absence of the TSIL. Changes of distribution ratio values of metal ions as a function of [DGA-TSIL] concentration are shown in **Fig. 5.5.** Am^{3+} was found to form 1:2 complexes with pure [DGA-TSIL][NTf_2] or [DGA-TSIL][PF_6] while the actinide ions were found to form 1:1 metal-ligand stoichiometric complexes with diluted [DGA-TSIL][NTf_2] and [CMPO-TSIL][NTf_2]. From the slope analysis method, La, Nd, Pr, Sm and Zr were found to be associated with two [DGA- TSIL][NTf_2] molecules in the ionic liquid, while Ce and Pd are associated with one ligand molecule. It is interesting to note that Y^{3+} extraction involves three ligand molecules, which may increase the lipophilicity of the complex manifested in high D_Y values It is also possible that nitrate ions can be part of the extracted species. This was confirmed by carrying out studies as a function of the nitrate ion concentration in the aqueous phase. While no change in the D_{Am} value was seen in the TODGA-IL extraction system, an increase in the D_{Am} values was observed in case of the DGA-TSILs. A slope value close to 1 for the log D_{Am} vs a_{NO3-} plots (**Fig. 5.6**) suggested the presence of one NO_3^- in the extracted species.

The K_{form} values, calculated from Eq. (5.12) are also listed in **Table 5.1(a)** along with the K'_{ex} values and the partition coefficient data. The formation constants (K_{form}) of the actinides follow the order: Am^{3+} > Pu^{4+} > Np^{4+} > NpO_2^{2+} > UO_2^{2+} > PuO_2^{2+} similar to that of the conditional extraction constants (K'_{ex}). The above trend can be explained in a similar manner as described for D_M. The extraction constants and the formation constants were found to be 10 times more in case of Np(IV) complex compared to Np(VI) complex and the constants were found to decrease with increase the chain length of the alkyl substituent on methylimidazolium ring i.e. $[C_4mim][NTf_2]$ > $[C_6mim][NTf_2]$ > $[C_8mim][NTf_2]$. The K'_{ex} and K_{form} for a particular diluent was found to follow the trend Np(IV) - $[CMPO\text{-}TSIL][NTf_2]$ complex > Np(IV) - $[DGA\text{-}TSIL][NTf_2]$ complex > Np(VI) – $[CMPO\text{-}TSIL][NTf_2]$ complex > Np(VI) – $[DGA\text{-}TSIL][NTf_2]$ complex. These facts reflect the more complexing ability of $[CMPO\text{-}TSIL][NTf_2]$ with tetra and hexa valent Np over $[DGA\text{-}TSIL][NTf_2]$ in $[C_4mim][NTf_2]$ medium (**Table 5.1(a)).** The conditional extraction constant values of the different metal ions follow the order: Y(III) > Sm(III) > Ce(IV) ~ Nd(III) > Pr(III) > Zr(IV) > La(III) > Pd(II) (**Table 5.1(b)**). The extraction constant values indicate that except for Pd^{2+}, all other metal ions are extracted to a very significant extent.

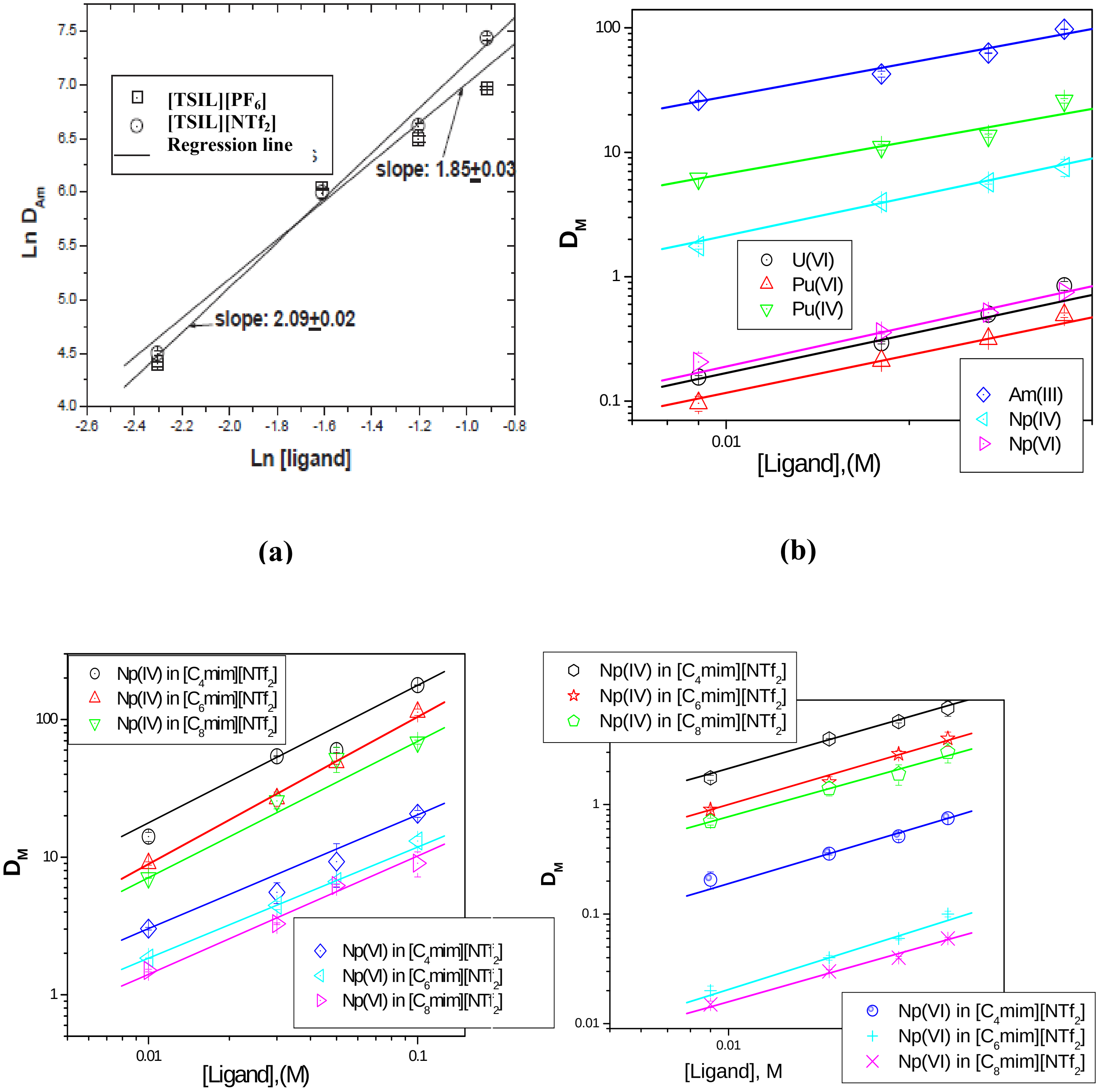

Ln D$_{Am}$
Ln [ligand]
[TSIL][PF$_6$]
[TSIL][NTf$_2$]
Regression line
slope: 1.85±0.03
slope: 2.09±0.02
7.5
7.0
6.5
6.0
5.5
5.0
4.5
4.0
-2.6
-2.4
-2.2
-2.0
-1.8
-1.6
-1.4
-1.2
-1.0
-0.8
D$_M$
[Ligand],(M)
U(VI)
Pu(VI)
Pu(IV)
Am(III)
Np(IV)
Np(VI)
100
10
1
0.1
0.01
Np(IV) in [C$_4$mim][NTf$_2$]
Np(IV) in [C$_6$mim][NTf$_2$]
Np(IV) in [C$_8$mim][NTf$_2$]
Np(VI) in [C$_4$mim][NTf$_2$]
Np(VI) in [C$_6$mim][NTf$_2$]
Np(VI) in [C$_8$mim][NTf$_2$]
[Ligand], M

(a)

(b)

(c)

(d)

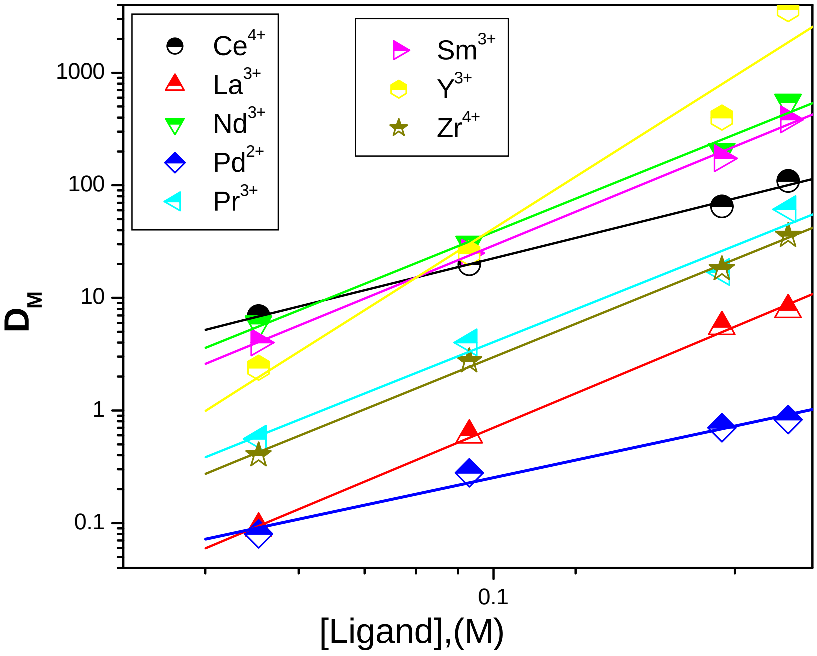

(e)

Fig. 5.5: (**a**) Dependence of D_{Am} on the concentration [DGA-TSIL][X] (where, X = NTf_2 and PF_6) in [C_4mim][NTf_2] and [C_4mim][PF_6]. Aqueous phase: 3 M HNO_3; (**b**) Variation of D_M with ligand concentration for different oxidation states of actinides. Aqueous phase: 0.5 M HNO_3; (**c**) Variation of D_{Np} (Np^{4+} and NpO_2^{2+}) with [CMPO-TSIL][NTf_2] concentration in [$C_n$mim][NTf_2] (n = 4, 6, 8). Aqueous phase: 3 M HNO_3; (**d**) Variation of D_{Np} (Np^{4+} and NpO_2^{2+}) with [DGA-TSIL][NTf_2] concentration in [$C_n$mim][NTf_2] (n = 4, 6, 8). Aqueous phase: 0.5 M HNO_3; (**e**) Variation of D_M with concentration of [DGA-TSIL][NTf_2] in [C_4mim][NTf_2] for the metal ions extracted from SHLW. Aqueous phase: 0.5 M HNO_3.

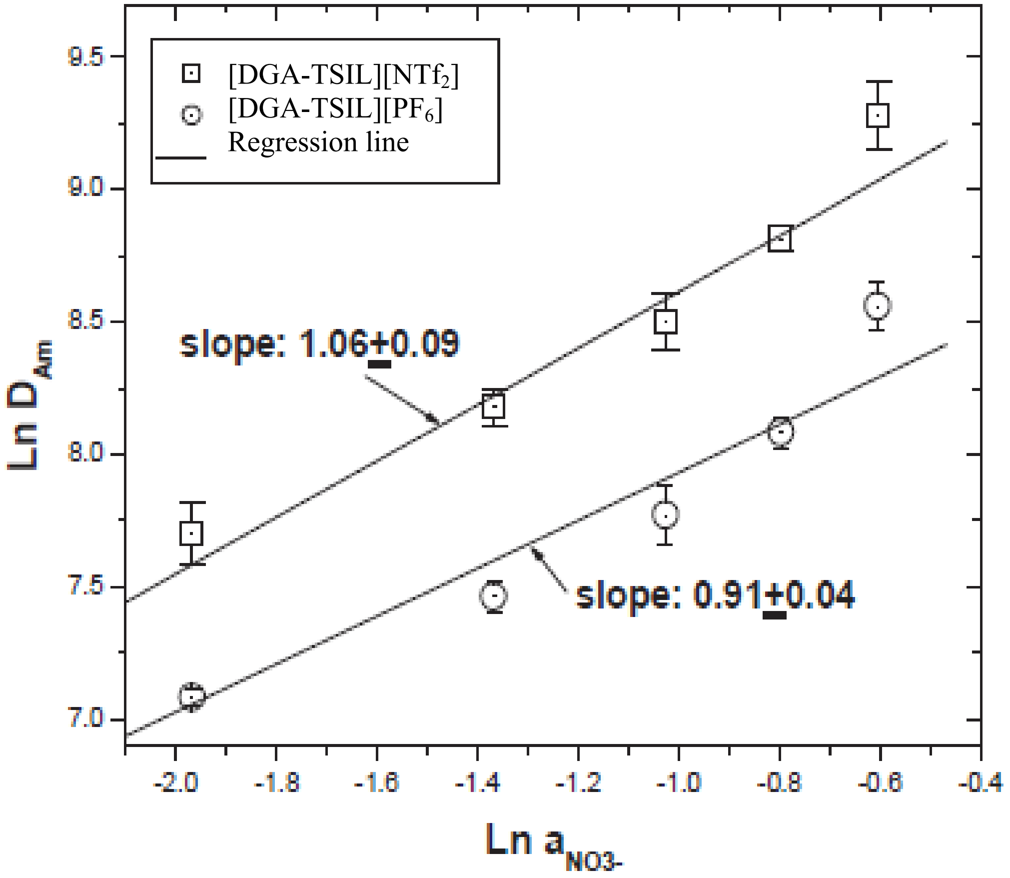

Fig. 5.6: Am^{3+} extraction profiles as a function of nitrate ion activity using [DGA-TSIL][NTf_2] and [DGA-TSIL][PF_6]

Table 5.1(a): Extraction and formation constant values for actinide ions in different oxidation states with different task specific ionic liquids

Metal ion	Diluent	Ligand	Feed acidity	Stoichiometry	K'_{ex}	K_{form}
Am(III)	[C_4mim][NTf_2]	[DGA-TSIL][NTf_2]	0.5 M	1:1	17.81×10^2	22.26×10^4
Pu(IV)	[C_4mim][NTf_2]	[DGA-TSIL][NTf_2]	0.5 M	1:1	3.63×10^2	7.26×10^4
Pu(VI)	[C_4mim][NTf_2]	[DGA-TSIL][NTf_2]	0.5 M	1:1	12.01	1.50×10^3
U(VI)	[C_4mim][NTf_2]	[DGA-TSIL][NTf_2]	0.5 M	1:1	20.40	2.91×10^3
Np(IV)	[C_4mim][NTf_2]	[CMPO-TSIL][NTf_2]	3 M	1: 1	17.37×10^2	11.58×10^4
	[C_6mim][NTf_2]			1: 1	12.02×10^2	8.01×10^4
	[C_8mim][NTf_2]			1: 1	6.76×10^2	4.51×10^4
	[C_4mim][NTf_2]	[DGA-TSIL][NTf_2]	0.5 M	1: 1	2.45×10^2	1.64×10^4
	[C_6mim][NTf_2]			1: 1	1.25×10^2	0.89×10^4
	[C_8mim][NTf_2]			1: 1	0.77×10^2	0.59×10^4
Np(VI)	[C_4mim][NTf_2]	[CMPO-TSIL][NTf_2]	3 M	1: 1	1.35×10^2	1.23×10^4
	[C_6mim][NTf_2]			1: 1	0.76×10^2	0.69×10^4
	[C_8mim][NTf_2]			1: 1	0.72×10^2	0.66×10^4
	[C_4mim][NTf_2]	[DGA-TSIL][NTf_2]	0.5 M	1: 1	0.26×10^2	0.17×10^4
	[C_6mim][NTf_2]			1: 1	0.03×10^2	0.027×10^4
	[C_8mim][NTf_2]			1: 1	0.02×10^2	0.013×10^4

Table 5.1(b): Stoichiometry of the metal-[DGA-TSIL][NTf_2] complexes and conditional extraction constants (with SHLW with 0.5 M HNO_3 as the feed)

Metal ion	Slope	Metal-ligand stiochiometry	Log K′ex
Ce^{4+}	1.16 ± 0.05	1:1	2.52 ± 0.11
La^{3+}	1.97 ± 0.06	1:2	1.81 ± 0.07
Nd^{3+}	1.90 ± 0.12	1:2	2.51 ± 0.15
Pd^{2+}	1.00 ± 0.1	1:1	0.40± 0.02
Pr^{3+}	1.88 ± 0.22	1:2	2.48 ± 0.17
Sm^{3+}	1.93 ± 0.07	1:2	3.39 ± 0.11
Y^{3+}	2.98 ± 0.23	1:3	4.59 ± 0.30
Zr^{4+}	1.90 ± 0.07	1:2	2.38 ± 0.09

5.5 Determination of thermodynamic parameters

As mentioned above, the extractability of the metal ions is dependent on the number of water molecules present in the extracted species which imparts the hydrophilicity. This is apart from the number of the organophilic extractant molecules present in the extracted species which impart lipophilicity. This can be quantified from the thermodynamic parameters such as entropy which takes the total number of reacting and product species into consideration. As the complexation / extraction reaction often involves replacement of inner-sphere water molecules, this will be reflected in the thermodynamic parameters. The Van't Hoff plots for different actinides from a 0.5 M HNO_3 feed solution using 3.6 x 10^{-2} M [DGA-TSIL][NTf_2] in

[C_4mim][NTf_2] are presented in **Fig. 5.7(a)**, while **Fig. 5.7(b)**, **Fig. 5.7(c)** and **Fig. 5.7(d)** presented the Van't Hoff plots for Np(IV) and Np(VI) using 0.01 M [CMPO-TSIL][NTf_2] in [$C_n$mim][NTf_2] (n = 4, 6, 8); Np(IV) and Np(VI) using 3.6 x 10^{-2} M [DGA-TSIL][NTf_2] in [$C_n$mim][NTf_2] (n = 4, 6, 8) and metal ion extracted from SHLW using 3.6 x 10^{-2} M [DGA-TSIL][NTf_2] in [C_4mim][NTf_2], respectively. The change in enthalpy (ΔH) during the complexation can be calculated from the slope ($-\Delta H/2.303\ R$) of the log D vs 1/T plots using the Van't Hoff equation (Chapter 3). The Gibb's free energy (ΔG) and the entropy change (ΔS) at a particular temperature were also calculated. The thermodynamic parameters for all the actinides were listed in **Table 5.2 (a),** while that for other metal ions co-extracted from SHLW were summarized in **Table 5.2(b)**. For all the actinides ions investigated, the D_M values decreased with temperature, indicating that the extraction processes are exothermic in nature. The change in enthalpy (ΔH) followed the trend $Np^{4+} > Am^{3+} > NpO_2^{2+} > Pu^{4+} > UO_2^{2+} > PuO_2^{2+}$, while the ΔG values followed a trend similar to that of the distribution ratios. The extraction of Am^{3+} is the most favourable amongst the actinide ions investigated in the present study, while that of PuO_2^{2+} is the least favourable. The entropy change decreased during the extraction process suggesting the loss of rotational and vibrational entropy of the ligand during complexation.

The change in enthalpy values were found to increase with the chain length of alkyl substituent of ionic liquid diluents for all the Np – TSIL systems, except Np(IV) - [DGA-TSIL][NTf_2] in [C_4mim][NTf_2] where the ΔH value changes marginally. The ΔG values for Np-TSIL systems were found to follow the order Np(IV) –[CMPO-TSIL][NTf_2] > Np(IV) – [DGA-TSIL][NTf_2] > Np(VI) – [CMPO-TSIL][NTf_2] > Np(VI) – [DGA-TSIL][NTf_2] i.e., Np(IV) and Np(VI) have preference for [CMPO-TSIL][NTf_2] over [DGA-TSIL][NTf_2] in ionic liquid medium.

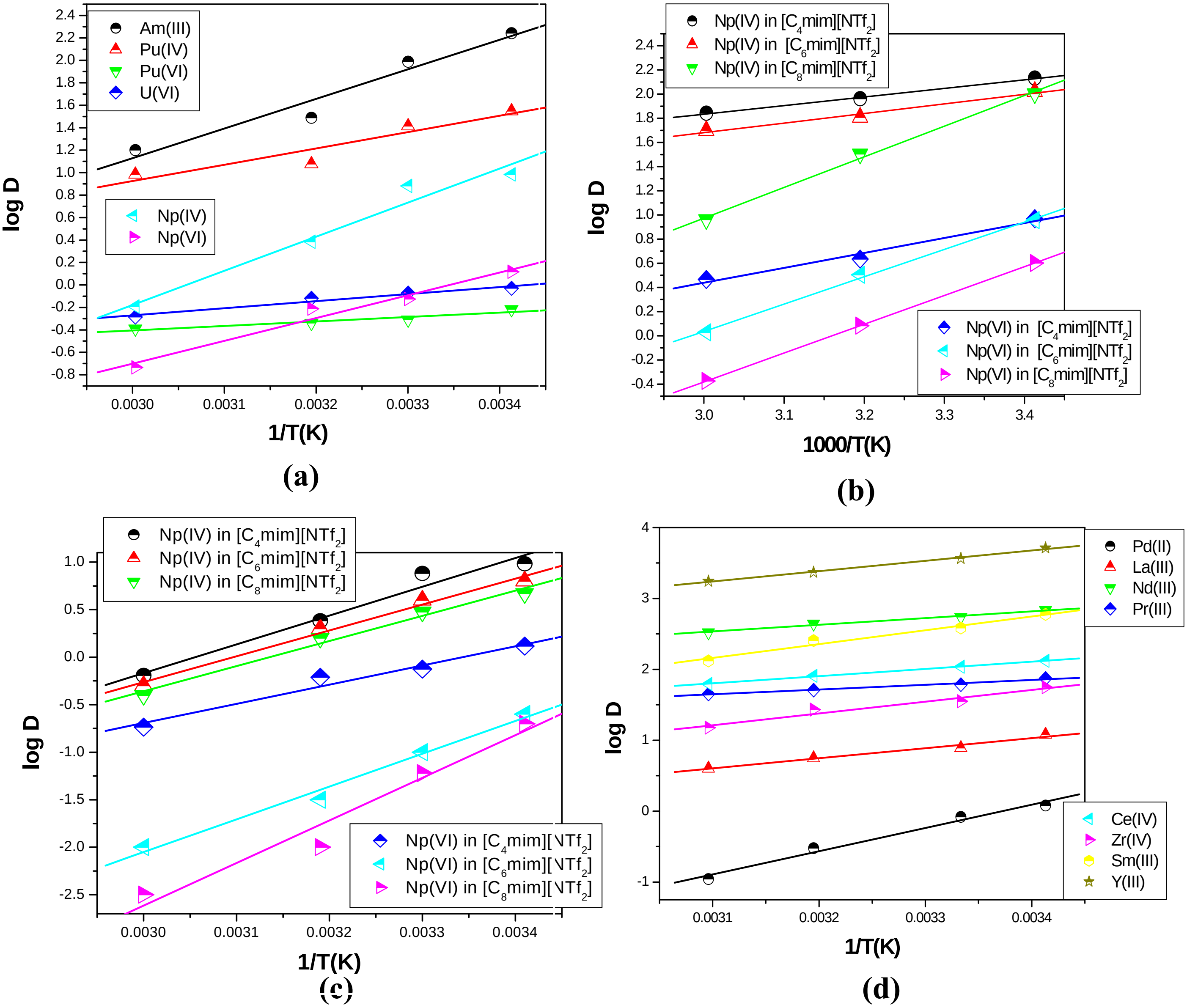

(a) **(b)**

(c) **(d)**

Fig. 5.7: Van't Hoff plots for (**a**) extraction of actinides using [DGA-TSIL][NTf$_2$]; (**b**) extraction of Np(IV) and Np(VI) using [CMPO-TSIL][NTf$_2$]; (**c**) extraction of Np(IV) and Np(VI) using [CMPO-TSIL][NTf$_2$]; (**d**) extraction of other metal ions using [DGA-TSIL][NTf$_2$]. [DGA-TSIL][NTf$_2$] conc. 3.6 x 10^{-2} M, [CMPO-TSIL][NTf$_2$] conc. 0.01 M. Diluent: [C$_4$mim][NTf$_2$]. Aqueous phase: 0.5 M HNO$_3$ (3 M HNO$_3$ for [CMPO-TSIL][NTf$_2$] system)

Table 5.2 (a): Thermodynamic parameters obtained using the Van't Hoff equation from the distribution ratio data obtained at varying temperatures for different oxidation states of actinides

Metal ion	Diluent	Ligand	Feed acidity	ΔH (kJ/mol)	ΔG (kJ/mol)	ΔS (J/mol/K)
Am(III)	$[C_4mim][NTf_2]$	$[DGA-TSIL][NTf_2]$	0.5 M	-50.4	-18.7	-230
U(VI)	$[C_4mim][NTf_2]$	$[DGA-TSIL][NTf_2]$	0.5 M	-12.0	-7.5	-65
Pu(VI)	$[C_4mim][NTf_2]$	$[DGA-TSIL][NTf_2]$	0.5 M	-7.6	-6.2	-45
Pu(IV)	$[C_4mim][NTf_2]$	$[DGA-TSIL][NTf_2]$	0.5 M	-27.8	-14.7	-141
Np(IV)	$[C_4mim][NTf_2]$	$[CMPO-TSIL][NTf_2]$	3 M	-13.6	-18.6	-16.7
	$[C_6mim][NTf_2]$			-15.1	-17.7	-8.5
	$[C_8mim][NTf_2]$			-48.4	-16.2	107
	$[C_4mim][NTf_2]$	$[DGA-TSIL][NTf_2]$	0.5 M	-58.1	-13.7	-148
	$[C_6mim][NTf_2]$			-52.2	-12.1	-134
	$[C_8mim][NTf_2]$			-50.7	-10.9	-133
Np(VI)	$[C_4mim][NTf_2]$	$[CMPO-TSIL][NTf_2]$	3 M	-23.5	-12.2	-37.7
	$[C_6mim][NTf_2]$			-43.3	-10.8	-108
	$[C_8mim][NTf_2]$			-45.6	-10.7	-116
	$[C_4mim][NTf_2]$	$[DGA-TSIL][NTf_2]$	0.5 M	-38.8	-8.2	-102
	$[C_6mim][NTf_2]$			-66.1	-3.3	-209
	$[C_8mim][NTf_2]$			-85.9	-1.3	-282

Table 5.2 (b): Thermodynamic parameters for the extraction of various metal ions present in the SHLW with 3.6 x 10^{-2} M DGA-TSIL in [C_4mim][NTf_2] (data obtained by ICP-AES)

Metal ion	ΔH (kJ/mol)	ΔG (kJ/mol)	ΔS (kJ/mol/K)
Pd(II)	-62.8	-2.3	-201.6
La(II)	-27.3	-10.43	-56.3
Nd(III)	-18.1	-20.03	6.3
Pr(III)	-12.9	-14.23	4.5
Ce(IV)	-19.4	-14.5	-16.6
Zr(IV)	-31.7	-13. 7	-60.1
Sm(III)	-37.3	-19.5	-59.6
Y(III)	-27.9	-26.4	-5.2

The change in entropy values for Np(IV) complexes were found to more positive with increase in the length of alkyl substituent while the reverse trend was observed in case of Np(VI) complexes (both either with [CMPO-TSIL][NTf_2] or [DGA-TSIL][NTf_2]) in ionic liquid medium. The change in enthalpy for the other metal ions extracted from SHLW using 3.6 x 10^{-2} M [DGA-TSIL][NTf_2] in [C_4mim][NTf_2] followed the trend: |ΔH (Pd)| > |ΔH (Sm)| > |ΔH (Zr)| > |ΔH (Y)| ~ |ΔH (La)| > |ΔH (Ce)| > |ΔH (Nd)| > |ΔH (Pr)|, while the change in Gibbs' free energy showed the following trend: Y(III) > Nd(III) ~ Sm(III) > Pr(III) ~ Ce(IV) > Zr(IV) > La(III) > Pd(II). For Nd(III) and Pr(III), the extraction process was found to be entropy driven, while for the other metal ions, the entropy change decreased with extraction.

5.6 Unique separation behavior of actinides and fission products

Preferential extraction of Eu^{3+} over Am^{3+} has been reported with DGA-based ligands, such as TODGA, T-DGA, and calix- DGA, in *n*-dodecane [189]. The task specific ionic liquids [DGA-TSIL][PF_6] and [DGA-TSIL][NTf_2] display unique separation behavior and the data are presented in **Table 5.3**. The $SF_{Eu/Am}$ values were in the range of 1.5 – 3.5 for TODGA in *n*-dodecane, [C_4mim][PF_6] and [C_4mim][NTf_2], which almost doubled for [DGA-TSIL][PF_6], though a value of 4.88 was observed for [DGA-TSIL][NTf_2] (**Table 5.3**). While Am(III) / Sr(II) separation factor (D_{Am}/D_{Sr}) values were 350, 140, and 150 for TODGA in *n*-dodecane, [C_4mim][PF_6], and [C_4mim][NTf_2], respectively [190], they increased substantially to 3.6×10^3 and 4.8×10^3 for [DGA-TSIL][PF_6] and [DGA-TSIL][NTf_2], respectively. This has a great relevance in getting better decontaminated minor actinide products and no special feed adjustment is required contrary to a previous report where the feed was adjusted to 6 M HNO_3 for achieving better decontamination from Sr [88]. High level waste solutions contain large amounts of U (in the range of 6 – 20 g/L) due to losses in the PUREX cycle. Am / U separation factor values are in the range of 10 - 26 for TODGA systems, which indicates the presence of significant concentrations of U in the minor actinide fraction, showing that a U recovery step is mandatory prior to the 'actinide partitioning' step [89]. The $SF_{Am/U}$ increased by one order of magnitude to 128 and 180 for the TSILs [DGA-TSIL][PF_6] and [DGA-TSIL][NTf_2], respectively, (**Table 5.3**) making U removal prior to minor actinide extraction redundant. Interestingly, the SF values of Am/Pu(IV) and Am/Np(IV) are in the same range. Furthermore, although [DGA-TSIL][PF_6] gave more favourable SF values for Eu / Am separation than [DGA-TSIL][NTf_2], an opposite trend was observed for the separation of the remaining elements investigated with respect to Am.

Table 5.3: Separation factor values for various actinide and fission product elements at 3 M HNO_3 feed conditions. No dilution was made for TSILs, while 1.0 x 10^{-2} M solutions were used for other solven

Ligand	$SF_{Eu/Am}$	$SF_{Am/Sr}$	$SF_{Am/Cs}$	$SF_{Am/U(VI)}$	$SF_{Am/Pu(IV)}$	$SF_{Am/Np(IV)}$
[DGA-TSIl][PF_6]	8.88	3.6 x 10^3	7.2 x 10^3	128	3.07	7.63
[DGA-TSIL][NTf_2]	4.89	4.8 x 10^3	8.5 x 10^3	181	3.9	11.9
TODGA in [C_4mim][PF_6]	1.65	140	280	26.3	1.75	4
TODGA in [C_4mim][NTf_2]	3.56	150	170	10.3	1.61	2.7
TODGA in *n*-dodecane	1.94	350	280	15.6	2.37	4.12

Note: SF is defined as the ratio of D values of the metal ions of interest

These results also suggest that [DGA-TSIL][NTf_2] has great potential from the separation point of view as well. Literature reports indicate that the nature of the organic diluent has a significant influence on the SF values. For instance, Sasaki *et al*. [62] reported SF values of ~1 and ~8.5 with ethyl acetate and *n*-dodecane, respectively, which increased to as high as 15 in case of *n*-hexane. Similar observations were made when DGA extractants were used in ionic liquids. The exceptionally high separation factor values obtained with the TSILs definitely make the DGA-functionalized ionic liquids excellent alternatives to TODGA, which has been proposed as one of the front runners to be used for the ‘actinide partitioning’ for the high level waste remediation.

5.7 Emission spectroscopic studies on the Eu^{3+} complexes

Though the solvent extraction data indicate that the trivalent metal ions (Am^{3+} and Eu^{3+}) are highly favoured to be extracted from the aqueous phase into the ionic liquid phase, it gives no information on the nature of the extracted species, i.e., whether the complexes are free from inner-sphere water molecules or not. Therefore, time resolved laser fluorescence spectroscopy (TRLFS) studies were carried out, using Eu^{3+} as a surrogate for the trivalent actinide ions. To determine the number of inner-sphere water molecules, an empirical formula was used (Chapter 4) [146,147]. The fluorescence spectrum of the Eu^{3+} aquo complex (containing 1.0×10^{-3} M Eu^{3+} in 5:1 acetonitrile and 3 M HNO_3) is presented in **Fig. 5.8**, which was compared with the emission spectra of the extracted complexes obtained with [DGA-TSIL][PF_6] and [DGA-TSIL][NTf_2]. Compared to the literature lifetime of 0.11 ms for the Eu^{3+} complex with nine water molecules, it is logical to assume the presence of 7-8 water molecules along with 1-2 nitrate ions in the inner coordination sphere of it in 5:1 acetonitrile and 3 M HNO_3 as the medium, for which a lifetime of 0.155 ms was measured (**Table 5.4**). **Fig. 5.8** also includes the emission spectra of the Eu^{3+} extracts (from 3 M HNO_3 feed solutions) obtained with pure [DGA-TSIL][PF_6] and [DGA-TSIL][NTf_2]. As shown in the **Fig. 5.8**, huge enhancements in the intensity of the emission spectra suggest strong complexation with both TSILs. The emission lifetime decay profile points to the existence of a single extracted species. Furthermore, the lifetime values of 1.564 ms for the Eu^{3+} extract with both the DGA-TSILs suggested complete removal of the inner-sphere water molecules. This is in sharp contrast to the lifetime value of 0.155 ms mentioned above.

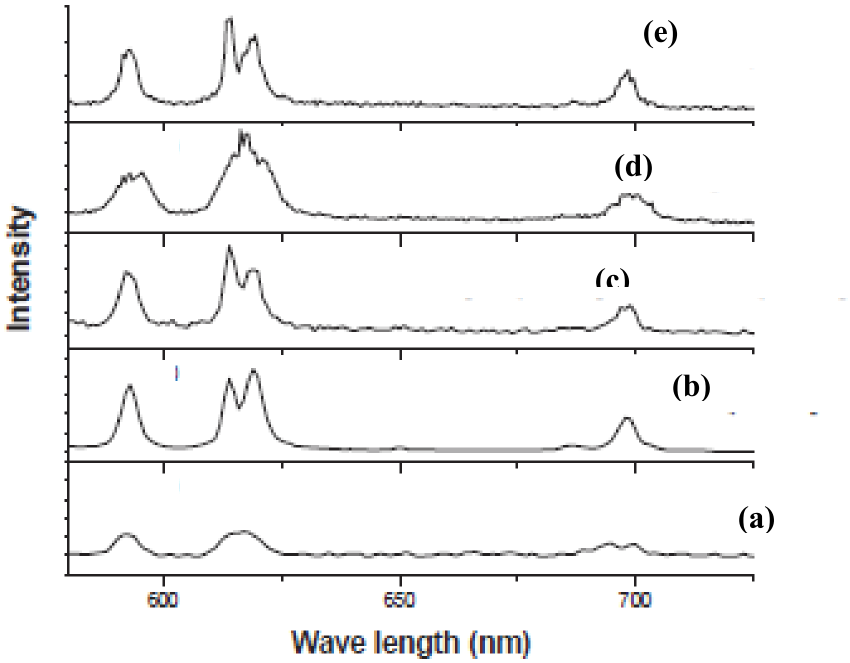

Fig. 5.8: Time resolved laser fluorescence spectroscopy studies. (**a**) 1.0 x 10^{-3} M Eu^{3+} in 5:1 acetonitrile–3 M HNO_3 mixture; (**b**) Eu(III) – extract using TODGA in [C_4mim][NTf_2]; (**c**) Eu(III)–extract using 3.6 x 10^{-2} M [DGA-TSIL][NTf_2] in [C_4mim][NTf_2]**;** (**d**) Eu(III)–extract obtained from [DGA-TSIL][PF_6]; (**e**) Eu(III) extract obtained from [DGA-TSIL][NTf_2]

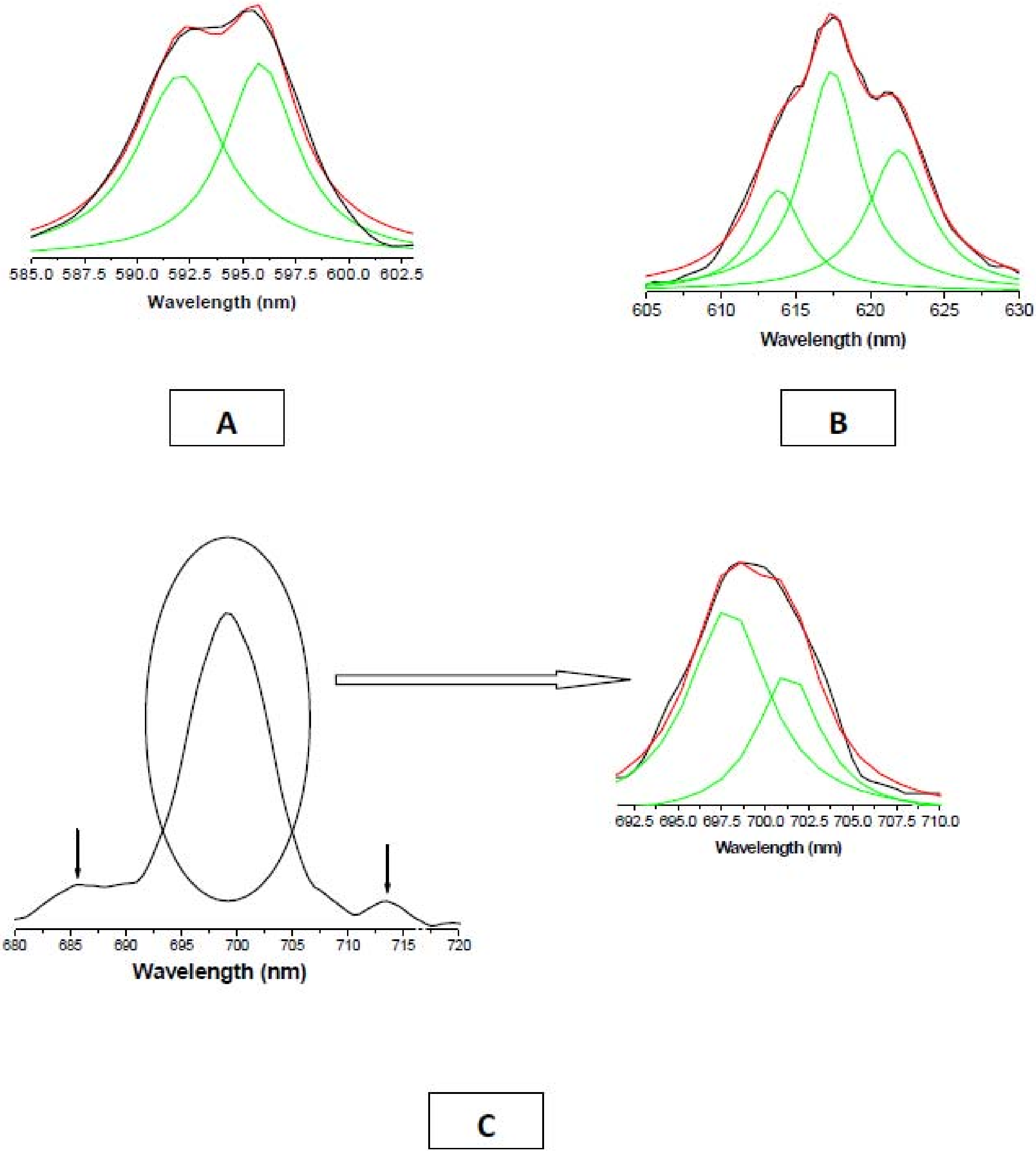

Fig. 5.9(a): Splitting pattern of different transitions in Eu^{3+}-[DGA-TSIL][NTf_2] complex, A – $^5D_0 \rightarrow {}^7F_1$ transition – 2 peaks, B - $^5D_0 \rightarrow {}^7F_2$ transition – 3 peaks, C – $^5D_0 \rightarrow {}^7F_4$ transition – 4 peaks, S_4 symmetry

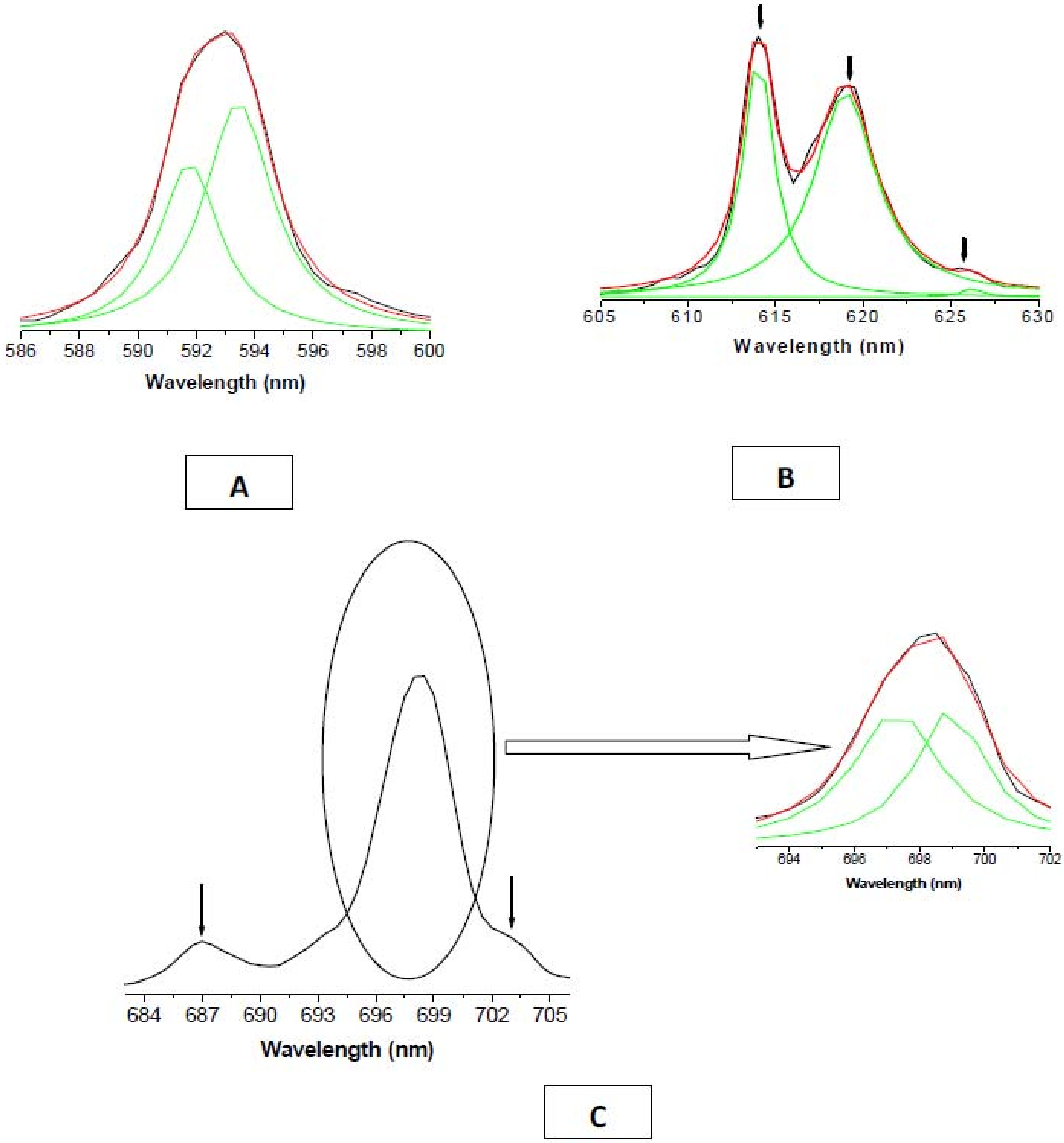

Fig. 5.9(b): Splitting pattern of different transitions in Eu^{3+}-[DGA-TSIL][PF$_6$] complex, A – $^5D_0 \rightarrow {}^7F_1$ transition – 2 peaks, B - $^5D_0 \rightarrow {}^7F_2$ transition – 3 peaks, C – $^5D_0 \rightarrow {}^7F_4$ transition – 4 peaks, S_4 symmetry

Table 5.4: Fluorescence spectroscopic data obtained for the different complexes / extracts of Eu^{3+}

System	Transition	Peak positions	Asymmetry factor	Life time (ms)	Expected number of water molecules
Eu^{3+} -Aquo complex in acetonitrile – water	$^5D_0 \rightarrow {}^7F_1$	592	1.649	0.155	8-9
	$^5D_0 \rightarrow {}^7F_2$	617			
	$^5D_0 \rightarrow {}^7F_3$	651			
	$^5D_0 \rightarrow {}^7F_4$	695, 700			
Eu^{3+} -extract with TODGA in $[C_4mim][NTf_2]$	$^5D_0 \rightarrow {}^7F_1$	593	1.985	2.172	0
	$^5D_0 \rightarrow {}^7F_2$	614, 619			
	$^5D_0 \rightarrow {}^7F_3$	650			
	$^5D_0 \rightarrow {}^7F_4$	687, 698			
Eu^{3+}- [DGA-TSIL]$[PF_6]$	$^5D_0 \rightarrow {}^7F_1$	593	1.953	1.564	0
	$^5D_0 \rightarrow {}^7F_2$	614, 619			
	$^5D_0 \rightarrow {}^7F_3$	654			
	$^5D_0 \rightarrow {}^7F_4$	698			
Eu^{3+} - [DGA-TSIL]$[NTf_2]$	$^5D_0 \rightarrow {}^7F_1$	594	1.774	1.564	0
	$^5D_0 \rightarrow {}^7F_2$	615, 617			
	$^5D_0 \rightarrow {}^7F_3$	651			
	$^5D_0 \rightarrow {}^7F_4$	699			
Eu^{3+} - [DGA-TSIL]$[NTf_2]$ in $[C_4mim][NTf_2]$	$^5D_0 \rightarrow {}^7F_1$	593	1.734	1.332	0
	$^5D_0 \rightarrow {}^7F_2$	614, 619			
	$^5D_0 \rightarrow {}^7F_3$	653			
	$^5D_0 \rightarrow {}^7F_4$	699			

The small lifetime can be attributed to non-radiative relaxations due to the coordinated water molecules [191]. The emission spectrum of the 10 times diluted extract (in the solvent system containing [DGA-TSIL][NTf_2] diluted with [C_4mim][NTf_2]) is also included in **Fig. 5.8**. The spectral pattern is not significantly different, and the lifetime data indicated that the extracted complex did not contain any inner-sphere water molecules. Consequently, there is no difference in the results obtained with pure [DGA-TSIL][NTf_2]. The splitting patterns of each transition was correlated to local symmetry around the Eu^{3+} ion was found to be S_4 [**Fig. 5.9(a), 5.9(b)**].

Judd–Ofelt intensity parameters were calculated and the Ω_2 values followed the trend: Eu^{3+}- [DGA-TSIL][NTf_2] > Eu^{3+}- [DGA-TSIL][PF_6] > Eu^{3+}- TODGA ([C_4mim][NTf_2]) > Eu^{3+}_{aq}. The variation of Ω_2 reflected by the hypersensitivity of the $^5D_0 \rightarrow {}^7F_2$ transition can be related to the variation in covalence of the Eu^{3+}-O bond. The large value of Ω_2 for the Eu^{3+} - DGA-TSIL complex suggests an enhanced covalency and strengthening the Eu^{3+}-O bond, i.e. a high bond energy short bond length. The lowest value of Ω_2 for the Eu^{3+}_{aq} system can be attributed to the low covalence of the Eu^{3+}-O bond. For all the complexes, the Ω_2 values are less than those of Ω_4. Ω_4, a measure of the long range ordering, follows the order: Eu^{3+}-[DGA-TSIL][NTf_2] > Eu^{3+}-[DGA-TSIL][PF_6] > Eu^{3+}-TODGA > Eu^{3+}_{aq}. The non-radiative transition lifetime (τ_{NR}) follows the trend: [DGA-TSIL][PF_6] ~ [DGA-TSIL][NTf_2] > TODGA > Eu^{3+}_{aq}, while a reverse trend was observed for their quantum efficiency values (η). In Eu^{3+}-DGA-TSIL complexes, where the anions are different, i.e., PF_6^- and NTf_2^-, the anions did not play any role to be distinguished by their τ_{NR} values. The branching ratio (β_n, n = 2, 4, 6) follows the order β_2 > β_4 > β_1, which revealed that Eu^{3+} resides in the asymmetric environment for all complexes. In all cases, the magnetic- and electric-dipole transition probabilities follow the order: A_{2ed} > A_{4ed} >

A_{md} (where A_{ed} and A_{md} are the electric- and magnetic-dipole radiative transition probabilities, respectively). Though there are significant differences in the electric-dipole transition values from complex to complex, the constancy of the magnetic-dipole transitions establishes the fact that there is no perturbation of the magnetic-dipole transitions by the crystal field. The radiative and non- radiative lifetime, the branching ratio of different transitions, the quantum efficiency, the probability of the electric-dipole and magnetic-dipole transitions, etc, are summarized in **Table 5.5**.

Table 5.5: Radiative parameters for Eu^{3+} - DGA complexes

system	Eu^{3+}-TODGA in $[C_4mim][NTf_2]$	Eu^{3+}-DGA-[DGA-TSIL]$[PF_6]$	Eu^{3+}-[DGA-TSIL]$[NTf_2]$
Ω_2	4.13×10^{-20}	4.26×10^{-20}	5.75×10^{-20}
Ω_4	5.23×10^{-20}	4.49×10^{-20}	5.90×10^{-20}
τ_R (sec)	2.24×10^2	2.40×10^2	2.42×10^2
τ_{NR} (sec)	2.80×10^2	4.00×10^2	3.98×10^2
η	0.44	0.37	0.38
A	1.98	1.95	1.77
Lifetime (ms)	2.17	1.56	1.56
N_{H2O}	0	0	0
N_{ligand}	2	2	2
β_1	0.19	0.18	0.18
β_2	0.48	0.46	0.48
β_4	0.30	0.31	0.31
A_{md}	42.59	42.60	42.41
A_{2ed}	107.14	110.01	114.85
A_{4ed}	67.01	73.70	75.35

5.8 Stripping studies

As mentioned earlier, it is required to understand the stripping behavior of the extracted metal ions from the TSIL based solvent systems. The acid concentration variation data suggest that the very high D_{Am} values obtained with both [DGA-TSIL][NTf_2] and [DGA-TSIL][PF_6] in the entire acidity range studied makes it rather difficult to effect satisfactory metal ion stripping. Therefore, it is known that metal ion stripping can be accomplished by the use of complexing agents such as 0.05 M EDTA or DTPA in 1 M guanidine carbonate [82,156] and about 50% stripping of Am^{3+} was seen from the extract in [DGA-TSIL][NTf_2] when a 4 times diluted solution in [C_4mim][NTf_2] was used. Summary of the stripping results are given in **Table 5.6**. It is possible to get quantitative stripping of the metal ion in about eight stages. On the other hand, > 90% stripping of the metal ion was possible in a single stage using 3.6×10^{-2} M [DGA-TSIL][NTf_2] in [C_4mim][NTf_2], which clearly shows that quantitative stripping is possible in two stages. The diluted TSIL extracts were checked for acid uptake, which was found to be negligible suggesting no pre-treatment of the metal ion loaded phase is required for the complexing agents to work effectively (valid for the lower stripping seen with the 4 times diluted solvent). Along with the exceptionally high Am(III) extraction, the stripping results demonstrate that the DGA-functionalized ionic liquids can be used for the extraction of ‘minor actinides’ from high level wastes, thereby addressing one of the most important issues involved in radioactive waste remediation.

A systematic study was also carried out to understand the stripping behavior of actinides in different oxidation states from the organic phase containing 3.6×10^{-2} M [DGA-TSIL][NTf_2]. 1 M Na_2CO_3 was found to be highly efficient for the quantitative recovery of hexavalent actinides (% stripping U(VI) = 99.3%, Pu(VI) = 98.9%, Np(VI) = 98.4%), whereas

0.5 M oxalic acid is fairly good for the stripping of tetravalent actinides with stripping percentages of 58.7% for Pu(IV) and 85.6% for Np(IV) in a single contact. It was also found that 0.5 M oxalic acid for Np(IV) and 1 M Na_2CO_3 for Np(VI) are suitable for quantitative stripping of loaded Np from [CMPO-TSIL][NTf_2] in [$C_n$mim][NTf_2] (n – 4, 6, 8). **Fig 5.10(a)** shows the % strippinig of actinide ions in different oxidation states from ionic liquid phase in a single contact while **Fig. 5.10(b)** and **Fig. 5.10(c)** give similar data for Np(IV) and Np(VI) from [CMPO-TSIL][NTf_2] and [DGA-TSIL][NTf_2], respectively in [$C_n$mim][NTf_2] (where, n = 4, 6, and 8)

Table 5.6: Stripping data obtained with the Am^{3+} extract made with the [DGA-TSIL][NTf_2]

Organic phase	Stripping solution	% stripping
[DGA-TSIL][NTf_2] 4 times diluted in [C_4mim][NTf_2]	1 M Guanidine carbonate + 0.05 M EDTA	49.9
	1 M Guanidine carbonate + 0.05 M DTPA	52.9
	0.1 M Citric acid + 0.4 M Formic acid + 0.4 M Hydrazine hydrate	1.2
[DGA-TSIL][NTf_2]10 times diluted in [C_4mim][NTf_2]	1 M Guanidine carbonate + 0.05 M EDTA	90.9
	1 M Guanidine carbonate + 0.05 M DTPA	90.3
	0.1 M Citric acid + 0.4 M Formic acid + 0.4 M Hydrazine hydrate	1.54

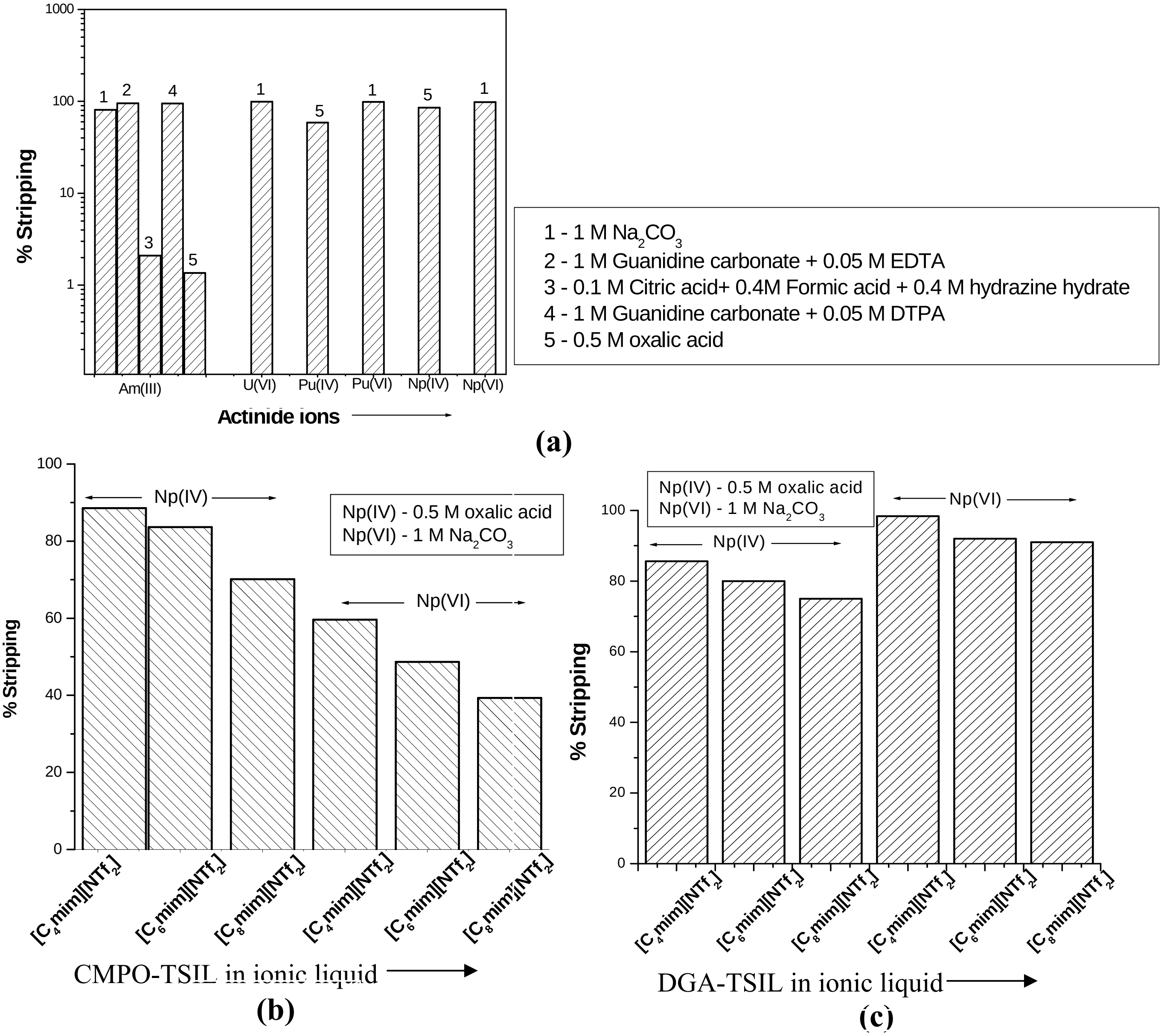

Fig. 5.10: Stripping data for **(a)** actinide ions in different oxidation states from 3.6 x 10^{-2} M [DGA-TSIL][NTf$_2$] in [C$_4$mim][NTf$_2$]; **(b)** Np(IV) and Np(VI) from 0.01 M [CMPO-TSIL][NTf$_2$] in [C$_n$mim][NTf$_2$] (n = 4, 6, 8); **(c)** Np(IV) and Np(VI) from 3.6 x 10^{-2} M [DGA-TSIL][NTf$_2$] in [C$_n$mim][NTf$_2$] (n = 4, 6, 8).

5.9 Radiolytic degradation and recycling possibilities

Radiolytic degradation studies were carried out by irradiating the DGA-TSIL based solvents to 1000 kGy gamma ray dose. The Am(III) extraction data obtained with the irradiated solvents are presented in **Fig. 5.11**, which clearly shows the relatively insignificant lowering in the D_{Am} values in case of [DGA-TSIL][NTf_2]. Although the radiolytic stability of [DGA-TSIL][PF_6] is less than that of [DGA-TSIL][NTf_2], it is still far superior to that of several ionic liquids based solvent systems reported in the literature [143,144]. This demonstrates that the DGA-TSILs are much more suitable for long term applications in radioactive waste processing as compared to other ionic liquid based solvents. Diglycolamides in *n*-dodecane show a very high radiolytic degradation (>95% with 1000 kGy (100 MRad) absorbed dose) [134,192]. That means that the DGA-TSILs are the most suitable solvents for 'actinide partitioning' from the recycling point of view as well, thus, making them 'green solvents' of very high potential for radioactive waste remediation applications.

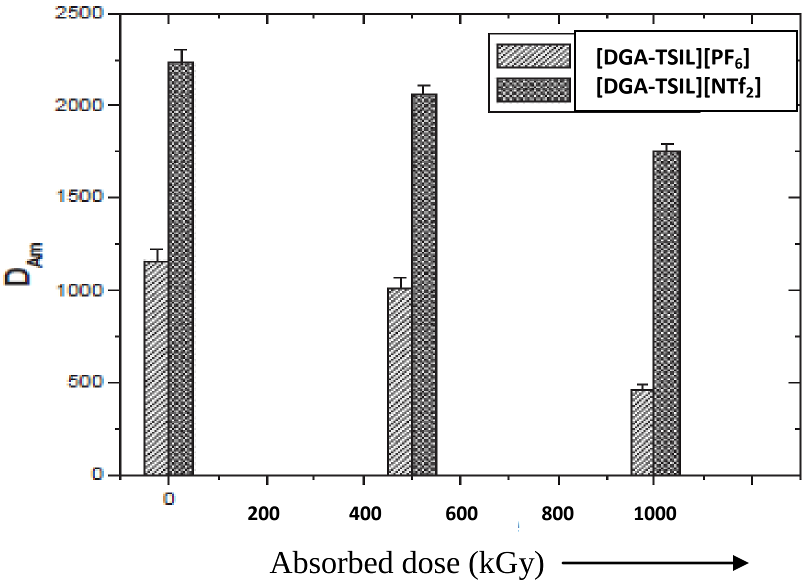

Fig. 5.11: Effect of absorbed gamma ray dose on Am(III) extraction. Aq. phase: 3 M HNO_3.

Though the radiation stability of the solvent system is reasonably good, an attempt was made to identify the degradation products. Since gamma radiation generally produces radicals, electron paramagnetic spectroscopic investigations of the 1000 kGy irradiated organic phase may lead to the identification of the radical species. EPR spectroscopic analysis of the spectra of the irradiated solvent system yielded a broad signal at g = 2.004 with a line width of 61 Gauss. From a deconvolution and simulation study, it was concluded that the EPR peak was a combination of two signals viz. of the methyl and the butylimidazolium radical [**Fig. 5.12(a)**]. Shkrob et al. [193] reported similar radicals upon the radiolysis of [C_{10}mim][NTf_2]. Since the concentration of [DGA-TSIL][NTf_2] is 3.6 x 10^{-2} M, it is likely that the radiolytic products mainly originate from the diluent. The butylimidazolium radical is responsible for the broad peak at ~2.004 with a line width of 61 Gauss, while the $CH_3\cdot$ radical is responsible for four signals, each separated by 17 Gauss with an intensity pattern of 1:3:3:1. From the integrated spectra, it was noticed that the overall intensity of the butylimidazolium radical is 5 times more intensive than that of the methyl radical.

EPR investigation was also carried out with pure [DGA-TSIL][NTf_2] and [DGA-TSIL][PF_6]. The major paramagnetic species reported to be obtained upon irradiation of NTf_2^- anion are $^{\cdot}CF_2SO_2NTf$ (with a triplet EPR signal having a relative intensity of 1:3:1) and $^{\cdot}CF_3$ (with a quartet EPR signal with a 1:3:3:1 relative intensity) radicals [194]. Shkrob et al. reported a plausible fragmentation mechanism of the NTf_2^- anion in [C_2mim][NTf_2] [195]. The relative yields of $^{\cdot}CF_3$ and $^{\cdot}CF_2SO_2NTf$ as compared to C_2mim^+ derived radicals are similar. Because of the large coupling constants due to ^{19}F nuclei (^{19}F, I = 1/2, 100% abundance), the above two radicals have a relatively small overlap with the central signal that originates from methylimidazolium ring/ C-H based radicals. Scanning of the EPR signal from 2870 to 3870 G revealed no signal from any fluorinated paramagnetic species. Variation of the temperature from 150 to 200 K, clearly indicated a triplet with g ~2.0038 G, wide shoulders separated by a large isotropic hyperfine coupling constant of 98 G and a smaller doublet with g ~2.0042 and a hyperfine coupling constant of ~28 G. These signals can be tentatively assigned to $Q_2H_2^{+\cdot}$ and $Q_2H\cdot$ [**Fig. 5.12(b)**], respectively [196]. $Q_2H\cdot$ is generated due to the electron attachment on the cation, while a plausible way for the formation of the former cation radical can be expressed as

$$Q_2H\cdot + H^+ = Q_2H_2^{+\cdot} \qquad (5.13)$$

On increasing the temperature to ~225 K an unresolved quartet at g ~2.0019 was observed with A ~18 G. This signal may be attributed to the methyl radical, as known from literature [194]. Beyond 250 K, the only signal persists with g ~2.0001 is attributed to the stable E'^{1} centered radical formed due to the irradiation of the quartz tube (**Table 5.7**) [197]. Reactive organic radicals being present in a liquid can diffuse easily and radical – radical recombination becomes more feasible upon increasing temperatures. The E_1' centered radical, generated due to glass container irradiation, is sufficiently stable even at 250 K where other signals have washed out. Similar EPR spectra were also observed for irradiated [DGA-TSIL][PF_6]. The total intensity of the signal, which is a measure of the amount of paramagnetic species present in the system, can be obtained by integration of the first derivative EPR signals. Thus, the obtained relative ratio of paramagnetic species was found to be 4:11 for [DGA-TSIL][NTf_2] : [DGA-TSIL][PF_6].

Table 5.7: Spin Hamiltonian parameters of the radicals obtained upon irradiation of [DGA-TSIL][NTf$_2$] at 77 K

Radical	Nature	g	A(G)
$Q_2H_2^{+\cdot}$	t, 1:2:1	2.0038	50
$Q_2H\cdot$	d, 1:1	2.0042	27
$CH_3\cdot$	q, 1:3:1	2.0019	20

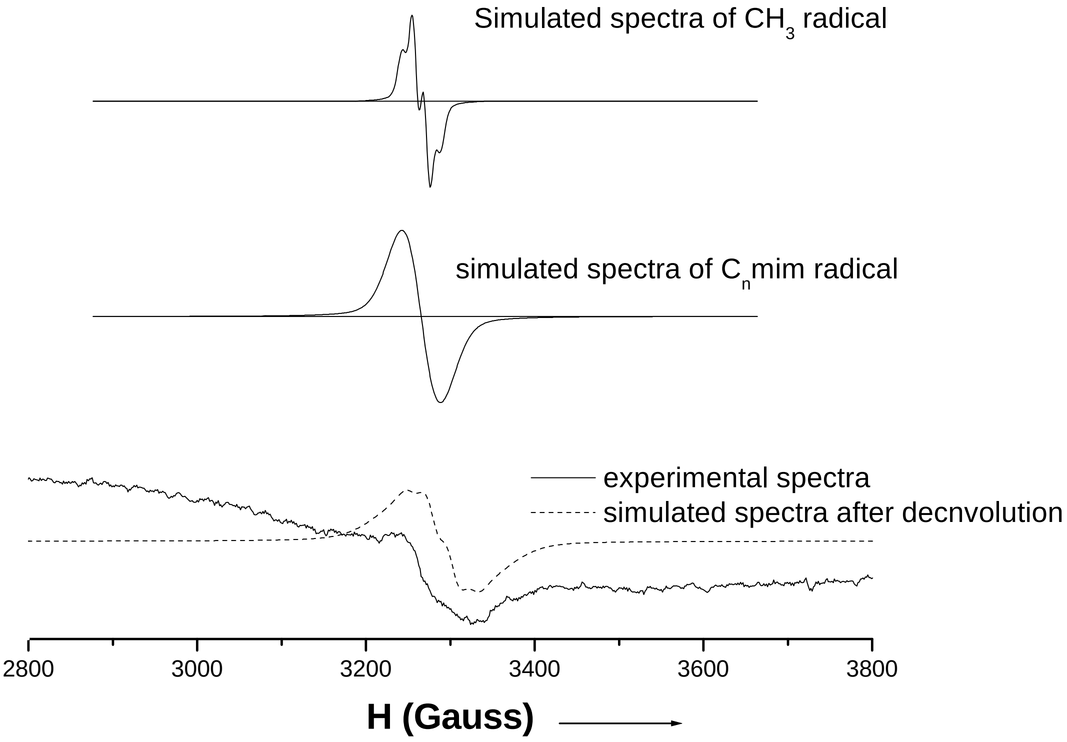

(a)

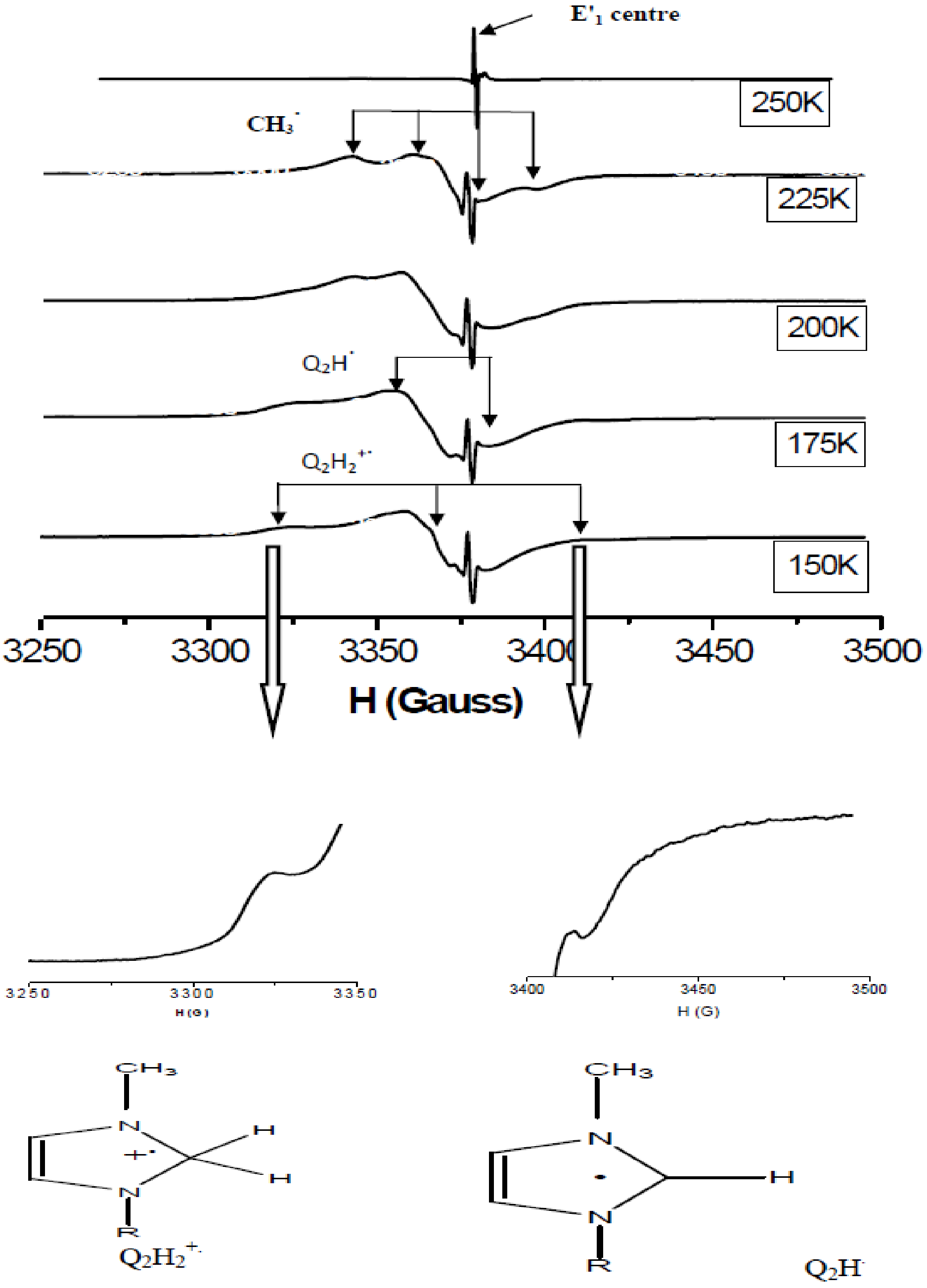

(b)

Fig. 5.12: EPR spectra of irradiated **(a)** 3.6 x 10^{-2} M [DGA-TSIL][NTf_2] in [C_4mim][NTf_2]; (**b**) pure [DGA-TSIL][NTf_2] at various temperature

5.10 UV-Vis spectroscopic investigations

5.10.1 Studies on UO_2^{2+} - [DGA-TSIL][Br] complex

A systematic study was carried out to understand the complexation of uranyl ion with [DGA-TSIL][Br] in room temperature ionic liquid. A series of peaks (426.406 nm, 439.218 nm, 460.867 nm, 476.881 nm, 491.903 nm) for U in dilute HNO_3 (0.1 M) and (431.923 nm, 445.459 nm, 462.965 nm, and 478.815 nm) for UO_2^{2+} - DGA-TSIL complex in ionic liquid were observed [**Fig. 5.13**]. A significant change in the peak positions as well as the spectral pattern suggested that the nature of the species differ from each other. An enhancement in the relative intensity at 478.815 nm for the UO_2^{2+} - [DGA-TSIL][Br] complex in [C_8mim][Br] can be attributed to the ability of the imidazolium cation to form hydrogen bond with NO_3^- of $UO_2(NO_3)_2$.[DGA-TSIL][Br] species. Sornein et al. [198] and Deetlefts et al. [199] also reprted similar enhancements at the low energy end of the spectra of the $UO_2Cl_4^{2-}$ complexes in [C_4mim][NTf_2]. The enhancement in the intensities of the peaks of the $UO_2Cl_4^{2-}$ was attributed to the hydrogen bonding of uranyl tetrachloro complex to a hydrogen donor atom [200]. The vibronic spacing of approximately 780.52 cm^{-1} can be attributed to the symmetric stretching vibration (ν_s) of UO_2^{2+} in the ground state while in uranyl-[DGA-TSIL][Br] complex it becomes 739.04 cm^{-1} suggesting decrease in the U-O bond energy upon complexation leading to weakening of the bonds (O=U=O) and increase in the bond lengths. The gorund state frequency of ν_s of $UO_2Cl_4^{2-}$ in [C_{10}mim][Br] was found to be approximately 750 cm^{-1} while that of $UO_2Cl_4^{2-}$ in [C_4mim][NTf_2] was reported as 825 cm^{-1} or 832 cm^{-1} from FT Raman spectral analysis of $UO_2Cl_4^{2-}$ in 40:60 $AlCl_3$ – [C_2mim][Cl] [200].

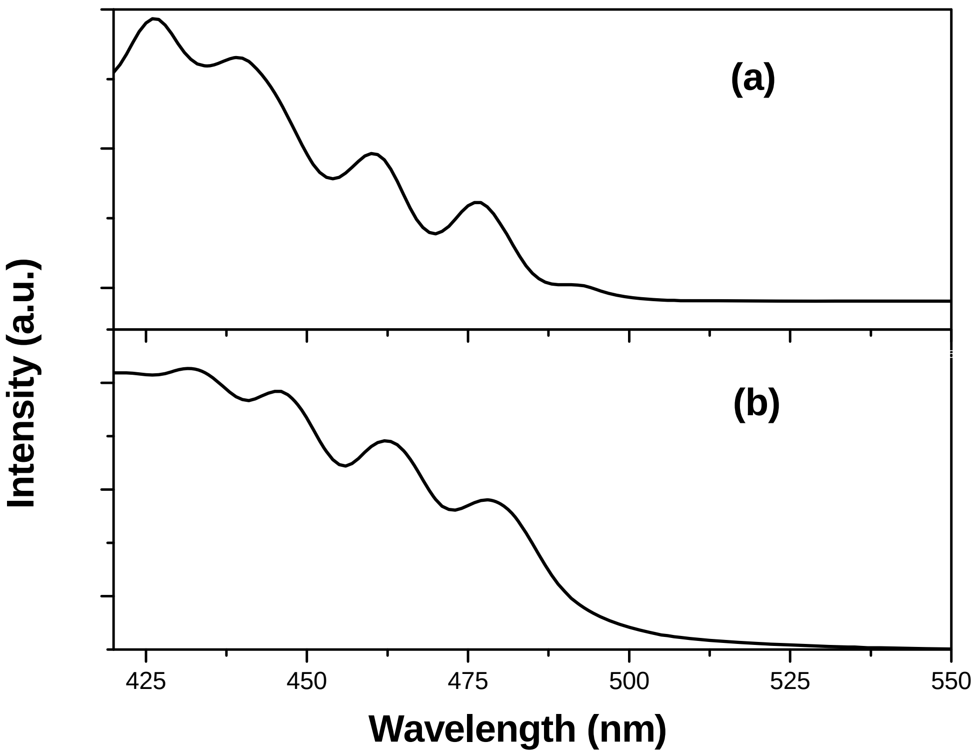

Fig. 5.13: UV-Vis specta of (**a**) UO_2^{2+} in dilute HNO_3 and (**b**) UO_2^{2+} - [DGA-TSIL][Br] complex

5.10.2 Studies on Np(IV) - TSIL complexes in [C_4mim][NTf_2]

The spectra of the naked ions of Np^{3+} and Np^{4+} showed many different overlapping bands and peak, primarily in the visual range, whereas the absorption of the neptunyl ions NpO_2^+ and NpO_2^{2+} have rather isolated strong absorption peaks [**Fig 5.14**]. The most significant peak in Np(IV) is at 700 nm which was found to be shifted towards higher wave length, ~735 nm for all the complexes of Np(IV). Similar shifts of 735 nm shoulder of Np(IV) in 3 M HNO_3 towards higher wavelength, ~762 nm was observed. All Np(IV) - CMPO complexes (in *n*-dodecane, in [C_4mim][NTf_2] and [CMPO-TSIL][NTf_2] in [C_4mim][NTf_2]) showed same amount of wavelength shifts for the two peaks mentioned above while for the peak at ~802 nm (in 3 M

HNO_3), the wave length shifts of Np(IV) - CMPO *n*-dodecane system is higher than that of Np(IV)-CMPO systems in the ionic liquid (CMPO and [CMPO-TSIL][NTf_2]). The overall shifts in wave length positions of Np(IV) and change in the structure of spectra revealed that the Np(IV) - CMPO complexes are entirely different from Np(IV) nitrate complex in 3 M HNO_3. It also revealed that out of these three systems, Np(IV)-CMPO complex in *n*-dodecane is entirely different than other two complexes. For Np(IV) – DGA complex, a drastic change in spectral characteristic was observed in UV-Vis spectra compared to Np(IV) in 3 M HNO_3. Though a shifts of ~30 nm towards higher wavelength was observed for ~700 nm peak of Np(IV) in HNO_3, an additional shoulder was observed for all Np(IV)-DGA complexes at lower wavelength values. The original shoulder at ~ 735 nm becomes less prominent on complexation of Np(IV) with all the diglycolamide moieties. The spectral characteristics of Np(IV)-TODGA in *n*-dodecane is entirely different from all other spectra whereas Np(IV)-TODGA complex in [C_4mim][NTf_2] and Np(IV) - [DGA-TSIL][NTf_2] complex in [C_4mim][NTf_2] showed considerable difference in their spectral characteristics. The spectra suggests that Np(IV)-TODGA complex in *n*-dodecane is entirely different than Np(IV)-DGA complexes in ionic liquid whereas significant difference is also observed in case of Np(IV)-TODGA complex in [C_4mim][NTf_2] and Np(IV)- [DGA-TSIL][NTf_2] complex in [C_4mim][NTf_2].

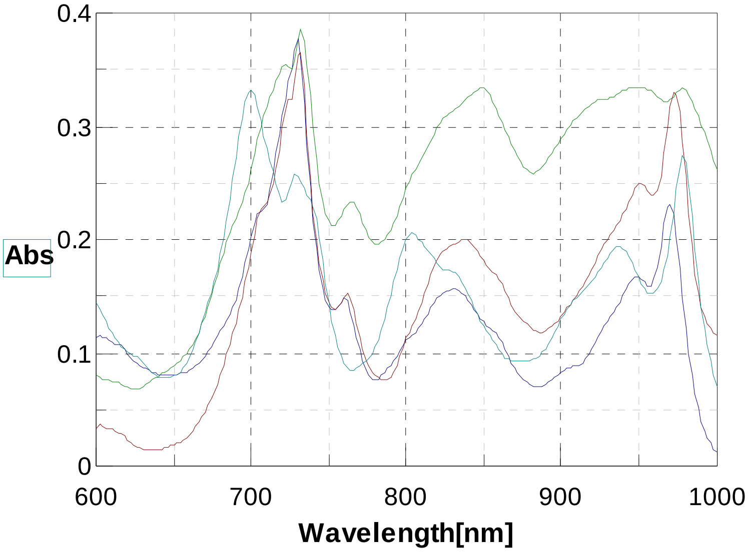

1: Greenish blue (Np(IV) vs 3 M HNO_3)

2: Green: (Np(IV) extracted in 0.1 M CMPO/ *n*-dodecane -vs- 0.1 M CMPO/ *n*-dodecane);

3: Red: (Np(IV) extracted in 0.1 M CMPO/ [C_4mim][NTf_2]-vs-0.1 M CMPO/[C_4mim][NTf_2]);

4: Blue: (Np(IV) extracted in 0.1 M [CMPO-TSIL][NTf_2] / [C_4mim][NTf_2]-vs-0.1 M [CMPO-TSIL][NTf_2] / [C_4mim][NTf_2])

(a)

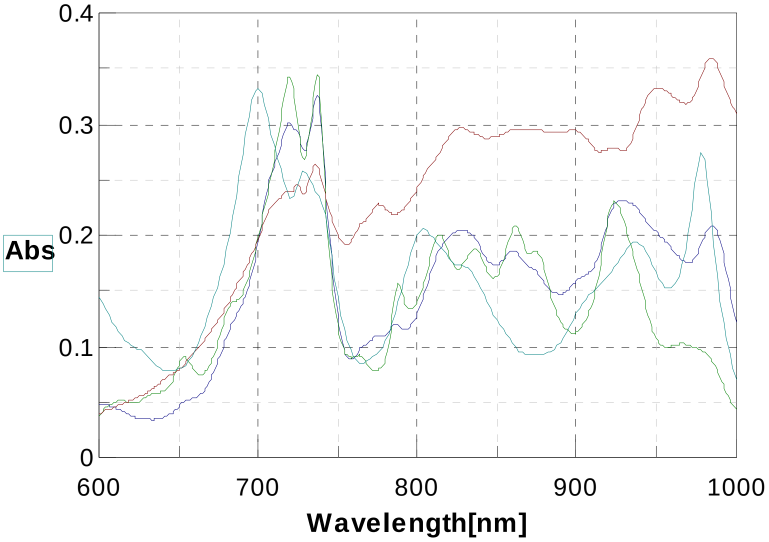

1: Greenish blue (Np(IV) vs 6 M HNO_3)

2: Green: (Np(IV) extracted in 0.36 M TODGA / [C_4mim][NTf_2]-vs- TODGA / [C_4mim][NTf_2]);

3: Red: (Np(IV) extracted in 0.36 M TODGA/*n*-dodecane-vs-TODGA/*n*-dodecane);

4: Blue: (Np(IV) extracted in 0.36 M [DGA-TSIL][NTf_2] / [C_4mim][NTf_2]-vs-[DGA-TSIL][NTf_2] / [C_4mim][NTf_2])

(b)

Fig 5.14: UV-vis spectra of Np(IV) in complexes with (**a**) CMPO based ligands; (**b**) DGA based ligands

5.11 Cyclic voltammetric studies

5.11.1 Studies on UO_2^{2+} - [DGA-TSIL][Br] complex in [C_8mim][Br]

Cyclic voltammetry is a sensitive technique to detect the electronic changes in local environment of the metal ions under study. Since complexation leads to the significant changes in the electronic environment of a given metal ion, cyclic votammogram of the complexed metal ion differs distinctly from that of the bare metal ion [201,202]. In the present case, a comparative study was carried out to understand the changes in the cyclic voltammogram due to the complexation of uranyl ion with [DGA-TSIL][Br] in [C_8mim][Br] (**Fig. 5.15**). The cathodic peak at -1.236 V for the bare uranyl ion in [C_8mim][Br], attributed to the reduction of U(VI) to U(IV), was found to be shifted towards more positive potential (E_p^c = -1.101 V) on complexation of the uranyl ion with [DGA-TSIL][Br]. On complexation, the overall charge density on the uranyl ion is decreased and less energy is required for the reduction of the UO_2^{2+} ion which is reflected in shifting of the reduction potential towards a less negative side. On the contrary, the reason behind the marginal shift of anodic peak potential on complexation (**Table 5.8**) is not clearly understood.

Table 5.8: Comparison of peak potentials and diffusion coefficient of bare uranyl ion and UO_2^{2+} - [DGA-TSIL][Br] complex in [C_8mim][Br]

System	UO_2^{2+} in [C_8mim][Br]	UO_2^{2+} -[DGA-TSIL][Br] complex in [C_8mim][Br]
E_p^c (V)	-1.236	-1.101
E_p^a(V)	-0.178	-0.188
D (cm^2s^{-1})	4.39×10^{-10}	5.40×10^{-11}

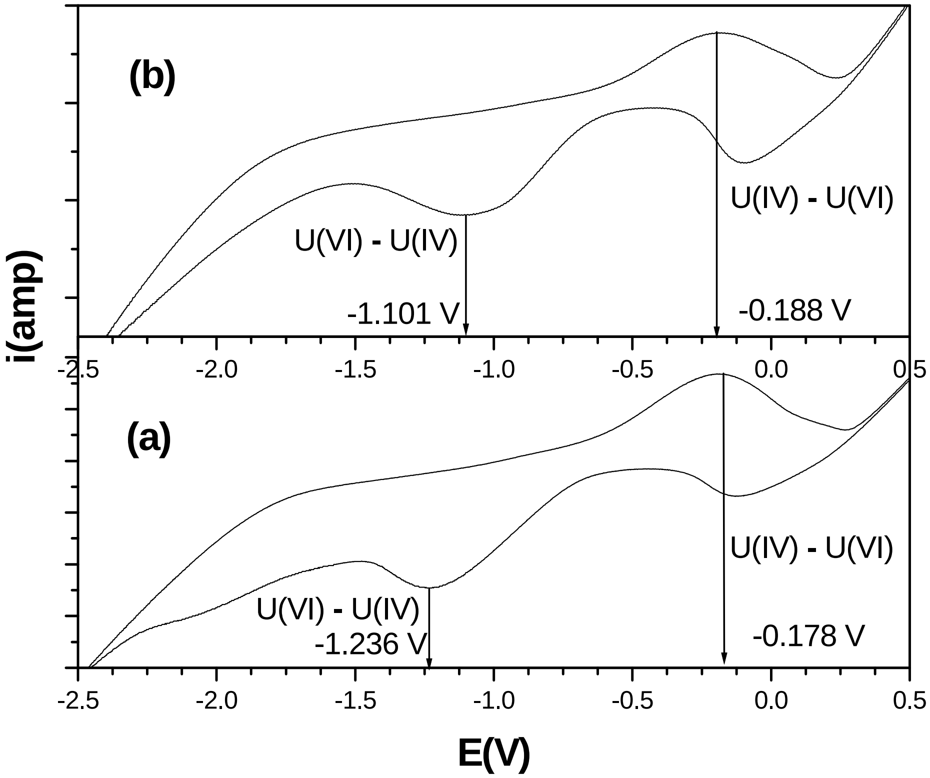

Fig. 5.15: Cyclic voltammogram of (**a**) bare UO_2^{2+} in [C_8mim][Br] and (**b**) UO_2^{2+} - [DGA-TSIL][Br] in [C_8mim][Br]

The general relationship between the cathodic diffusion peak current [$(i_p^c)_{diff}$] and scan rate for a soluble- soluble irreversible / quasi-reversible system can be given as [151]

$$(i_p^c)_{diff} = 0.496\ nFAC_0^* \sqrt{D_0}\ (\alpha n_\alpha F\nu/RT)^{1/2} \qquad (5.14)$$

where, A is the electrode area in cm^2 (= 1.68 cm^2), C_0^* is the concentration of the corresponding metal ion in mol.cm^{-3}, D_0 is the diffusion coefficient in cm^2s^{-1}, F is the faraday constant, n is the number of exchanged electrons (= 2 for U), ν is potential sweep rate in Vs^{-1}, α is the charge transfer coefficient, n_α is the number of electrons transferred in the rate determining step, T is the value of absolute temperature in K. If this relation was valid, cathodic peak current $(i_p^c)_{diff}$ vs. $\nu^{1/2}$ should give a straight line whose slope was 0.496 $nFAC_0^*\sqrt{D_0}\,(\alpha n_\alpha F/RT)^{1/2}$. In this term, the only unknown product, αn_α, obtainable from the equation below is substituted in the value of slope given above to yield the diffusion coefficient, D_0.

$$E_p^c - E_{p\,1/2}^c = 1.857RT/\alpha n_\alpha F \quad (5.15)$$

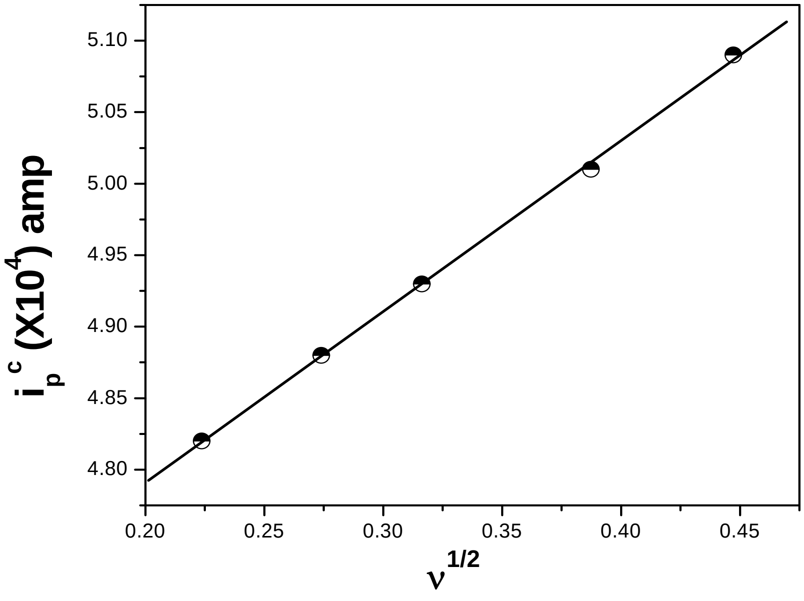

Fig 5.16: Variation of cathodic peak current with the square root of scan rate at 303 K for UO_2^{2+} - [DGA-TSIL][Br] in [C_8mim][Br]

A plot of i_p^c vs $\nu^{1/2}$ gave a straight line (**Fig 5.16**) and from the slope value the diffusion coefficient of the UO_2^{2+}-DGA-TSIL was calculated at 303 K. The diffusion coefficient of the uranyl complex (5.40×10^{-11} cm^2s^{-1}) was found to be 10 times more than that of the bare uranyl ion (4.39×10^{-10} cm^2s^{-1}) in [C_8mim][Br] as reported earlier [203]. This increase in the diffusion coefficient on complexation can be attributed to the increase in the size of the uranyl – [DGA-TSIL][Br] complex as compared to the bare uranyl ion in [C_8mim][Br].

5.11.1.1 Kinetics of complexation

Due to the addition of the [DGA-TSIL][Br] in [C_8mim][Br] containing uranyl ion, the peak current was found to decrease due to complexation of uranyl ion with [DGA-TSIL][Br]. The decrease in the peak current which is a measure of complexation was found to follow a time profile (**Fig.5.17(a)**) and can be expressed by the following equation

$$i_p^c = (2.474 \pm 0.008) + (0.448 \pm 0.012) \exp[-t/(34.77 \pm 2.75)] \qquad (5.16)$$

suggesting that the complexation follows slower kinetics and is ‘first order reaction’ with a rate constant of 4.8×10^{-4} s^{-1}. This compares very well with the of Eu^{3+} - TODGA complex in [C_8mim][Br] which was found to be 5.5×10^{-4} s^{-1}. **Fig. 5.17(a)** revealed that i_p^c decreases drastically upto 120 min. followed by a marginal decrease. It can be concluded that ~120 min is required to achieve complete complexation of uranyl ion with diglycolamide functionalized task specific ionic liquid. Time profile saturating near 120 minutes was also observed during liquid-liquid extraction of uranyl ion from 3 M HNO_3 to the organic phase containing [DGA-TSIL][NTf_2] in [C_8mim][NTf_2] (**Fig. 5.17(b)**). Due to the hydrophilic nature of bromide form of the DGA-TSIL, the hydrophobic [DGA-TSIL][NTf_2] was used. Similar observation was made during the liquid – liquid extraction of actinides in different ionic liquids using multiple diglycolamide-functionalized ligands and relatively slower kinetics of complexation was attributed to the high viscosity coefficient of the ionic liquids compared to the conventional molecular solvents. In viscous medium, due to high diffusion coefficient of the reacting species, their approach towards each other for the formation of the complex requires longer time which was reflected in their complexation kinetics.

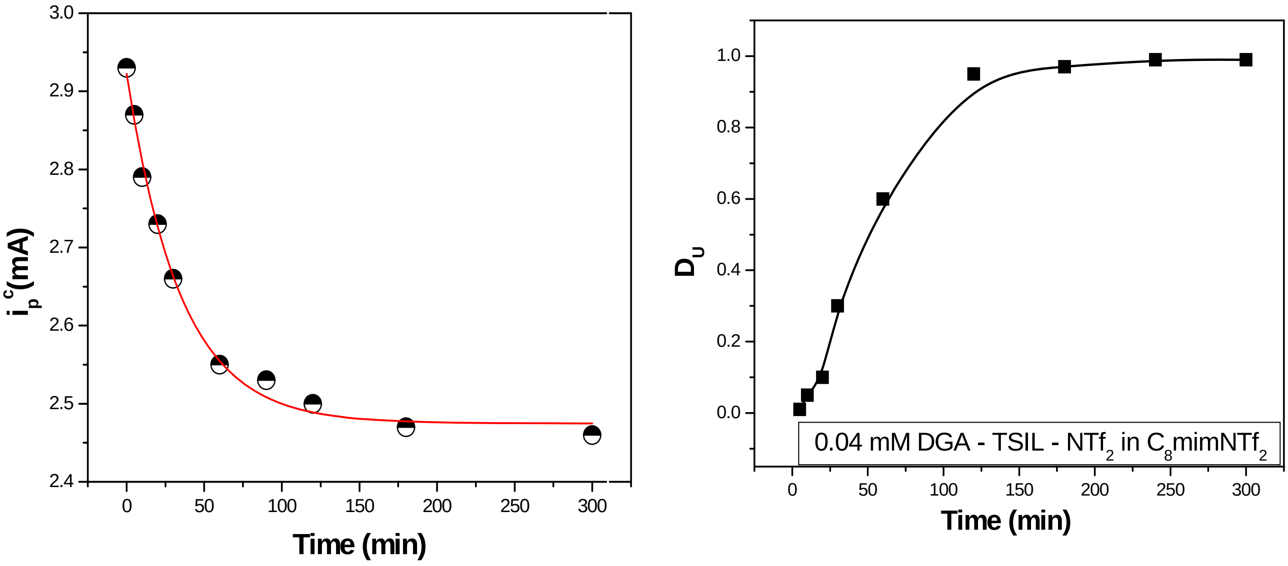

(a) **(b)**

Fig. 5.17: Studies on time profiles of **(a)** cathodic peak current (i_p^c) during the titration of 200 mM UO_2^{2+} in [C_8mim][Br] by 1 mM [DGA-TSIL][Br] in [C_8mim][Br] at 300K with scan rate 1vs^{-1}; (**b**) during the extraction of uranyl ion into 0.4 M [DGA-TSIL][NTf_2] in [C_8mim][NTf_2] at 303 K

5.11.1.2 Determination of the stoichiometry of the complex

To understand the complexation, the preliminary step is to determine the stoichiometry of the metal – ligand complex. In the present study, an attempt was made to determine the stoichiometry of the uranyl – DGA-TSIL complex by the electrochemical as well as the liquid-liquid extraction method. Both the methods were used to calculate the formation constants of the complex.

The amperometric titration curve for uranyl ion with [DGA-TSIL][Br] in [C_8mim][Br] is shown in **Fig.5.18**. It was observed that a steady decrease in uranyl ion oxidation current after addition of each aliquots of the ligand into the electrochemical cell. The inflection point was used to calculate the stoichiometry of the metal – ligand complex. The conditional formation constant of the complex can be obtained from the following equation [73,152]

$$i_p^2 = (-K_f)\,(i_{po}^2 - i_p^2) / [\text{DGA-TSIL}] + i_p^{02} - [\text{DGA-TSIL}] \qquad (5.17)$$

where, K_f is formation constant of the complex, i_p^o is oxidation current of U in the absence of [DGA-TSIL][Br], i_p is oxidation current of U in the presence of [DGA-TSIL][Br]. From the slope of the plot of i_p^2 vs (i_{po}^2-i_p^2) (**Fig. 5.18**) the ‘conditional formation constant (K_f)’ was determined as 1.01×10^3 M^{-1}. Solvent extraction data also indicated the formation of 1:1 metal-ligand stoichiometric complex with the formation constant (K_f) of 1.05×10^3 M^{-1}.

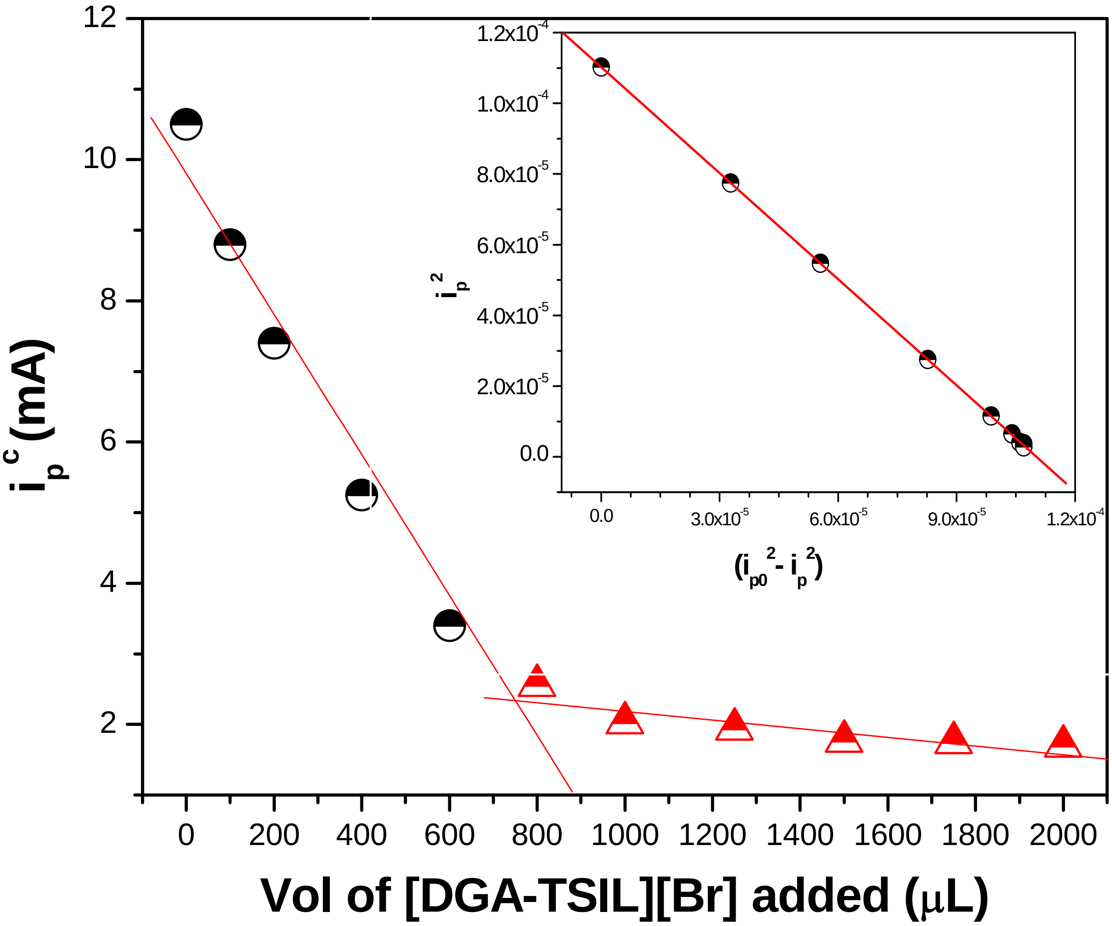

Fig. 5.18: Amperometric titration curves of uranyl ion by [DGA-TSIL][Br] in [C_8mim][Br] at 303 K. Inset: Plot of i_p^2 vs (i_{po}^2-i_p^2) to determine the formation constant of Uranyl – [DGA-TSIL][Br] complex in [C_8mim][Br]

5.11.2 Studies on Np(IV) complexes with [DGA-TSIL][NTf_2] and [CMPO-TSIL][NTf_2] in [C_4mim][NTf_2]

It was of interest to understand the effect of the nature of TSIL on the redox behavior of Np. **Fig. 5.19(a)** gives the cyclic voltammograms (CV) for Np(IV) extracts of TODGA and [DGA-TSIL][NTf_2] in [C_4mim][NTf_2] while **Fig. 5.19(b)** gives that for Np(IV) extracts of CMPO and [CMPO-TSIL][NTf_2] in [C_4mim][NTf_2]. The CVs for the blank solutions, i.e. aqueous nitric acid, TODGA, CMPO, and the respective TSIL solutions in [C_4mim][NTf_2] did not give any peaks in the scanned voltage range except a reduction peak at ~ -0.4 V which was originally found in the bare [C_4mim][NTf_2]. From both the figures, it is seen that the cathodic part of the potential window for the organic solutions is extended much more as compared to that in nitric acid medium. The CVs are characterized by their cathodic (E_p^c) and anodic (E_p^a) peak potentials and corresponding peak currents (i_p^c, i_p^a). Each peak signifies an electron transfer reaction. In both the figures, the $\Delta E_p = |E_p^c - E_p^a| > 0.059$ V, theoretically predicted for one electron redox reaction which shows that the reaction is not reversible but could be quasi-reversible or irreversible. Furthermore, the ratio of the currents (i_p^c/i_p^a) was found to be < 1 indicating the partial adsorption of the species. From **Fig. 5.19**, CV of Np in aqueous nitric acid (**Fig.5.19(a)**), the reduction peak potentials for Np(VI) / Np(V) occur at ~ 1.17 V, and for Np(V)/Np(IV) at ~0.56 V. A shoulder seen at ~ -0.13 was attributed to the Np(IV) to Np(III) [197]. On the reverse side, oxidation peak potentials noted for Np(III)/Np(IV) occur at ~ 0.086 V, for Np(IV)/Np(V) at ~1.0 V and the peak at ~1.26 V was attributed to the oxidation of Np(V) to Np(VI). These potentials are somewhat close to those reported previously [204-206]. The differences could be partly due to the fact that the reference electrode used in the previous studies, was Ag/AgCl, whereas Pt was used as the pseudo reference electrode in the present work.

Table 5.9: E_p^c, E_p^a and formal potential $E^{0'}$ values for Np in all the systems studied.

System	E_p^c, V (Np(IV)/Np(III))	E_p^a, V (Np(III)/Np(IV))	$E^{0'} = (E_p^c + E_p^a)/2$
Aqueous HNO_3	-0.14	0.086	-0.027
0.01 M TODGA in $[C_4mim][NTf_2]$	-1.0	-0.66	-0.83
0.1 M $[CMPO\text{-}TSIL][NTf_2]$ in $[C_4mim][NTf_2]$	-0.78	0.23	-0.28
0.1 M CMPO in $[C_4mim][NTf_2]$	-0.82	-0.083	-0.45

Since, the oxidation state of Np was adjusted to IV just before the extraction by the ligands, a clear reduction peak at ~ -0.82 V and oxidation peak at -0.66 V were attributed to the conversion of Np(IV) to Np(III) and Np(III) to Np(IV), respectively, for the Np-TODGA complexes in RTIL. Similarly, in the case of $[DGA\text{-}TSIL][NTf_2]$, the oxidation peak occurred at -0.37 V and the reduction peak at -0.78 V. In the case of $[CMPO\text{-}TSIL][NTf_2]$ or CMPO in RTIL, a similar situation was seen. The reduction peaks for Np(IV)/Np(III) were seen at -0.58 V and -0.92 V for $[CMPO\text{-}TSIL][NTf_2]$ and CMPO in RTIL, respectively, whereas the oxidation peaks are at 0.23 and at -0.083 V for the same order of ligands. These potentials were tabulated in **Table 5.9**. An empirical correlation can be made between the formal potentials ($E^{0'}$) and the distribution ratio value (D) of the trivalent metal ion. More negative $E^{0'}$, implied higher D values implying more stability for the +3 state in the organic medium which is aptly illustrated with Am(III) as an example (**Table 5.9)**.

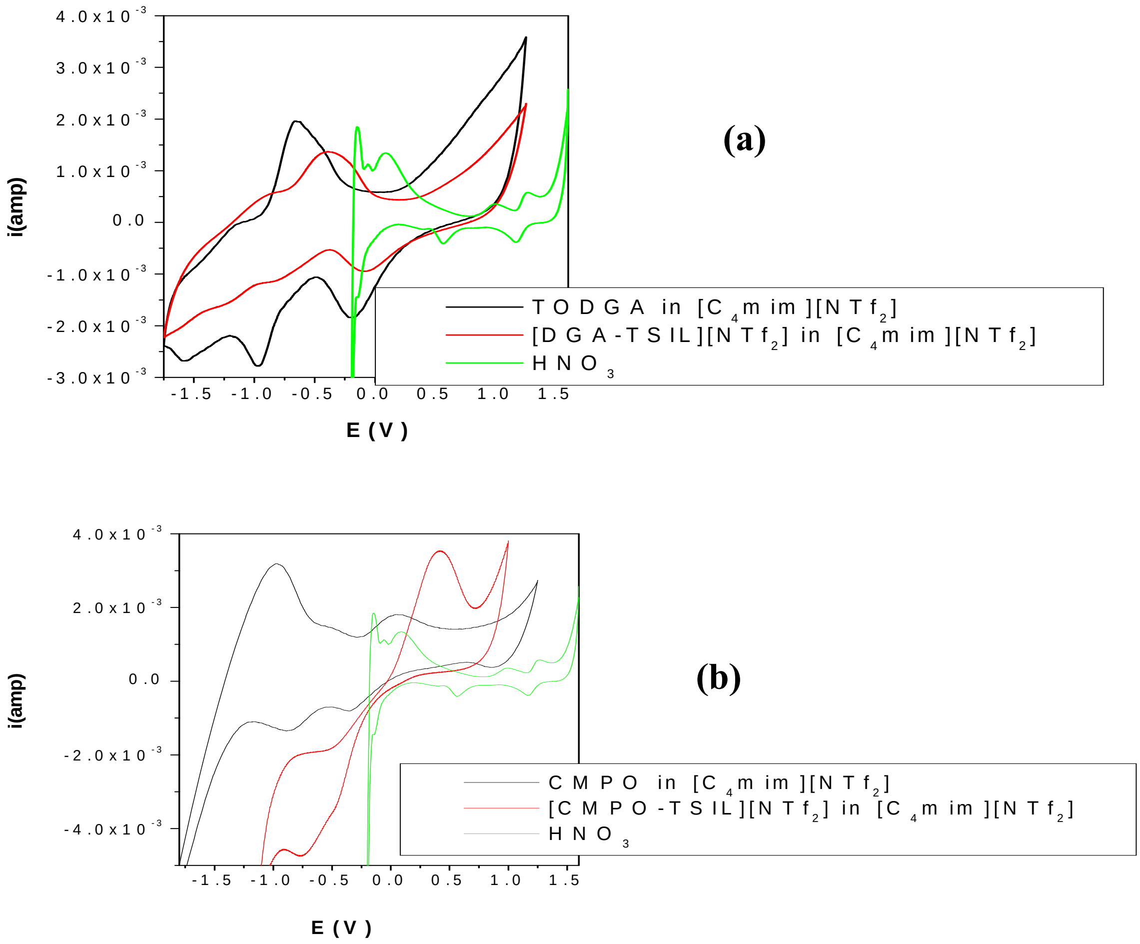

Fig 5.19: **(a)** CV for Np in aqueous nitric acid and Np extracted into 0.1 M TODGA , 0.1 M [DGA-TSIL][NTf_2] in [C_4mim][NTf_2], T – 298 K, scan= 0.1 V/s; (**b**) CV for Np in aqueous nitric acid and Np extracted into 0.1 M CMPO, 0.1 M [CMPO-TSIL][NTf_2] in [C_4mim][NTf_2], T – 298 K, scan - 0.1 V/s

5.12 Theoretical studies

It was of interest to understand the structures of the actinide ion complexes with the DGA-TSIL. All the bare ligand and metal-ligand complex structures have been optimized considering the DGA-TSIL ligand as tri-dentate one. The M-O bond length values have been found to be almost comparable in case of $[Am(DGA\text{-}TSIL)_2]^{5+}$ and $[Eu(DGA\text{-}TSIL)_2]^{5+}$, and five membered rings were formed during the complexation with DGA-TSIL ligand [**Fig. 5.20**]. However, metal-oxygen bond lengths have been found to be smaller when carbonyl oxygen atoms were involved in the bonding, in the cases of both the complexes and the americium-oxygen bond length values were smaller as compared to the corresponding Eu-O bond lengths in $[Am(DGA\text{-}TSIL)_2]^{5+}$ and $[Eu(DGA\text{-}TSIL)_2]^{5+}$ complexes, respectively. It can be rationalized from the fact that each of the carbonyl groups are attached with the less hard nitrogen atom, which in turn affected the bonding of the carbonyl oxygen atoms with the metal ions with a slightly smaller value of Am-O bond lengths. On the other hand, the metal-oxygen bond lengths were higher for the Eu^{3+} complexes when ether oxygen was involved in the bonding. Both the gas phase and solvent phase complexation energies support this trend. According to the gas phase complexation energy results, the Eu(III) complexes have been found to be more stable than the complexes with Am(III). However, solvent phase complexation energy trend was just opposite. The reason was suggested as the high dehydration energy requirement for Eu^{3+} complexation as compared to that of Am^{3+} due to smaller ionic radius of Eu^{3+}, and ligand has no role in controlling the selectivity. Therefore, the calculated complexation energy values obtained using COSMO approach always favour Am^{3+} complex to be more stable as compared to the Eu^{3+} complex for both of the ligands.

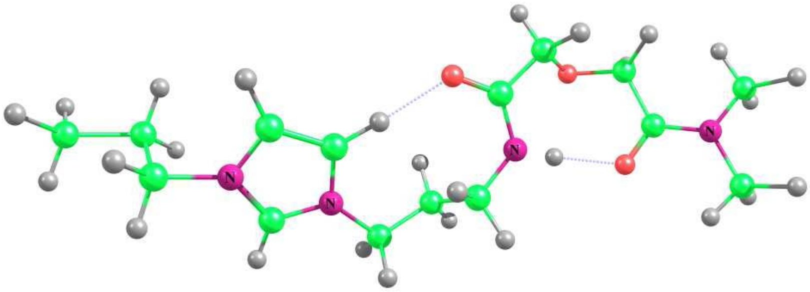

$[DGA\text{-}TSIL]^{+}$

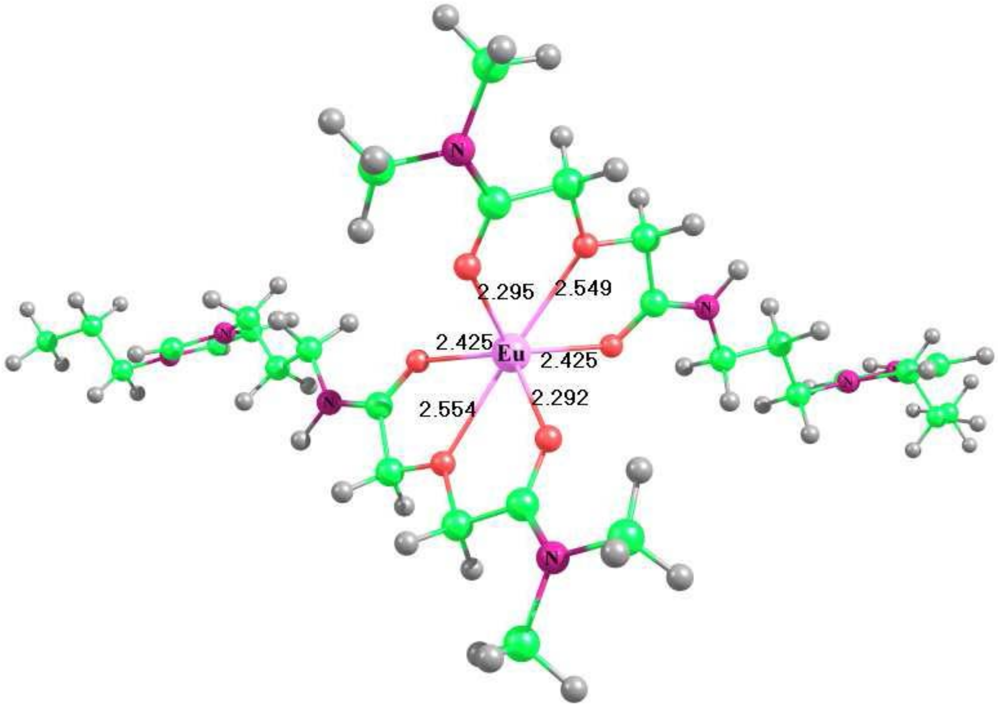

$[Eu(DGA\text{-}TSIL)_2]^{5+}$

Fig. 5.20: Optimized structures of the $[DGA\text{-}TSIL]^{+}$ bare ligand and its complexes with Eu^{3+}.

5.13 Summary

The extraction of several actinide ions in different oxidation states was investigated from nitric acid solutions using diglycolamide functionalized task specific ionic liquids. The trivalent actinide ions were extracted most favourably followed by the tetravalent actinide ions, while the hexavalent actinides were least extracted. Ligand concentration variation studies and slope analysis methods indicated the extraction of 1:1 species for all actinide ions. The solvent extraction studies indicated that a cation-exchange extraction mechanism was operative. Luminescence studies indicated the presence of single species in Eu^{3+} – DGA-TSIL extracts with no inner-sphere water molecules. Furthermore, it revealed that Eu^{3+} resides in a highly asymmetric environment with S_4 local symmetry. Stripping studies indicated that complexing agents such as EDTA and DTPA in guanidine carbonate are effective strippants for the trivalent actinide ions, while sodium carbonate and oxalic acid are effective strippants for the hexa and the tetravalent actinide ions, respectively. The thermodynamics studies indicated that the hexavalent actinides are less favourably extracted due to less effective interaction between the metal ions and the ligand, while the trivalent ions were instantaneously extracted due to large negative ΔG values, which were less negative for the tetravalent ions. DGA-TSILs appear to be a very promising extractant for actinide separations from high level waste solutions. Extraction studies involving simulated high level waste revealed that Zr(IV), Pd(II), Y(III), La(III), Ce(IV), Pr(III), Nd(III), and Sm(III) were co-extracted along with the minor actinides

CHAPTER- 6

Extraction of radio strontium from nuclear waste solution using crown ethers in room temperature ionic liquids

^{90}Sr ($T_{1/2}$ = 28.5 years) is one of the most important fission products present in high-level waste (HLW) solution generated during the reprocessing of spent nuclear fuel. The separation of long-lived ^{90}Sr from HLW prior to the vitrification of the latter is helpful not only in reducing the volume of the disposable waste but also in reducing the risk of matrix deformation caused by the generated heat [207]. In addition, the separated radionuclide has many applications, viz. as a power source for thermoelectric and thermo-mechanical power generators. For the separation of radio strontium from nitric acid feed solutions (HLW usually contains 1 – 3 M nitric acid), several methods such as precipitation, ion exchange and solvent extraction have been reported [208]. Out of these, solvent extraction methods with crown ether ligands are particularly interesting due to the ease of operation of the separation technique and high specificity of the extractants [209]. Dicyclohexano-18-crown-6 (DCH18C6) has been reported to be quite effective for Sr^{2+} extraction from nitric acid medium [210], whereas the more organophilic 4, 4' (5')-di-*tert*-butyldicyclohexano-18-crown-6 (DTBCH18C6) has shown significantly improved extraction properties [211]. Horwitz et al. [211,212] had developed the strontium extraction (SREX) process using DTBCH18C6 in 1-octanol as the diluent. The SREX process, though found promising, the use of large volumes of solvents is one of the major disadvantages and can add to the volatile organic compound (VOC) burden. Therefore, there is a need to search for alternative extraction systems with low VOC inventory.

There are several literature reports on the extraction of Sr^{2+} using RTILs [85,86,213-215]. Dai et al. [85] reported unusually high D_{Sr} values ($>10^4$) using DCH18C6 in ionic liquids such as $[C_n\text{mim}][\text{NTf}_2]$ from weakly acidic aqueous nitrate solutions. Using similar concentrations of the crown ether in $CHCl_3$ and 1-octanol, the D_{Sr} values were reported to be less than 1 and 0.01, respectively. Visser et al. [86], however, had indicated that the D_{Sr} values were much lower (<

10) with the same crown ether when RTIL counter anion was changed to PF_6^- . DTBCH18C6 is reported to be a superior extractant than DCH18C6 in the ionic liquid medium as well, and a 10 -fold increase in the D_{Sr} value was reported with the former extractant using $[C_4mim][PF_6]$ as the diluent [86]. Luo et al. [213] had used DCH18C6 in an imidazolium-based RTIL for Sr^{2+} extraction and had observed that the presence of Na^+ ions suppressed Sr^{2+} extraction significantly. Though there are several literature reports on Sr^{2+} extraction using crown ethers and RTILs, a detailed investigation with reference to the separation from HLW is lacking. Furthermore, though there are several reports on the radiolytic stability of the crown ethers in ionic liquid medium [216-218], it is of interest to make a comparative study of the Sr^{2+} extraction using both DCH18C6 and DTBCH18C6 in $C_n$mimPF_6 as well as $[C_nmim][NTf_2]$ as the ionic liquid medium under identical experimental conditions. The present study deals with the evaluation of several RTILs, $[C_nmim][PF_6]$ and $[C_nmim][NTf_2]$, where n = 4, 6 or 8 as the diluents while DCH18C6 and DTBCH18C6 were used as the extractants for the extraction of radio strontium from nitric acid solutions. The structures of DCH18C6 and DTBCH18C6 are given below.

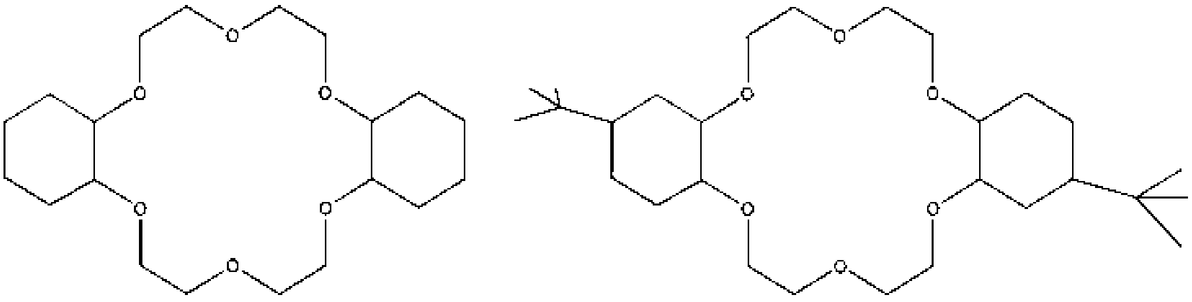

DCH18C6 **DTBCH18C6**

Fig. 6.1: Structures of the ligands used in Chapter-6

6.1 Evaluation of the RTILs containing DTBCH18C6

Extraction of Sr^{2+} was carried out using the six RTILs, viz. $[C_4mim][PF_6]$, $[C_6mim][PF_6]$, $[C_8mim][PF_6]$, $[C_4mim][NTf_2]$, $[C_6mim][NTf_2]$ and $[C_8mim][NTf_2]$ containing the two crown ethers, viz. DCH18C6 and DTBCH18C6. Studies carried out with no extractant from aqueous feed solution of 3 M HNO_3 indicated negligible extraction of Sr^{2+} with all the ionic liquids (**Table 6.1**). The solubility of the crown ether was also studied with the RTILs. The crown ethers were relatively easily dissolved in the ionic liquids and the distribution ratio values for Sr^{2+} were obtained with 0.01 M DTBCH18C6 in all the six ionic liquids from 3 M HNO_3 as the feed solution (Table 6.1). The table also lists the D_{Sr} values for DCH18C6 under identical conditions for comparison purposes. The D_{Sr} values indicated that the extraction efficiency decreased with increasing alkyl group size in the ionic liquids. As indicated in **Table 6.1**, the butyl-substituted ionic liquids displayed more favourable extraction of Sr^{2+} than the others, while ionic liquids with PF_6^- anions showed higher Sr^{2+} extraction compared to that with the ionic liquids with NTf_2^- as the counter anion. A distribution coefficient value of 2.05 was obtained with 0.01 M DTBCH18C6 in $[C_4mim][PF_6]$ from 3 M HNO_3 (**Table 6.1**). Chun et al. [219] had carried out a systematic investigation on the role of alkyl chain length in imidazolium-based RTILs and observed that the extraction efficiency decreased with increasing alkyl chain length. They had also reported that though the extraction properties were far superior with the RTILs such as $[C_4mim][PF_6]$ than with $[C_8mim][PF_6]$, the former is about 10 times more soluble in the aqueous phase leading to significant solvent loss during the extraction process. The superior extraction properties of $[C_4mim][PF_6]$ and $[C_4mim][NTf_2]$ were explained on the basis of the solubility of the ionic liquid into the aqueous phase as per the following extraction equilibrium as suggested by Dietz et al. [220]:

$$Sr^{2+}_{aq} + nCE_{IL} + 2C_nmim^+_{IL} = Sr\,[CE]_n{}^{2+} + 2C_nmim^+_{aq} \qquad (6.1)$$

Table 6.1: Distribution ratio values of Sr^{2+} with pure RTILs and with 0.01 M crown ether in RTIL. Aqueous phase: 3 M HNO_3.

Diluent	D_{Sr} in the absence of crown ethers	D_{Sr} in the presence of 0.01 M crown ethers DTBCH18C6	D_{Sr} in the presence of 0.01 M crown ethers DCH18C6	Dynamic viscosity (mPa.s) of ionic liquid
$[C_4mim][PF_6]$	1.5 x 10^{-3}	2.05 ± 0.01	0.97 ± 0.02	250.16
$[C_6mim][PF_6]$	3.0 x 10^{-3}	1.31 ± 0.01	0.71 ± 0.01	308.56
$[C_8mim][PF_6]$	3.1 x 10^{-3}	1.20 ± 0.03	0.53 ± 0.01	694.25
$[C_4mim][NTf_2]$	1.8 x 10^{-3}	1.02 ± 0.01	0.47 ± 0.01	46.408
$[C_6mim][NTf_2]$	1.6 x 10^{-3}	0.62 ± 0.01	0.35 ± 0.01	52.022
$[C_8mim][NTf_2]$	1.9 x 10^{-3}	0.49 ± 0.01	0.23 ± 0.01	72.639

The cation exchange extraction mechanism suggests appreciable solubility of the cationic part of the ionic liquid into the aqueous phase as indicated in equation (6.1). The C_4mim^+ ion has higher solubility in the aqueous phase compared to the C_6mim^+ and C_8mim^+ ions and hence is responsible for higher extraction of Sr^{2+}. Literature reports have indicated DTBCH18C6 to be a far superior extractant for Sr^{2+} than the analogous DCH18C6 [220]. This was attributed to the aggregation of DCH18C6 which decreased the Sr^{2+} extraction at higher crown ether concentrations, leading to a plateau in the extraction profile. Therefore, most of the following studies involved Sr^{2+} extraction using DTBCH18C6 in the six ionic liquids mentioned above. In certain cases, Sr^{2+} extraction using DCH18C6 was carried out for comparison purposes.

6.2. Time of equilibration

The equilibration time has a significant role on the extraction by RTILs. In view of high viscosity of the RTILs, it is expected that the rate of mass transfer will be slower and, consequently, the equilibrium will be attained at a relatively longer time than those observed with common molecular diluents. **Fig. 6.2** gives the profiles of Sr^{2+} extraction from 3 M HNO_3 feeds using 0.01 M DTBCH18C6 in the six RTILs. Compared to the PF_6^- based ionic liquids, the NTf_2^- based ionic liquids facilitated faster mass transfer and hence the time to attain equilibrium was lower.

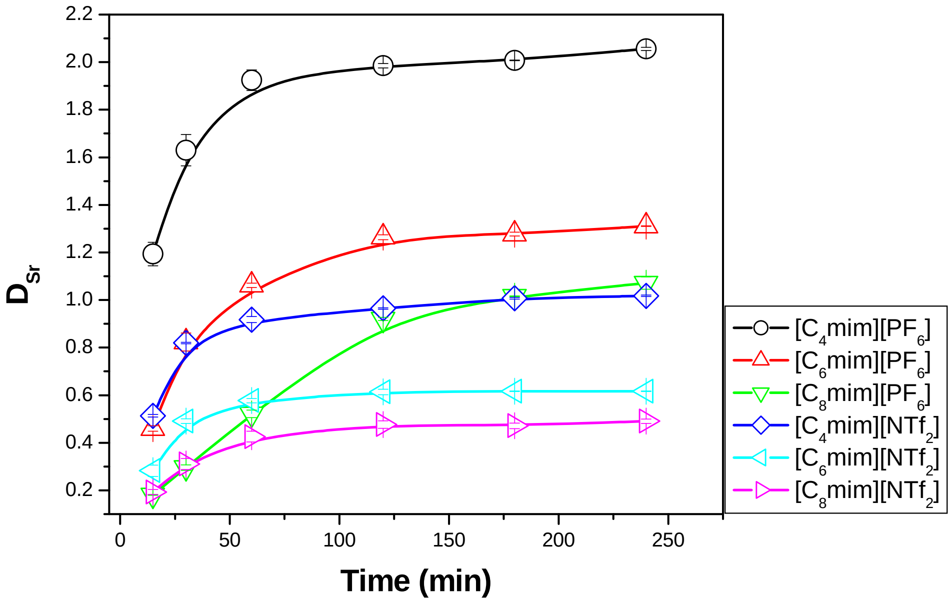

Fig. 6.2: Effect of time of equilibration on Sr^{2+} extraction using 0.01 M DTBCH18C6. Aqueous phase: 3 M HNO_3

About 60 minutes were needed for obtaining steady D_{Sr} values with all the three ionic liquids with NTf_2^- counter anions. However, the PF_6^- based ionic liquids required significantly larger time to attain equilibrium, and more than 4 h were required when [C_8mim][PF_6] was used as the diluents (**Fig. 6.2)**. On the other hand, about 2 h were required to obtain equilibrium D_{Sr} values when both [C_4mim][PF_6] and [C_6mim][PF_6] were used as the diluents. In view of the relatively faster attainment of equilibrium and higher distribution coefficient values, [C_4mim][PF_6] and [C_4mim][NTf_2] were used as the diluents in subsequent studies. In other cases, wherever required, all the solvent systems consisting of both the crown ethers in all the six ionic liquids were investigated.

6.3 Effect of HNO_3 concentration on Sr^{2+} extraction

Extraction of Sr^{2+} from nitric acid feed conditions has significance from the radioactive waste management point of view. Moreover, HLW can have wide ranging acidities and can contain from 1 to 4 M nitric acid. Therefore, it was of interest to understand the effect of nitric acid concentration on the extraction of Sr^{2+} using 0.05 M DCH18C6 or DTBCH18C6 in [C_4mim][PF_6] as well as in [C_4mim][NTf_2] as the organic diluents. The D_{Sr} values decreased continuously with increasing acidity (**Fig. 6.3)** from 0.01 to 3 M HNO_3, beyond which an increase in Sr^{2+} extraction was noticed. As per equation (6.1), which shows an cation-exchange mechanism, the extraction of Sr^{2+} is independent of nitric acid concentration. Therefore, the observed trend in Sr^{2+} extraction can be attributed to the extraction of nitric acid by the crown ethers as per the following extraction mechanism:

$$H^+_{aq} + nCE_{IL} + C_nmim^+_{IL} = H^+\cdot n[CE]_{IL} + C_nmim^+_{aq} \qquad (6.2)$$

Extraction of nitric acid by the crown ether can lead to a decrease in the effective ligand concentration in the ionic liquid phase, thereby decreasing Sr^{2+} extraction. The extraction of nitric acid was verified by titration of the ionic liquid phase, which indicated significant amounts of acid uptake by the ionic liquid phase (**Table 6.2)**. **Table 6.2** also indicates that the acid uptake of the solvent containing DTBCH18C6 is slightly higher than that containing DCH18C6, and no significant variation was seen when changing the alkyl group of the ionic liquids. The upward trend in the extraction profiles suggests a possible change in the extraction mechanism. Dietz et al. [220] had suggested the possibility of both cation-exchange and ion-pair extraction mechanism in RTIL based solvent systems depending on the experimental conditions. The latter mechanism involves the participation of nitrate anion as follows:

$$Sr^{2+}_{aq} + CE_{IL} + 2NO_3^-{}_{aq} = Sr \cdot (CE)_n^{2+} .(NO_3^-)_{2,IL} \qquad (6.3)$$

This suggests that the increase in the Sr^{2+} extraction at higher acidities (**Fig. 6.3**) could be attributed to the ion-pair extraction mechanism presented in Equation (6.3). Furthermore, the decrease in Sr^{2+} extraction with increasing acidity was noticed to be much sharper in $[C_4mim][NTf_2]$ than that observed in $[C_4mim][PF_6]$. This is rather intriguing and could be one of the reasons for proposing the NTf_2^- as a better medium of extraction than the PF_6^- medium, as the extraction and stripping of the metal ion may be possible by suitably tuning the acidity of the aqueous phase.

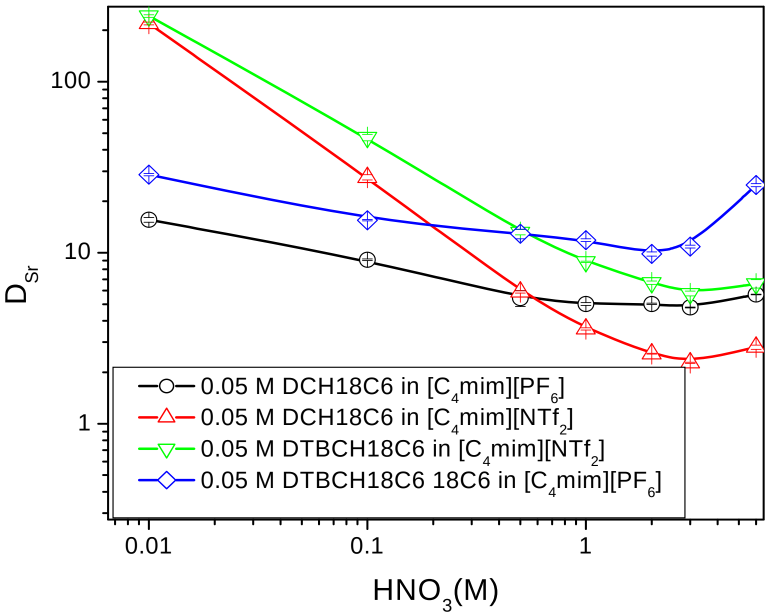

Fig. 6.3: Effect of aqueous feed acidity on the extraction of Sr^{2+} using DCH18C6 and DTBCH18C6 in [C$_4$mim][PF$_6$] and [C$_4$mim][NTf$_2$]

Table 6.2: Sr and nitric acid extraction data with the two crown ethers in the six RTILs. Crown ether concentration: 0.01 M; aqueous phase: 3 M HNO_3. The error in the % E data is less than 2%

Ligand	Diluent	% Sr^{2+} extraction	% Acid extraction
DCH18C6	$[C_4mim][PF_6]$	49.2 (32.0)	12. 7 (12.7)
DCH18C6	$[C_6mim][PF_6]$	41.5 (25.9)	13.6 (11.5)
DCH18C6	$[C_8mim][PF_6]$	34.6 (18.7)	13.7 (11.4)
DTBCH18C6	$[C_4mim][PF_6]$	67.2 (51.7)	14.8 (13.7)
DTBCH18C6	$[C_6mim][PF_6]$	56.7 (38.3)	14.4 (13.3)
DTBCH18C6	$[C_8mim][PF_6]$	54.5 (32.9)	13. 6 (12.5)

Note: The values inside the parentheses are for NTf_2 analog of the RTILs

6.4. Effect of crown ether concentration on Sr^{2+} extraction

Sr^{2+} extraction was also studied as a function of DTBCH18C6 concentrations at a fixed nitric acid concentration using all the six RTILs. The log–log plots of the D_{Sr} versus crown ether concentration are shown in **Fig. 6.4**, and the slope values of the linear graphs are listed in **Table 6.3**. As indicated in the table, the dependence of the ligand concentration on Sr^{2+} extraction is very close to 1, and hence Equation (6.1) can be presented as

$$Sr^{2+}_{aq} + CE_{IL} + 2C_nmim^{+}_{IL} = Sr^{2+}\cdot CE_{IL} + 2C_nmim^{+}_{aq} \qquad (6.4)$$

The two phase extraction equilibrium constant of Sr^{2+} for the above equilibrium reactions can be gives as follows:

$$K_{ex} = ([Sr^{2+} \cdot CE]_{IL} [C_n mim^+]_{aq}^2) / ([Sr^{2+}]_{aq} [CE]_{IL} [C_n mim^+]_{IL}^2) \qquad (6.5)$$

The D_{Sr} is the ratio of the concentration of Sr^{2+} in the IL phase to the total concentration of the metal ion in the aqueous phase. In the above equation, as the values of $[C_n mim^+]_{aq}$ and $[C_n mim^+]_{IL}$ do not change significantly, these two terms may be taken as constant. Therefore, equation (6.5) can be modified as

$$K_{Sr} . P_{Cnmim+} = D_{Sr} / [CE]_{IL} = K'_{ex} \qquad (6.6)$$

here K'_{ex} is the conditional extraction constant and P_{Cnmim+} is the partition coefficient of the alkyl methylimidazolium cation. Taking logarithm one can obtain:

$$\log D_{Sr} = \log K'_{ex} + \log [CE]_{IL} \qquad (6.7)$$

K'_{ex} is calculated from the intercept of the log D_{Sr} versus log $[CE]_{IL}$ plots at a constant nitric acid concentration. log K'_{ex} values were calculated for both DCH18C6 and DTBCH18C6 in all the six ionic liquids and are listed in **Table 6.3**. For comparison purpose, the log K'_{ex} values for analogous extraction systems with DCH18C6 as the extractant are also included in **Table 6.3**. As expected, the extraction constants are significantly lower with DCH18C6 than those obtained with DTBCH18C6, which may be attributed to the difference in their organophilicity and aggregation tendencies [211]. The complex formation equilibrium in an ionic liquid can be described by the following equations.

$$Sr^{2+}_{IL} + CE_{IL} = Sr^{2+} \cdot CE_{IL} \qquad (6.8)$$

The complex formation constants (K_{form}) can be given by the following equation.

$$K_{form} = [Sr^{2+}.CE]_{IL} / ([Sr^{2+}]_{IL}\ [CE]_{IL}) \qquad (6.9)$$

$$K_{form} = K'_{ex}\ [Sr^{2+}]_{aq} / [Sr^{2+}]_{IL} \qquad (6.10)$$

$$K_{form} = K'_{ex} / P_{Sr} \qquad (6.11)$$

where, P_{Sr} is the partition coefficient of Sr^{2+} defined as the ratio of Sr^{2+} concentration in the ionic liquid phase to that in the aqueous phase. The P_{Sr} values for different ionic liquids are listed in **Table 6.1**.

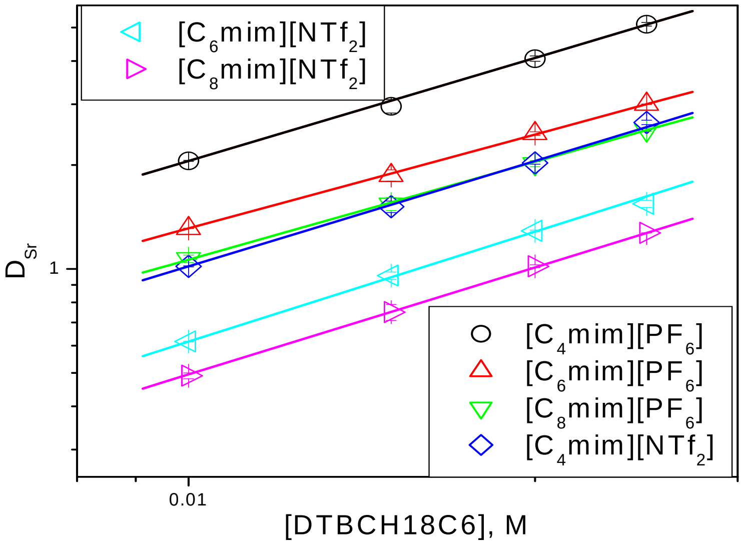

Fig. 6.4: Effect of crown ether (DTBCH18C6) concentration on Sr^{2+} extraction using all the six ionic liquids as the diluents. Aqueous phase: 3 M HNO_3.

The log K_{form} values were calculated from equation (6.11) and are listed in **Table 6.3**. For comparison purpose, the log K_{fom} values for DCH18C6 are also included in the table. The formation constants in IL media were found to be higher with DTBCH18C6 than those obtained with DCH18C6. A literature report [220] showed that the complex formation constant for Sr^{2+} with DCH18C6 in a polar medium such as MeOH to be around 5 (log K), which is more or less comparable to the values reported in the polar ionic liquid medium as reported in this study. Furthermore, it was interesting to observe that the log K_{form} values were higher in PF_6^- based IL than in the NTf_2^- based ILs (**Table 6.3**).

Table 6.3: Slopes and intercept values of the log D_{Sr} – log [DTBCH18C6] plots

Diluent	Slope	Intercept	Log K'_{ex}	Log K_{fom}
$[C_4mim][PF_6]$	0.99 ± 0.01	2.30 ± 0.02	2.30 ± 0.02 (1.98 ± 0.03)	5.14 ± 0.03(4.81 ± 0.01)
$[C_6mim][PF_6]$	0.90 ± 0.01	1.92 ± 0.01	1.92 ± 0.01(1.85 ± 0.04)	4.44 ± 0.04(4.37 ± 0.03)
$[C_8mim][PF_6]$	0.94 ± 0.03	1.91 ± 0.04	1.91 ± 0.04 (1.74 ± 0.01)	4.42 ± 0.04(4.25 ± 0.02)
$[C_4mim][NTf_2]$	1.01 ± 0.03	2.04 ± 0.06	2.04 ± 0.06(1.66 ± 0.02)	4.77 ± 0.06(4.40 ± 0.01)
$[C_6mim][NTf_2]$	1.06 ± 0.04	1.90 ± 0.07	1.90 ± 0.07(1.54 ± 0.03)	4.71 ± 0.03(4.34 ± 0.02)
$[C_8mim][NTf_2]$	1.030 ± 0.018	1.75 ± 0.03	1.75 ± 0.03(1.42 ± 0.04)	4.41 ± 0.04(4.14 ± 0.05)

Notes: The conditional extraction constant (K'_{ex}) and formation constant (K_{fom}) are also listed in the table. Values in parentheses refer to the data for DCH18C6 as the extractant

6.5. Extraction from simulated high-level waste

The application of the Sr^{2+} extraction studies can be made in the recovery of radio strontium (^{90}Sr) from actual HLWs. However, such attempts require elaborate safety arrangements including a hot cell facility. It was thus decided to use simulated high-level waste

(SHLW) the composition of which is given in Chapter 4. The D_{Sr} values with SHLW as the feed are shown in **Fig. 6.5**. For comparison purpose, D_{Sr} values with 3 M HNO_3 as the feed are also shown in the figure. The figure indicates that with SHLW as the feed, the D_{Sr} values are about 30 – 40% lower than the values observed with 3 M HNO_3 as the feed. Secondly, the D_{Sr} values were nearly double with the PF_6^- based ionic liquids as compared to those obtained with the NTf_2^- based ionic liquids when 3 M HNO_3 was used as the feed, whereas the values were more favourable with the former solvent when SHLW was used as the aqueous phase. It was noteworthy, however, that the D_{Sr} values were still significantly higher for effecting quantitative Sr extraction using counter-current extraction. The major hurdle in such studies is the slow extraction kinetics.

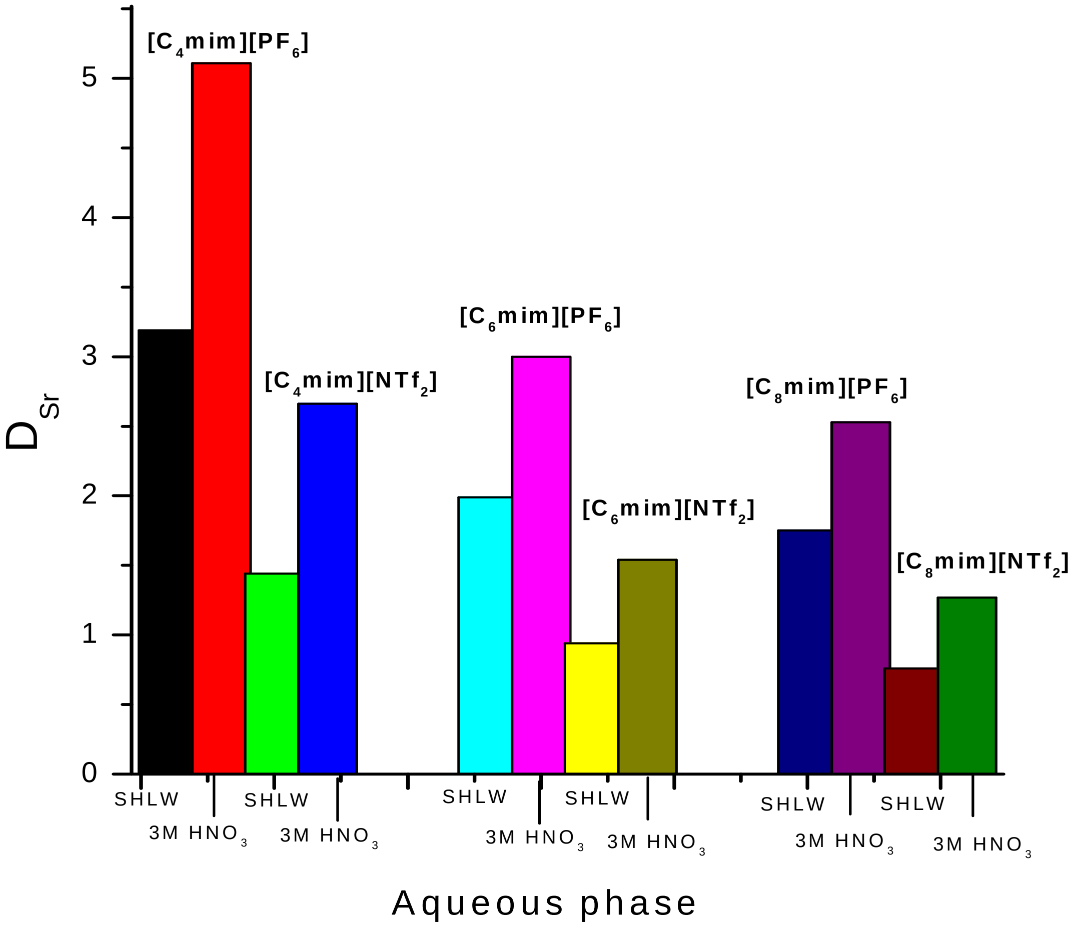

Fig. 6.5: Comparative evaluation of Sr^{2+} extraction from 3 M HNO_3 and SHLW using 0.025 M DTBCH18C6 in $[C_4mim][PF_6]$ and $[C_4mim][NTf_2]$

6.6. Radiolytic degradation studies

Radiolytic degradation studies were carried out by using irradiated solvents containing both the crown ethers, viz. DCH18C6 and DTBCH18C6, in all the six ionic liquids. The absorbed dose was limited to 1000 kGy in line with the standard practice [216]. The plots of D_{Sr} with varying absorbed dose (500 and 1000 kGy) are shown in **Fig. 6.6(a)** and **6.6(b)**, respectively, for 0.05 M solutions of DCH18C6 and DTBCH18C6 in all the six ionic liquids. For comparison purpose, D_{Sr} values with unirradiated solvents are also included in the figures. It was interesting to note that though DTBCH18C6 was a superior extractant than DCH18C6, its radiolytic stability was significantly poorer than that of the latter extractant. Yuan et al. had investigated the radiolytic degradation of DCH18C6 in [C_4mim][PF_6] and reported similar decrease in Sr^{2+} extraction with the irradiated solvents up to 550 kGy [217-218]. This could have serious consequences on the long-term usage of the ionic liquid based solvent systems. The solvent system can be recycled after simple washing with distilled water. Skrob et al. [216] had carried out a detailed investigation on the radiolytic degradation of crown ethers in ionic liquids by Electron Paramagnetic Resonance (EPR). Their results indicated generation of acid due to the radiolysis of the solvents which adversely affected the extraction of the metal ions especially at higher absorbed dose values. This usually influences the extraction (to a much larger extent the back extraction) behaviour of the metal ion. The influence of the radiolytic degradation products on Sr^{2+} extraction has been to a varying extent depending on the medium of extraction. Takagi et al. [221] reported the significant role of the nature of the diluents on metal ion extraction. They have reported that the D_{Sr} values even increased with increasing absorbed dose in certain diluents. This study, however, has shown lowering of the D_{Sr} values with increased absorbed dose. The highly viscous nature of the solvent system has led to high-local degradation of the solvent (as the free radical scavenging may be lower), which was reflected in the sharp fall in the D_{Sr} values.

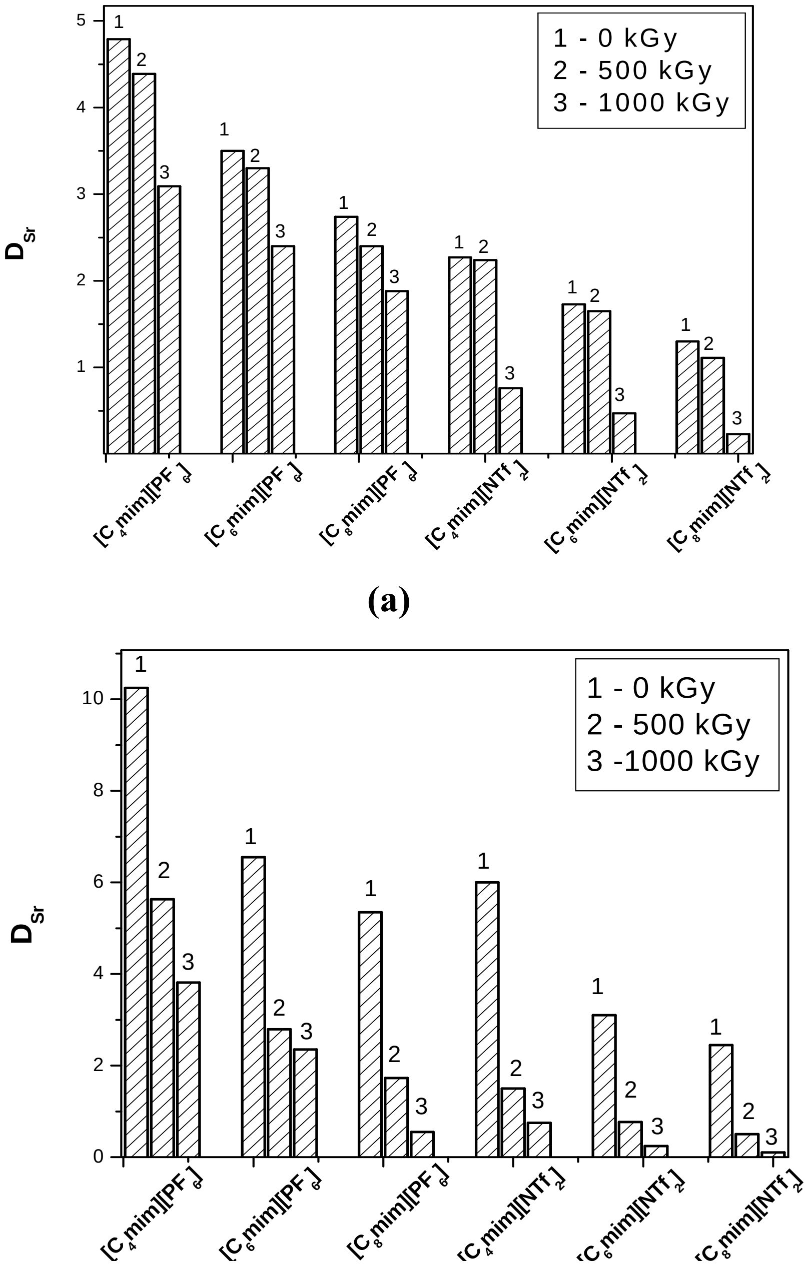

Fig. 6.6: Effect of absorbed irradiation dose on Sr^{2+} extraction using (**a**) 0.05M DCH18C6 and (**b**) DTBCH18C6. Aqueous phase: 3M HNO_3.

6.7 Summary

This study suggests that extraction of ^{90}Sr from the nitric acid medium can be carried out effectively employing crown ethers as the extractant with various commercially available RTILs, which can be a viable alternative to the toxic and volatile molecular diluents. The extraction of the metal ion was significantly higher with ionic liquids as the diluents, particularly in the lower actinides than with the molecular diluents such as 1-octanol. Studies on the extraction of Sr^{2+} from SHLW waste have yielded promising results and suggested that the ionic liquid-based solvent system can be used for radio-strontium extraction from radioactive waste solutions. The studies on the nature of the extracted species indicated extraction of 1:1 metal–ligand complexed species with an ion-exchange extraction mechanismin at HNO_3 concentrations < 3 M. The formation constants were also calculated and found to be comparable to those obtained in a polar medium. The changes in either cationic or anionic part of the ionic liquid which is responsible for changing the overall viscosity coefficient of the media was found to affect the extraction kinetics of Sr^{2+} into room temperature ionic liquid. Radiolytic degradation studies were also carried out and indicated decrease in Sr^{2+} extraction with increase in the absorbed dose. Furthermore, though DTBCH18C6 is a superior extractant than DCH18C6, the radiolytic stability of the former is relatively poor as compared to the latter extractant, suggesting that the recovery of ^{90}Sr from radioactive wastes should be more effective using DCH18C6 as the extractant rather than DTBCH18C6.

CHAPTER- 7

Summary & Conclusions

The main objectives of the Thesis include investigations on the extraction/ separation behavior of actinides in different oxidation states using several newly synthesized diglycolamide functionalized calix[4]arenes, tripodal diglycolamides in ionic liquids and also to evaluate several task specific ionic liquids. This was primarily due to the fact that the conventional molecular diluents are volatile, inflammable and very often toxic. On the other hand, ionic liquids promise to be 'green' alternatives to the molecular diluents. Performance of diglycolamide functionalized ionic liquid was compared with CMPO functionalized ionic liquid in selected cases. The studies also include the mechanism of extraction, nature of the species involved in extraction including stiochiometry, inner/outer sphere complex, covalecy in metal-ligand bond, and the kinetics and thermodynamics studies associated in the extraction process. Electrochemical studies were also carried out to understand the redox possibilities, which may help in metal ion stripping. Studies were also carried out to determine the complex formation constants and diffusivities. Substituted crown ether based ligands in RTIL were also investigated for the extraction of ^{90}Sr, which is one of the long lived fission products in high level nuclear waste solution. The results of the experimental work carried out as a part of this Thesis have been briefly summarized in this Chapter.

1. **Tripodal diglycolamide (T-DGA):** The solvent extraction studies of Am(III) using T-DGA in various room temperature ionic liquids clearly demonstrate that the ionic liquid medium extracts the metal ions more efficiently as compared to molecular diluents such as *n*-dodecane. Furthermore, the tripodal diglycolamide (T-DGA) is a far superior extractant as compared to TODGA. It extracts Am(III) from acidic feed solutions with [C_4mim][NTf_2] as the ionic liquid.

- The metal ion extracts followed a cation-exchange mechanism at lower acidity and a solvation mechanism at higher acidities. Though the extraction of the tetravalent actinide ion was much lower as compared to the trivalent lanthanide and actinide ions (both Eu(III) and Am(III) were better extracted), the extraction of the hexavalent actinyl ion was insignificant.
- The extracted species was a 1: 1 complex formed between Am(III) and T-DGA with no inner-sphere water molecules, which was confirmed by the TRLFS studies using the analogous Eu^{3+} complexes. The stripping results were encouraging with the possibility of > 99% stripping after three stages using complexing agents such as EDTA or DTPA in guanidine carbonate.
- The thermodynamics of extraction indicated a highly entropy driven reaction, suggesting the removal of a large number of water molecules from the inner-coordination sphere. Radiolytic stability studies showed a significantly higher stability of the ionic liquid solvent systems as compared to those reported previously in the literature, which may lead to possible long term recycling options making it one of the promising ‘green’ solvents.

2. **Diglycolamide functionalized calix[4] arenes (C4DGA):** A series of diglycolamide-functionalized calix[4]arenes (L-I – L-VI) in RTIL ([C_8mim][NTf_2]) were evaluated for actinide extraction.
    - Slower kinetics was observed for the extraction of actinides using all the C4DGA ligands in [C_8mim][NTf_2] as compared to the molecular diluents. This fact can be attributed to higher viscosity coefficient of the ionic liquid. Almost 2 h were required to reach the equilibrium distribution ratio values.

- Unlike the molecular diluents, a decrease in the distribution ratio of americium with increasing aqueous phase acidity was observed for all the C4DGA – RTIL systems (except for L-VI) which can be attributed to the predominance of cation-exchange mechanism during metal ion extraction. However, remarkable acidity independent actinide extraction was observed with a both-rim diglycolamide-functionalized calix[4]arene (L-VI) in [C_8mim][NTf_2].
- In the series of C4DGA ligands studied, L-I and L-IV were found to be the most promising extractants. The ligand with a short spacer was found to be a better extractant in comparison to its analog with a longer spacer probably because of the better pre-organization of the diglycolamide moieties on the calixarene platform as a result of restricted C−C single bond rotation.
- At lower feed acidity, the coordinating ability of the carbonyl oxygen is enhanced because of the electron density on the amidic nitrogen atom to which a group with a +I effect is attached, while at comparatively higher feed acidity the steric crowding around the coordinating group plays a significant role.
- In case of both rim functionalized DGA molecule (L-VI), the metal ion binds to the DGA groups attached to one side of the calix[4]arene, while the other side is either uncoordinated or complexed with hydronium ion (H_3O^+).
- Am^{3+} was found to form complex with 1:1 stoichiometry with all the C4DGA ligands in [C_8mim][NTf_2].
- Metal - C4DGA complexes in ionic liquid were found to be thermodynamically favorable. The overall extraction process was exothermic in nature with a decrease in the overall entropy of the system.

- The trend of the extraction efficiency of the C4DGAs in [C_8mim][NTf_2] was found to be $Eu^{3+} > Am^{3+} > Pu^{4+} > PuO_2^{2+} > UO_2^{2+} > Sr^{2+} > Cs^{+}$. The separation factors (SF) for Am^{3+} with respect to UO_2^{2+}, Cs^{+}, Sr^{2+}, Pu^{4+}, and PuO_2^{2+} are 130, 1040, 470, 3.2, and 90, respectively with L-I in [C_8mim][NTf_2], which increased enormously to 4670, 13120, 4990, 130, and 4160, respectively, for L-IV in [C_8mim][NTf_2]. It can be inferred that L-IV is not only a better ligand with respect to the higher extraction efficiency of americium; it also shows a significantly favorable separation behavior.
- A radiolytic stability study indicated that L-I and LIV can be used for actinide partitioning up to a 500 kGy dose, without significant decrease of the extraction efficiency.
- Similar to the T-DGA based solvent system complexing agents were used for quantitative back extraction of actinides from ionic liquid phase.
- The extraction of Am(III), Pu(IV), Np(IV), U(VI) and Pu(VI) was studied from simulated high-level waste (SHLW) solutions using several Calix-DGA ligands in RTIL (L-I, L-II, L-V, L-VI and L-VII). The trend of extraction of the actinides was found out to be Am(III) > Pu(IV) > Np(IV) > U(VI) ~ Pu(VI).
- Reasonably, good extraction of Am(III) was obtained with 5.0×10^{-4} M ligand solutions suggesting that higher concentrations of the ligand can be used for a higher loading of the metal ions. Studies on the extraction of other metal ions revealed that Na, K, Pd, Fe, Sr, Mn, Pd, Ce, Ru and Ba remained un-extracted by all the systems while Y, La, Sm, Y, Pr, Nd, Zr and Mo were found to be extracted into the organic phase alongwith the actinides.

- Extraction of Am^{3+} was carried out using a both-rim diglycolamide-functionalized calix[4]arene with eight DGA pendent arms (L-VI) in several organic diluents and the observed extraction trend was: nitrobenzene > *n*-dodecane (with 5% *iso*-decanol as phase modifier) > phenyltrifluoromethylsulphone (PTMS) > hexone > 2-nitrophenyloctylether > 1-octanol > chloroform at 0.1 M HNO_3, which changed at higher acidities (3 M) showing crossovers between the nitrobenzene – *n*-dodecane and the PTMS–hexone pairs. The extraction behaviour was correlated with various parameters such as Schmidt's diluent parameter, dielectric constant.
- The extraction was found to be a spontaneous process giving 1:1 species. The observed exceptional extraction behaviour of the L-VI ligand in room temperature ionic liquid does not take place in the molecular diluents studied.
- Fluorescence spectroscopy was employed to get insights into the Eu^{3+} complexation of a series of C4DGA ligands in ionic liquid. Lifetime data of the Eu^{3+}–C4DGA complexes revealed the presence of single species and the absence of inner sphere water molecules except for Eu^{3+}- L-VII complex (with 5 water molecules). The high intensity $^5D_0\rightarrow{}^7F_2$ transition suggested that the local environment around the Eu^{3+} ion is highly asymmetric with respect to the inversion symmetry, while the splitting pattern of the different transitions exhibited that all the Eu^{3+} - C4DGA complexes exhibit C_{4V} symmetry except for Eu^{3+} - L-VII, which was found to exhibit either C_1, C_2, or C_S symmetry. The transition strength of the $^5D_0\rightarrow{}^7F_0$ line was found to be proportional to the crystal field parameter, while that of the $^5D_0\rightarrow{}^7F_2$ line was insensitive to the crystal field parameter. The $^5D_0$-$^7F_1$ splitting varied linearly with the energy of the $^5D_0\rightarrow{}^7F_0$

transition. Similarly, a linear relationship between the energy of the $^5D_0 \rightarrow {}^7F_0$ transition and that of the $^5D_0 \rightarrow {}^7F_1$ transition was observed.

- The branching ratio (β_n; n=2, 4, 6) follows the trend $\beta_2 > \beta_4 > \beta_1$, which reveals that Eu^{3+} resides in an asymmetric environment in case of all complexes. In all the cases, the magnetic- and electric-dipole transition probabilities behave in the fashion of $A_{2ed} > A_{4ed} > A_{md}$. Judd and Offelt parameters (Ω_2, Ω_4) were calculated for all the samples. Steric crowding around ligating site decrease the proximity of metal ion with carbonyl oxygen as a result the bond length increases and the covalency decreases which was signature by decrease in Ω_2 value while Ω_4 value signifies the long range ordering.

3. **TSILs:** Two new diglycolamide based task-specific ionic liquids (DGA-TSILs) were evaluated for the extraction of actinides and lanthanides from acidic feed solutions and the performance of [DGA-TSIL][NTf_2] was compared with that of [CMPO-TSIL][NTf_2] for Np extraction.

    - D_M values that were obtained with the trivalent actinide (Am^{3+}) and lanthanide ions (Eu^{3+}) by using the DGA-TSILs were unusually high compared to analogous solvent systems, whereas the hexavalent uranyl ion and the Cs^+ and Sr^{2+} ions were practically unextracted. The distribution- ratio values follow the trend $Eu^{3+} > Am^{3+} >> Pu^{4+} > Np^{4+} >> UO_2^{2+} >> Sr^{2+} \sim Cs^+$, which suggests that the DGA-TSILs also formed reverse micelles similar to TODGA/*n*-dodecane system.
    - The kinetics of extraction was rather slow and about 6 h were required to attain equilibrium D_{Am} value using pure DGA-TSILs, dilution in [C_4mim][NTf_2]

afforded reasonably faster mass transfer due to decrease in viscosity which improved the extraction kinetics.

- The distribution ratio values for different actinides were found to decrease with increase in feed acidity indicating the predominance of the cation-exchange mechanism.
- Slope ratio method revealed that though Am^{3+} formed 1:2 complex with pure DGA-TSILs alongwith the incorporation of one NO_3^- ion in the complex, on dilution with [C_4mim][NTf_2], [DGA-TSIL][NTf_2] formed 1:1 complex with different oxidation states actinides.
- The radiolytic stability of [DGA-TSIL][NTf_2] was found to be much better than [DGA-TSIL][PF_6]. EPR spectral analysis revealed the formation of methyl radical and methylimidazolium based radicals on exposure of 1000 kGy gamma dose on DGA-TSILs.
- Buffered complexing agents such as EDTA and DTPA can be effectively used as strippants.
- The emission lifetime decay profile of luminescence spectra of Eu^{3+} - DGA-TSIL complexes pointed to the existence of single extracted species. Furthermore, the lifetime values of 1.564 ms for the Eu^{3+} extract with both the DGA-TSILs suggest complete removal of the water molecules from the inner coordination sphere. This is in sharp contrast to the lifetime value of 0.155 ms mentioned above.
- The Ω_2 follows the trend of Eu^{3+}- [DGA-TSIL][NTf_2] > Eu^{3+}- [DGA-TSIL][PF_6] > Eu^{3+}- TODGA ([C_4mim][NTf_2]) > $Eu^{3}{}_{+aq}$. The variation of Ω_2 reflected by the

hyper-sensitivity of the $^5D_0\rightarrow{}^7F_2$ transition can be related to the variation in covalence of the Eu^{3+}-O bond. The splitting patterns of each transition were correlated to local symmetry around the Eu^{3+} ion was found to be S_4.

- The thermodynamics studies indicated that the hexavalent actinides are less favourably extracted due to less effective interaction between the metal ions and the ligand, while the trivalent ions were instantaneously extracted due to large negative ΔG values, which were less negative for the tetravalent ions. All the extraction processes were found to be exothermic with overall decrease in entropy value.
- The selectivity of the extraction of trivalent lanthanides and actinides over other elements was studied in SHLW which revealed that Zr(IV), Pd(II), Y(III), La(III), Ce(IV), Pr(III), Nd(III), and Sm(III) were co-extracted along with minor actinides. At 0.01 M HNO_3 as the feed, the distribution ratio of the metal ions follows the trend: $D_Y > D_{Ce} > D_{Nd} > D_{Sm} > D_{Pr} > D_{La} > D_{Pd} > D_{Zr}$.

4. **Sr^{2+} - Substituted crown ether:** Extraction of radiostrontium from dilute nitric acid solutions was studied using two Sr^{2+} selective crown ethers, viz. dicyclohexano-18-crown-6 and 4,4′(5′)-di-tert-butyl-dicyclohexano-18-crown-6, in several room temperature ionic liquids([$C_n$mim][X], where, n = 4, 6, 8 and X = PF_6 and NTf_2).

   - The study suggested that the extraction of ^{90}Sr from the nitric acid medium can be carried out effectively employing crown ethers as the extractant with various commercially available RTILs, which can be a viable alternative to the toxic and volatile molecular organic diluents. The extraction of the metal ion was significantly higher with ionic liquids as the diluent than that with the molecular diluents such 1-octanol. Studies on the extraction of Sr^{2+} from SHLW waste have shown promising results and suggest that the ionic liquid-based solvent system can be used for radio-strontium extraction from radioactive waste solutions.

- The studies on the nature of extracted species indicated extraction of 1:1 metal–ligand complexed species with a cation-exchange extraction mechanism. The formation constants were also calculated and found to be comparable to those obtained in polar medium.
- Radiolytic degradation studies were also carried out and indicated decrease in Sr^{2+} extraction with increase in absorbed dose. Furthermore, though DTBCH18C6 is a superior extractant than DCH18C6, the radiolytic stability of the former is relatively poor as compared to the latter extractant, suggesting that the Sr recovery from radioactive wastes should be carried out using DCH18C6 as the extractant rather than DTBCH18C6.

Future perspectives

The Thesis demonstrated the highly favourable extraction trivalent lanthanides and actinides using multiple diglicolamide functionalized ligands in room temperature ionic liquids, which are considered as alternative diluent to the commonly used volatile organic diluents. The extraction mechanism, kinetics, thermodynamics and the nature of the species involved in extraction were also investigated. DGA functionalized ionic liquids were also studied. The following can be part of the future studies.

1. The major challenge in recovery of minor actinides and fission products from high level waste would be the radiation degradation of the RTIL based solvent systems. We have seen the degradation after 1000 kGy of radiation dose. It is required process actual high level wate for actinide partitioning using these solvent systems.
2. More theoretical modeling study is required for detailed investigation of the mechanism of the extraction of actinides into ionic liquid phase. Theoretical approach is also required to understand the favourable configurations of ligands and their mode of ligation.
3. Stripping from ionic liquid phase is one of the challenging jobs. Though we have used complexing agents which were found to be suitable for quantitative stripping of actinides from ionic liquid phase, electro-deposition can be cleaner option for stripping. Significant efforts are required in this direction also.
4. One of the problems in using ionic liquids for the extraction of actinides is the rather high solubility of its cations/ anions during cation exchange mechanism. R & D efforts are required to synthesize ionic liquids with lower aqueous solubilization. Similar thoughts were also found in the literature by Dietz et al [220].

5. Viscosity of ionic liquids makes the mass transfer slower during the extraction of metal ions. So appropriate cation and anion combinations are required to achieve desired physico-chemical properties of RTILs to be used in plant scale.
6. More detailed studies are required to justify the real 'greenness' of the ionic liquid solvents.
7. Efforts are needed in the synthetic schemes of RTILs, so that the costs of the RTILs decrease making the solvents more viable for plant scale applications rather than its only lab scale uses.

REFERENCES

References

1. www.iaea.org Nuclear Technology Review, September 2011.
2. IAEA Electricity information, 2010, World Nuclear Association, Nuclear Engineering International.
3. IAEA Nuclear Technology Review 2009, IAEA, Vienna, (2009) 3.
4. World Nuclear Association, Nuclear power in India, http://www.worldnuclear. org/info/inf53.htm
5. PhD thesis of Raut D. R., Mumbai University (2011).
6. Holder J.V, *Radiochim. Acta*, 25 (1978**)** 171.
7. Crowley K.D., Nuclear waste disposal: The technical challenges, *Physics Today*, 50 (1997) 32.
8. Baisden P.A., Choppin G.R*., UNESCO Encyclopedia of Life Support Systems*, Radiochemistry and Nuclear Chemistry, *Nuclear Waste Management and the Nuclear Fuel Cycle Chapter*.
9. Baisden P. A., Choppin G. R., *Nuclear Waste Management and the Nuclear Fuel Cycle.* In *Radiochemistry and Nuclear Chemistry*; Nagyl, S., Ed.; Encyclopedia of Life Support Systems (EOLSS); EOLSS Publishers: Oxford, U.K., 2007.
10. Johnson J., *Chem. Eng. News*, 76 (1998) 25.
11. Madic C., Ouvrier N., *Radiochim. Acta,* 96 (2008) 183.
12. Ahrland S., Liljenzin J.O., Rydberg J., Solution Chemistry, In "*Comprehensive Inorganic Chemistry*", J.C. Bailar Jr., H.J. Emeleus, R. Nyhlom and A.F.T. Dickenson (Eds.), Pergamon Press, Oxford, 5 (1973) 465-535.

13. Cunningham B.B., “Proc. of XVII international congress of pure and applied chemistry”, Butterworths, London. Vol. 1, P. 64.
14. Spitsyn V.I., Gelman A.D., Krot N.N., Mefodiyeva M.P., Zacharova F.A., Komokov Y.A., Shilov V.P., Smirnovam I.V., *J. Inorg. Nucl. Chem.*, 31 (1969) 2733.
15. Wick O.J., “*Plutonium Hand Book: A Guide to the Technology*”, Gordon and Breach, New York, 1 (1967) 438.
16. Rainey R.H., USAEC Report CF-59-12-95 (1959).
17. Cleveland J.M., “*The chemistry of plutonium*”, Gordon and Breach, New York (1970) 84.
18. Janes A.D., Choppin G.R., *Actinides Rev.*, 1 (1969) 311.
19. Pearson R.G., *J. Am. Chem. Soc.*, 85 (1963) 3533.
20. Sekine T., Hasegawa Y. (Eds.) “*Solvent Extraction Chemistry: Fundamentals and Applications*”, Marcel Dekker, New York (1977), 60.
21. Bagawade S.V., Vasudeva Rao P.R., Ramakrishna V.V., Patil S.K., *J. Inorg. Nucl. Chem.*, 40 (1978) 1913.
22. Ramanujam A., Nadkarni M.N., Ramakrishna V.V., Patil S.K., *J. Radioanal. Chem.*, 42 (1978) 349.
23. Patil S.K., Ramakrishna V.V., Kartha P.K.S., Gudi N.M., *Sep. Sci. Technol.*, 15 (1980) 1459.
24. Benedict M., Pigford T.H., Levi H.W., “*Nuclear Chemical Engineering*”, 2nd Edition, McGraw Hill Book Company (1981), 172.
25. McKay H.A.C., Miles J.H., Swanson J.L., Applications of Tributyl Phosphate in Nuclear Fuel Reprocessing, In “*Science and Technology of Tributyl Phosphate*”, W.W. Schulz,

L.L. Burger, J.D. Navratil and K.P. Bender (Eds.), CRC Press Inc., Boca Raton, Florida, 3 (1990) 55.

26. Nash K., *Solv. Extr. Ion Exch*. 11 (1993) 729.
27. Nash K., *Sep. Sci. Technol.,* 34 (1999) 911.
28. Marcus Y., *Ion Properties*, Marcel, Dekker, New York, (1997).
29. Pearson R. G., *J. Am. Chem. Soc.,* 85 (1963) 3533.
30. Diamond R. M., Street K., Seaborg G. T., *J. Am. Chem. Soc.,* 76 (1954) 1461
31. Jensen M. P., Bond A. H., *J. Am Chem Soc*., 124 (2002) 9870.
32. Musikas C., Cuillerdier C., Livet J., Forchioni A., Chachaty C., *Inorg. Chem.,* 22 (1983) 2513.
33. McKibben J. M., *Radiochim. Acta,* 36 (1984**)** 3.
34. Horwiz E. P., Schulz W. W., *The TRUEX Process: A Vital Toll for Disposal of US Defense Nuclear Waste*, Elsevier, London (1991**)** 21.
35. Horwitz E. P., Kalina D. G., Diamond V., Vandegrift D. G., Schultz W. W., *Solv. Extr. Ion Exch.,* 3 (1985**)** 75.
36. Zhu Y., Jiao R., *Nucl. Technol.,* 108 (1994**)** 361.
37. Cuillerdier C., Musikas C., *Sep. Sci. Technol., 26* (1991) 1229.
38. Morita Y., Glatz J. P., Kubota M., Koch L., Pagliosa G., Roemer K., Nicholl A., *Solv. Extr. Ion Exch.,* 14 (1996**)** 385.
39. Modolo G., Seekamp S., Vijgen H., Scharf K., Baron P., *Recent developments in the ALINA process for An(III)/Ln(III) group separation during the partitioning of minor actinides, Proceedings of the 8th International Conference on Radioactive Waste*

Management and Enviromental Remediation. ICEM 01, Bruges, Belgium, Sept. 30–Oct. 4 (2001) ASME.

40. Liljenzin J. O., Persson G., Svantsesson I., Wingefors S., *Radiochim. Acta,* 35 (1984) 155.
41. See: www.acsept.org.
42. Siddall T. H. *J.*, *Inorg. Nucl. Chem*., 25 (1963**)** 883.
43. Siddall T. H. *J.*, *Inorg. Nucl*. Chem., 26 (1964**)** 1991.
44. Rozen A. M., Volk V. I., Vakhrushin A. Yu., Zakharkin B. S., Kartasheva N. A., Krupnov B. V., Nikolotova Z. I., *Radiochemistry,* 41 (1999**)** 215.
45. Sasaki Y., Umetani S., *J. Nucl. Sci. Tech*., 43 (2006) 794.
46. Kulyako Y. M., Malikov D. A., Chmutova M. K., Litvina M. N., Myasoedov B. F., *J. Alloys Compd*., 760 (1998) 271.
47. Kulyako Y., Malikov D., Trofimov T., Chmutova M., Myasoedov B., *J. Nucl. Sci. Technol*., 3 (2002) 302.
48. I.Malofeeva G., Chmutova M. K., Rozhkova L. S., Petrukhin O. M., Spivakov B.Ya., Myasoedov B. F., *Radiochemistry*, 40 (1998) 241.
49. Kolarik Z., Horwitz E. P., *Solv. Extr. Ion Exch*., 6 (1988) 247.
50. Nagasaki S., Kinoshita K., Wisnubroto D. S., Enokida Y., Suzuki A., *J. Nucl. Sci. Technol*., 29 (1992) 671.
51. Mathur J. N., Murali M. S., Natarajan P. R., Badheka L. P., Banerji A., *Talanta*, 39 (1992) 493.
52. Horwitz E. P., Kalina D. G., Kaplan L., Mason G. W., Diamond H., *Sep. Sci. Technol.*, 17 (1982) 1261.
53. Musikas C., *Sep. Sci. Technol.*, 23 (1988) 1211.

54. Chan G. Y. S., Drew M. G. B., Hudson M. J., Iveson P. B., Liljenzin J., Skålberg M., Spjuth L., Madic C., *Dalton Trans*. (1997) 649.
55. Mowafy E. A., Aly H. F., *Solv. Extr. Ion Exch*., 24 (2006) 677.
56. Narita H., Yaita T., Tamura K., Tachimori S., *J. Radioanal. Nucl. Chem*., 239 (1999) 381.
57. Spjuth L., Liljenzin J. O., Hudson M. J., Drew M. G. B., Iveson P. B., Madic C., *Solv. Extr. Ion Exch*., 18 (2000**)** 1.
58. Lumetta G. J., Rapko B. M., Garza P. A., Hay B. P., *J. Am. Chem. Soc.,* 124 (2002) 5644.
59. Sasaki Y., Choppin G. R., *Anal. Sci.*, 12 (1996) 225.
60. Sasaki Y., Choppin G. R., *Radiochim. Acta*, 80 (1998) 85.
61. Tachimori S., Sasaki Y., Suzuki S., *Solv. Extr. Ion Exch*., 20 (2002) 687.
62. Sasaki Y., Sugo Y., Suzuki S., Tachimori S., *Solv. Extr. Ion Exch*., 19 (2001) 91.
63. Narita H., Yaita T., Tachimori S., *Solv. Extr. Ion Exch.*, 22 (2004) 135.
64. Zhu Z. X., Sasaki Y., Suzuki H., Suzuki S., Kimura T., *Anal. Chim. Acta*, 527 (2004) 163.
65. Sasaki Y., Rapold P., Arisaka M., Hirata M., Kimura T., Hill C., Cote G., *Solv. Extr. Ion Exch.,* 25 (2007) 187.
66. Sasaki Y., Zhu Z. X., Sugo Y., Kimura T., *J. Nucl. Sci. Technol.*, 44 (2007) 405.
67. Murillo M. T., Espartero A. G., Sánchez-Quesada J., Mendoza J. de, Prados P., *Solv. Extr. Ion Exch.*, 27 (2009) 107.
68. Jańczewski D., Reinhoudt D. N., Verboom W., Hill C., Allignol C. , Duchesne M., *New J. Chem*., 32 (2008) 490.
69. Matloka K., Gelis A., Regalbuto M., Vandegrift G., J. Scott M., *Dalton Trans.,* 23 (2005) 3719.

70. Matloka K., Gelis A., Regalbuto M., Vandegrift G., Scott M. J., *Sep. Sci. Technol.*, 41 (2006) 2129.
71. Iqbal M., Mohapatra P. K., Ansari S. A., Huskens J., Verboom W., *Tetrahedron,* 68 (2012) 7840.
72. Billard I., Ouadi A., Gillard C., *Anal. Bioanal. Chem*., 400 (2011) 1555.
73. Binnemann K., *Chem. Rev.,* 107 (2007) 2592.
74. Mudring A.V., Tang S., *Eur. J. Chem*, 41 (2010) 2569.
75. Seddon K.R., *Nat. Mater.,* 2 (2003) 363.
76. Wilkes J.S., *Green Chem.,* 4 (2002) 73.
77. Giridhar P., Venkatesan K.A., Srinivasan T.G., Rao V., *J. Radioanal. Nucl. Chem.,* 265 (2005) 31.
78. Giridhar P., Venkatesan K.A., Srinivasan T.G., Rao V., *J. Nucl. Radiochem Sci.,* 5 (2004) 21.
79. Lohithakshan K.V., Agarwal S.K., *Radiochim. Acta*, 96 (2008) 93.
80. Lohithakshan K.V., Agarwal S.K., *Radiochim. Acta*, 99 (2011) 201.
81. Visser A.E., Rogers R.D., *J. Solid State Chem.,* 171 (2003) 109
82. Nakashima K., Kuboto F., Maruyama T., Goto M., *Ind. Eng. Chem. Res.,* 44 (2005) 4368.
83. Shimojo K., Kurahashi K., Nagnawa H., *Sol. Extr. Ion Exch.,* 19 (2008) 62.
84. Sun X., Wu D., Chen Ji., Li D., *J. Chem. Technol. Biotechnol.*, 82 (2007) 267.
85. Dai S., Barnes C.E., Ju Y.H., *Dalton Trans.,* 8 (1999) 1201
86. Visser A.E., Swatloski R.P., Reichert W.M., Griffin S.T., Hartman D.H., Rogers R.D., *Ind. Eng. Chem. Res.,* 39 (2000) 3596.

87. Visser A.E., Swatloski R.P., Reichert W.M., Mayton R., Sheff S.A., Wierzbicki D., Jr. J.H., Rogers R.D., *Envir. Sci. Tecnol.,* 36 (2002) 2523.
88. Ouadi A., Gadenne B., Hessemann P., Moreau J.E., Billard I., Gaillard C., Mekki S., Moutiers G., *Chem. Eur. J.,* 12 (2006) 3074.
89. Ouadi A., Klimshuc O., Gaillard C., Billard I., *Green Chem.,* (2007) 1160.
90. Luo H., Dai S., Bonnesen P.V., Buchanan A.C., *J. Alloy and Compds.,* 418 (2006) 195.
91. Odinets I.L., Sharova E.V., Artishn O.I., Lyssenkao K.A., Nelyubina Y., Myasoedova V., Galina V., Molochincova N.P., Zakharchenro E.A., *Dalton Trans.,* 39 (2010) 4170
92. Mehdi H., Binnemans K., Hecke V., Meervelt L.V., Nockemann P., *Chem. Commun.* (2010) 234.
93. Sun X., Ji Y., Hu F., He Bo., Chen Ji., Li D., *Talanta,* 81 (2010) 1877.
94. Mohapatra P.K., Ph.D. Thesis, University of Bombay (1993).
95. Ansari S.A., Mohapatra P.K., Iqbal M., Kandwal P., Huskens J., Verboom W., *J. Membr. Sci.*, 430 (2013) 304.
96. Herbst R.S., Law J.D., Todd T.A., Romanovskiy V.N., Babain V.A., Vyatcheslav M.E., Smirnov I. V., Zaitsev B.N., *Solv. Extr. Ion Exch*., 20 (2002) 429.
97. Mohapatra P.K., Bhattacharya A., Manchanda V.K., *J. Hazard. Mater.,* 181 (2010) 679.
98. Mohapatra P.K., Manchanda V.K., *J. Incl. Phenom. Mol. Recog. Chem*., 25 (1996) 257.
99. Ansari S.A., Gujar R.B., Prabhu D.R., Pathak P.N., Mohapatra P.K., *Solv. Extr. Ion Exch.*, 30 (2012) 457.
100. Mathur J. N., Murali M. S., Nash K. L., *Solvent Extr. Ion Exch*., 19 (2001) 357.
101. Paiva A. P. and P. Malik, J. Radioanal. Nucl. Chem., 261 (2004) 485.
102. Serrano-Purroy D., Christiansen B., Malmbeck R., Glatz J. P., Baron P., Proc. Global

2003, New Orleans, USA, November 16–20 (2003).

103. Ansari S. A., Pathak P. N., Hussain M., Prasad A. K., Parmar V. S., Manchanda V. K., *Solvent Extr. Ion Exch.,* 23 (2005) 463.
104. Wilden A., Schreinemachers C., Sypula M., Modolo G., *Solvent Extr. Ion Exch.*, 29 (2011) 190.
105. Jensen M. P., Yaita T., Chiarizia R., *Langmuir*, 23 (2007) 4765.
106. Dam H. H., Reinhoudt D. N., Verboom W., *Chem. Soc. Rev.*, 36 (2007) 367.
107. Mohapatra P. K., Iqbal M., Raut D. R., Verboom W., Huskens J., Manchanda V. K., *J. Membr. Sci.,* 375 (2011) 141.
108. Adam C. J., Earle M. J., Seddon K. R., *Green Chem*., 2 (2000) 21.
109. Toma S., Gotov B., Solkaniova E., *Green Chem*., 2 (2000) 149.
110. Song C. E., Roh E. J., *Chem. Commun*. (2000) 837.
111. Dyson P. J., Ellis D. J., Parker D. C., Welton T., *Chem. Commun*. (1999) 25.
112. Huddleston J. G., Willauer H. D., Swatloski R. P., Visser A. N., Rogers R. D., *Chem. Commun*, (1998) 1765.
113. Blanchard L. A., Hancu D., Beckman E. J., Brennecke J. F., *Nature*, 399 (1999) 28–29.
114. Fadeev A. G., Meagher M. M., *Chem. Commun*. (2001) 295.
115. Cocalia V. A., Jensen M. P., Holbrey J. D., Spear S. K., Stepinskim D. C., Rogers R. D., Dalton Trans. (2005) 1966.
116. Sun I. W., Hussey C. L., Inorg. Chem., 28 (1989) 2731.
117. Hussey C. L., in Chemistry of Non-aqueous Solvents: Current Progress, ed. G. Mamantov and A. I. Popov, VCH, New York (1994).
118. Freemantle M., *Chem. Eng.News*, 78 (2000) 37.

119. Wasserschield P., Keim W., *Angew Chem., Int. Ed.,* 39 (2000) 3773.

120. Welton T., *Chem. Rev*., 99 (1999) 2071.

121. Antony J. A., Maginn E. J., Brennecke J. F., *J. Phys. Chem. B*, 105 (2001) 10942.

122. Huddleston J. G., Visser A. E., Reichert W. M., Willauer H. D., Broker G. A., Rogers R. D., *Green Chem*., 3 (2001) 156.

123. Han D., Row K. H., *Molecules*, 15 (2010) 2405.

124. Jensen M. P., Dzielawa J. A., Rickert P., Dietz M. L., *J. Am. Chem. Soc*., 124 (2002) 10664.

125. Visser A. E., Jensen M. P., Laszak I., Nash K. L., Choppin G. R., Rogers R. D., *Inorg. Chem.*, 42 (2003) 2197.

126. Shimojo K., Goto M., *Anal. Chem*., 76 (2004) 5039.

127. Jensen M. P., Neuefeind J., Bietz J. V., Skanthakumar S., Soderholm L., *J. Am. Chem. Soc*., 125 (2003) 15466.

128. Schurhammer R., Wipff G., *J. Phys. Chem. B*, 111 (2007) 4659.

129. Shimojo K., Kurahashi K., Naganawa H., *Dalton Trans*. (2008) 5083.

130. Turanov A. N., Karandashev V. K., Baulin V. E., *Solvent Extr. Ion Exch*., 28 (2010) 367.

131. Luo H., Dai S., Bonnesen P. V., Buchanan III A. C., Holbrey J. D., Bridges N. J., Rogers R. D., *Anal. Chem*., 76 (2004) 3078.

132. Ansari S. A., Mohapatra P. K., Raut D. R., Manchanda V. K., *Radiochim. Acta*, 99 (2011) 713.

133. Mohapatra P. K., Iqbal M., Raut D. R., Verboom W., Huskens J., Godbole S. V., *Dalton Trans.*, 41 (2012) 360.

134. Gujar R. B., Ansari S. A., Prabhu D. R., Mohapatra P. K., Pathak P. N., Sengupta A.,

Thulasidas S. K., Manchanda V. K., *Solv. Extr. Ion Exch*., 30 (2012) 156,

135. Modolo G., Hanna A., Schreinemachers C., Vijgen H., *Solvent Extr. Ion Exch*., 25 (2007) 703.
136. Panja S., Mohapatra P. K., Tripathi S. C., Gandhi P. M., Janardan P., *J. Membr. Sci*., 403–404 (2012) 71.
137. Haynes W. M., Handbook of chemistry and physics, CRC Press, Florida (1992).
138. Rout A., Venkatesan K. A., Srinivasan T. G., Vasudeva Rao P. R., *J. Radioanal. Nucl. Chem.,* 290 (2011) 215.
139. Shen Y., Tan X., Wang L., Wu W., *Sep. Purif. Technol*., 78 (2011) 298.
140. Ansari S. A., Mohapatra P. K., Prabhu D. R., Manchanda V. K., *J. Membr. Sci*., 298 (2007) 169.
141. Giridhar P., Venkatesan K. A., Srinivasan T. G., Rao P. R. V., *J. Nucl. Radiochem. Sci*., 5 (2004) 17.
142. Singh T., Kumar A., J. Phys. Chem. B, 112 (2008) 12968.
143. Xu C., Yuan L., Shen X., Zhai M., *Dalton Trans*., 39 (2010) 3897.
144. Allen D., Baston G., Bradley A. E., Gorman T., Haile A., Hamblett I., Hatter J. E., Healey M. J. F., Hodgson B., Lewin R., Lovell K. V., Newton B., Pitner W. R., Rooney D. W., Sanders D., Seddon K. R., Sims H. E., Thied R. C., Green Chem., 4 (2002) 152.
145. Gujar R. B., Ansari S. A., Bhattacharyya A., Kanekar A. S., Pathak P. N., Mohapatra P. K., Manchanda V. K., *Solv. Extr. Ion Exch*., 30 (2012) 278.
146. Horrocks W. D., Sudnick D. R., *J. Am. Chem. Soc.*, 101 (1979) 334.
147. Horrocks W. D., Sudnick D. R., *Acc. Chem. Res*., 14 (1981) 384.
148. Colette S., Amekraz B., Madic C., Berthon L., Cote G., Moulin C., *Inorg. Chem*., 43

(2004) 6745.

149. Pathak P. N., Ansari S. A., Godbole S. V., Dhobale A. R., Manchanda V. K., *Spectrochim. Acta, Part A*, 73 (2009) 348.

150. Jagadeeswara Rao C, Venkatesan K.A, Nagarajan K, Srinivasan TG, Vasudeva Rao PR, *J Nucl Mat*, 399 (2010) 81.

151. Jagadeeswara Rao C, Venkatesan K.A, Nagarajan K, Srinivasan T.G., Vasudeva Rao P.R., *Electrochim Acta*, 54 (2009) 4718.

152. De Castro C.S. P., De Souza J. R., Junior C. B., *Biophysical Chemistry*, 112 (2004) 59.

153. Wang W.J., Lin J., Wang A., Zheng P., Wang M., Wang B., *Inorg. Chim. Acta,* 149 (1988) 151.

154. Kolarik Z., *Solvent Extr. Ion Exch*., 32 (2013) 24.

155. Suzuki H., Sasaki Y., Sugo Y., Apichaibukol A., Kimura T., *Radiochim. Acta,* 92 (2004) 463.

156. Nakashima K., Kubota F., Maruyama T., Goto M., *Anal. Sci*., 19 (2003) 1097.

157. Yuan L., Peng J., Xu L., Zhai M., Li J., Wei G., *Dalton Trans*., 2008, 6358.

158. Shkrob I. A., Marin T. W., Bell J. R., Luo H., Dai S., Hatcher J. L., Rimmer R. D., Wishart J. F., *J. Phys. Chem*., 116 (2012) 2234.

159. Judd B. R., *Phys. Rev.*, 127 (1962) 750.

160. Malta O. L., Britob H. F., Menezesb J. F. S., Gongalves e Silva F. R., Alves S., Farias Jr., F. S., de Andrade A. V. M., *J. Lumin.,* 75 (1997) 255.

161. de Sa G. F., Malta O. L., de Mello Donega C., Simas A. M., Longo R. L., Santa-Cruz P. A., da Silva Jr. E. F., *Coord. Chem. Rev.*, 196 (2000) 165.

162. Kumar A., Rai D. K., Rai S. B., *Spectrochim. Acta A*, 58 (2002) 2115.

163. Lina H., Yanga D., Liua G., Maa T., Zhaia B., Ana Q., Yua J., Wangb X., Liub X., Pun E. Y. B., *J. Lumin.,* 113 **(**2005) 121.

164. Kumar M., Seshagiri T. K., Godbole S. V., *Phys. B*, 410 **(**2013) 141.

165. Nagaishi R., Arisaka M., Kimura T., Kitatsuji Y., *J. Alloys Comp*., 431 **(**2007) 221

166. Zhang P., Kimura T., *Solv. Extr. Ion Exch.*, 24 **(**2006) 149.

167. Görller-Walrand C., Binnemans K., In *Handbook on the Physics and Chemistry of Rare Earths*; K. A. Gscheidner and L. Eyring, Eds.; Elsevier: Amsterdam, 1996; Vol. 23, pp 121-283.

168. Werts M.H.V., Jukes R.T.F., Verhoeven J.W., Phys. Chem. Chem. Phys. 4 (2002) 1542.

169. Guo X., Wang X., Zhang H., Fu L., Guo H., Yu J., Carlos L.D., Yang K., Microporous Mesoporous Mater. 116 (2008) 28.

170. Guo X., Guo H., Fu L., Zhang H., Carlos L.D., Deng R., Yu J., J. Photochem. Photobiol. A-Chem. 200 (2008) 318.

171. Wen S., Zhang X., Hu S., Zhang L., Liu L., J. Rare Earth 26 (2008) 787.

172. Sharma J.N., Ruhela R., Hareendaran K.N., Mishra S.L., Suri A.K., *J. Radioanal. Nucl. Chem*., 278 (2008) 173.

173. W.M. Haynes (Ed.), Handbook of Chemistry and Physics, CRC Press, **1992**

174. Raut D.R., Mohapatra P.K., Ansari S.A., Godbole S.V., Iqbal M., Manna D., Ghanty T.K., Huskens J., Verboom W., *RSC Advances*, 3 (2013) 9296.

175. Marcus Y., *Solv. Extr. Ion Exch*., 7 (1989) 567.

176. Shimdt V.S., Mezhov E.A., Novikova S.S., *Radiokhimiya,* 9 (1967) 700

177. W.M. Haynes (Ed.), Handbook of Chemistry and Physics, CRC Press, **1992**

178. Ansari S.A., Pathak P. N., Mohapatra P. K., Manchanda V. K., *Chem. Rev.*, 112 **(**2012)

1751.

179. Gujar R. B., Ansari S. A., Murali M. S., Mohapatra P. K., Manchanda V. K., *J. Radioanal. Nucl. Chem*., 284 (2011) 377.

180. Raut D.R., Mohapatra P.K., Ansari S.A., Godbole S.V., Iqbal M., Manna D., Ghanty T.K., Huskens J., Verboom W., *RSC Advances*, 3 (2013) 9296.

181. Carda-Broch S., Berthod A., Armstrong D. W., *Anal. Bioanal. Chem*., 375 (2003) 191.

182. Modolo G., Asp H., Vijgen H., Malmbeck R., Magnusson D., Sorel C., *Solv. Extr. Ion Exch*., 26 (2008) 62.

183. Sun X., Luo H., Dai S., *Chem. Rev*., 112 (2012) 2100.

184. Li N., Fang G., Liu B., Zhang J., Zhao L., Wang S., *Anal. Sci.* 26 (2010) 455.

185. Loe-Mie F., Marchand G., Berthier J., Sarrut N., Pucheault M., Blanchard-Desce M., Vinet F., Vaultier M., *Angew. Chem. Int. Ed.*, 49 (2010) 424.

186. Rout A., Venkatesan K. A., G.Srinivasan T., Vasudeva Rao P. R., *Sep. Purif. Technol.,* 76 (2011) 238.

187. Magnusson D., Christiansen B., Glatz J.-P., Malmbeck R., Modolo G., Purroy D., Sorel C., *Solv. Ext. Ion Exch.,* 27 (2009) 26.

188. Rout A., Venkatesan K. A., Srinivasan T. G., Vasudeva Rao P. R., *Radiochim. Acta,* 98 (2010) 459.

189. Visser A. E., Swatloski R. P., Reichert W. M., Mayton R., Sheff S., Wierzbicki A., Davis J. H., Rogers Jr., R. D., *Chem. Commun.* (2001) 135.

190. Harjani J. R., Friscic T., MacGillivray L. R., Singer R. D., *Dalton Trans.* (2008) 4595.

191. Choppin G. R., Peterman D. R., *Coord. Chem. Rev*., 174 (1998) 283.

192. Sharma J. N., Ruhela R., Singh K. K., Kumar M., Janardhanan C., Achuthan P. V.,

Manohar S., Wattal P., Suri A. K., *Radiochim. Acta,* 98 (2010) 485.

193. Shkrob I.A., Marin T.W., Chemerisov S.D., Hatcher J.L., Wishart J.F., *J. Phys. Chem. B* 115 (2011) 3889.
194. Shkrob I. A., Wishart J. F., *J. Phys. Chem. B*, 113 **(**2009) 5582.
195. Shkrob I. A., Marin T. M., Chemerisov S. D., Wishart J. F., *J. Phys. Chem. B*, 115 (2011) 3872.
196. Shkrob I. A., Chemerisov S. D., Wishart J. F., *J. Phys. Chem. B*, 111 **(**2007) 11786.
197. Ikeda-Ohno A., Hennig C., Rossberg A., Funke H., Scheinost A. C., Bernhard G., Yaita T., *Inorg Chem*., 47 (2008) 8294.
198. Sornein M. O., Cannes C., Naour C. Le, Lagarde G., Simoni E., Barthet J.C., *Inorg. Chem.*, 45 (2006) 10419.
199. Deetleft M., Hussey L.C., Mohammed T.J., Seedon K.R., van den Berg J.A., Jora J.A., *Dalton Trans*. (2006) 2334.
200. Nockemann P., Servaes K., Deun R. V., Hecke K.V., Meervelt L.V., Binnemann K., Walrand C., *Inorg. Chem*., 26 (2007) 11335.
201. Swiatek J., *J. Coord. Chem*, 33 (1994), 191.
202. Swiatek J., Pawalowski T., Gasiorowski K., *Inorg. Chim. Acta*, 138 (1987) 79.
203. Niu J., Cheng G., Dong S., *Electrochim. Acta*, 39(1994) 2455.
204. Yamamura T., Watanabe N., Yano T., Y. Shiokawa, *J. Electrochem Soc*., 152 (2005) A830.
205. Kim Seong-Yun, Asakura T., Morita Y., *Radiochim. Acta*, 93 (2005) 767.
206. Aoyagi H., Kitatsuji Y., Yoshida Z., Kihara S., *Analytica Chim. Acta*, 538 (2005) 283.

207. Feasibility of Separation and Utilization of Cesium and Strontium from High Level Liquid Waste, IAEA Technical Report Series No. 356, 1993, p. 5, ISBN: 92-0-102093-7.
208. Schulz W.W.,Bray L.A., *Sep. Sci. Technol.*, 22 (1987) 191.
209. Gerow I.H., Smith Jr. J.E., Davis, Jr., M.W., *Sep. Sci.Technol.*, 16 (1981) 519.
210. Blasius E., Klein W., Schon U., *J. Radioanal. Nucl. Chem.,* 89 (1985) 389.
211. Horwitz E.P., Dietz M.L., Fisher D.E., *Solvent Extr. Ion Exch.*, 8 (1990) 557.
212. Horwitz E.P., Dietz M.L., Fisher D.E., *Solvent Extr. Ion Exch.*, 9 (1991) 1.
213. Luo H., Dai S., Bonnesen P.V., Buchanan III, A.C. *ACS Symposium Series*, Oxford University Press, 943 (2006) 146.
214. Luo H., Huang J.F., Dai S., *Sep. Sci. Technol.*, 45 (2010) 1679.
215. Luo H., Dai S., Bonnesen P.V., Haverlock T.J., Moyer B.A., Buchanan III, A.C., *Solvent Extr. Ion Exch.*, 24 (2006) 19.
216. Shkrob I.A., Marin T.W., Dietz M.L., *J. Phys. Chem.* B, 115 (2011) 3903.
217. Yuan L., Peng J., Xu L., Zhai M., Li J., Wei G., *J. Phys. Chem.* B, 113 (2009) 8948.
218. Yuan L., Peng J., Xu L., Zhai M., Li J., Wei G., *Dalton Trans.* (2008) 6358–6360.
219. Chun, S.; Dzyuba, S.V.; Bartsch, R.A., Anal. Chem., 73 (2001) 3737.
220. Dietz M.L., Dzielawa J.A., Laszak I., Young B.A., Jensen M.P., *Green Chem.*, 5 (2003) 682–685.
221. Takagi N., Izumi Y., Ema K., Yamamoto T., Nishizawa K., *Solvent Extr. Ion Exch.*, 17 (1999) 1461.